THE UNIVERSITY OF HULL

THE STRUCTURE AND KINETICS OF OIL-IN-WATER MICROEMULSIONS STABILISED BY NONIONIC SURFACTANTS

being a Thesis submitted for the Degree of

Doctor of Philosophy

in the University of hull

by

Jane Susan Morris B.Sc.

September 1995

ACKNOWLEDGEMENTS

I would like to express my sincere gratitude to my supervisor Dr. Paul Fletcher for his advice, guidance, encouragement and enthusiasm during the period of my research. Thanks are also due to Professor Josef Holzwarth at the Max Planck Institute in Berlin for his invaluable help with the ILTJ experiments, and to Dieter Bauer for his technical assistance with same, and finally to my fellow colleagues in Hull for many helpful discussions, in particular Dr. F. Klinkhammer and Dr. K. Suhling.

I am also grateful to the S.E.R.C. for the award of a three year studentship, and to the D.A.A.D for financial assistance during my period of research in Berlin.

September 1995

ABSTRACT

This thesis is concerned with the behaviour of the single phase (1ϕ) alkane oil-in-water (O/W) microemulsions stabilised by nonionic surfactants of the general structure H-$(CH_2)_n(OCH_2CH_2)_m$-OH, abbreviated to C_nE_m. The aims were to attempt to characterise their behaviour in terms of the effect of the different constituents n, m, and alkane oil chain length (x).

Initially the limiting temperature phase boundaries of the 1ϕ region were established by measurements of turbidity. Turbidity was found to be at a minimum at the lower temperature phase boundary (the solubilisation phase boundary, SPB), and at a maximum at the upper temperature phase boundary (UTPB). The temperature position of the 1ϕ region was found to be increased by increasing m or x, and decreased by increasing n. The width of the temperature range was generally found to be decreased by increasing the ratio of oil to surfactant (R). For a series of decane-in-water microemulsions stabilised by surfactants having a constant ratio n/m=2, the SPB was found to be little affected by an increased overall surfactant length, whereas the UTPB was found to be increased.

The microemulsion droplet sizes were determined by both static and dynamic light scattering (turbidity and PCS respectively). The particle size was measured at varying temperatures and was found to be at a minimum at the SPB and to increase with temperature (explaining the increase of turbidity with increasing temperature). The increased particle size was assumed to correspond to clustering or growth of the microemulsion droplets. The size measured at the SPB was assumed to be that of the individual droplets at their preferred size. The hydrodynamic radius (r_h) of the droplet at the SPB was used to calculate the area (A_s) occupied per surfactant molecule at the interface between the droplet core and the surfactant monolayer. A_s was found to be increased by increasing n, and decreased by increasing x, whereas m was found to have little effect.

Turbidity measurements were found to be a simple method of measuring the extent of clustering or growth of the droplets with increasing temperature. From this information the equilibrium constant (K) and the associated standard enthalpy, entropy and Gibbs free energy changes were obtained. A simple scheme of droplet aggregation was postulated in which K for the addition of one droplet to an existing cluster (equating to growth by the equivalent of one droplet at the preferred size) was constant regardless of cluster size. The model was found to fit well to a middle range droplet

concentration of 0.04 - 0.10 M. Measurements at lower droplet volume fractions were found to be too inaccurate, and K was found to decrease for fractions greater than this range. A model which would accommodate the decrease in K with higher droplet volume fraction would be highly complex and include further estimated parameters. It was therefore deemed appropriate to employ the simple model for comparison within the relevant range of droplet volume fraction. As expected K was found to increase with increasing temperature for all systems. The large positive enthalpy (of the order of 1000 $kJmol^{-1}$) obtained for all systems accounts for the strong temperature dependence of the behaviour of these microemulsions. The positive entropy change (of the order of 3 $JK^{-1}mol^{-1}$) was attributed to the increasing disorder of the water molecules following dehydration from the surfactant head group region. The removal of water from the head groups has the additional effect of increasing inter-head group and therefore inter-droplet attractions thus promoting clustering or growth. The resulting negative Gibbs free energy (of the order of -14 $kJmol^{-1}$) indicates that the clustering/growth process is spontaneous and entropically driven. The clustering/growth process was found to be dependent on the packing density of the surfactant head groups at the droplet monolayer surface. Assuming clustering occurs the thermodynamic parameters were calculated per mole of surfactant molecules involved in the droplet contact zone of the clusters. Droplets having the more widely spaced (less closely packed) head groups were found to have a larger enthalpy and entropy change, probably as a result of the greater requirement for dehydration of the head groups.

A temperature jump method was employed to study the kinetics of the clustering/growth process. The results were found to be consistent with the equilibrium data, in that the rates of the clustering/growth process were found to be dependent on the packing density of the surfactant head groups. Droplets having the less closely packed head groups were found to cluster more slowly, again an indication of the greater difficulty in dehydrating the head groups. The activation energy was also calculated for the clustering/growth process, and was found to be of the order of a few hundred $kJmol^{-1}$, but no discernible trends with molecular structure of the components were observed.

PUBLICATIONS

Work contained within this has given rise to the following publication, first presented at the 10th International Symposium on Surfactants in Solution, Caracas, Venezuela, June 1994:

Turbidity of oil-in-water microemulsion droplets stabilised by nonionic surfactants.
P. D. I. Fletcher and J. S. Morris, Colloids and Surfaces, A:Physiochemical and Engineering Aspects 98, (1995) 147 - 154.

GLOSSARY

Some abbreviations and terms used in this thesis are given below. Others are defined as appropriate within the text.

1ϕ	single phase microemulsion region
Abs	absorbance
A_h	area occupied per surfactant head group at the droplet monolayer surface
A_s	area occupied by a surfactant molecule at the droplet core/surfactant monolayer interface
ΔA	change in interfacial area
c	concentration
C_c	cluster concentration
C_d	dropet concentration
cmc	critical micelle concentration
$c\mu c$	critical microemulsion concentration
CW	Continuous Wave
δ	thickness of the surfactant monolayer in a microemulsion droplet
D	diffusion coefficient
E_{act}	activation energy
γ	surface tension
γ_c	minimum surface tension at the cmc, or $c\mu c$
ΔG^o	standard Gibbs free energy change
Γ	surface excess concentration
H_1	hexagonal phase
ΔH^o	standard enthalpy change
I_1	cubic phase
ILTJ	Iodine Laser Temperature Jump
φ	polydispersity
k	Boltzmann's constant
K	equilibrium constant
k_f	forward (clustering/growth) rate constant
k_{obs}	the observed first order rate constant for the clustering/growth process
k_r	reverse (clustering/growth) rate constant
L_1	isotropic single phase micellar solution
L_α	lamellar phase

λ	wavelength of light
μ	chemical potential
n	average number droplets at the preferred size in a cluster
N	number of particles per unit volume
η	viscosity
N_{agg}	aggregation number
O/W	oil-in-water
PCS	Photon Correlation Spectroscopy
r_c	radius of microemulsion droplet core
r_h	hydrodynamic radius of microemulsion droplet
R	molar ratio of oil to surfactant
R'	gas constant
SPB	solubilisation phase boundary
ΔS^o	standard entropy change
T	absolute temperature
T-jump	temperature jump
TRF	Time Resolved Fluorescence
τ	turbidity
τ_o	minimum turbidity at the SPB
UV/VIS	ultraviolet/visible
UTPB	upper temperature phase boundary of the 1ϕ region
V_m	molecular volume of the dispersed phase of a microemulsion
V_p	scattering volume of particle
W/O	water-in-oil

CONTENTS

APPENDIX IV

The minimum absorbance values measured for each C_nE_m/x-alkane oil system with varying surfactant concentration. Data used in chapters 5 and 6.

APPENDIX V

The hydrodynamic radii measured by PCS at the SPB for each C_nE_m/x-alkane oil system. Data used in chapter 4.

APPENDIX VI

The observed rate constant measured for each C_nE_m/x-alkane oil system. Data used in chapter 6.

CHAPTER ONE

1 Introduction. Surfactant behaviour.

1.1 Surfactant structure

Surfactants (surface active agents) gain their name from their behaviour at surfaces and interfaces, caused by their amphiphilic nature. Surfactant molecules are composed of a non-polar hydrophobic section and a polar hydrophilic section. The hydrophobic part, usually referred to as the tail, is most commonly a long alkyl substituent which may be linear or branched or consist of more than one chain. Surfactants are classified according to the nature of the charge on the head group. They may be anionic, often sulphates, or carboxylates; cationic, which are generally derived from substituted ammonium compounds; zwitterionic, in which the head group contains both anionic and cationic groups; or non-ionic. The present study is concerned with an important class of non-ionic surfactants based on polyoxyethylene which have the general formula $C_nH_{2n+1}(OCH_2CH_2)_mOH$, abbreviated to C_nE_m. Illustrations of surfactant behaviour discussed in the rest of this chapter will be for these C_nE_m surfactants. Examples of the different types of surfactants are given in Figure 1.1.

Figure 1.1 Examples of the different surfactant types.

Anionic: Sodium dodecyl sulphate (SDS) $CH_3(CH_2)_{11}\text{-}O\text{-}SO_3^-Na^+$.

Cationic: Dodecyl trimethyl-ammonium bromide (DTAB)
$CH_3(CH_2)_{11}N^+(CH_3)_3Br^-$

Zwitterionic: C-betaine series

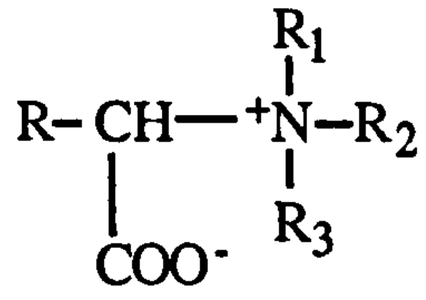

where R = a long hydrophobic tail, R_{1-3} = hydrogen or short alkyl chain.

Non-ionic: Hexa-oxyethylene-n-dodecyl ether
$C_{12}H_{25}(OCH_2CH_2)_6OH$ (abbreviated to $C_{12}E_6$)

1.2 Surfactant adsorption and aggregation in aqueous solutions

1.2.1 Adsorption

The amphiphilic nature of surfactants determines their adsorption at surfaces and interfaces, and aggregation in the bulk phase. The surfactant molecules try to orientate themselves such that the hydrophobic tail is in a hydrophobic environment, and the hydrophilic heads are in a hydrophilic environment.

At low concentrations of surfactant in water, the surfactant molecules exist as monomers, with some adsorbing at the air water interface forming a monolayer, with the heads in the water and the tails lying out of the water surface. The migration to the surface is caused by the tendency of the hydrophobic tails to minimise contact with water. The hydrophobic tail causes increased ordering of the surrounding water molecules resulting in increased hydrogen bonding in the region - this is termed the hydrophobic effect[1]. The ordering is entropically unfavourable and is therefore minimised by migration of the monomer to the surface. The adsorption at the surface is spontaneous and therefore the free energy of the system decreases, which is achieved by a lowering of the surface tension, defined as the reversible work required to form a unit area of surface at constant temperature, pressure and composition. The relationship between the amount of surfactant adsorbed at a surface and the surface tension at constant temperature and pressure, is given by the Gibbs adsorption equation[2] (equation 1.2a).

$$-d\gamma = \Sigma_i \Gamma_i \, d\mu_i \qquad (1.2a)$$

where γ = the surface tension with units of mN/m.

Γ_i = the surface excess concentration of species i. This is the extra amount of species i that is adsorbed due to the presence of the surface.

μ_i = the chemical potential of species i.

Σ_i = the summation for all species i.

---

[1]C. Tanford,"The Hydrophobic Effect: Formation of Micelles and Biological Membranes", 2nd Edition, Wiley, New York, 1980.

[2]R. Aveyard, D. A. Haydon, "An Introduction to the Principles of Surface Chemistry", Cambridge University Press, 1973.

Assuming ideal behaviour the chemical potential of species i is related to the concentration (c_i) by:

$$\mu_i = \mu_i^o + RT\ln c_i \qquad (1.2b)$$

where μ_i^o is the chemical potential of species i in a standard state (commonly 1 M), assumed to behave ideally;

therefore the change in chemical potential is given by

$$d\mu_i = RTd\ln c_i \qquad (1.2c)$$

and substituting into the Gibbs adsorption equation yields, for a nonionic surfactant:

$$-d\gamma = \Sigma_i \Gamma_i RTd\ln c_i \qquad (1.2d)$$

1.2.2 Aggregation

Increasing the surfactant concentration leads to more adsorption at the surface, with further reduction of the surface tension, until a concentration is reached at which the extra monomers can no longer adsorb at the surface and begin to form aggregates (micelles). The surfactant monomers orientate themselves within the micelles such that the hydrocarbon tails are in the centre away from the water with the head groups at the surface, these are termed *normal micelles*[3] in which the monolayer is said to have a positive curvature (Figure 1.2.1). The concentration at which the micelles begin to form is termed the *critical micelle concentration* (cmc). The surface tension reaches a minimum (γ_c) at the cmc, and thereafter remains approximately constant for increasing surfactant concentration (Figure 1.2.2). The cmc of a surfactant can therefore be determined by this abrupt change in γ. A compilation of cmc values for different surfactants has been given by Mukerjee and Mysels[4]. The cmc's for the non-ionic C_nE_m surfactants are very low, e.g. 4×10^{-5} mol l^{-1} for $C_{12}E_5$ whereas the cmc's of ionic surfactants having the same hydrocarbon chain are generally higher e.g. 1.3×10^{-3} mol l^{-1} for SDS.

---

[3]J. W. McBain, C. S. Salmon, J. Amer. Chem. Soc. 1920, 45, 426.
[4]P. Mukerjee, K. J. Mysels, "Critical Micelle Concentrations of Aqueous Surfactant Systems", National Bureau of Standards, Washington, 1971.

Figure 1.2.1 Schematic diagram of surfactant aggregation in water.

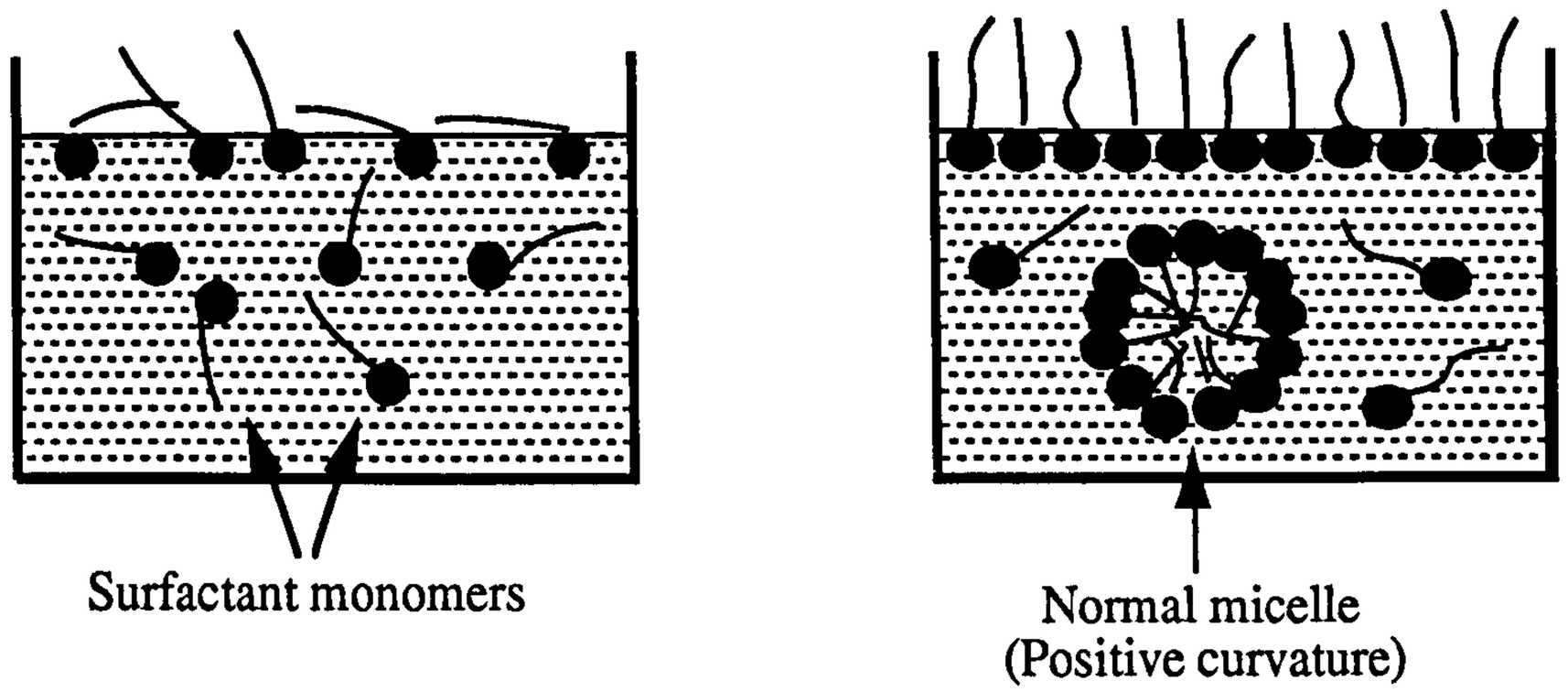

Figure 1.2.2

The variation of surface tension (γ) with surfactant concentration in the binary surfactant/water system, showing the cmc occurring at minimum tension (γ_c).

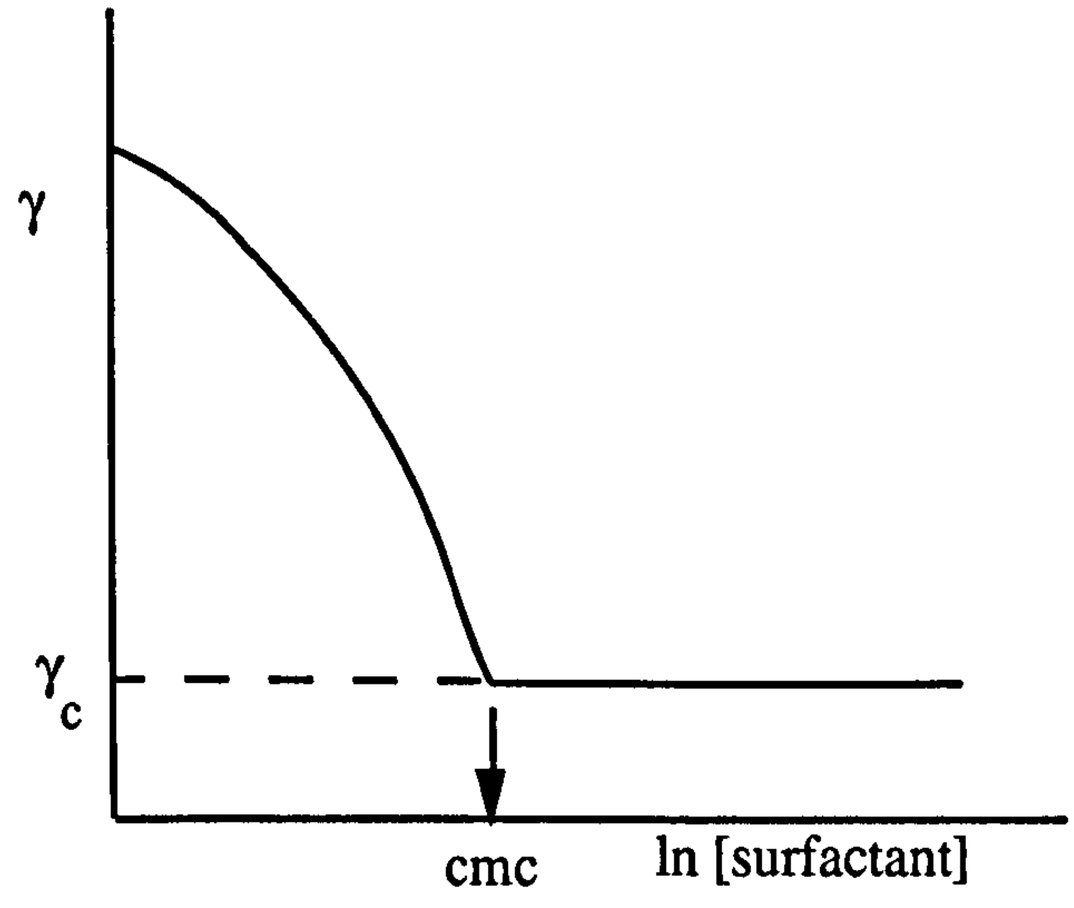

1.2.3 Micellar shape and growth

As discussed above, aggregation into micelles is driven by the tendency of the surfactant hydrophobic tail groups to orientate themselves such that they are away from water. Aggregation does not continue indefinitely but is limited by repulsive forces between the head groups. For ionic head groups this force is electrostatic repulsion between the charges, for nonionic surfactants steric hindrance and hydration provide the

repulsive force. The formation of micelles is therefore determined by the opposing forces of the tail and head groups. The structure of the surfactant therefore determines the size and shape of the micelle within packing restraints. Also important are the solution conditions such as the surfactant concentration, electrolyte concentration and temperature. The number of surfactant molecules constituting one micelle (the aggregation number) can be in the range from fifty to a few thousand. The standard free energy required to micellise one mole of surfactant (ΔG^o) is related to the cmc by:

$$\Delta G^o = RT\ln(cmc) \qquad (1.2e)$$

where ideal behaviour is assumed for both the monomer and micellar state. For a homologous series of surfactants ΔG^o is found to decrease linearly with increasing hydrophobic tail length, the contribution to free energy for each additional methylene group has been found to be of the order of -3 $kJmol^{-1}$ [5].

At low aggregation numbers micelles tend to be spherical. The maximum radius of a spherical micelle is the all trans-length of the surfactant tail group. Therefore, to grow the micelle must change it's surface curvature forming a non-spherical shape. Increasing the surfactant concentration, or other factors which allow micellar growth such as temperature for nonionic surfactant, therefore leads to rod or disc shaped micelles (Figure 1.2.3). As the concentration is increased leading to higher volume fraction of micelles, the micelles start to pack together due to space limitations. Disc micelles will pack into lamellar structures (L_α) of surfactant bilayers separated by layers of water. Rod micelles will pack into a hexagonal array (H_1) which may then form lamellae. Spherical micelles initially pack into a regular cubic array (I_1), which may then progresses through a hexagonal structure to a lamellar phase. These close packed arrangements of micelles hence form structured liquids known as *liquid crystals* (also known as mesophases or intermediate phases) since they are more structured than normal liquids but less structured than normal solid crystals.

The phase diagram of temperature versus concentration for $C_{12}E_6$ in water is given in Figure 1.2.4[6] where the formation of H_1 and L_α mesophases are seen. An additional feature on this diagram is the transition from a one phase isotropic micellar solution (L_1) to two liquid phases on increasing the temperature. The increase in temperature causes the micellar aggregates to attract each other to the extent that they

---

[5]J. M. Corkill, J. F. Goodman, J. R. Tate, Trans. Faraday Soc.,1964, 60, 996.
[6]J. S. Clunie, J. F. Goodman, P. C. Simons, Trans. Faraday Soc. 1969, 65, 287.

Figure 1.2.3

Schematic diagram of the possible shape changes with growth for normal micelles.

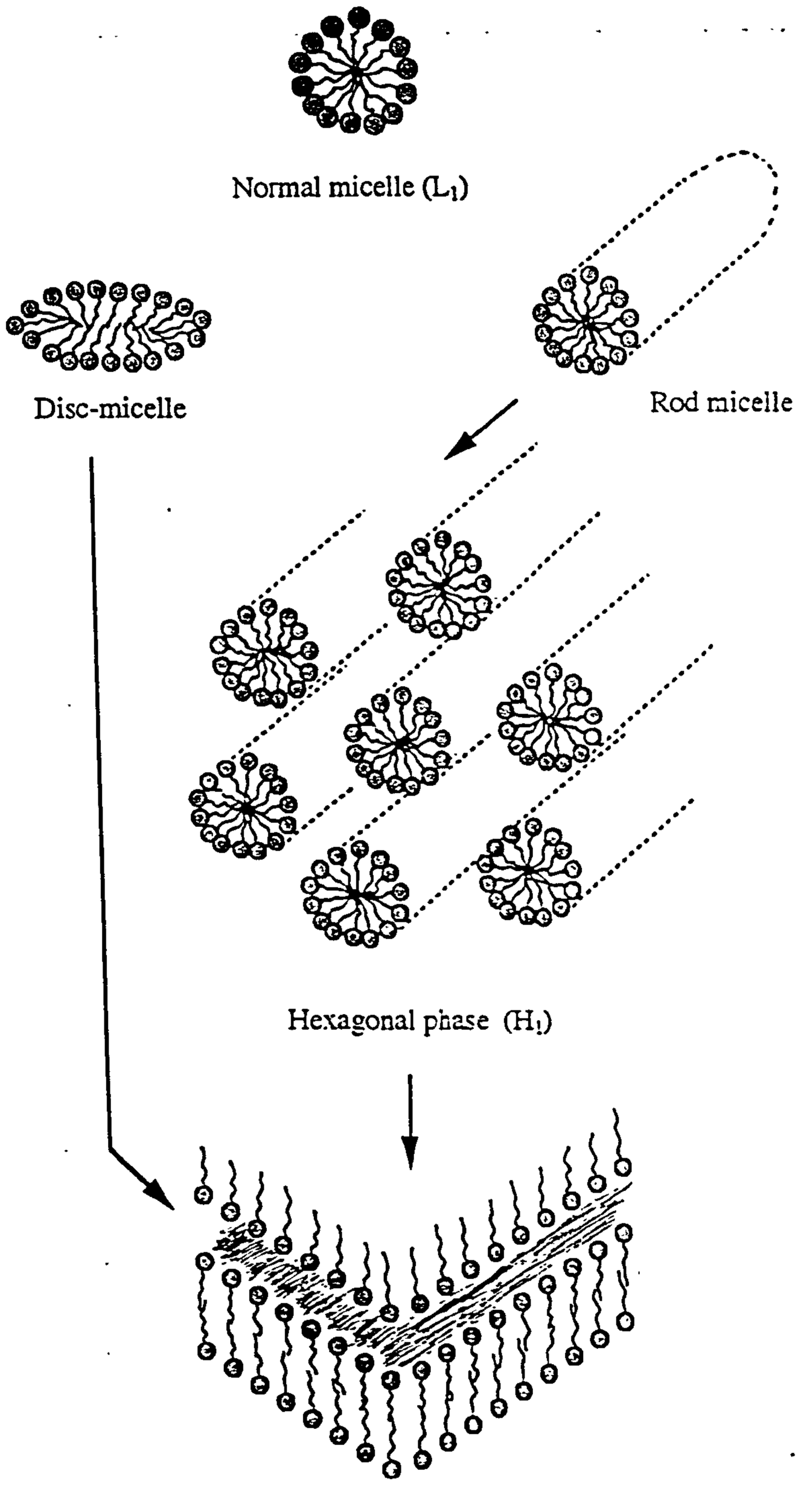

separate out forming a surfactant rich upper phase, with the lower phase being mainly water. The temperature at which this separation occurs is accompanied by a clear to cloudy transition on warming the solution. This temperature is therefore known as the *cloud point*, and is used as a test for purity of the surfactant. Most C_nE_m surfactants show the cloud point phenomenon.

Figure 1.2.4 The phase diagram of $C_{12}E_6$ in water (reproduced from reference 6).

L_1 = the isotropic single phase micellar solution

H_1 = hexagonal phase

L_α = lamellar phase

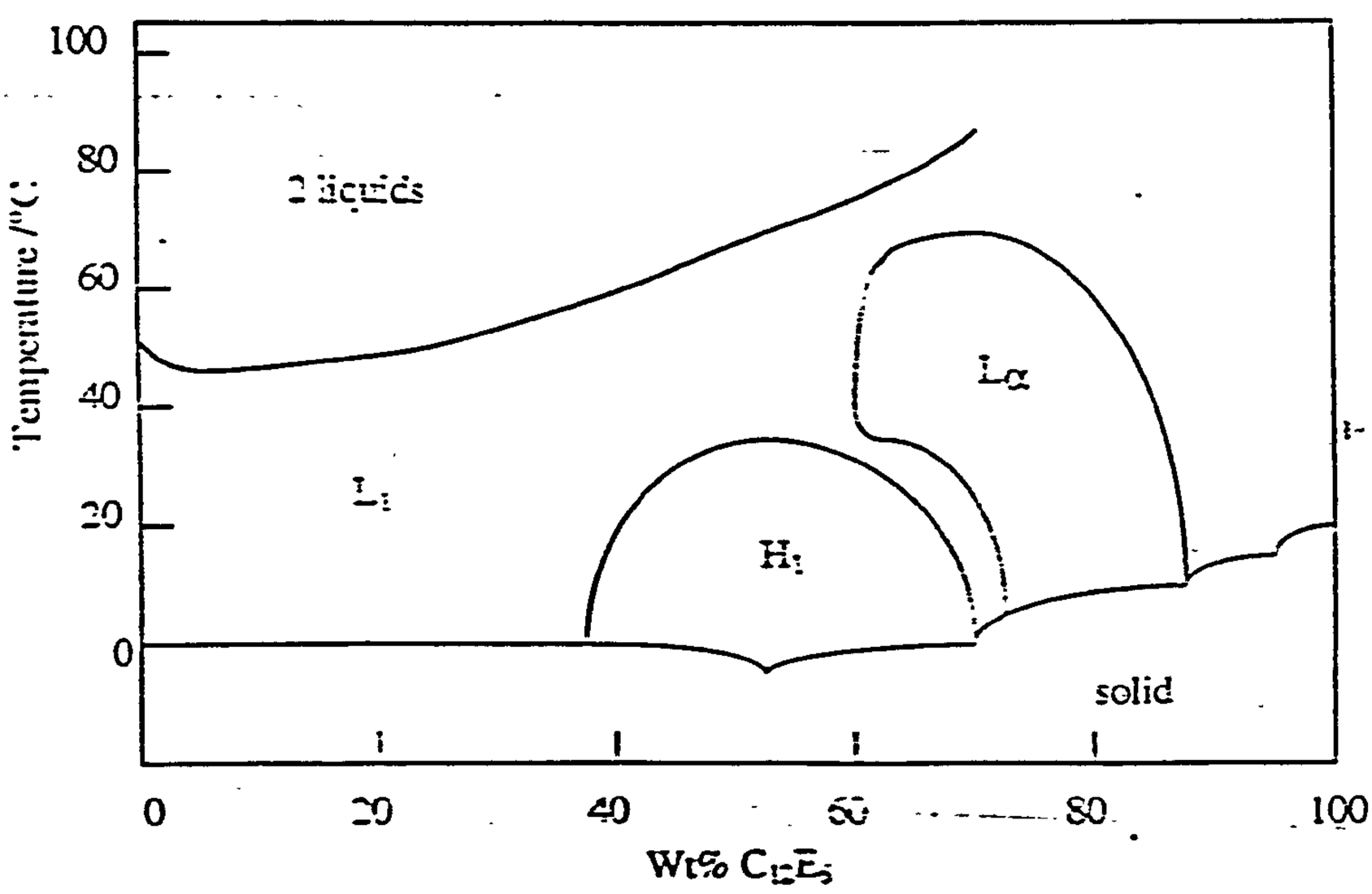

1.3 Aggregation in apolar liquids

The addition of surfactant to apolar solvents produces aggregation into *reverse micelles* (Figure 1.3.1) in which the polar head groups are in the centre and the apolar tail groups on the outside protruding into the solvent (forming a negatively curved monolayer). Unlike surfactants in water, adsorption *does not* occur at the air/oil interface. A layer of head groups has a higher energy than the apolar surface, and thus the head groups generally prefer oil to air. The driving force for reverse micellisation is the inter head group attraction which may be ionic, or due to dipole-dipole attractions. In some cases there can be hydrogen bonding between the head groups in the centre of the aggregates, forming a more hydrophilic region. Aggregation in apolar liquids is very sensitive to traces of water which may increase the bonding between head groups by acting as an H-bonding bridge between head groups, sticking them together. Aggregation in oil generally occurs over a wide concentration range and thus a "cmc" in the oil is not appropriate. Jones et al[7] have shown that the degree of aggregation of C_nE_m surfactants in oil is low and only small micelles containing between 5 and 15 surfactant monomers are formed.

Figure 1.3.1 Schematic diagram of surfactant aggregation in oil.

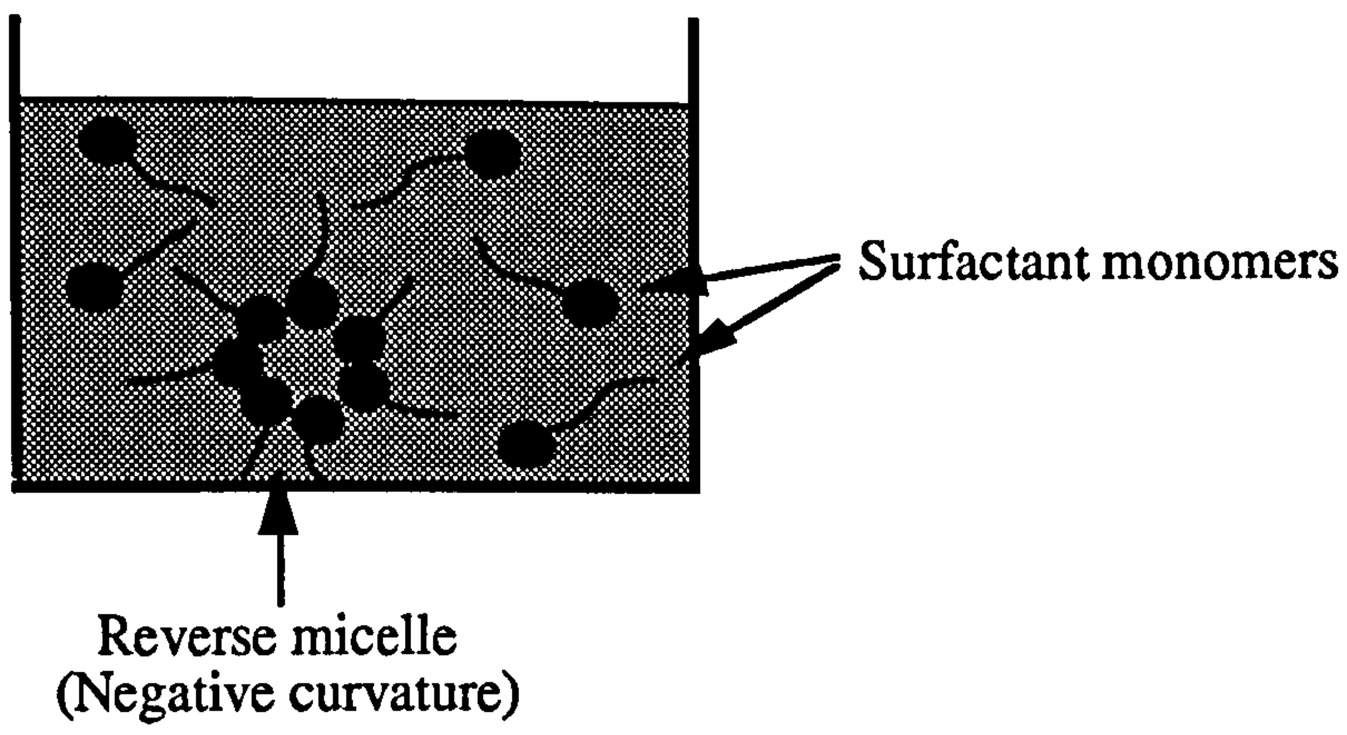

[7]P. Jones, E. Wyn-Jones, G. J. Tiddy, J. Chem. Soc. Faraday Trans. 1987, 83, 2735.

1.4 Surfactant adsorption and aggregation in ternary systems with oil and water

1.4.1 Adsorption at the oil/water interface

Oil and water do not mix, and will exist as two separate phases if added together. Oil generally forms the upper phase, and water the lower phase with an interfacial tension occurring between the two phases. If surfactant is added to such a system the molecules will partition between both phases, non-ionic surfactants of the C_nE_m type generally partition in favour of alkane oils[8]. Unfavourable interactions will occur between the head groups and the oil, and between the tail groups and the water. These interactions will be minimised by the preferential location of the surfactant molecules at the oil/water interface, where the head groups will prefer to lie in the water phase, and the tail groups in the oil phase. Adsorption at the interface lowers the interfacial tension in an analogous way to that described earlier for surfactants in water (section 1.2). As the concentration of surfactant is increased, more adsorption occurs at the interface to a maximum point when no more will adsorb. At this point the interfacial tension reaches a minimum (γ_c) and remains approximately constant with increasing surfactant concentration. Any extra surfactant molecules will thereafter aggregate together with the head groups in contact with the water and the tail groups with the oil. These aggregates are therefore able to "mix" oil with water by containing (*solubilising*) one phase inside the aggregates which are then dispersed in the continuous phase. If the surfactants aggregate in the water, the surfactant molecules form a monolayer coating the droplet surface with the head groups on the outside in contact with the water, and the tail groups on the inside in contact with oil solubilised in the centre (Figure 1.4.1a). A dispersion of oil in water is therefore possible. If aggregates occur in the oil, reverse droplets occur, with water forming the droplet core and the surfactant molecules in the monolayer orientated such that the heads are on the inside in contact with the water, and the tails on the outside in contact with the oil, (Figure 1.4.1b) thus allowing a dispersion of water in oil. Oil/water/surfactant systems containing these dispersed droplets in the continuous medium are called *microemulsions* and the concentration of surfactant at which the aggregates start to form is called the *critical microemulsion concentration (cμc).* Dispersions of oil in water are thus termed oil-in-water (O/W) microemulsions, and dispersions of water in oil are termed water-in-oil

---

[8]R. Aveyard, B. P. Binks, S. Clark, P. D. I. Fletcher, J. Chem. Soc. Faraday Trans. 1990, 86, 3111.

(W/O) microemulsions.

Figure 1.4.1 Schematic diagram of microemulsion droplets.

(a) Oil-in-water microemulsion droplet

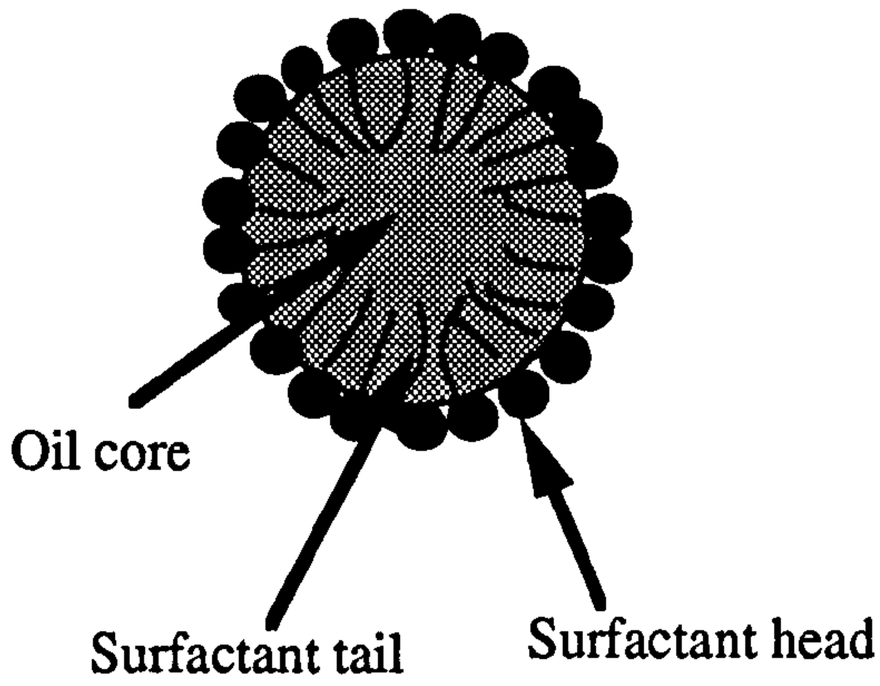

(b) Water-in-oil microemulsion droplet

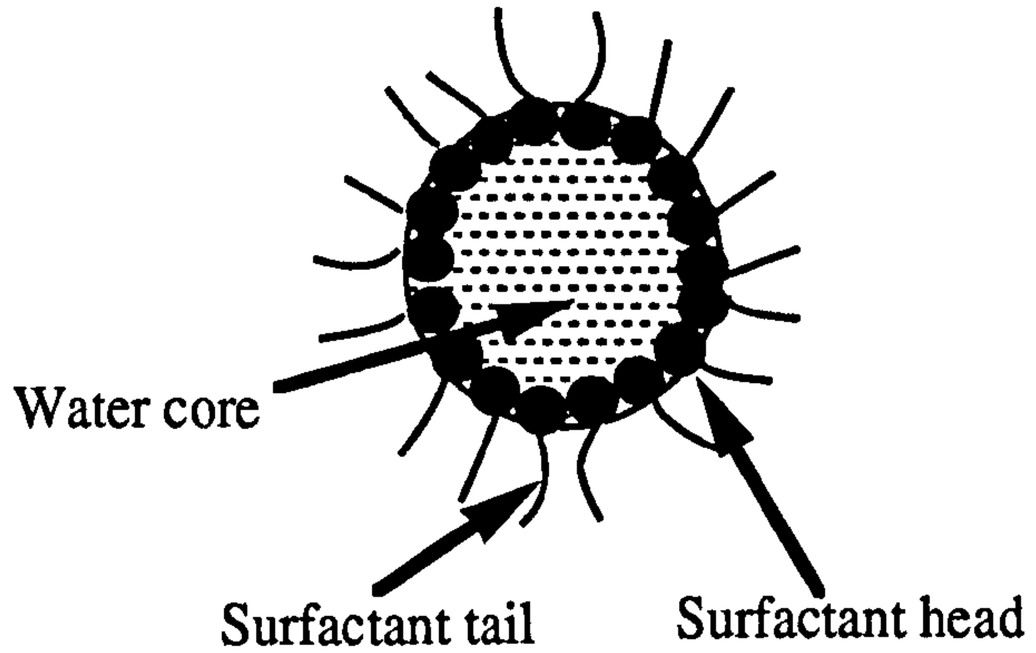

1.4.2 The phase behaviour of oil/water/surfactant systems.

In oil/water/surfactant systems the type of aggregate which occurs depends on the nature of the surfactant and the solution conditions such as the surfactant concentration, electrolyte concentration and temperature. Changing the solution conditions can lead to a progression of different phases which has been studied extensively for nonionic surfactants by Shinoda *et al*[9] and Kahlweit[10]. The work in this thesis is concerned with nonionic surfactants on which further discussion of microemulsion phase behaviour will concentrate. For a fixed oil/water/nonionic surfactant composition, changing the temperature causes a phase progression as shown schematically in Figure 1.4.2.

At low temperatures the surfactants aggregate in the water forming an O/W microemulsion phase in equilibrium with excess oil. This termed a Winsor I system. The surfactant monolayer within an O/W droplet is said to have a positive curvature. On increasing the temperature three phases may exist with the formation of a middle surfactant rich phase in equilibrium with excess oil and excess water phases. The aggregate structure within the surfactant rich phase can be bicontinuous or L_α in structure which contain comparable amounts of oil and water both of which form continuous domains with the monolayer having approximately zero mean curvature. Increasing the temperature still further causes the aggregates to form in the oil forming

---

[9]K. Shinoda, H. Kunieda, J. Disp. Sci. Tech., 1982, 3, 233.
[10]M. Kahlweit, R. Strey, Angew. Chem. Int. Ed. Engl.,1985, 24, 654.

Figure 1.4.2

A schematic diagram of the progression of phase behaviour, post cμc interfacial tension (γ_c) and surfactant monolayer curvature with temperature for an oil/water/nonionic surfactant system at fixed composition.

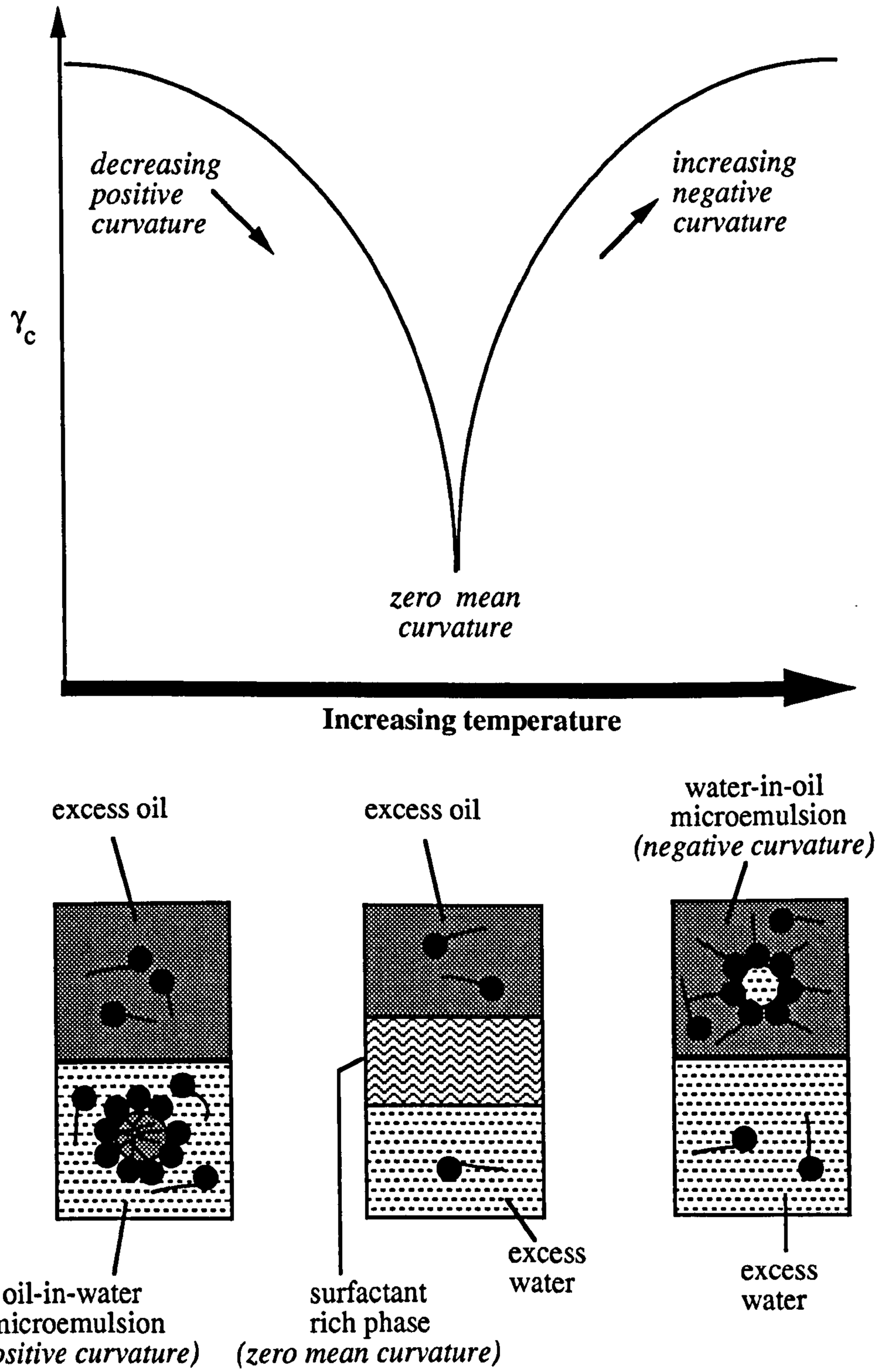

a W/O microemulsion in equilibrium with excess water. The curvature of the monolayer is defined here as negative for a W/O droplet. The changing preferred curvature of the monolayer causes a corresponding variation in the interfacial tension of the flat interface separating the bulk phases. The interfacial tension decreases with increasing temperature from Winsor I reaching a minimum at the Winsor III system, thereafter increasing again for the Winsor II system. The type of aggregation of surfactants in oil and water systems therefore depends on the tendency of the monolayer to curve, which is determined by the system conditions.

When microemulsions are in equilibrium with an excess of the dispersed phase the droplets are free to solubilise more or less of the dispersed component, growing or shrinking in size until the system free energy is minimised. When this point is reached the droplet monolayer is said to be at it's *preferred curvature* and thus the droplet is at it's *preferred size*. The free energy of formation of a dilute microemulsion phase arises from two main contributions. An unfavourable (positive) contribution results from the formation of a large increase in the oil-water interface of the system, which may be equated to the product of the tension of the curved interface, (γ) and the increase in the interfacial area (ΔA). A favourable contribution results from the increase in entropy associated with dispersion of the droplets in the continuous phase, this term is given by the product of the absolute temperature (T) and the dispersion entropy (ΔS). The resulting free energy of formation (ΔG) is given by the difference between these two terms (equation 1.4a).

$$\Delta G = \gamma \Delta A - T\Delta S \qquad (1.4a)$$

Microemulsions form spontaneously (ΔG is negative) only when the tension is low enough such that the favourable entropy term outweighs the unfavourable tension term[11]. Hence microemulsion formation is always associated with ultra low values of the interfacial tension (of the order of 10^{-1} - 10^{-4} mNm^{-1}).

The extent of curvature of the surfactant monolayer thus determines the amount of solubilisation of the dispersed phase and hence the size of the droplets. The amount of solubilised material within the droplets can be expressed as the molar ratio of dispersed component to surfactant within the aggregate (equation 1.4b):

$$R = [\text{dispersed component}] / ([\text{surfactant}] - c\mu c) \qquad (1.4b)$$

[11]E. Ruckenstein, J. Chi, J. chem. Soc. Faraday Trans. II, 1975, 71, 1690.

For O/W microemulsions stabilised by C_nE_m surfactants (in the absence of an excess oil phase) the cμc term can be ignored since, as discussed in section 1.2.2, the cmc in water is very low, and is similar both for micelles and microemulsion aggregates.

A schematic diagram of the structural parameters of a microemulsion droplet are shown in Figure 1.4.3 for spherical monodisperse droplets. The radius of the microemulsion droplet core (r_c) is simply related to R by:

$$r_c = 3V_mR/A_s \qquad (1.4c)$$

where V_m is the molecular volume of the dispersed phase, and A_s is the area occupied by a surfactant molecule at the interface between the droplet core and the surfactant monolayer. The hydrodynamic radius (r_h) of the microemulsion droplet is therefore given by:

$$r_h = r_c + \delta \qquad (1.4d)$$

where δ is the thickness of the surfactant monolayer and includes any entrapped solvent.

Figure 1.4.3

A schematic representation of the structural parameters of microemulsion droplets, shown for an oil-in-water droplet. $\mathbf{r_h}$ is the hydrodynamic radius of the droplet, $\mathbf{r_c}$ is the radius of the core, δ is the thickness of the surfactant monolayer including any entrapped solvent, $\mathbf{A_s}$ is the area occupied by a surfactant molecule at the interface between the droplet core and the surfactant monolayer.

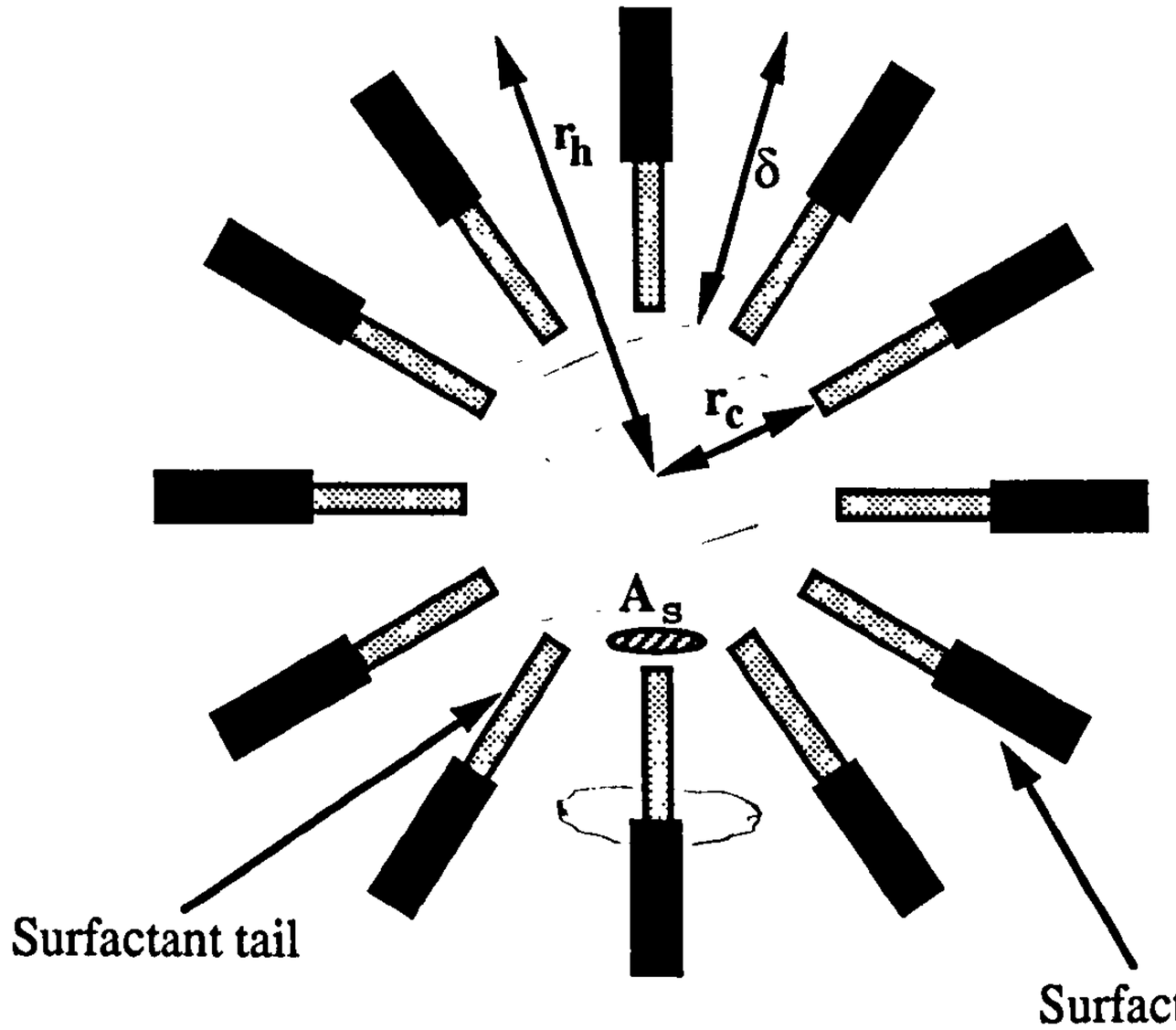

1.4.3 Factors affecting monolayer curvature

The preferred curvature of the monolayer (and thus the Winsor phase type) can be changed by varying the nature of the surfactant or the solution conditions as discussed below.

1) *The molecular structure of the surfactant.*

The relevant sizes of the head and the tail groups of the surfactant affect the geometry of the monolayer. A larger head promotes a positive curvature, whereas a larger tail promotes a negative curvature (Figure 1.4.4 (a) and (b) respectively).

Figure 1.4.4 The effect of surfactant structure on preferred monolayer curvature.

(a) A larger head group promotes a more positive curvature, leading to an oil-in-water microemulsion

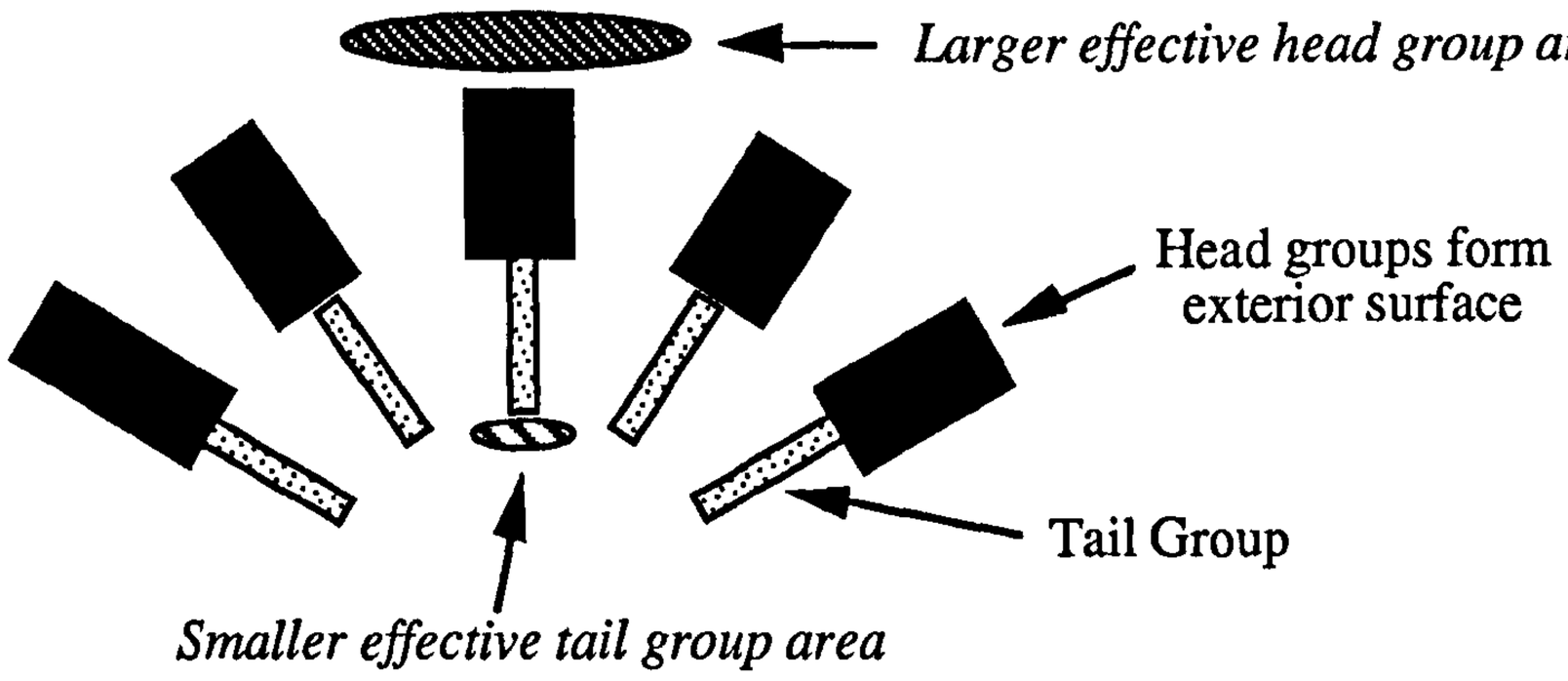

(b) A larger tail group promotes a more negative curvature, leading to a water-in-oil microemulsion.

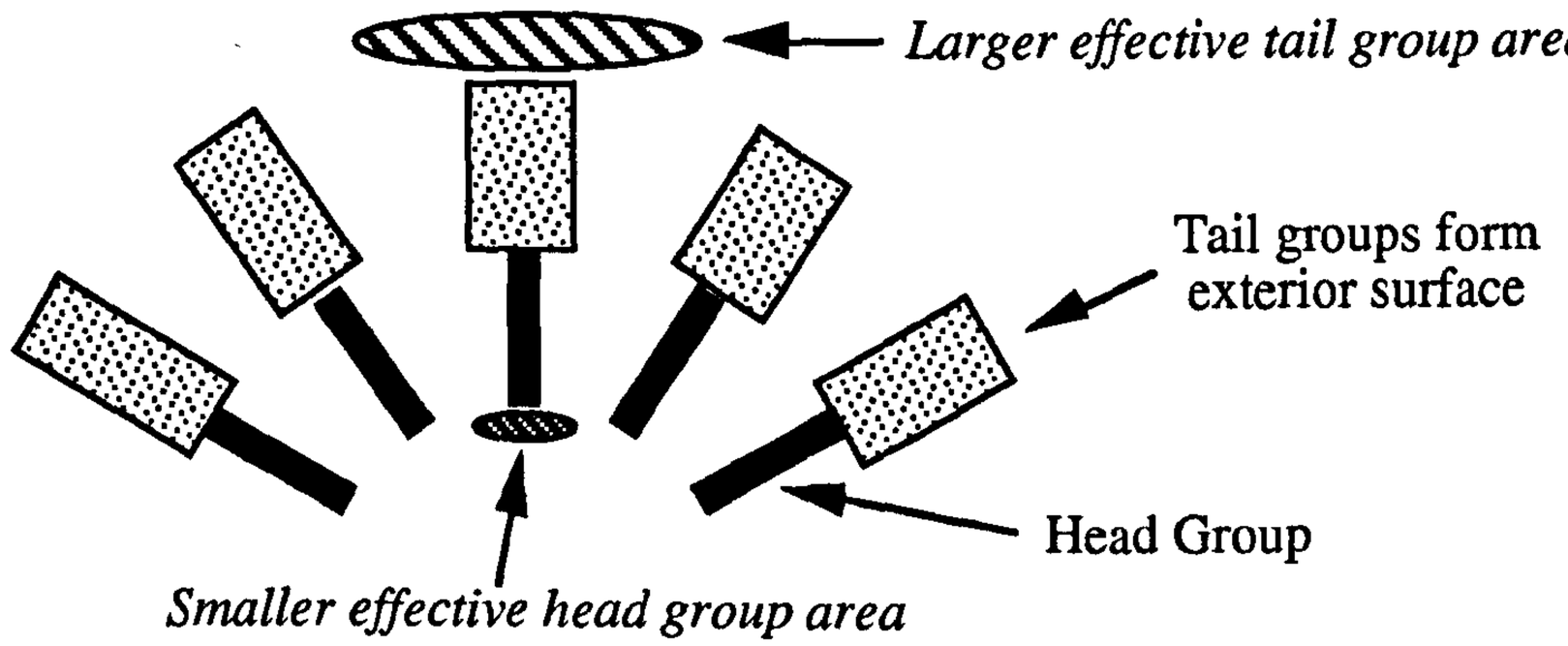

2) *Temperature.*

For non-ionic surfactants an increase in temperature leads to dehydration of the head groups resulting in a smaller effective head group area and thus promoting a more negative curvature[12]. Increasing temperature for ionic surfactants produces a more positive curvature[13], possibly due to increased surfactant dissociation leading to increasing electrostatic repulsion between the head groups and hence resulting in a larger effective head group area.

---

[12]K. Shinoda, H. Kunieda, T. Ari, H. Saijo, J. Phys. Chem. 1984, 88, 5126.
[13]R. Aveyard, B. P. Binks, J. Mead, J. Chem. Soc. Faraday Trans. 1985, 1, 81, 2169.

3) *Salt concentration.*

Addition of salt produces a more negative curvature in both ionic and non-ionic surfactants. For ionic head groups, salt screens the charges thus reducing electrostatic repulsion promoting a smaller effective head group area[14]. Non-ionic head groups require a larger salt concentration before a significant change in the effective head group area results in a change in the monolayer curvature. It is thought that salt competes with the head groups for hydration water, thus effectively dehydrating the head group causing the head group area to shrink, often called "salting out" of the head groups.[15].

4) *Nature of the oil.*

The effective area per surfactant tail group is affected by the nature of the oil phase. A decrease in the length of an alkane oil has been shown to increase this effective tail group area, and it has been postulated that shorter chain oils penetrates the surfactant tails in a monolayer to a greater extent [16] thus producing a more negative curvature. Aromatic oils have a similar effect.

5) *Addition of a cosurfactant*

Cosurfactants are extra surface active molecules, such as medium chain length alcohols, which adsorb within the surfactant monolayer and are added such that the curvature property of the monolayer can be adjusted. The effect on the curvature depends on the structure of the cosurfactant as for the main surfactant of the monolayer (*cf.* 1 above).

1.4.4 The relationship between interfacial tension and microemulsion droplet size.

The interfacial tension is related to the free energy difference between the interfacial film at the planar interface separating the bulk phases, and the curved monolayer surrounding the droplets. The tension contains contributions from the energies required to bend the monolayer and energies associated with the entropy

---

[14]Surfactants and Inter facial phenomena, ED. M. J. Rosen, John Wiley & Sons, New York, 1989.
[15]Surfactant Systems - their chemistry, pharmacy and biology, D. Attwood, A. T. Florence, Chapman & Hall, London and New York, 1983.
[16]R. Aveyard, B. P. Binks, P. D. I. Fletcher, Langmuir, 1989, 5, 1210.

change involved in the dispersion process[17]. As discussed previously it is observed that the interfacial tension remains constant at concentrations above the cμc, and since the entropy contribution from dispersion is expected to be dependent on the surfactant concentration, it is assumed that this contribution must be small. The bending energy contribution is therefore expected to be the dominant factor. The energy required to bend a unit area of surface is given by[18]:

$$W_{bend} = K_b/2\ (1/r_1 + 1/r_2 - 2/r_0)^2 + K_e/r_1r_2 \qquad (1.4e)$$

where r_1 and r_2 are the principal radii of curvature, r_0 is the spontaneous radius which describes the tendency of the monolayer to curve toward either the oil (i.e. r_0 is positive) or the water (r_0 is negative), K_b is the bending rigidity constant, and K_e the elastic constant of Gaussian curvature. (Note that this model ignores any entropy contributions).

The radius (r) of the aggregates formed can be approximately related to the interfacial tension above the cμc by equation 1.4f[19]:

$$r^2 \sim (2K_b + K_e)/\gamma_c \qquad (1.4f)$$

Large droplets are therefore expected to be formed only when the interfacial tension is ultra low.

1.5 The behaviour of single phase oil-in-water microemulsions stabilised by nonionic surfactants of the C_nE_m type.

For a particular composition of surfactant, oil and water (i.e. R value) within a well defined temperature range, the dispersed phase can be fully solubilised within the microemulsion droplets thus forming a single phase (1ϕ). A schematic representation of the 1ϕ region for an O/W system stabilised by a nonionic surfactant is given in Figure 1.5.1. For an O/W system the lower temperature phase boundary corresponds to the separation of excess oil, and is termed the solubilisation phase boundary (SPB).

---

[17]M. E. Cates, D. Andelman, S. A. Safran, D. Roux, Langmuir, 1988, 4, 802.
[18]W. Helfrich, W. Harbich, 1987, in "Physics of Amphiphilic Layers", Eds. J. Meunier, D. Langevin, N. Boccara, Berlin, Heidelberg, New York.
[19]B. P. Binks, J. Meunier, O. Abillon, D. Langevin, Langmuir, 1989, 5, 415.

The upper temperature phase boundary (UTPB) corresponds to the separation of a surfactant rich phase.

Figure 1.5.1

A schematic representation of the single phase region for an O/W microemulsion stabilised by nonionic surfactant.

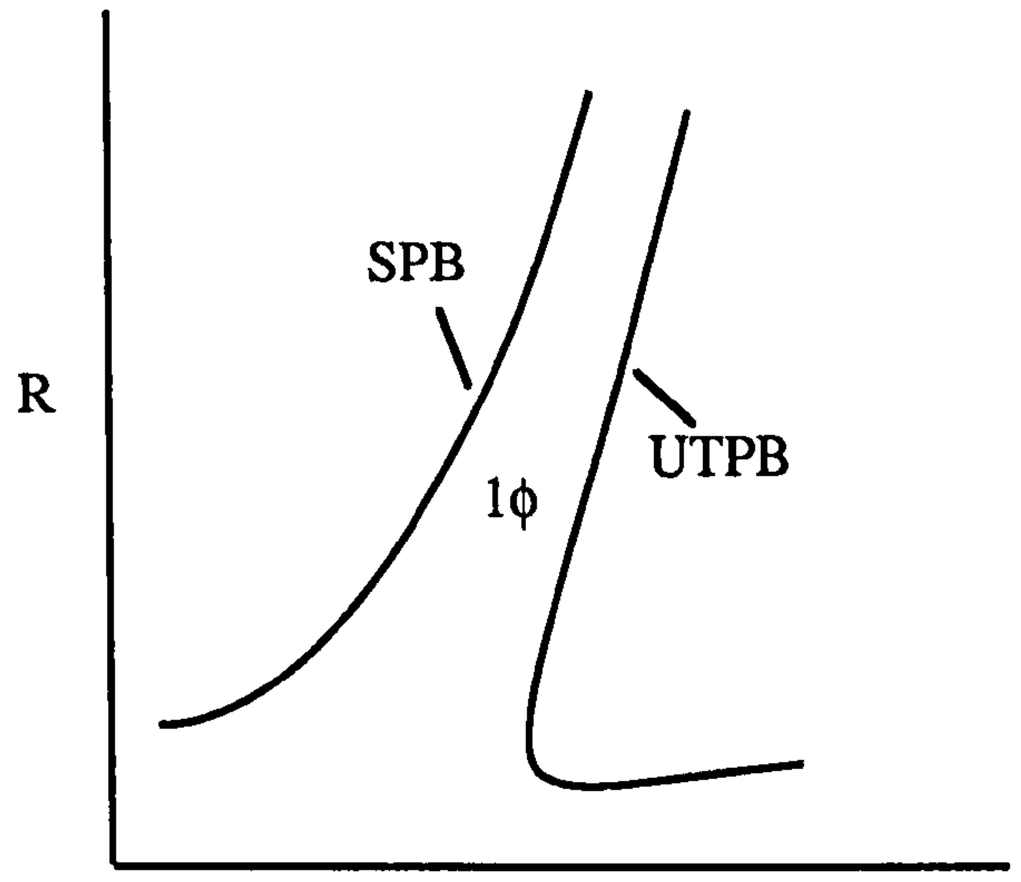

Microemulsion droplet sizes are very small with diameters of the order of 5 - 100 nm, the single phase microemulsion region therefore scatters light only weakly and appears transparent for smaller droplets, and slightly bluish for larger droplets. At the SPB the droplets are at their preferred curvature, where inter-droplet interactions are at a minimum[16,20], and the droplets thus behave as weakly interacting spheres. It can be observed that increasing the temperature from the SPB causes the solution to scatter more light (manifested in the solution becoming more turbid). The increase in light scattering indicates that increasing the temperature causes the formation of larger particles. This is consistent with the aggregates either clustering or growing, which proceeds until a temperature is reached at which phase separation occurs (i.e. the UTPB).

The question of whether clustering or growth occurs as temperature is increased across the 1ϕ O/W region is not fully resolved. Separation at the UTPB into an L_α

---

[20]J. Kizling, P. Stenius, J. Colloid Int. Sci., 1987, 118, 2, 482.

phase with excess water would indicate that growth of the droplets has occurred. Microemulsion droplets grow by becoming non-spherical forming rod or disc shapes which may form L_α phases on packing together (similarly to micelles in the binary surfactant/water system section 1.2). Separation into drop-rich and drop-poor phases with no L_α phase observed indicates that clustering of droplets of the original preferred size has occurred. The diagram of the phase behaviour of $C_{12}E_5$ with decane at a fixed R value of 2.64, with increasing temperature and droplet volume fraction is given in Figure 1.5.2, reproduced from work by Olsson and Wennerström [21]. Above the UTPB of the single O/W microemulsion phase region (denoted L in this diagram) there is a narrow temperature range between approximately 30 and 31°C where the nature of the phase is uncertain. This may correspond to a " cloud point" separation where droplet rich and droplet poor phases separates, suggesting clustering of droplets has occurred. On increasing the temperature above this region an L_α phase separates out in equilibrium with excess water (L_α + W) (spherical droplets may eventually form L_α on close packing). Further increases in temperature lead to a pure L_α phase. The progression of phase boundaries with increasing temperature from the L_α phase is the reverse of those already discussed, leading to the single phase W/O microemulsion (L_3), then the two phase L_3 plus excess water system (L_3 + W). This diagram also clearly shows that the position of the SPB and the UTPB of the L region are unaffected by the droplet volume fraction up to values approaching 0.4.

The phase diagram for an approximately constant concentration of $C_{12}E_5$ (15 - 18 wt.%) with varying wt.% of tetradecane (i.e. R value) is given in Figure 1.5.3[7]. The phase variation with temperature on the water rich side of the diagram shows a similar phase progression as that discussed above for $C_{12}E_5$ with decane, from the 1ϕ O/W microemulsion through an L_α phase to the 1ϕ W/O microemulsion . The $C_{12}E_5$/tetradecane system also shows a temperature "gap" (approximately in the range 35 - 40°C) between the 1ϕ region and the L_α phase, where the nature of the phase is uncertain. K. Suhlung[22] also observed a 2ϕ region with no L_α phase on increasing the temperature above the UTPB of the 1ϕ O/W region for the same system, between a concentration range of 0.04 and 0.12 M for $C_{12}E_5$ at R = 1.86.

---

[21]U. Olsson, H. Wennerström, Adv. in Colloid and Int. Sci. 1994, 49, 113.
[22]K. Suhlung, unpublished work, Hull University, 1995.

Figure 1.5.2

The variation in oil/water (D_2O)/surfactant phase behaviour with temperature and droplet volume fraction (Φ) for a fixed surfactant:oil ratio of 0.815 (equivalent to an R value of 2.64) for $C_{12}E_5$ with decane. Reproduced from reference 14.

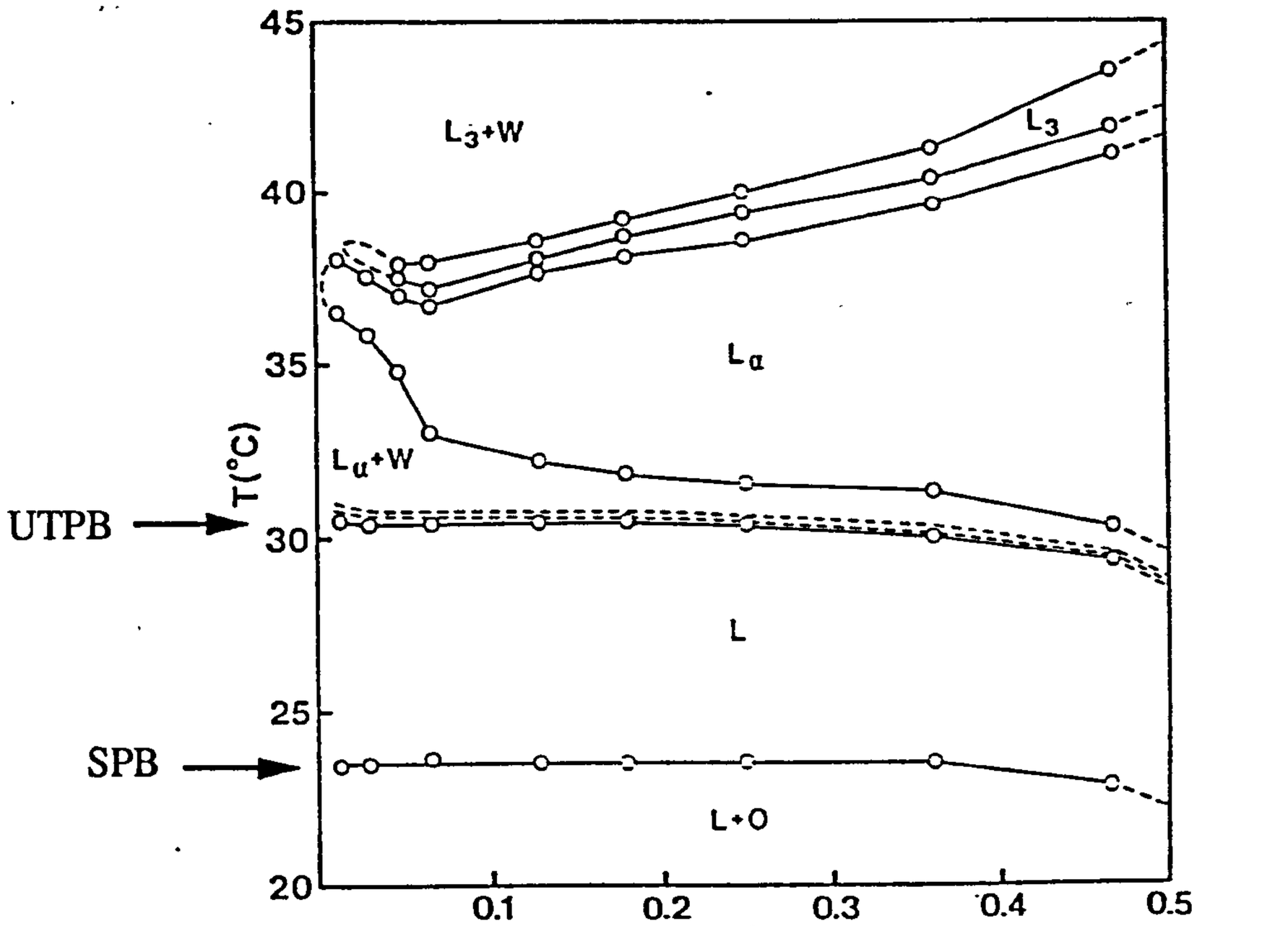

Figure 1.5.3

The variation in oil/water/surfactant phase behaviour with temperature and wt.% tetradecane at an approximately constant concentration of $C_{12}E_5$ (15 - 18 wt.%), indicating the temperature phase "gap" (see text). Reproduced from reference 7.

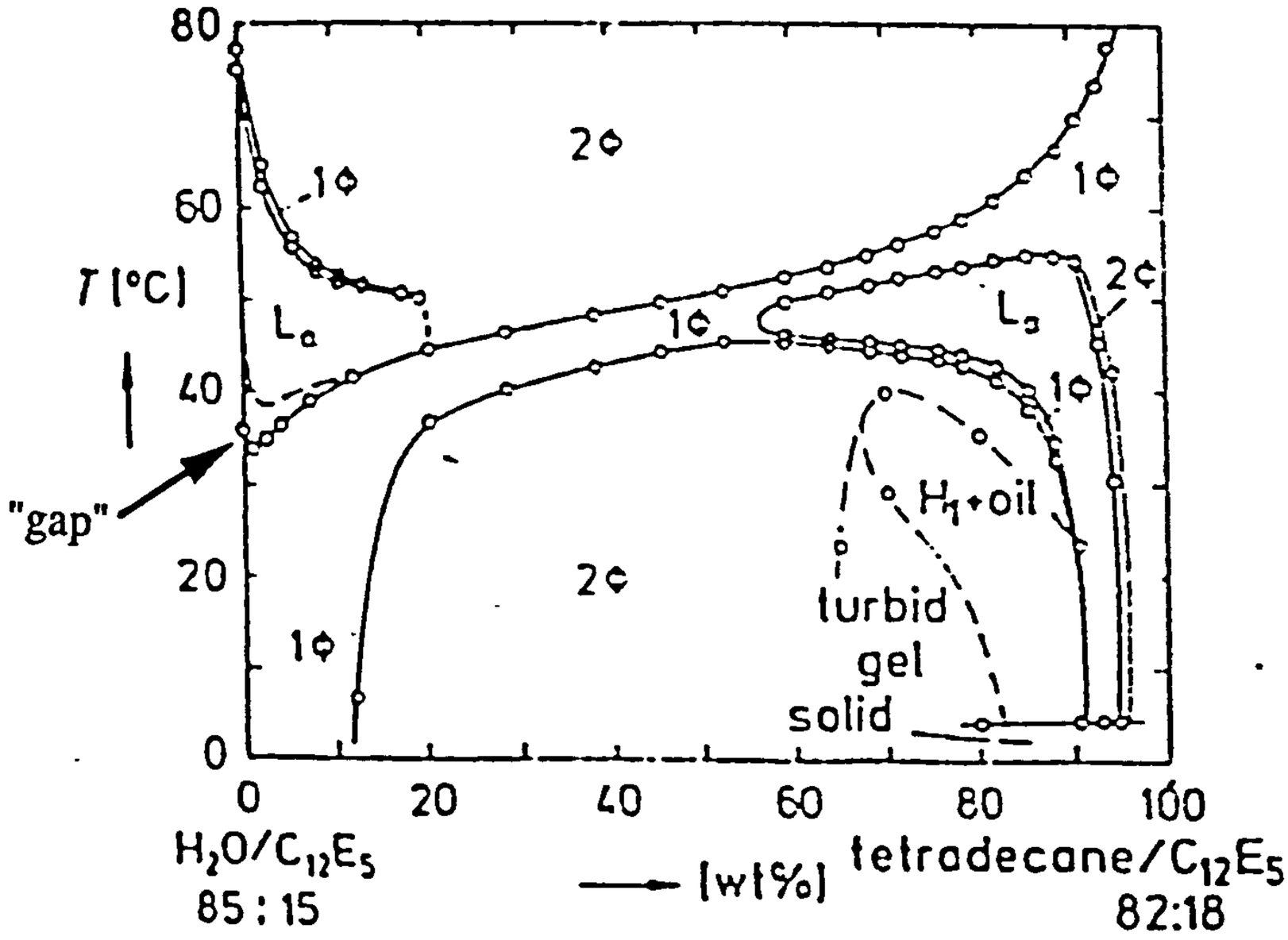

1.6 Microemulsion droplet kinetics.

Much of the interest in surfactant/oil/water systems is in the kinetically stabilised structures of emulsions and foams, but there has been little study into their kinetic behaviour. Emulsions are dispersions of oil in water, or water in oil, stabilised by surfactants, and differ from microemulsions in that they are not thermodynamically stable, and the droplet sizes are much larger, of the order of μm compared with the nm sized microemulsion droplets. Emulsions are therefore often termed *macro*emulsions, and their behaviour is related to that of microemulsions, which are easier to study.

Previous work[23-28] using probe molecules in, for example, stopped flow, and time resolved fluorescence (TRF) techniques have shown that microemulsion droplets exchange components in a rapid dynamic equilibrium. The overall process has been postulated as follows. Two droplets approach each other and form a non-coalesced encounter pair, coalescence of the encounter pair may then occur and form a short lived droplet dimer of indeterminate shape, reseparation then occurs into two separate droplets (Figure 1.6.1).

Figure 1.6.1

A schematic representation of the coalescence of two droplets to form a short lived droplet dimer.

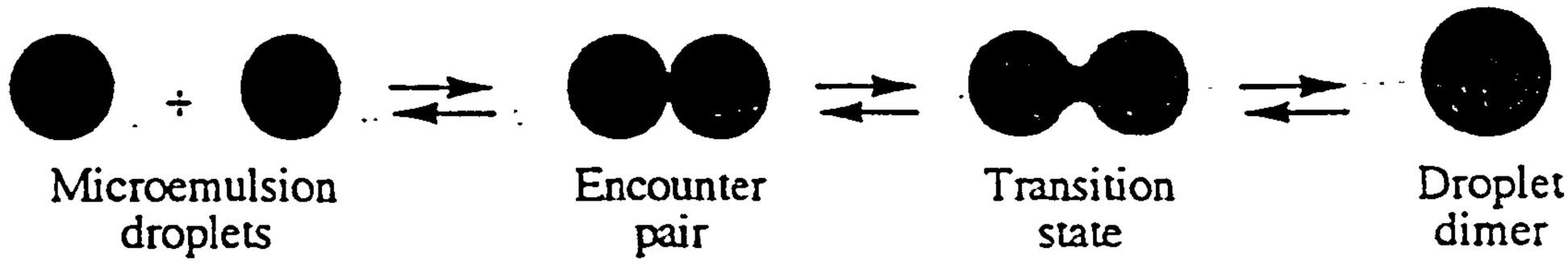

---

[23]S. Clark, P. D. I. Fletcher, X. Ye, Langmuir, 1990, 6, 1301.
[24]H. F. Eicke, J. C. W. Shepherd, A. J. Steinman, J. Colloid & Int. Sci. 1976, 56, 168.
[25]S. S. Atik, J. K. Thomas, J. Amer. Chem. Soc. 1981, 103, 3543.
[26]P. D. I. Fletcher, A. M. . Howe, B. H. Robinson, J. Chem. Soc. Faraday Trans. 1987, 1, 83, 985.
[27]P. D. I. Fletcher, D. Parrott, In "Chemical and Biological Reactions in Compartmentalised Liquids", Eds. W. Knoche, R. Schomacker, Springer-Verlag, Berlin, 1989.
[28]A. S. Bommarius, J. F. Holzwarth, D. I. C. Wang, T. A. Hatton, J. Phys. Chem. 1990, 94, 7232.

The exchange of components may therefore take place either between the encounter pair, by passage of components through the area of compression of the surfactant monolayers at the collision point, or through the redistribution of components in a droplet dimer. Fletcher *et al*[26], deduced that in the W/O microemulsions of AOT/heptane/water system the exchange is most likely to occur within a coalesced droplet-dimer, since the exchange rate for different species of probe molecules was found to be independent of species type, whereas exchange through the surfactant bilayer of an encounter pair would be expected to be highly species dependent. Further support for this process is given through the observation that mixing microemulsions of large and small droplets results, over a period of a few seconds, in a microemulsion of intermediate sized droplets, which reorganisation would appear to be unlikely to occur via a non-coalesced encounter pair. Work by Fletcher *et al* [29] on the rate of formation of the droplet encounter pair, (clustering) measured by a temperature jump method for the $C_{12}E_5$/tetradecane O/W system, yields a value for this initial rate constant to be of the order of 10^7 $M^{-1}s^{-1}$. The coalescence exchange rate constant for the same system measured by TRF[16] was found to be of the order of 10^9 $M^{-1}s^{-1}$.

The different measurements of the rates of droplet encounter pair, and probe exchange cited above, both showed that the rates were much slower near to the SPB, and therefore that there is an energy barrier to the processes. Contributions by various factors are expected to affect the rate:

(i) the energy concerned with the approach of the droplets,
(ii) the preferred curvature of the surfactant monolayer,
(iii) the energy required to bend the surfactant monolayer,
(iv) the energy required to desorb surfactant from the droplet surface, thus allowing exchange of contents.

Chapter six in this thesis investigates the effect on the rate of the encounter pair formation (clustering of two droplets) in the single phase O/W microemulsion regions of a homologous series of C_nE_m surfactants and alkane oils.

---

[29] P. D. I. Fletcher, J. F. Holzwarth, J. Phys. chem. 1991, 95, 2550.

1.7 Presentation of the thesis.

The aim of the work in this thesis was to characterise the behaviour of the single phase alkane(x)-in-water microemulsions stabilised by the nonionic C_nE_m surfactants, with a view to establishing the effect of the different constituents, x, n, and m. The same homologous series of systems varying in n, m and x were therefore studied throughout the work.

Chapter two describes the experimental techniques employed. Chapter three establishes the phase behaviour with temperature, in particular the position of the SPB. Chapter four describes the determination of microemulsion droplet sizes using light scattering techniques (turbidity and PCS), and from this the area occupied per surfactant molecule at the droplet core/surfactant monolayer interface is calculated and compared for the different systems. Turbidity data are used in chapter five to determine the equilibrium constant and the thermodynamic changes (ΔG^o, ΔH^o, and ΔS^o) occurring as temperature is increased over the 1ϕ region. Chapter six describes the use of a temperature jump technique to study the kinetics of the clustering/growth behaviour of microemulsion droplets in the 1ϕ region. The forward and reverse rate constants are obtained for the clustering/growth process, and from this the associated activation energies. Finally chapter 7 summarises the main conclusions of the thesis.

CHAPTER TWO

2 Experimental methods and materials

2.1 Materials

Table 2.1*a* summarises the source and purity of materials used. Water was purified by passage through an Elga Prima reverse osmosis unit followed by a Milli-Q reagent water system. The surface tension of the water was 71.9 mN/m at 25°C, in agreement with the best literature values[1]. Surfactants were used as supplied without further purification. All oils were passed twice over aluminium oxide (BDH chromatographic grade) to remove any polar impurities prior to use.

Table 2.1*a* Materials used

Chemical	Source	Purity
C_8E_5	Bachem	>98%
$C_{10}E_5$	Nikkol	98%
$C_{12}E_4$	Nikkol	98%
$C_{12}E_5$	Nikkol	98%
$C_{12}E_6$	Nikkol	98%
$C_{12}E_7$	Nikkol	98%
$C_{14}E_5$	Nikkol	98%
$C_{14}E_7$	Nikkol	98%
n-Heptane	Merck	>99%
n-Decane	Fluka	>98%
n-Tetradecane	Fluka	>99%

The purity of the surfactants were tested by determination of the cloud point (discussed in section 1.2.3) of a 1 weight % solution of the surfactant in water. The results are tabulated in table 2.1*b*, and were found to be in good agreement with literature data.

---

[1]J. Timmermans, "Physical Constants of Pure Organic Compounds", Elsevier, New York, 1950.

Table 2.1*b* Surfactant cloud point (°C) data.

	This Work	Literature Values	
Surfactant	Cloud Point (1 wt. %)	Cloud Point	Wt %
C_8E_5	not determined	63.6[2]	1.0
		63.6[3]	1.0
$C_{10}E_5$	44.7 ± 0.2	45.0[4]	1.0
$C_{12}E_4$	6.7 ± 0.1	7.0[5]	0.5
		6.6[2]	1.0
$C_{12}E_5$	31.6 ± 0.1	31.5[4]	1.0
		31.4[5]	1.0
		31.7[2]	1.0
$C_{12}E_6$	52.6 ± 0.2	52.5[4]	1.0
		52.5[5]	1.0
		50.8[2]	1.0
$C_{12}E_7$	61.7 ± 0.1	65.0[4]	1.0
		62.0[6]	unspecified
$C_{14}E_5$	24.0 ± 0.1	No literature data available	
$C_{14}E_7$	58.6 ± 0.1	58.7[4]	1.0
		58.2[7]	1.0

2.2 Methods

2.2.1 Preparation of Oil-in-water Microemulsions

The surfactant was first dissolved in a little water. Oil was then added to produce the [oil]/[surfactant] ratio required, and the system made up to the mark with water. The microemulsion phase is in some cases very slow to form, especially for the longer chain surfactants, since it appears that liquid crystalline phases are formed on initial

---

[2]K. V. Schubert, R. Strey, M. Kahlweit, J. Coll. & Int. Sci, 1991, 141, 21-29.
[3]J. R. MacNab, Hull University, Unpublished data.
[4]Nikkol Catalogue.
[5]R. Aveyard, T. Lawless, J. Chem. Soc. Faraday Trans. 1, 1986, 83, 2951-2963.
[6]A. W. Rosen, M. J. Rosen, J. Am. Oil. Chem. Soc. 1981, 58, 1062.
[7]M. Corti, C. Minero, V. Degiorgio, J. Phys. Chem.,1984, 88, 309.

mixing at room temperature. For this reason the system was heated to a temperature above the UTPB, with a little gentle shaking to melt any liquid crystal phases present, then cooled to the single phase microemulsion temperature region.

2.2.2 Photon Correlation Spectroscopy (PCS)

The PCS apparatus used for this work, shown schematically in figure 2.2.2*a*, consisted of the following components. The one phase microemulsion samples were contained in a 10 mm path length stoppered Hellma Quartz type 6110-blue cuvette, and were positioned in a thermostatted Malvern Instruments (PCS 100SM) goniometer. The temperature was regulated to a precision of 0.1 ^{o}C using a combination of a Malvern temperature controller (PCS 8) and an external Grant water circulating thermostat. A Spectra-Physics 15mW He-Ne laser (λ=632) illuminated the sample and scattering was collected at 90^{o} to the laser beam by a Malvern photomultiplier. Intensity variations were analysed using a Malvern digital correlator, model K7072 and the autocorrelation function (described in chapter 4) displayed on the screen of the incorporated Commodore Pet computer. A hard copy of the results was obtained through the use of an on-line Taxan/Kaga KP-210 printer (exact Epson FX-80 emulator).

During the work described in this thesis the PCS apparatus was updated, and the following changes made:

(i) The He-Ne laser was replaced with a Cyonics Uniphase Argon Ion 75mW (λ=488nm) model 2213-75SLYV, including a remote interface controlling unit;
(ii) The Malvern K7072 correlator was replaced with a Malvern 7032 Multi-8 correlator;
(iii) The computer was replaced with an NEC Powermate SX/16i, incorporating the new PCS Software for Windows (1992 version).

Microemulsion droplet sizes measured using the updated PCS apparatus were found to be in good agreement with those obtained using the old system, (see table 2.2.2). All droplet sizes for decane-in-water microemulsions stabilised by $C_{12}E_7$ were measured using only the updated PCS.

Figure 2.2.2*a* Schematic diagram of the photon correlation spectrometer apparatus. P. M. is the photomultiplier.

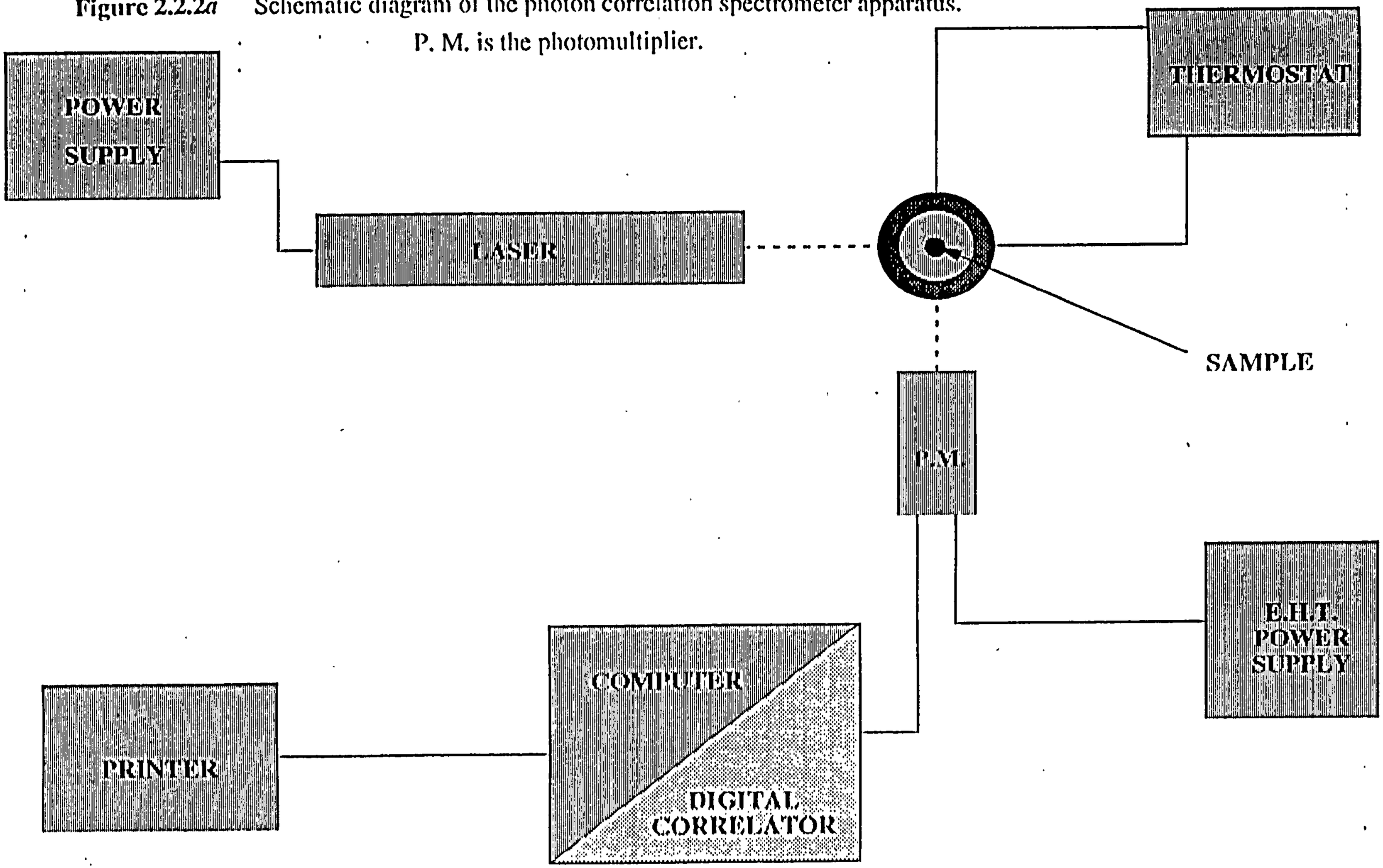

Figure 2.2.2*b*

Typical PCS correlogram trace obtained for 0.01 M $C_{12}E_7$ with decane at R = 3.70.

C12E7/C10/R=3.70
Laser=70.3
Apperture=50
File data from A:\BC12E7.SIZ Record 1
S4700

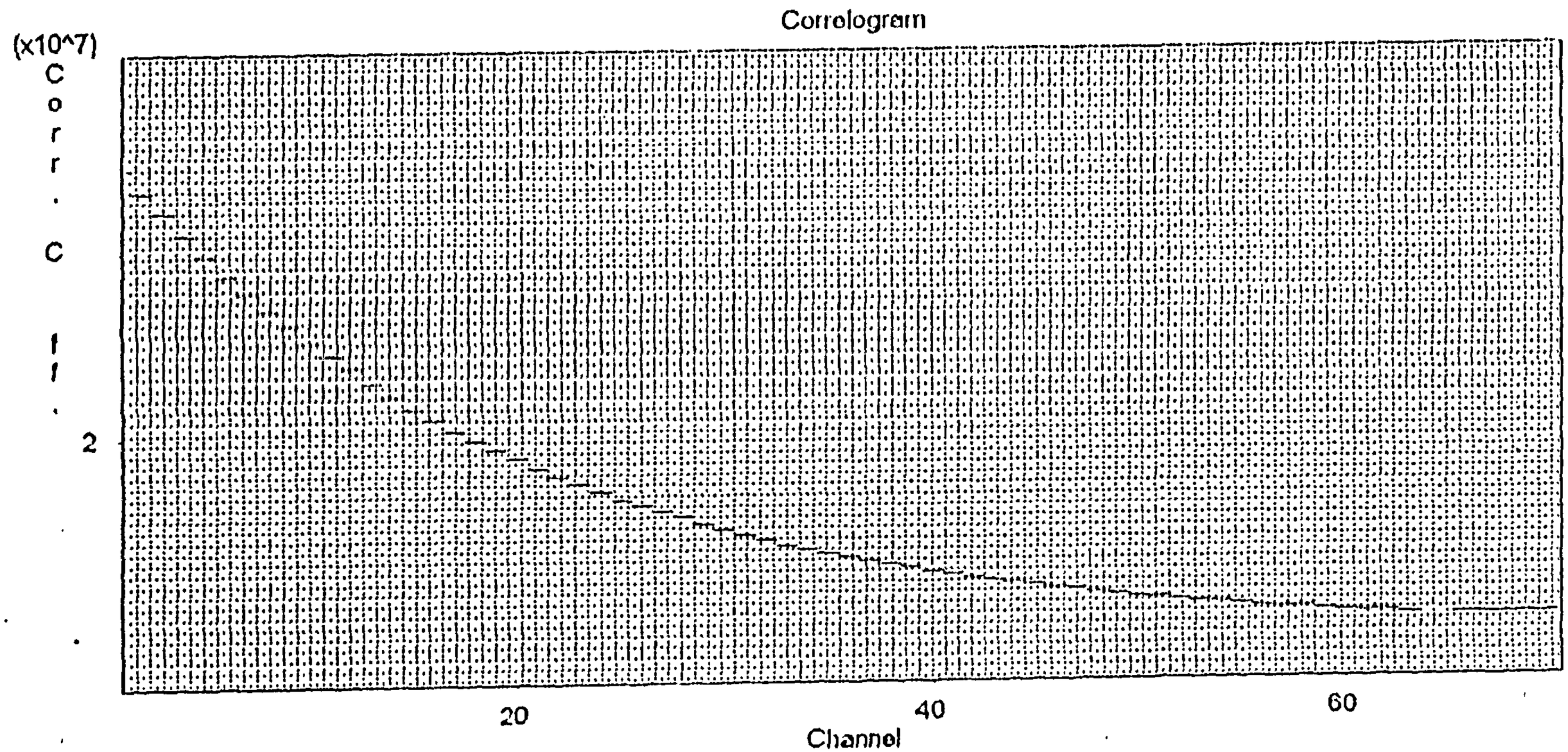

RecAngle	KCps	ZAve	Poly	Fit Error	Time	Function	Analysis	File	Title
1 90.0	527.7	21.6	0.003	0.00080	17:40:31	Data	Monomodal	BC12E7	C12E7/C10/R=3.70

Table 2.2.2

Comparison of the hydrodynamic radii (r_h) measured using the old and updated PCS systems. All data is by J. Morris except * from B. P. Binks, PhD thesis, Hull University, 1986, p. 79.

	r_h (nm)		
Microemulsion system	Old PCS	Updated PCS	% Difference
5 mM AOT / heptane, R_{water}=51.1	10.3*	10.6	3%
$C_{10}E_5$ / decane, R=3.12	11.3	11.1	1%
$C_{12}E_4$ / decane, R=2.89	10.2	10.6	4%
$C_{12}E_5$ / heptane, R=11.6	24.5	23.5	4%

Samples were thermostatted within the PCS for a minimum of 15 minutes prior to the measurement to allow pre-equilibrium to the selected temperature. Each size measurement involved collecting data from successive experimental periods ("bursts") of 1 second duration. To avoid any scattering due to dust affecting the autocorrelation function, a rejection algorithm was implemented. For each "burst", the routine calculated the normalised, time-averaged value of the measured scattered intensity from the total count of the scattered photons collected in that "burst". This value was compared with the average value calculated from the intensity at very long times (compared to the period of the fluctuations) as determined through the use of four delay channels. If the maximum fractional difference between these two values was outside a set value, the data of that "burst" was rejected. Otherwise, the data was collected and averaged.

A typical correlogram obtained for a microemulsion sample is shown in figure 2.2.2*b* (from the updated PCS).

2.2.3 Turbidity

Turbidities were measured as absorbances using a UV/VIS spectrophotometer. Turbidity is related to absorbance by equation 2.2.3, where l is the path length and = 1cm in this work.

$$\tau l = 2.303 \text{ Absorbance} \qquad (2.2.3)$$

The absorbance results presented in chapters 3-5 were measured using a Perkin-Elmer Spectrophotometer 550 thermostatted by a Grant LTD 6 circulating thermostat. Polystyrene covers were placed over each cell and holder, to minimise temperature gradients occurring in the sample. The absorbance readings versus time were recorded using a Chessel chart recorder to enable the determination of the equilibrium i.e. time independent, reading. Turbidities for the kinetic study (chapter 6) were measured using a Shimadzu UV-2100 spectrophotometer.

For all turbidity measurements matched Hellma Quartz measuring cells, type 6110-Blue, of 10mm path length were used. The reference cell contained Milli-Q water and a thermocouple for direct temperature determination. The thermocouple was calibrated using a mercury thermometer (accurate to within $0.1^{o}C$) and the readings corrected accordingly. The measuring cell was rinsed, filled with the sample, and stoppered. To allow for any difference between the cells, the absorbance reading when both cells were filled with Milli-Q water was noted at the beginning and end of each experiment and the sample readings adjusted accordingly.

A steady absorbance reading for the microemulsion could also imply that the microemulsion had phase separated, i.e. that it had been equilibrated at a temperature either below the SPB or above the UTPB. To ascertain if phase separation had occurred, the sample was inspected visually and gently shaken immediately after each measurement and the absorbance re-read. Lack of phase separation was clearly indicated if the absorbance value after shaking was found to be the same as that before.

2.2.4 Iodine Laser Temperature Jump (ILTJ)

Relaxation methods for the study of fast reactions or processes depend on the ability to alter one physical condition of the system, such as pressure, electric field or temperature, virtually instantaneously, and to monitor the relaxation of the sample to the resulting new equilibrium position. Most chemical processes show a variation with temperature, and thus the temperature jump (T-jump) method is one of the most useful ways of investigating fast reactions.

In the microemulsion systems studied in this thesis the increase in turbidity caused by increasing temperature, (as described in chapter 4), has been used in a T-jump method using an iodine laser as the energy source. The iodine laser has been shown[8] to provide the most useful heating source for performing T-jump experiments in aqueous solutions as it provides simple direct homogeneous heating with no requirement for addition of electrolyte, and no side effects such as transient electric fields or shockwaves experienced from Joule heating and pressure jump methods respectively. At the wavelength at which the iodine laser operates, 1.315 μm, the absorption coefficient of water is close to 1 cm^{-1} allowing a water layer of 2 by 10 mm to be heated by approximately one degree on application of a laser pulse of a few joules energy. Longer wavelengths are absorbed more strongly by water and result in inhomogeneous heating of the sample. Shorter wavelengths are only weakly absorbed and would require higher power lasers. The ILTJ technique used in this work was developed by Professor Josef Holzwarth at the Fritz-Haber Institut der Max Planck Gesellschaft Berlin [9].

The iodine laser was first mentioned by Kasper and Pimental [10]and operates by flashing perfluoroisopropyliodide (i-C_3F_7I) with UV-light, resulting in electronically excited iodine atoms whose stimulated emission produces laser pulses at 1.315μm with a photoenergy of 0.94eV.

$$C_3F_7I + hw_{uv} \rightarrow C_3F_7 + I^* \qquad \text{(excitation)}$$

$$I^* \rightarrow I + hw_{laser} \qquad \text{(laser action)}$$

The iodine laser system is shown schematically in figure 2.2.4*a*. Linear xenon flash lamps are situated inside an aluminium reflector around the laser tube. The laser tube is filled with pure gaseous C_3F_7I, and the pressure controlled by equilibration with a thermostat filled with liquid C_3F_7I. A low inductance capacitor charged up to 40 kV is discharged through the flash lamps by triggering the spark gap, and the resulting UV light radiates the tube exciting the C_3F_7I. Dissociation into the excited state is almost 100%, and after laser action has occurred most of the fragments recombine to reform

---

[8]J.F.Holzwarth, V. Eck and A. Genz, in "Spectroscopy and the Dynamics of Molecular Biological Systems", Academic Press. Inc. (London) Ltd. p. 351 (1985)
[9]J.F.Holzwarth, Fritz-Haber Institut der Max Planck Gesellschaft, Faradayweg 4-6, D-14195 Berlin, Germany.
[10]Kasper, J.V.V. and Pimental, G.C., Appl. Phys. Lett., 1964, 5, p.231.

Figure 2.2.4*a* The iodine laser used in T-jump experiments.

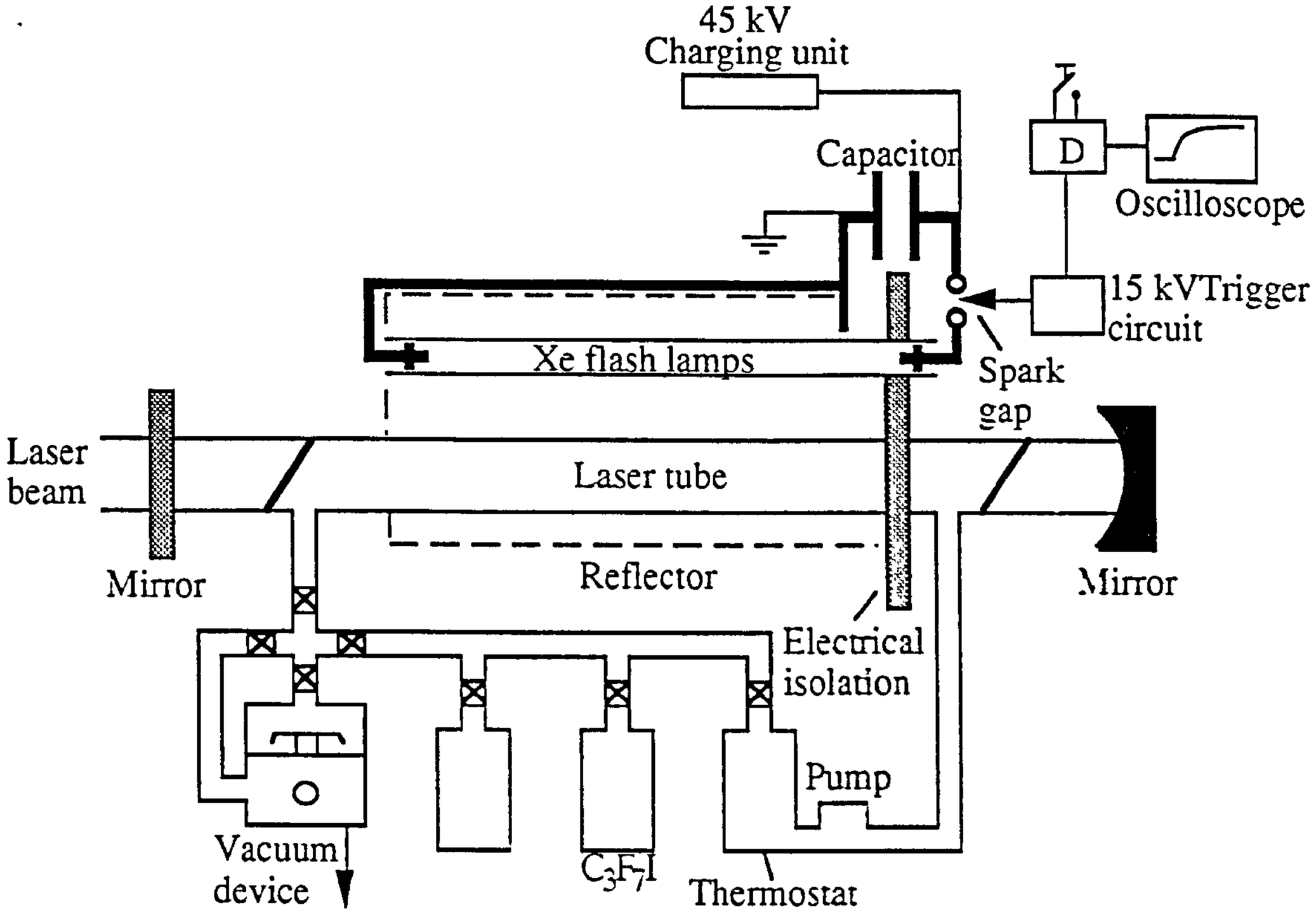

The thermostat, pump, and the vacuum device make up the gas recycling and cleaning system for the laser tube.

the laser gas. The output energy is kept constant from shot to shot by a gas recycling system which removes any remaining iodine molecules and decomposed laser gas by circulating C_3F_7I through a thermostat held at 260 K. The vacuum system allows cleaning of the laser gas circuit of oxygen. The output energy of 2 J is released in a time of 2.4 μs and shows a simple exponential decay with time.

A schematic diagram representing the whole T-jump apparatus is shown in figure 2.2.4*b*. The one phase microemulsion sample was placed in a Hellma quartz measuring cell of path length 5 mm with respect to the heating laser flash, and 10 mm with respect to the monitoring laser beam. The cell was held in position inside a metal box thermostatted by a Haake water circulator. The iodine laser pulse was triggered and directed onto the sample, passing through twice (by use of a mirror placed behind the sample) to ensure greater homogeneity of heating. The repetition rate possible for the laser flash is limited by the requirement to change the gas fill after every shot, which in practise means a maximum repeat rate of about four per minute. Typical T-jumps observed for the focusing arrangement used in this work were 0.4 - 1.0 ^{o}C. The changes in turbidity of the sample after the T-jump were detected by the use of a dual beam from a continuous wave (CW) laser at 407 nm. The split beam comprised a reference beam, and a monitoring beam passing through the sample at 90^{o} to the iodine laser flash. Figure 2.2.4*c* schematically shows the relative geometry of the laser flash, monitoring beam and sample. Turbidity changes as low as 0.005 cm^{-1} could be detected.

Figure 2.2.4*b* ILTJ apparatus

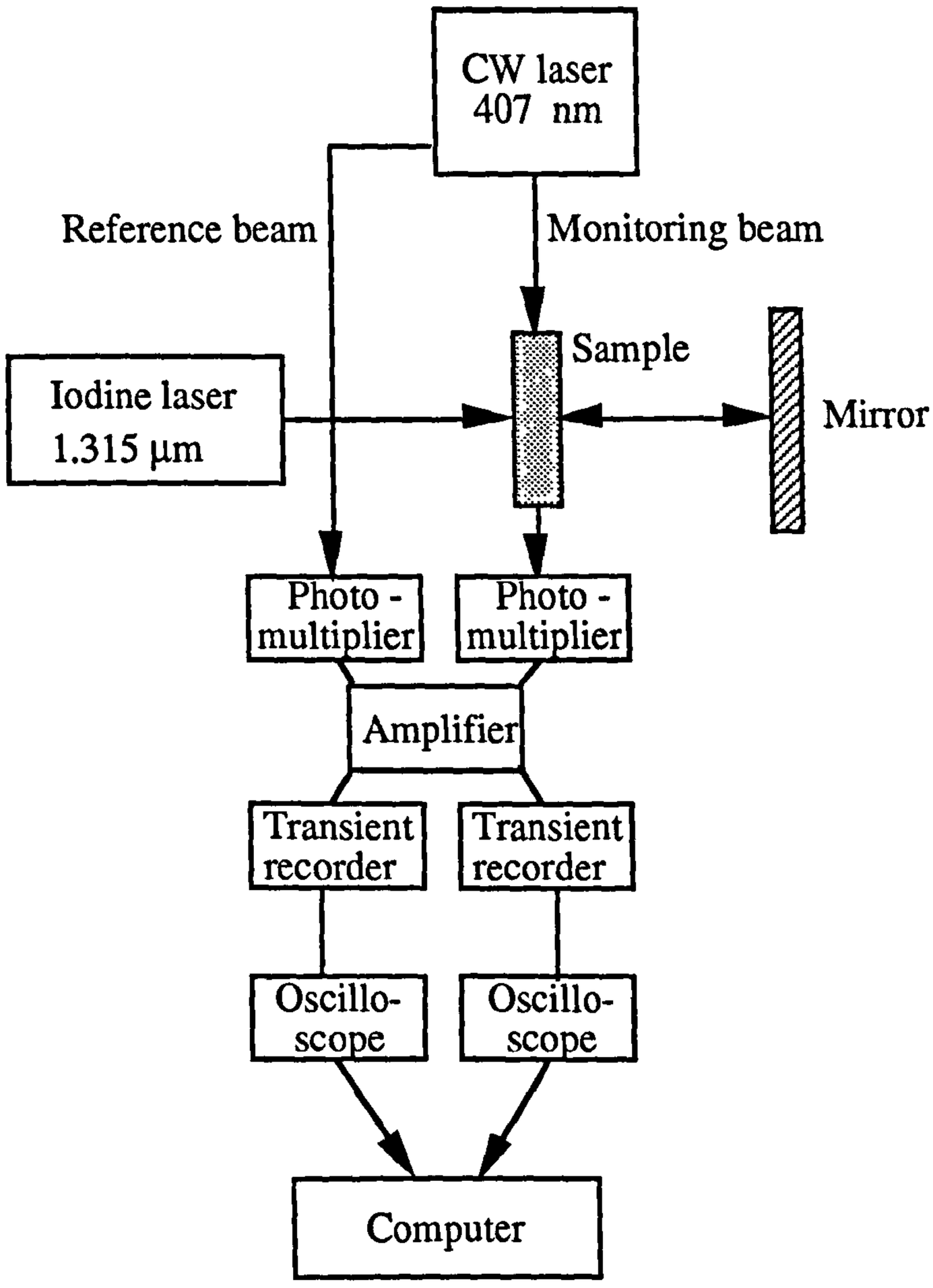

Figure 2.2.4*c*

A schematic diagram showing the alignment of the CW laser and the iodine laser beams in the sample cell. The CW monitoring laser beam passes at 90^{o} through the section of the sample heated by the iodine laser flash.

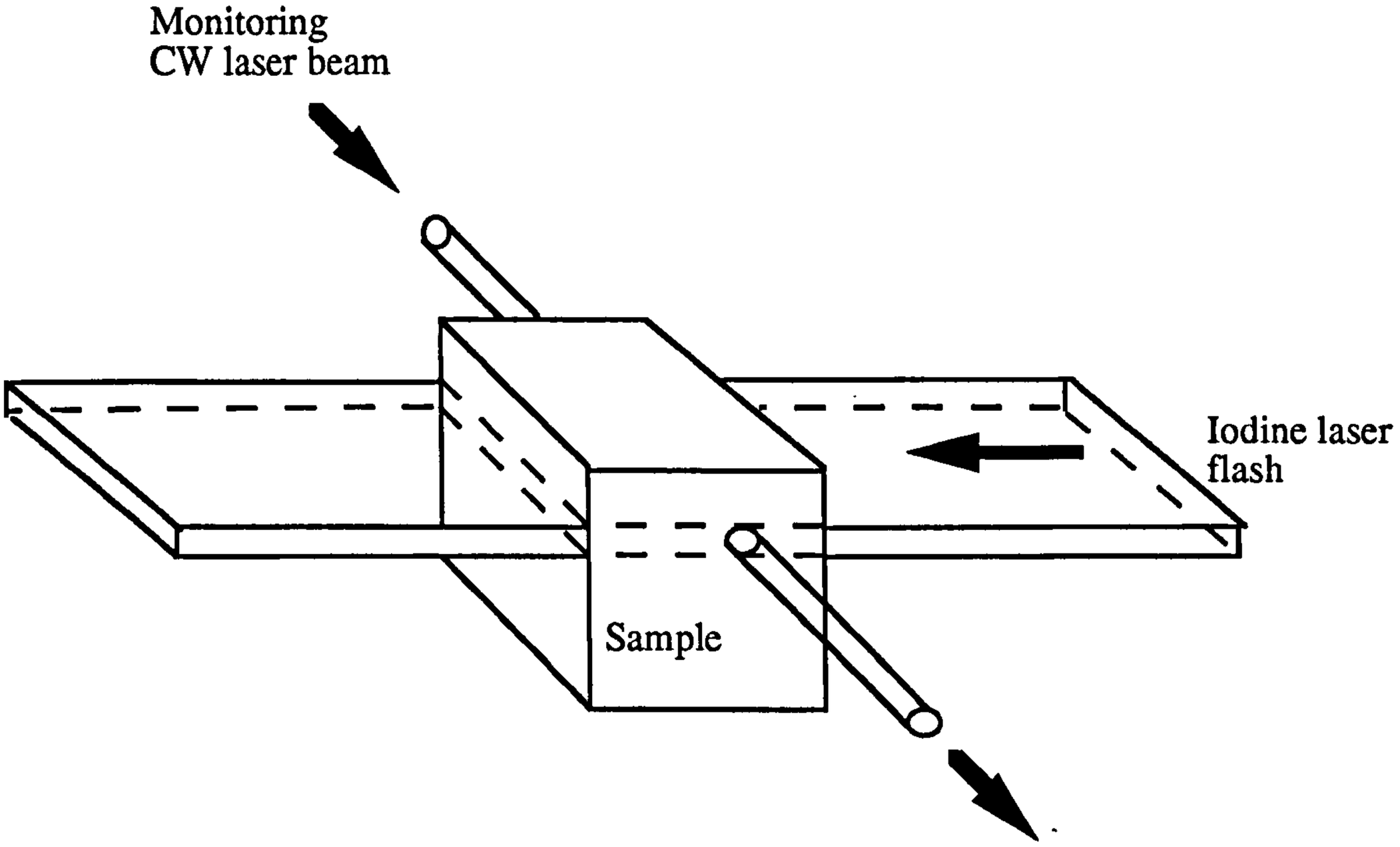

The signal from the reference beam was subtracted from the monitoring beam to correct for any fluctuations in the incident intensity of the CW laser. The resulting signal was captured using two transient recorders whose combined time ranges recorded the full progress of the signal from the initial T-jump to the cooling curve after relaxation has occurred. Four timebases were chosen. The first (t_1) was typically 68 μs to capture the initial strike of the iodine laser flash, the second and third (t_2, t_3) were a few milliseconds to enable the full turbidity relaxation curve to be recorded. The fourth (t_4) was a few seconds to capture the full cooling curve and to confirm that the turbidity of the sample returned to its original value. The cooling time was typically 2 - 4 s. A schematic representation of the four timebases recorded from the two recorders is shown in figure 2.2.4*d*. The time base which contains the full exponential trace of the T-jump was recorded, t_3 in this example, and fitted by the theoretical single exponential curve. The fastest relaxation time measurable is 1 μs. Transients with low signal to noise ratio were averaged over 2 - 10 T-jump shots before calculation to improve the

signal to noise ratio. Figure 2.2.4*e* shows the experimental signals recorded for a single shot for 0.12 M $C_{12}E_7$ with decane at R = 2.5 (2.2.4*e* (i)), and for an averaged signal for 0.01 M $C_{12}E_5$ with decane at R = 2.5 (2.2.4*e* (ii)).

Figure 2.2.4*d*

A schematic representation of the four timebases (t_1, t_2, t_3, t_4) recorded from the two transient recorders in the ILTJ experiments. Typical values are t_1 = 68ms; t_2 = 2 ms; t_3 = 4 ms; t_4 = 10 s. Timebase 1 shows the initial laser strike, t_2 the start of the relaxation curve, t_3 the full turbidity relaxation curve and t_4 the cooling curve.

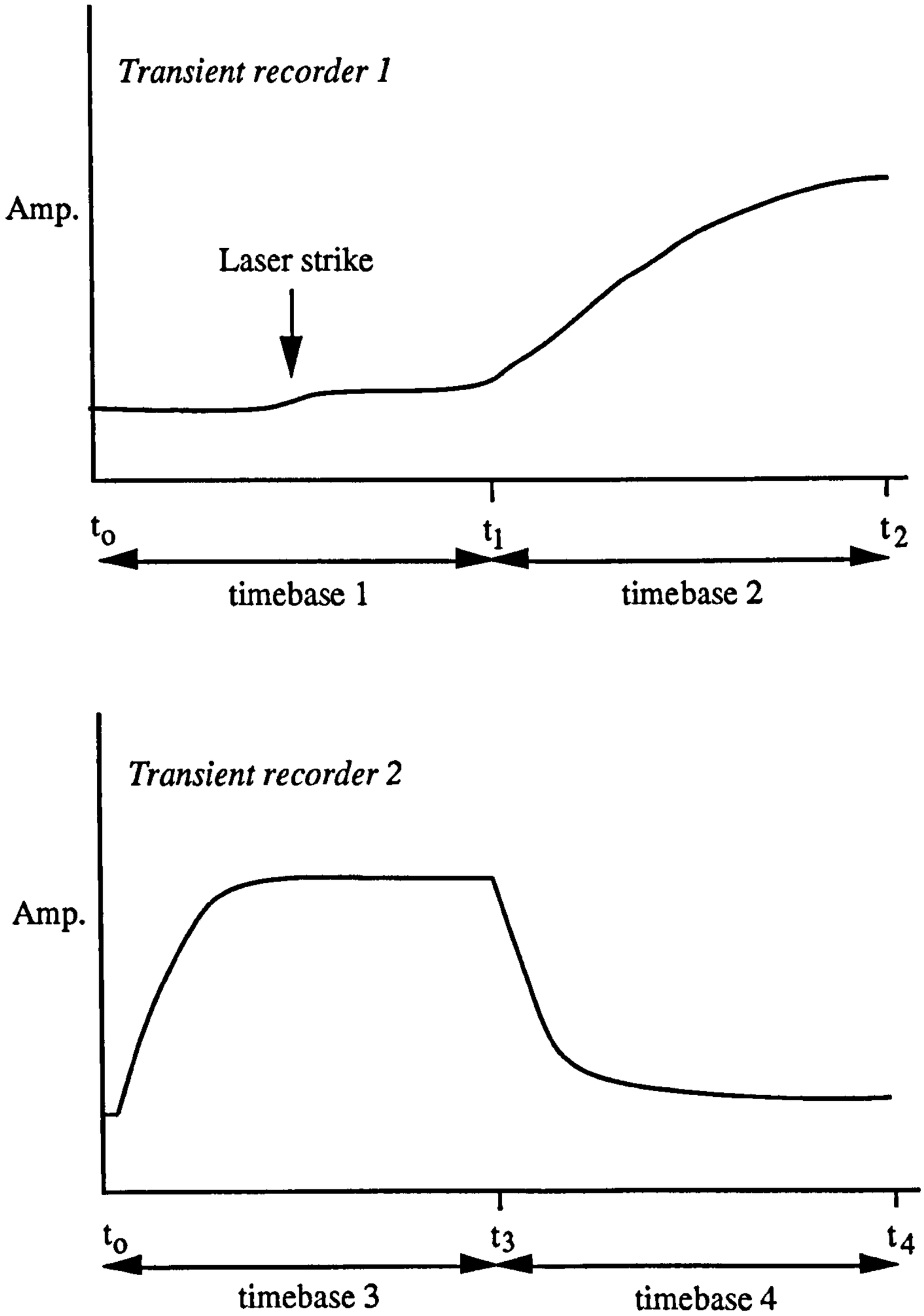

Figure 2.2.4*e*

Typical signals recorded over four timebases following a T-jump experiment.

(i) The signal obtained from a single shot for 0.12 M $C_{12}E_7$ with decane at R = 2.5.

t_1 = 68 μs; t_2 = 2 ms; t_3 = 4 ms; t_4 = 10 s.

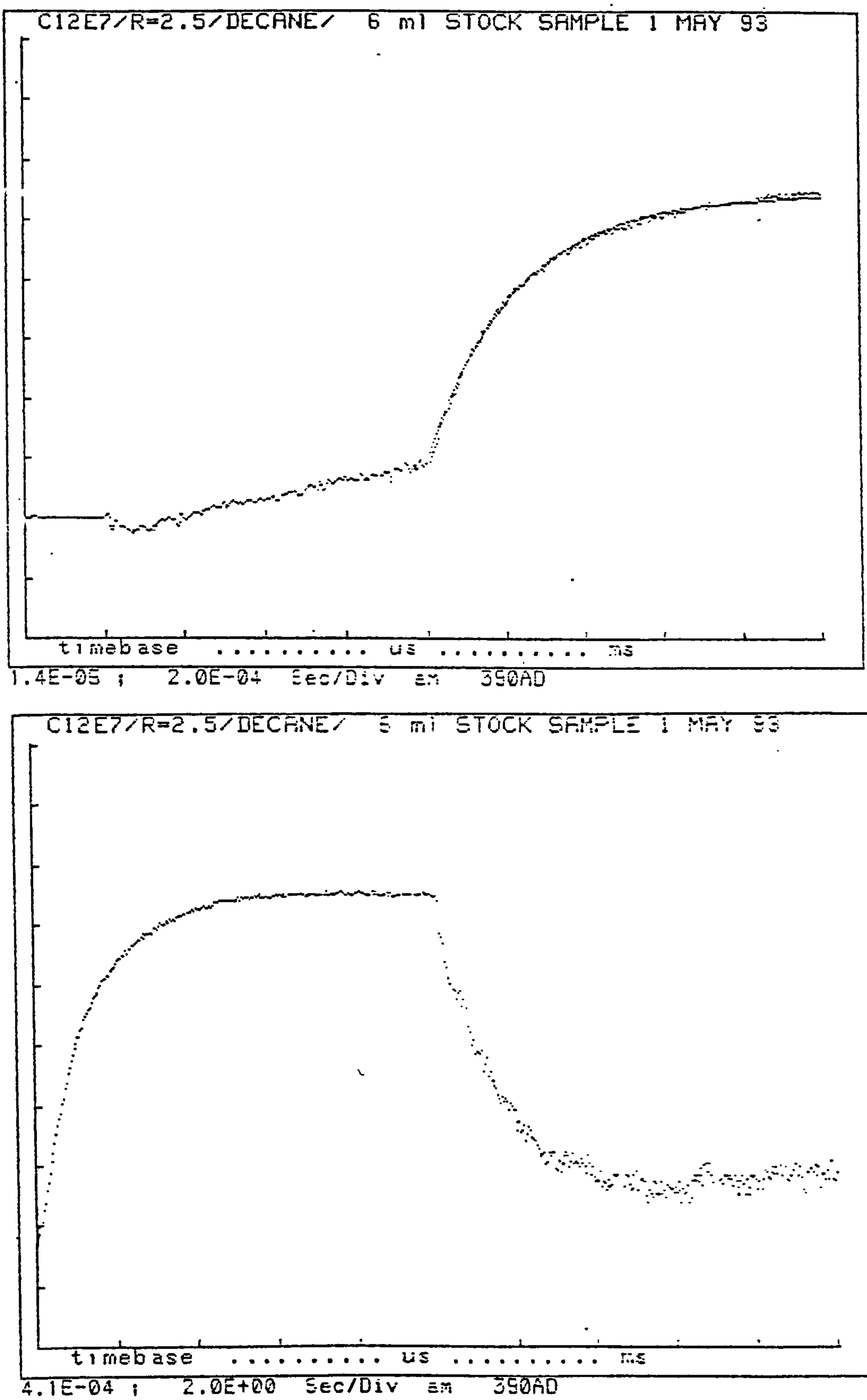

Figure 2.2.4*e*

Typical signals recorded over four timebases following a T-jump experiment.

(ii) The signal obtained from an average of 7 shots for 0.01 M $C_{12}E_5$ with decane at R = 2.5. t_1 = 68 ms; t_2 = 40 ms; t_3 = 100 ms; t_4 = 10 s.

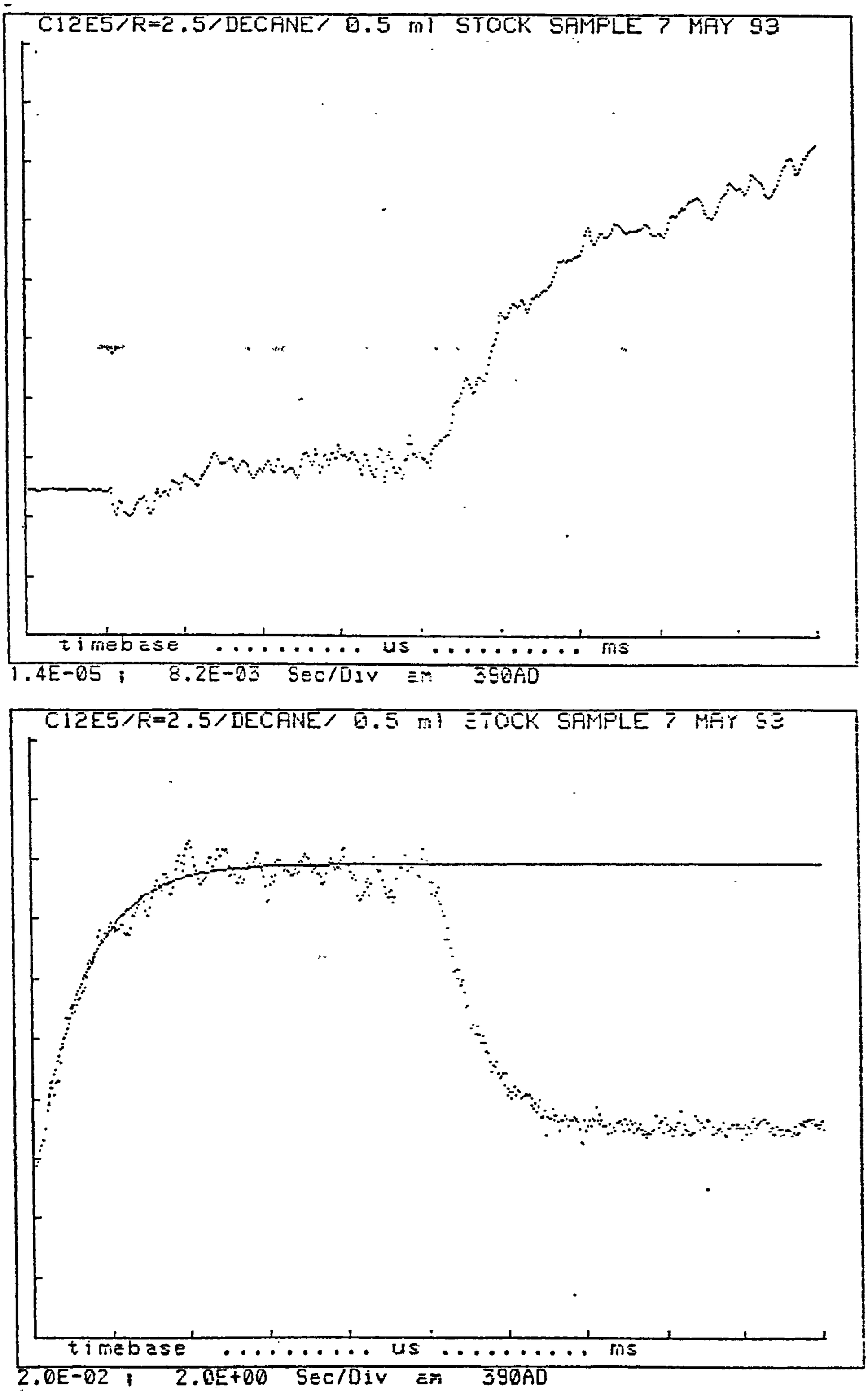

CHAPTER THREE

3. Oil-in-water microemulsion single phase domains for the C_nE_m/alkane oil/water microemulsion systems.

3.1 Introduction

Determination of the phase behaviour of the single phase (1ϕ) regions of the C_nE_m/alkane oil/water microemulsion systems are necessary before detailed kinetic studies can be made. These 1ϕ regions exist in one small corner near the water apex of the full three component phase triangle. The position of the 1ϕ region is dependent on the conditions of the system, such as the structure of the oil and surfactant, and the oil/surfactant ratio (R), and should follow the rules of preferred curvature as described in section 1.4.2. For a specific R the 1ϕ microemulsion region exists only within a limited temperature range. The lower limiting temperature of this range is that at which the surfactant is first able to completely solubilise the available oil at the so called solubilisation phase boundary (SPB), forming a transparent single phase of individual microemulsion droplets. At the upper limiting temperature of the 1ϕ region clusters of drops or larger drops begin to separate into drop rich-drop poor phases, or water + lamellar liquid crystal (L_α) phases respectively. As described later in section 4.3.2, the turbidity of a sample increases with temperature from a minimum at the SPB to a maximum at the UTPB, corresponding to clustering or growing of the microemulsion droplets, and hence these turbidity measurements have been used to determine the temperature range within which the single phase microemulsion regions exist. The temperatures shown for the SPB's are only approximate for the low R values (R = 1 or below, where R refers to the molar ratio of oil to surfactant), since in this region the turbidity often remains constant over a few ^oC, and as the turbidities were measured only to ascertain the minimum turbidity (to be used in droplet size calculations (chapter 4)). The true limiting temperature of the SPB at these lower R values is likely to be lower than that shown. Olsson *et al*[1] indicated the difficulty in determining these solubilisation phase boundaries since solubilisation and the reverse process, phase separation, are very slow (of the order of a few days) for these systems, and requires the boundary to be determined by both increasing and decreasing the temperature around the phase boundary region.

---

[1]U. Olsson, P. Schurtenberger, Langmuir, 1983, 9, 3389

3.2 Effect of the surfactant concentration on the single phase o/w microemulsion region for $C_{12}E_6$ with decane

For weakly interacting systems at low volume fractions, the amount of oil which is able to be solubilised per mole of surfactant is not expected to be affected by the surfactant concentrations used if above the cmc of surfactant in water . The cmc for C_nE_m surfactants in water is very low (of the order of 4×10^{-5} M [2]) and thus the phase boundaries measured in this work are not expected to be sensitive to the surfactant concentrations used within this work. Figure 3.2 shows that the effect on the single phase O/W microemulsion temperature phase boundaries of differing concentrations of surfactant in the $C_{12}E_6$/decane/water system is minimal, and agrees with previous work on $C_{12}E_4$ with heptane[3].

3.3 The effect of varying n, m, or x for C_nE_m surfactant with x alkane oil on the position of the 1ϕ region.

Figures 3.3(a - d) show the effects that different carbon chain length of the surfactant (n), E group length (m), overall surfactant length (where n/m = 2) and the chain length (x) of the alkane oil have on the position of the o/w microemulsion single phase region. The results compare favourably with previous work on the same or similar systems[4 -8] . Figure 3.3*a* (i) also includes PCS data for the $C_{12}E_5$ system at the SPB showing good agreement with the turbidity data. Table 3.3 summarizes the results.

The results for the varying surfactant head, tail or alkane oil chain length conform to the general behaviour of nonionic surfactant / alkane / water systems as discussed in terms of the effect of the variable on the preferred monolayer curvature (chapter 1). For an increase in the overall surfactant length where the ratio of head to tail group length remains the same, the temperature of the solubilisation phase boundary is found to be

---

[2]"Critical Micelle Concentrations of Aqueous Surfactant Systems", P. Mukerjee & K. J. Mysels, NSRDS-NBS 36, U.S. Government Printing Office, Washington D.C., 1971.
[3]D. I. Horsup, PhD thesis, University of Hull, 1991.
[4] R. Aveyard, T. A. Lawless, J. Chem. Soc. Faraday Trans. 1, 1986, 82, 2951
5 S. Friberg, I. Lapczynska, Progr. Colloid & Polymer Sci. 56, 1975, 16.
6 F. Harusawa, S. Kakamura, T. Mitsui, Colloid & Polymer Sci. 252, 1974, 613.
7 H. Kunieda, K. Shinoda, J. Dispersion Science & Technology, 3(3), 1982, 233.
8 D. Wielebinski, G. H. Findenegg, Progr. Colloid & Polymer Sci. 77, 1988, 100.

unchanged, whereas the upper temperature phase boundary is increased. The preferred curvature of the droplet formed at the SPB is dependent on the balance of the opposing forces between between the head and tail group of the surfactant, as this balance is the same for this particular surfactant series, then the temperature of the SPB is expected to be the same. On increasing the temperature, however, other factors come into effect. Increasing the temperature from the SPB causes the droplets to cluster or grow, and as seen in chapter 4, the longer surfactants form a less closely packed monolayer, which would allow more stable clusters to form since the monolayers from approaching droplets are more able to interpenetrate and thus hold the droplets together (discussed in chapters 5 & 6), a longer head group is even more advantageous. If growth of the droplet occurs, the more widely spaced head groups facilitate the process by allowing further negative curvature i.e. more extension of the monolayer is able to take place due to less obstruction by head groups.

Table 3.3 The effects of the molecular structure of constituents on the O/W microemulsion phase regions for C_nE_m / x alkane / water systems.

Increase in Variable	Temperature of 1ϕ Region	Figure
n	Decreased	3.3*a* (i) & (ii)
m	Increased	3.3*b* (i) & (ii)
overall surfactant length (for n/m = 2)	Unchanged SPB Increased UTPB	3.3*c*
x	Increased	3.3*d*

3.4 Conclusions

The temperature range over which the 1ϕ region exists is dependent on the structure of the surfactant and the alkane oils, the concentration of surfactant has little effect on its position. For these C_nE_m/alkane oil/water systems the temperature range of this region is increased by increasing the head group size of the surfactant or the

alkane oil chain length, and decreased by increasing the length of the surfactant hydrocarbon chain. Increasing the overall length of the surfactant for a consistent n/m ratio of n/m = 2 has no effect on the SPB temperature due to the opposing effects of the tail and head group, whereas the UTPB is increased i.e. the 1ϕ region is stable over a wider temperature range.

Figure 3.2

The effect of surfactant concentration on the position of the 1ϕ o/w microemulsion region for three concentrations of $C_{12}E_6$ with decane.

Circles = 0.093 M, squares = 0.033 M, diamonds = 0.016 M $C_{12}E_6$.
Open symbols denote the SPB, solid symbols denote the UTPB.

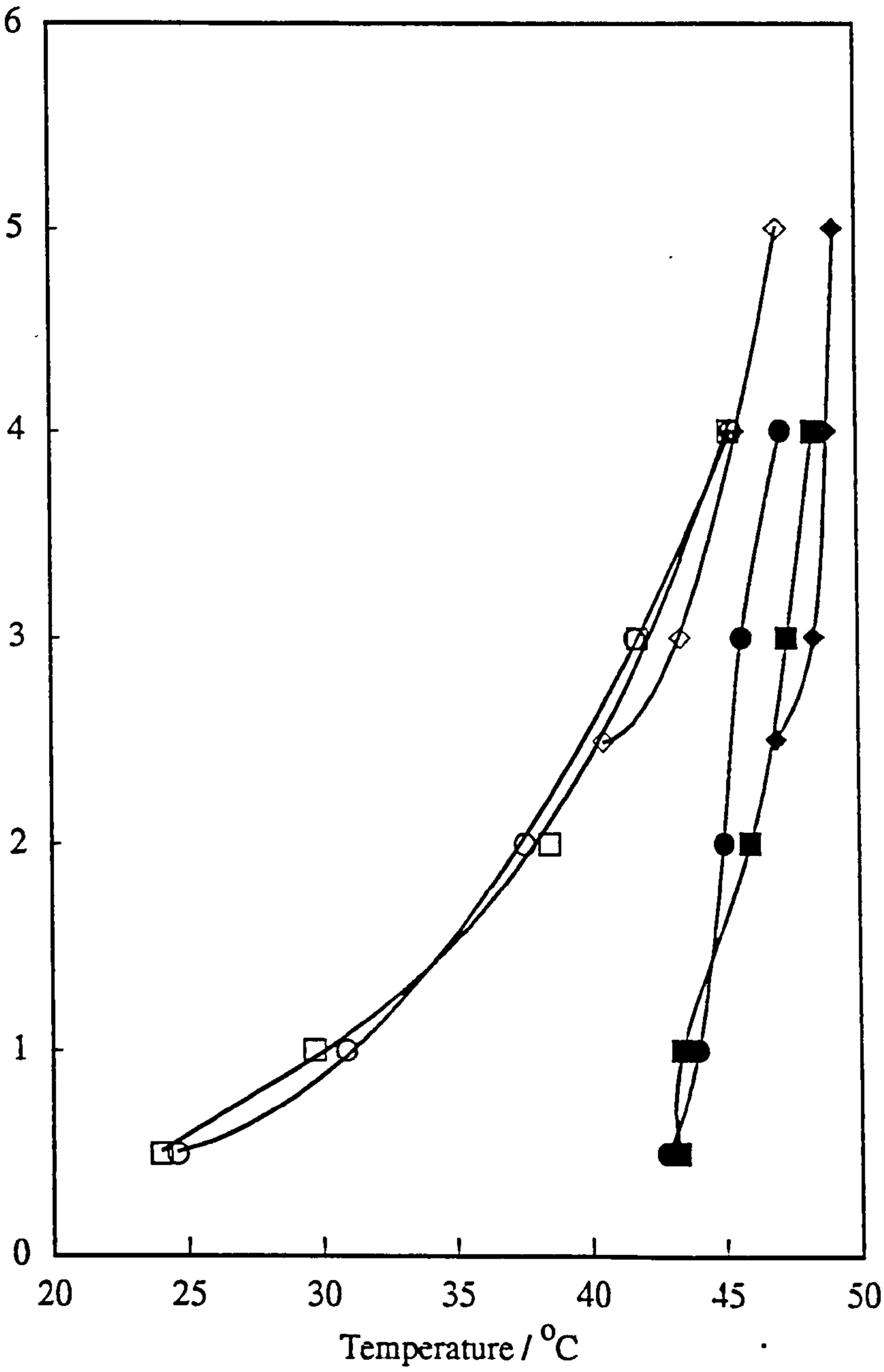

Figure 3.3

(a) The effect of surfactant hydrocarbon tail group length on the position of the 1ϕ o/w microemulsion region.
(i) C_nE_5 with decane at surfactant concentrations of 0.09 M C_8E_5, 0.08 M $C_{10}E_5$, 0.09 M $C_{12}E_5$, and 0.05 M $C_{14}E_5$.
Open symbols denote the SPB, solid symbols denote the UTPB.
✖ = PCS data for 0.01 M $C_{12}E_5$ at the SPB, showing good agreement with turbidity data.

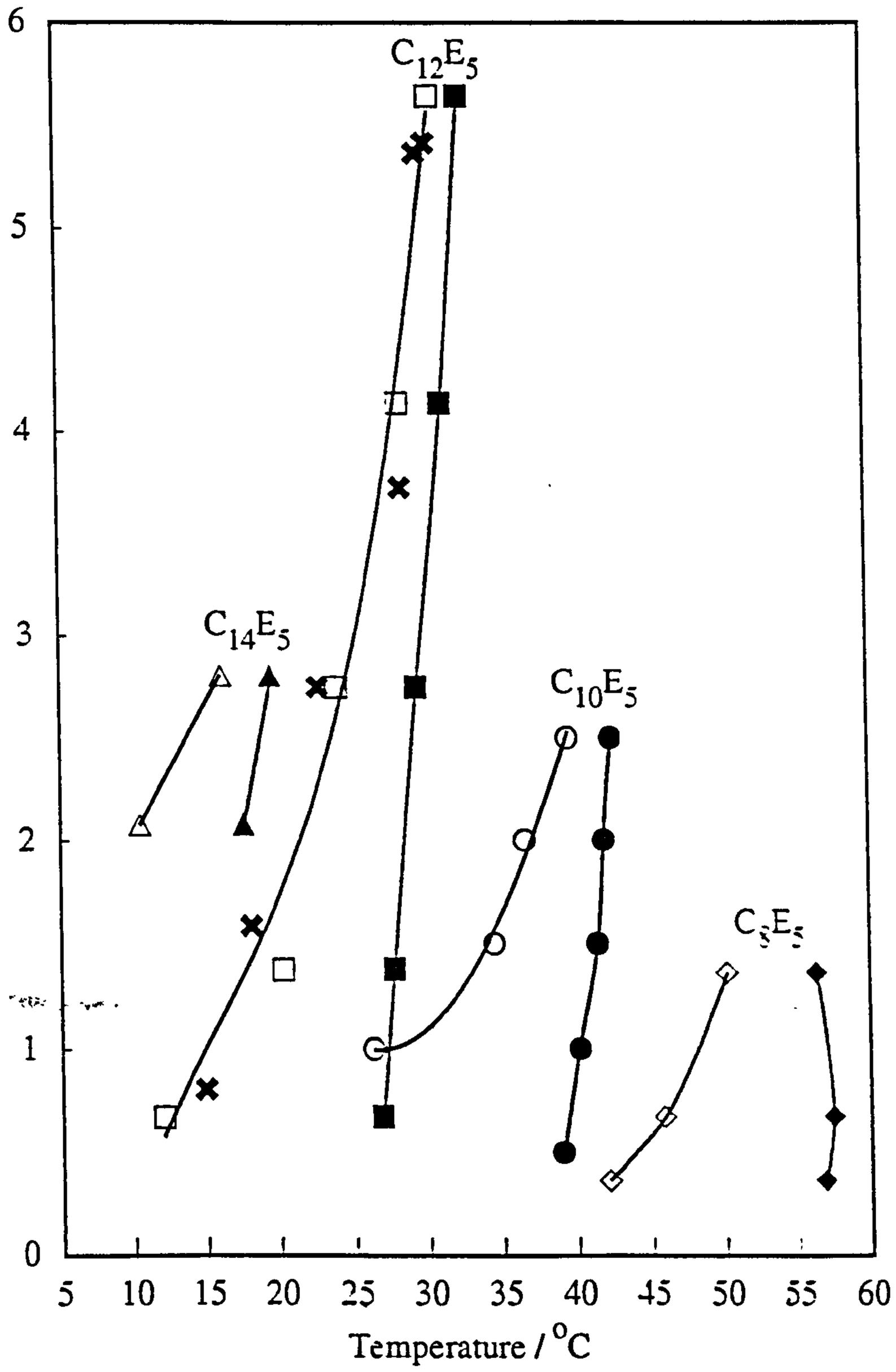

Figure 3.3

(a) The effect of the surfactant hydrocarbon tail group length on the position of the 1ϕ o/w microemulsion region.

(ii) C_nE_7 with decane, at surfactant concentrations of 0.09 M .
Open symbols denote the SPB, solid symbols denote the UTPB.

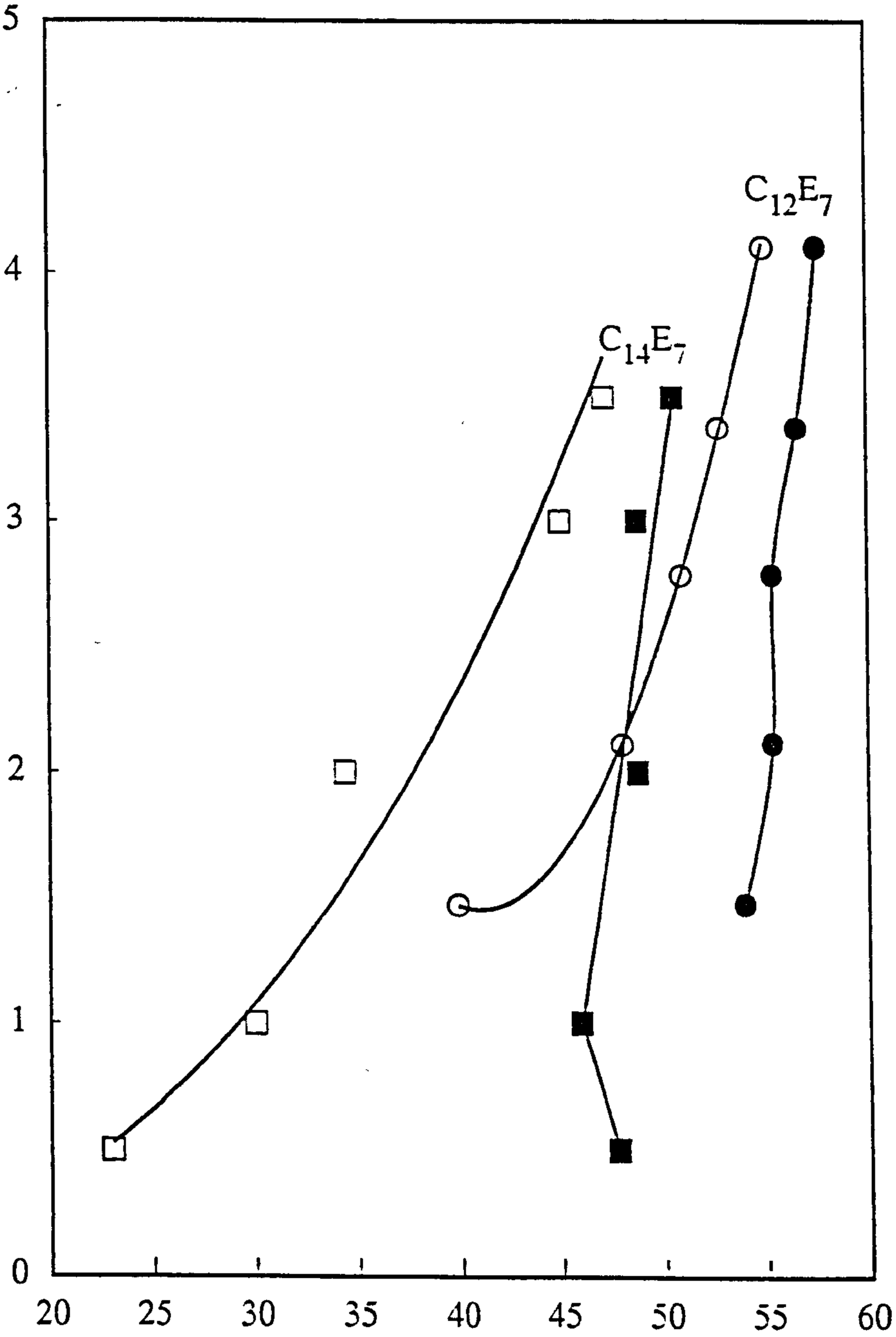

Figure 3.3

(b) The effect of surfactant head group size on the position of the 1ϕ o/w microemulsion region.

(i) $C_{12}E_m$ with decane, at surfactant concentrations of 0.09 M. Open symbols denote the SPB, solid symbols denote the UTPB.

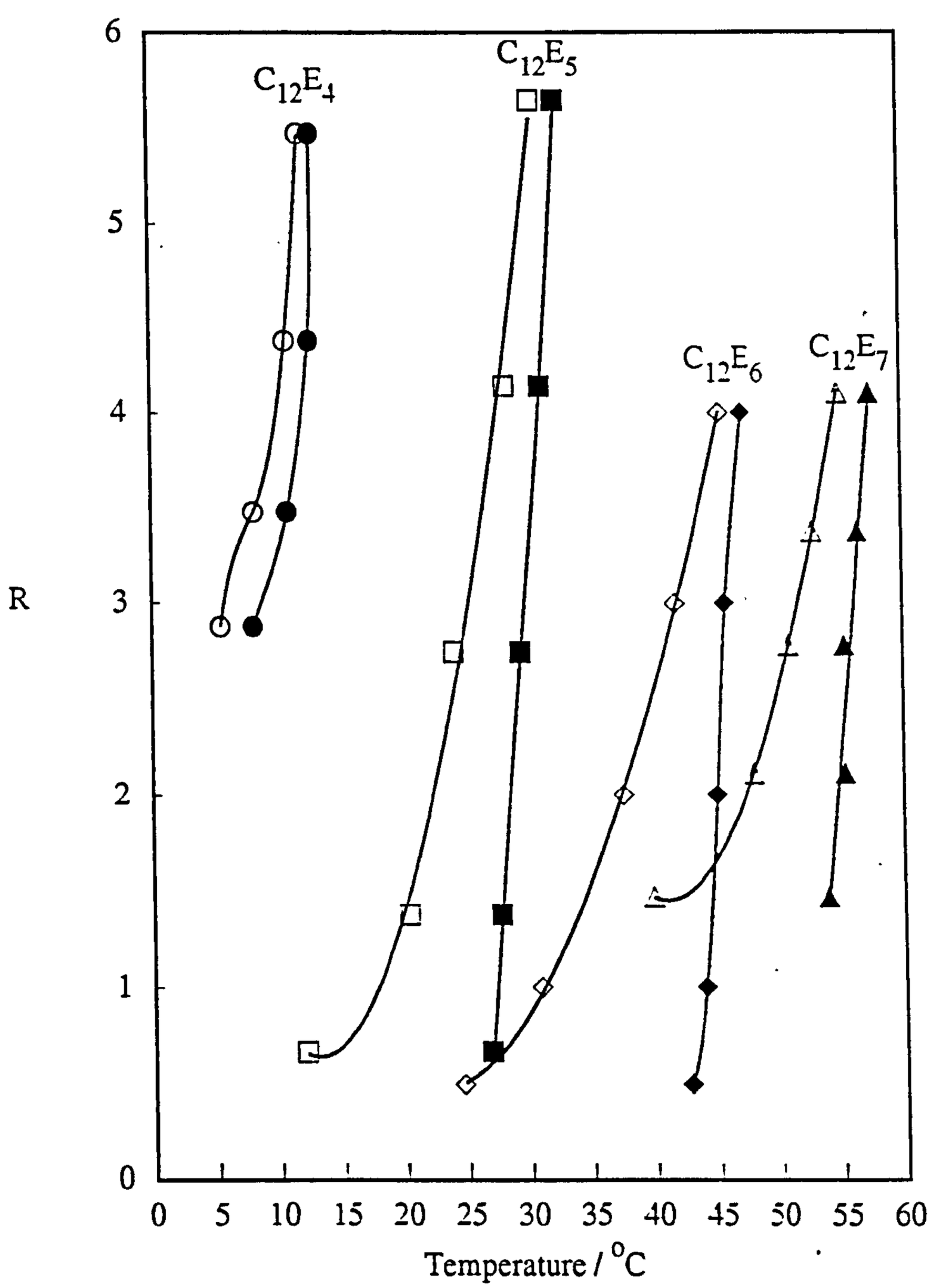

Figure 3.3

(b) The effect of the surfactant head group size on the position of the 1ϕ o/w microemulsion region.

(ii)$C_{14}E_m$ with decane, at concentrations of 0.05 M $C_{14}E_5$, and 0.09 M $C_{14}E_7$.
Open symbols denote the SPB, solid symbols denote the UTPB.

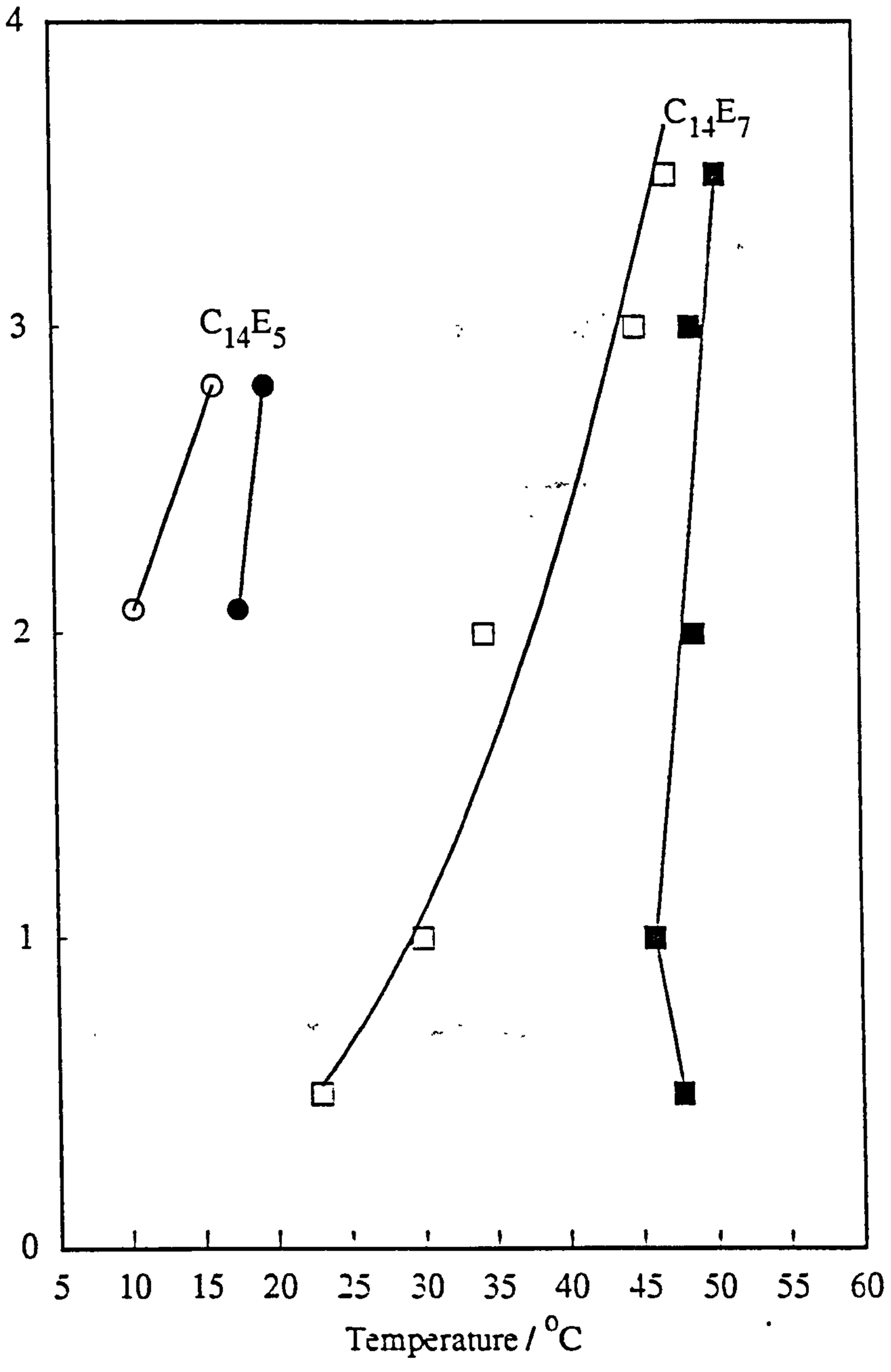

Figure 3.3

(c) The effect of overall surfactant length on the position of the 1ϕ oil-in-water microemulsion region.

Circles = $C_{10}E_5$, squares = $C_{12}E_6$, diamonds = $C_{14}E_7$.
Open symbols denote the SPB, solid symbols denote the UTPB.

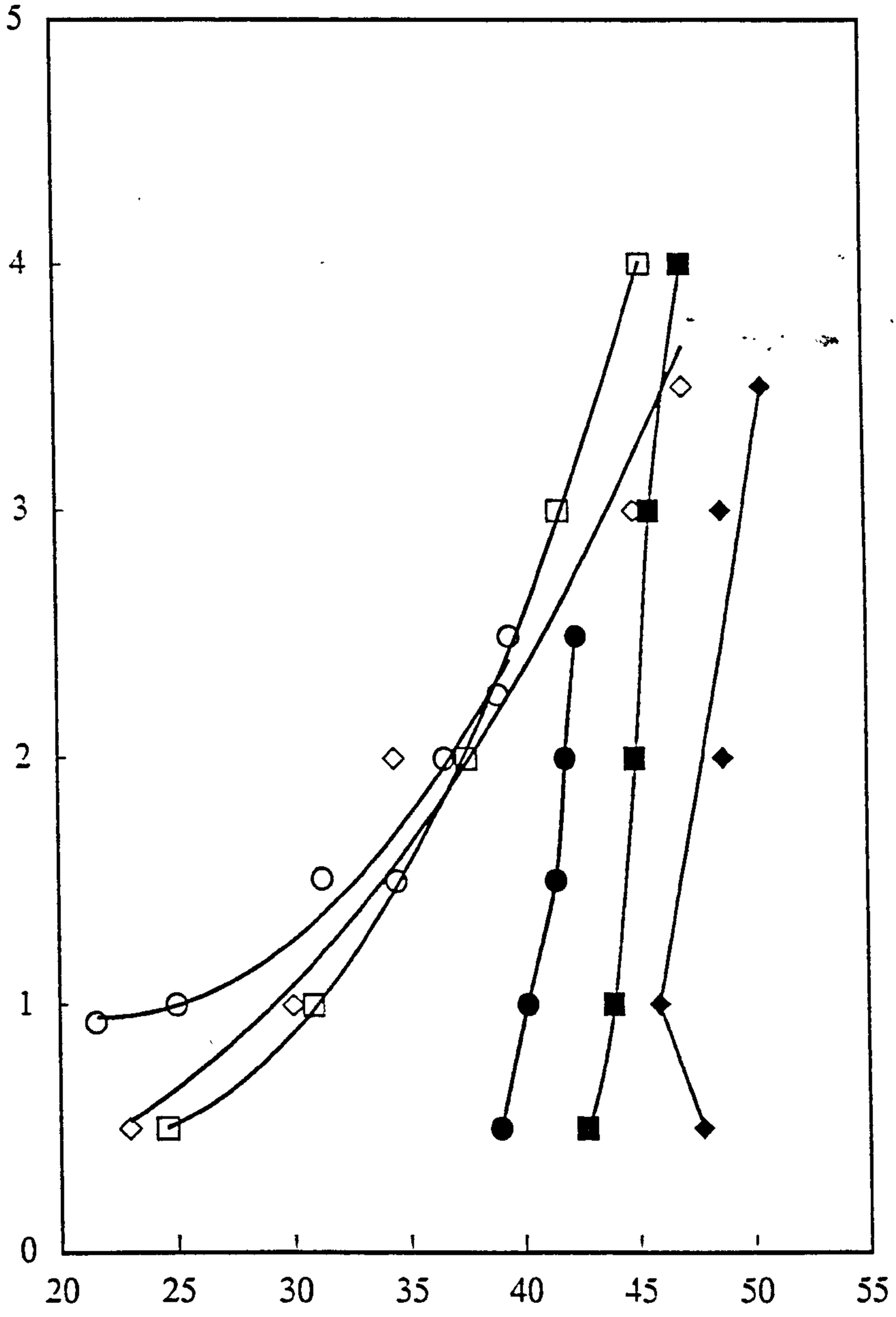

Figure 3.3

(d) The effect of the alkane oil chain length on the position of the 1ϕ region of o/w microemulsions stabilised by $C_{12}E_5$.

Surfactant concentrations of 0.09 M were used with heptane (C7) and decane (C10). Data from reference 9 for 0.014 M $C_{12}E_5$ with tetradecane (C14) is also shown. Open symbols denote the SPB, solid symbols denote the UTPB.

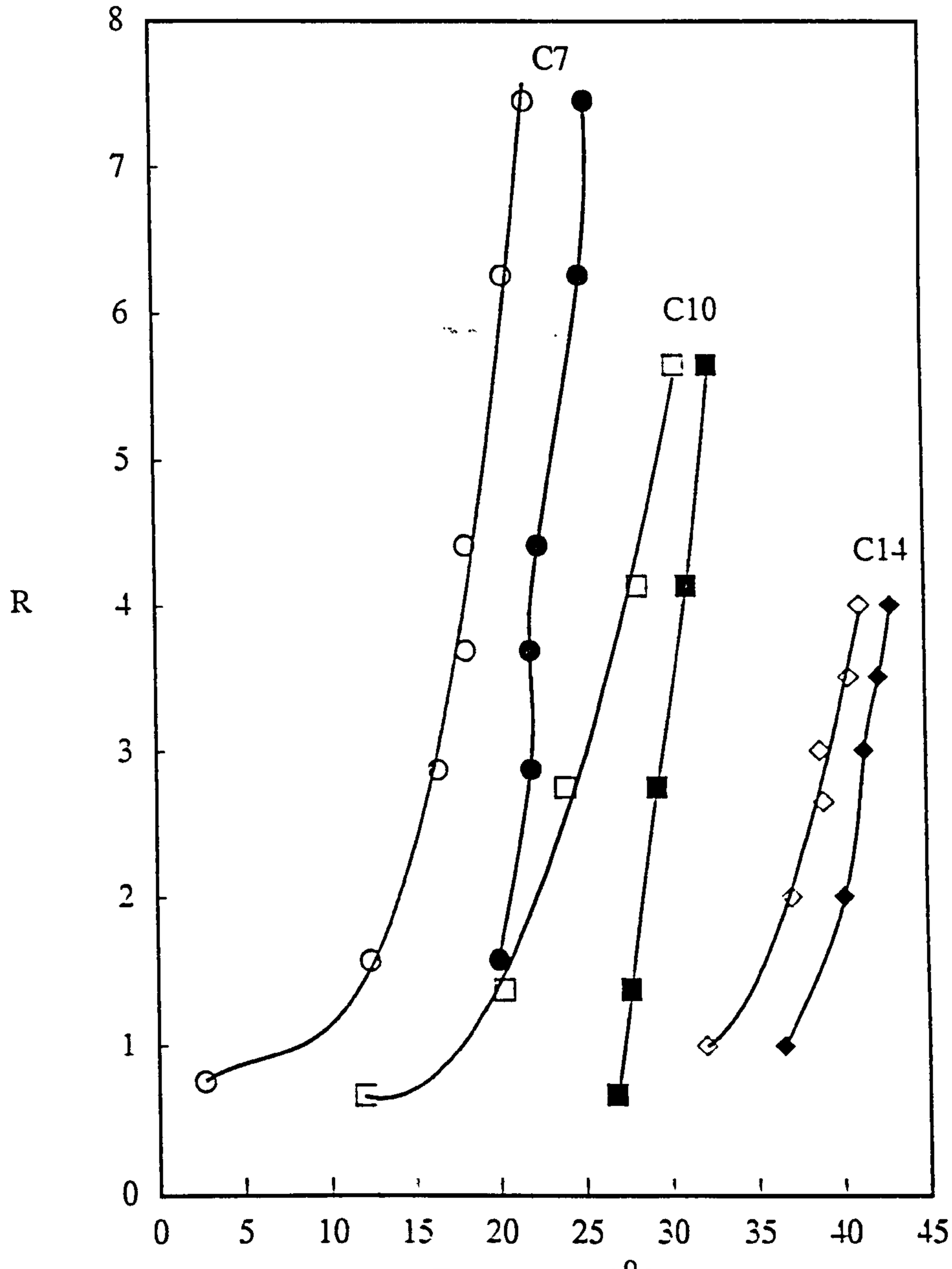

[9] P. D. I. Fletcher, J. F. Holzwarth, J. Phys Chem, 1991, 95, 2550-2552.

CHAPTER FOUR

4. The structure of oil-in-water microemulsion droplets at the solubilisation phase boundary.

4.1 Introduction.

The microemulsion droplets at the SPB were assumed to be spherical and monodisperse. The hydrodynamic radius of the droplets can be calculated from equation 1.4d (from section 1.4, chapter 1). Turbidity and PCS methods were used to determine the size parameters of the microemulsion droplets for a range of surfactant systems in which the chain lengths of the tail and head groups of the surfactant and the alkane oil are systematically varied.

4.2 PCS results

4.2.1 Background

PCS (also known as dynamic light scattering) uses a coherent laser beam source. Analysis of the scattered light signal from the particles in a colloidal suspension yields information about particle motion and, in turn, the distribution of particle sizes[1] . PCS has been extensively used for particle sizing in microemulsion systems[2 3,4].

If a dispersion of static colloidal particles is considered as forming a 3 - dimensional array then, on illumination by a coherent light source, a characteristic random diffraction or "speckle" pattern will be produced. Bright and dark areas will arise from constructive and destructive interference of the scattered light. In a real solution the particles are continually moving under Brownian motion and hence the diffraction pattern bright spots will move randomly. A detector positioned to register the intensity of the bright spots will then yield a signal which fluctuates significantly about a mean value. The characteristic frequency of these random intensity fluctuations contains information on the particle motion and hence its size. Small, fast moving particles produce high frequency fluctuations whereas larger, slower moving particles give lower frequencies. The PCS signal was analysed according to the cumulants

---

[1]P.N.Pusey, in Colloidal Dispersions,ed, J.W.Goodwin, p. 129, Royal Society of Chemistry, London, (1982)
[2]R. Aveyard, B. P. Bimks, P. D. I. Fletcher, Langmuir, 1989, 5, 1210.
[3]A.M.Cazabat and D.Langevin, J.Chem.Phys., 1981, 6, 74, 3148.
[4]R.A.Day, B.H.Robinson, J.H.R.Clarke, and J.V.Doherty, J. Chem. Soc. Faraday Trans. 1979, 1, 75, 132.

analysis to yield a mean diffusion coefficient of the particles[5]. For non-interacting spherical particles, the hydrodynamic radius is related to the diffusion coefficient by the following equation :

$$r_h = \frac{kT}{6\pi\eta D} \qquad (4.2.1a)$$

where: k = Boltzmann's constant
T = the absolute temperature
η = the viscosity of the continuous solvent
D = the mean diffusion coefficient.

The cumulants analysis also yields a value of the normalised first moment (ψ, equal to the so-called "polydispersity") of the expansion of the scattered intensity autocorrelation function which provides a measure of the polydispersity of particle sizes.[5]

For the measurements described here, the volume fraction of the droplets was always less than a few %, since it has been shown that for these systems interactions between droplets can be neglected at these low volume fractions[11].

4.2.2 The variation of the average hydrodynamic radius and polydispersity with temperature.

The average hydrodynamic radius and the corresponding polydispersity were measured as a function of temperature for each microemulsion sample. Figure 4.2.2*a* for $C_{12}E_5$ with decane shows the typical behaviour. The apparent hydrodynamic radius increases with temperature, with a more pronounced increase as the upper phase boundary is approached. As discussed in chapter 1, at the solubilisation phase boundary the droplets have been shown to behave as weakly interacting spheres. The increase in the apparent radius of the droplets with increasing temperature is consistent with *either* clustering of droplets (with no change of droplet size) *or* droplet growth.

---

[5]"Particle sizing by light scattering - an application manual", Malvern Instruments Ltd., Spring Lane South, Malvern, Worcester. WR14 1AT. U. K.

Figure 4.2.2*a*
PCS measurements for 0.01 M $C_{12}E_5$ with decane

(i) Variation of the mean hydrodynamic radius with temperature.

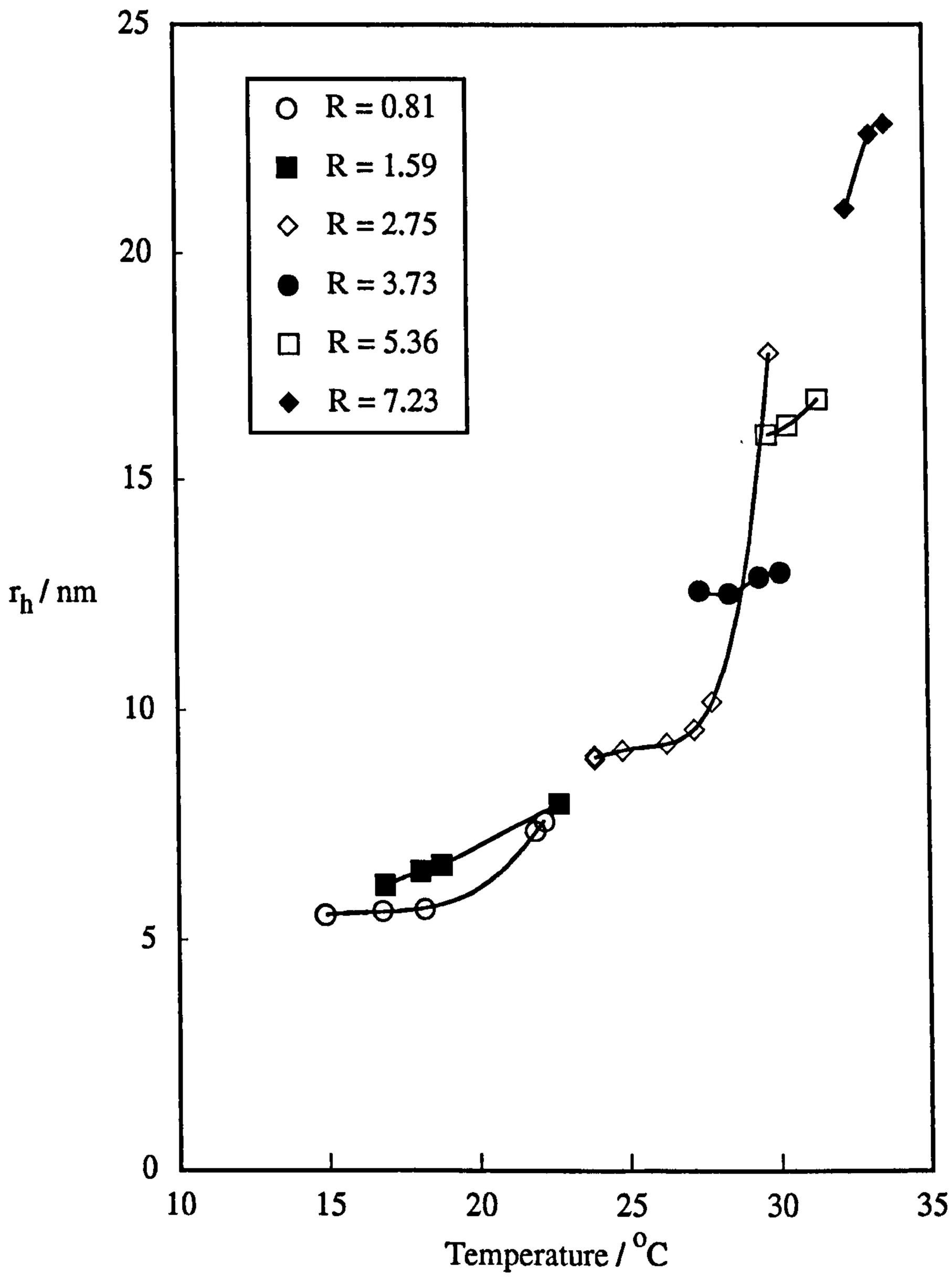

Both interpretations have been suggested as explanations for experimental results for this type of micromemulsion system [2,6].

Figure 4.2.2a (ii) shows the variation of polydispersity with temperature for this system which is typical for the other microemulsions studied. In general, Ψ is found to be approximately 0.05 at the SPB and to increase as the UTPB is approached. For low R values (data not shown) the apparent value of Ψ was found to be 0.1 - 0.2. However, these values were judged to be unreliable because of the low precision of the data caused by the weak scattering from these samples.

[6]M. Leaver, I. Furo, U. Olsson, submitted to Langmuir, December 1994.

Figure 4.2.2*a*
PCS measurements for 0.01 M $C_{12}E_5$ with decane.

(ii) Variation of polydispersity (Ψ) with temperature.

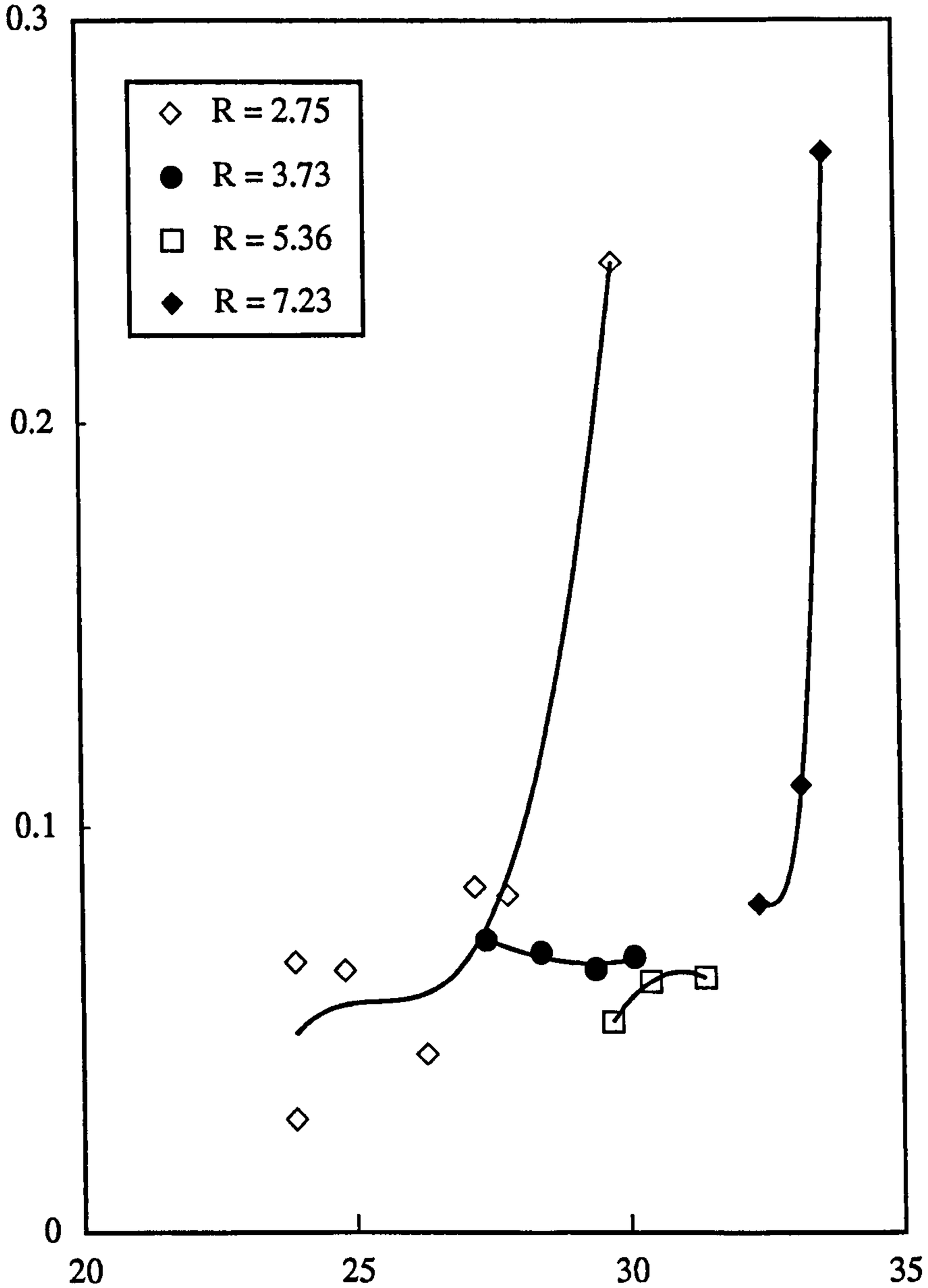

4.2.3 *The variation of the hydrodynamic radius with R at the SPB for the different microemulsion systems.*

For each microemulsion system, the droplet hydrodynamic radii for the different R values at the temperature corresponding to the SPB were obtained from plots of the type shown in Figure 4.2.2*a*. Also included in these figures are the plots obtained from the turbidity data fitted to model one (section 4.3.1) showing good agreement with PCS data. Equation 4.1*a* predicts that the radius of the droplet should increase linearly with R, with the slope and the intercept of the r_h v R line yielding the A_s and δ values respectively. Figure 4.2.3*a* (i) for $C_{12}E_5$ with decane shows a typical example of such a plot. It is interesting to note that Olsson *et al* [7] found by self-diffusion studies and PCS, a value for r_h of 9.5 ± 0.3 nm for $C_{12}E_5$ with decane at a surfactant to oil weight ratio of 0.82 (corresponding to R = 2.65), which agrees with that found in this work of 9.3 nm for this R value. All the systems studied gave data of precision comparable to 4.2.3*a* except for $C_{10}E_5$ with decane, where the "scatter" of the data was unusually high (Figure 4.2.3*a*(ii)). The reason for this poor precision remains unclear. An example of a system showing very good precision is given in Figure 4.2.3.*a*(iii) for $C_{12}E_6$ with decane.

The PCS data produce good linear plots in agreement with equation 4.1*a* which predicts a linear variation should be obtained only if A_s is constant for all R values. However, as discussed in reference 8, the PCS data is insensitive to variations in A_s for r_h values comparable to δ, i.e. R less than 1 or 2. The linearity of the plots show only that A_s is independent of R at high R values. Hence the A_s values derived from the slopes of these plots are valid only for high R values greater than 1 or so.

Table 4.4 gives the values of A_s and δ found for the systems studied. The values for $C_{12}E_5$ with heptane and $C_{12}E_5$ with tetradecane are quoted from reference 2. Detailed discussion of the values is postponed until section 4.4 following a comparison with the parameters derived from turbidity measurements.

---

[7] U. Olsson, P. Schurtenberger, Langmuir, 1993, 9, 3389.
[8] P. D. I. Fletcher, R. Johansson, J. Chem. Soc. Faraday Trans. 1994, 90 (23), 3567.

Figure 4.2.3*a*
Variation of r_h with R as determined by both PCS (open squares and solid line) and turbidity (dashed line, fitted to model 1).

(i) Typical plot shown by $C_{12}E_5$ with decane at a surfactant concentration of 0.01 M for PCS and 0.09 M for turbidity.

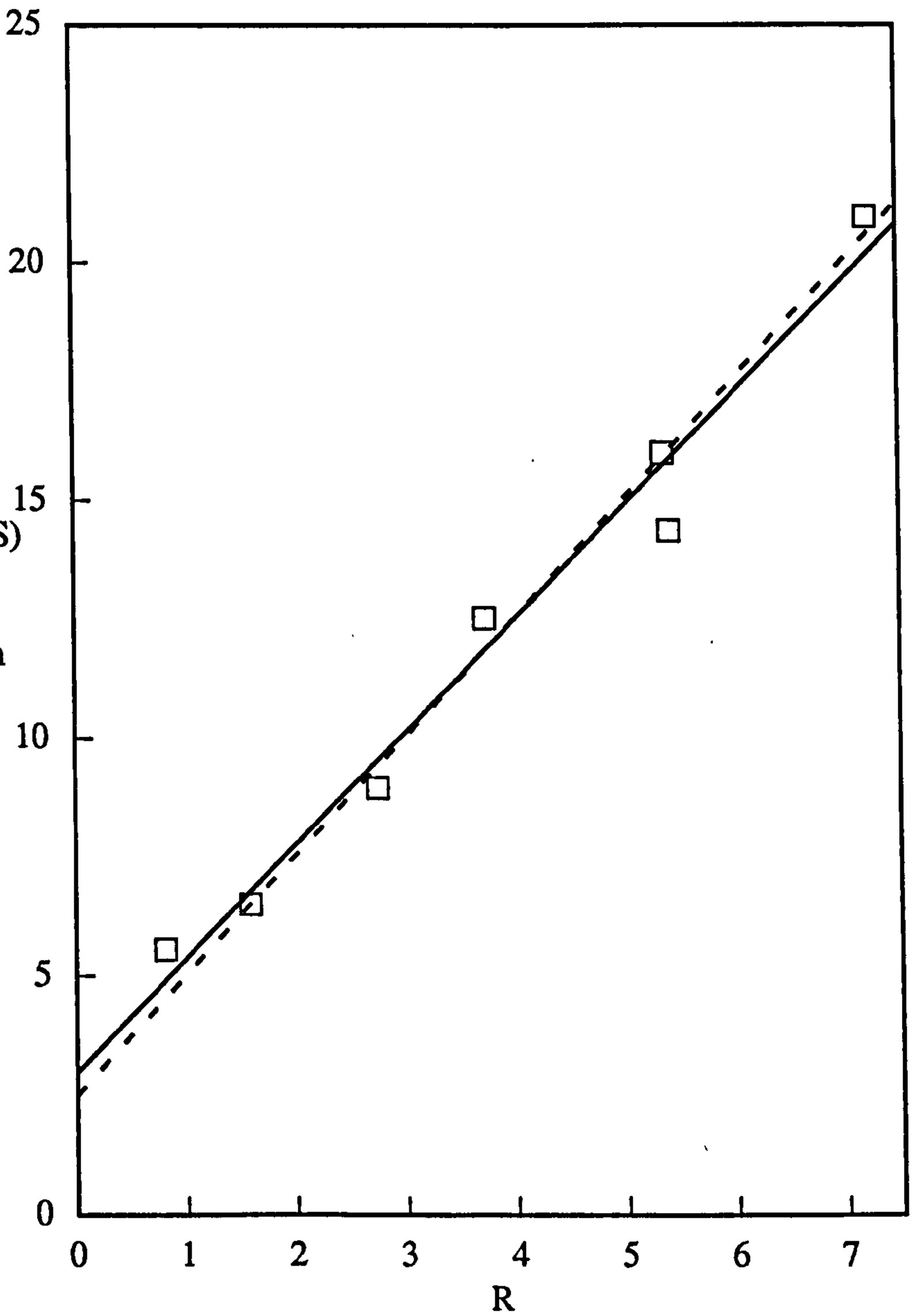

Figure 4.2.3*a*
Variation of r_h with R by both PCS and (open squares and solid line) and turbidity (dashed line, fitted to model 1).

(ii) r_h versus R for $C_{12}E_5$ with decane using surfactant concentrations of 0.01 M for PCS and 0.08 M for turbidity. This shows the difficulty found in obtaining good agreement of PCS data for this one system, though the fitted line through the points agrees favourably with the turbidity data.

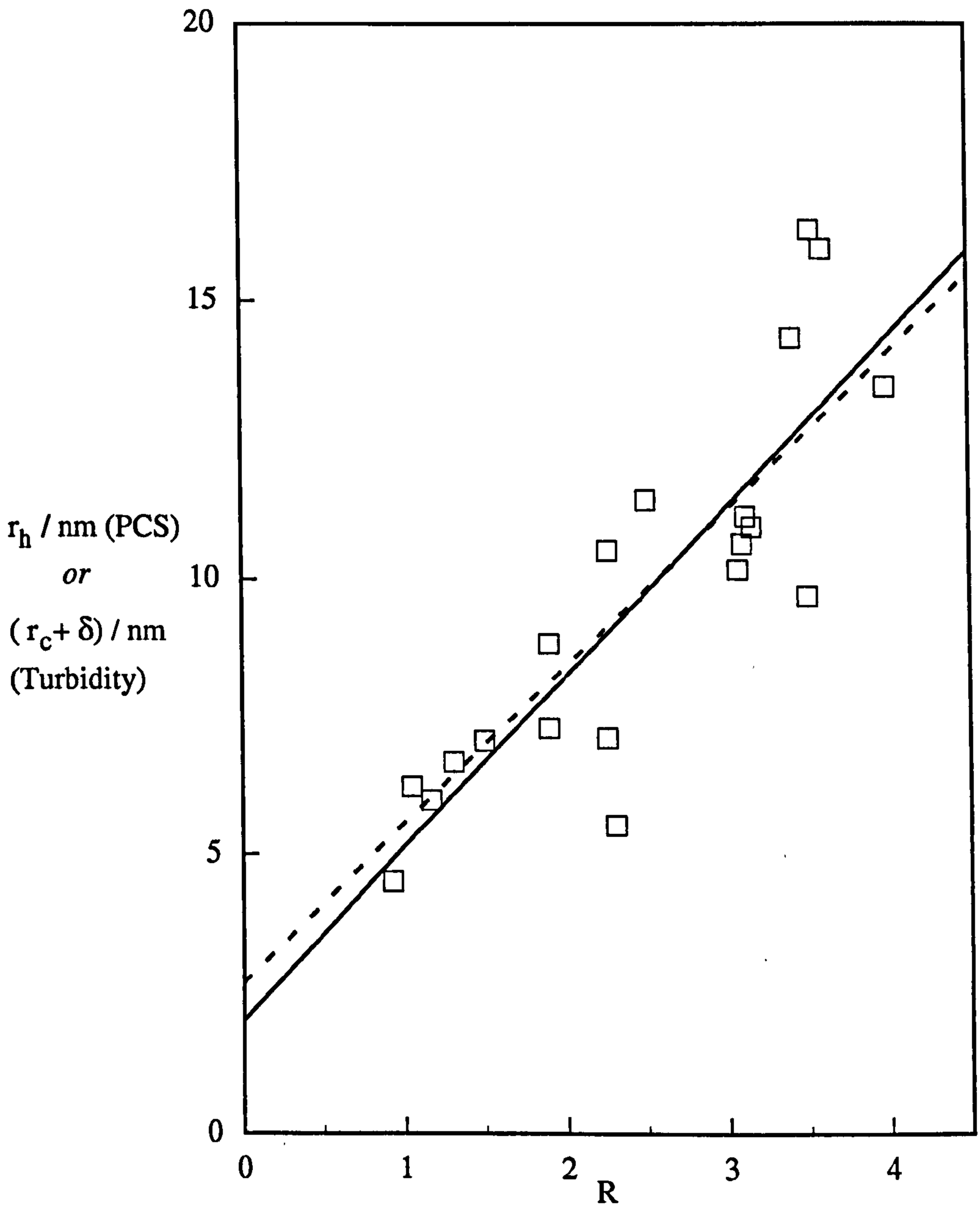

Figure 4.2.3*a*
Variation of r_h with R as determined by both PCS (open squares and solid line) and turbidity (dashed line, fitted to model 1).

(iii) Plot showing good precision from PCS data for $C_{12}E_6$ with decane at a surfactant concentration of 0.01 M for PCS and 0.093 M for turbidity.

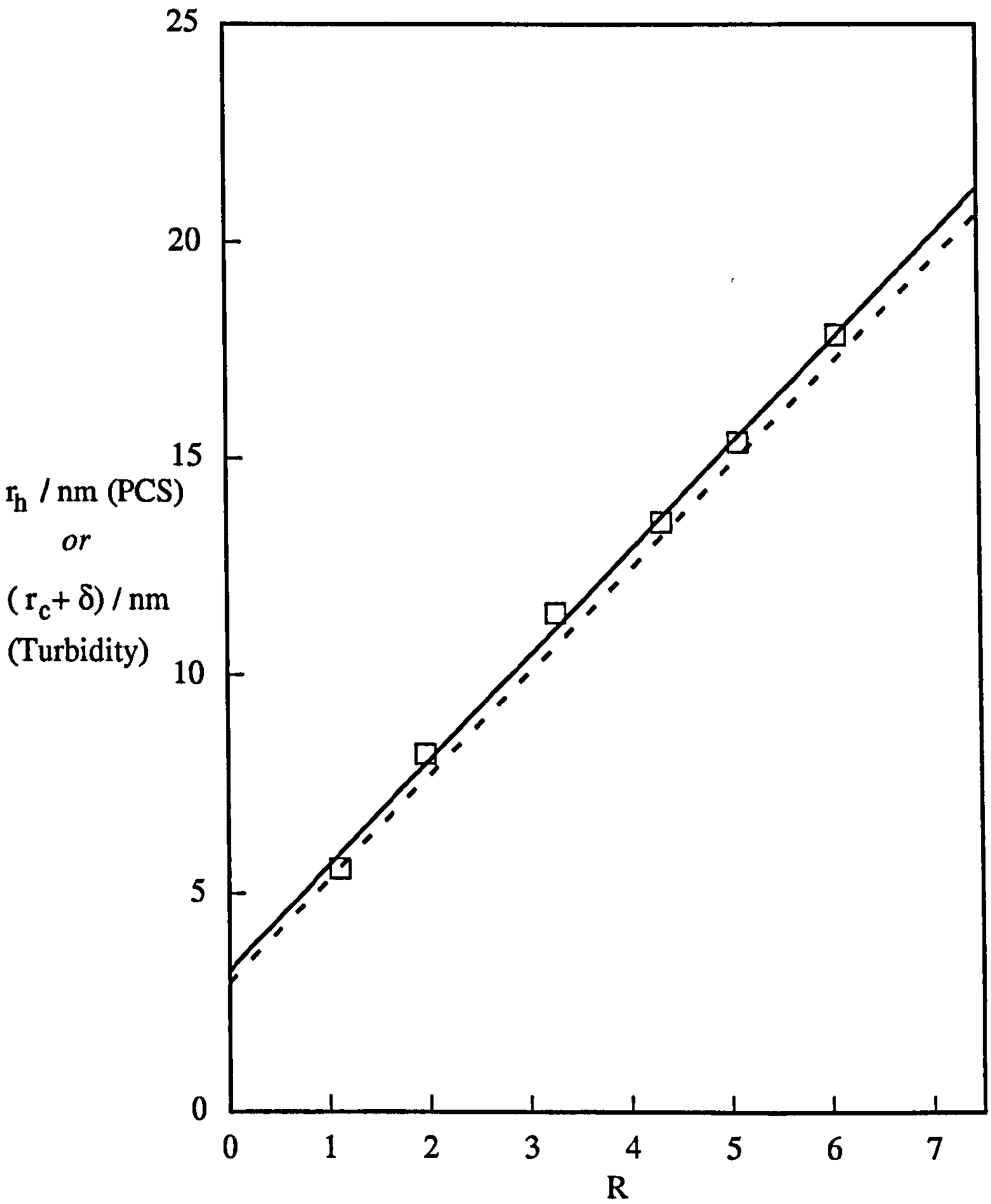

4.3 Turbidity results

4.3.1 Turbidity - basic theory.

Turbidity (τ) is a measure of the reduction in intensity of light as it passes through a sample due to the scattering process. It is defined by the following equation in which l is the path length, and I_t and I_o are the intensities of transmitted light and incident light respectively[9].

$$\tau l = -\ln(I_t/I_o) \qquad (4.3.1a)$$

The turbidity of a dispersion, for a non-polarised incident beam, of non-interacting spheres of radius much less than the wavelength of the incident light is given by the following equation 4.3.1*b*.

$$\tau = (24\pi^3/\lambda^4)P^2NV_p^2 \qquad (4.3.1b)$$

where λ = wavelength of light in the medium

N = number of particles per unit volume

V_p = particle scattering volume

and P is a factor containing the refractive indices of the particle and the solvent.

There is an uncertainty in the calculation of parameter P due to the difficulty in assigning values of refractive index to the different regions of the microemulsion droplet. This uncertainty arises because the surfactant tails are likely to be penetrated by the oil and the heads by the water solvent to a degree which is unknown. Two models for the calculation of P were tested (Figure 4.3.1*a*):

[9]Hunter, R. J. Foundations of Colloid Science, Clarenden Press, Oxford, U.K., 1986, Vol. 1.

Figure 4.3.1*a*

The two refractive index models used in particle calculations from turbidity data.

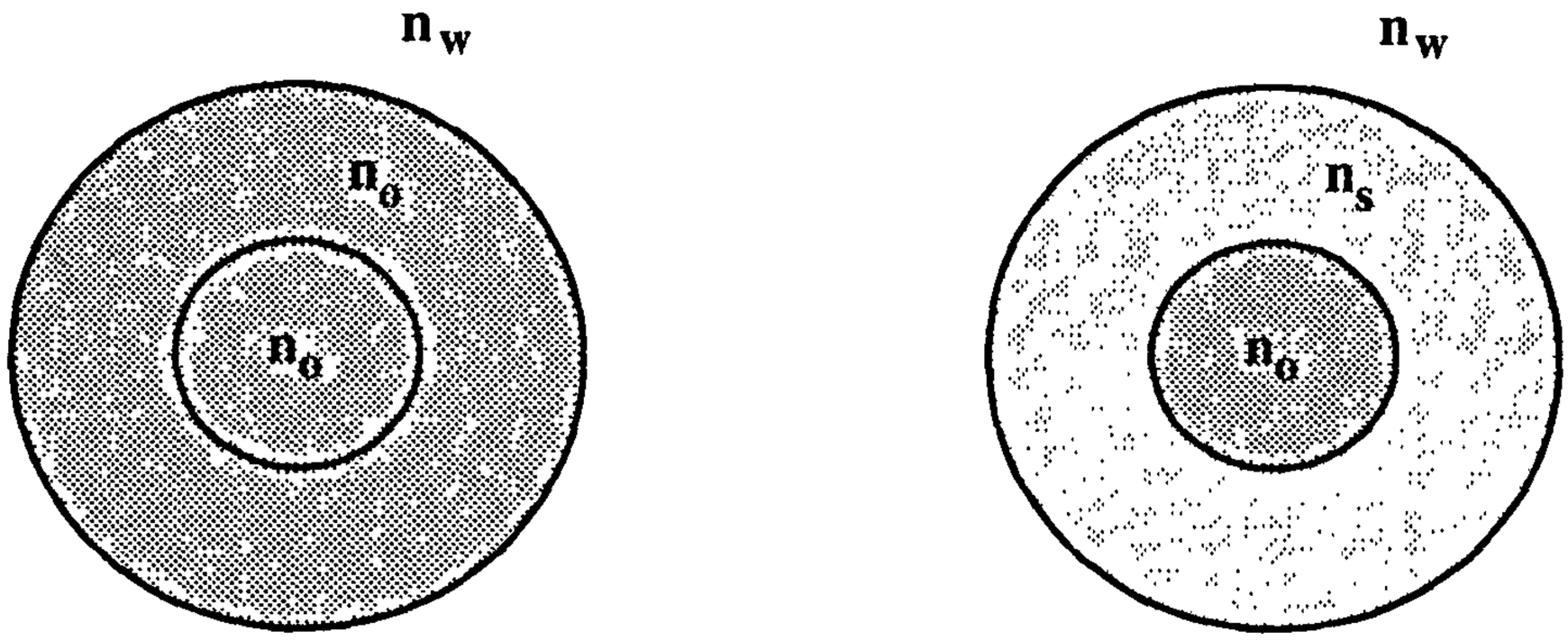

Model 1 **Model 2**

Model 1 The scattering particle was assumed to have a *constant refractive index* equivalent to that of the pure oil (n_o). This suggests that the scattering particle is comprised of the oil core plus the surfactant hydrocarbon tail length, and assumes that the surfactant heads have the same refractive index as the surrounding water (n_w). In this case δ represents the surfactant tail length and P is given by equation 4.3.1*c*:

$$P_1 = \{(n_o^2 - n_w^2)/(n_o^2 + 2n_w^2)\}^2 \qquad (4.3.1c)$$

Model 2 The scattering particle is assumed to have a *dual refractive index* comprising that of the oil core, assumed to have the refractive index of the pure oil (n_o), and that of the surfactant shell, assumed to have the refractive index of the pure surfactant (n_s). In this case both the surfactant tail and the head contributes to the scattering particle and δ therefore represents the full length of the surfactant. The parameter P then becomes[10]:

$$P_2 = \frac{(m_2^2 - 1)(m_1^2 + 2m_2^2) + q^3(2m_2^2 + 1)(m_1^2 - m_2^2)}{(m_2^2 + 2)(m_1^2 + 2m_2^2) + q^3(2m_2^2 - 2)(m_1^2 - m_2^2)} \qquad (4.3.1d)$$

where q = radius of the core divided by the overall radius.

$m_1 = n_o/n_w$

$m_2 = n_s/n_w$

---

[10]"The scattering of light and other magnetic radiation", M. Kerker, 1969, Academic Press Inc., London.

For these systems the droplets (at the SPB) have been shown to interact according to a hard sphere potential[11]. This requires a further adjustment to the turbidity equation to allow for the dependence on the volume fraction of particles (ϕ), equation 4.3.1*e*:[12]

$$\tau_{HS} = (\text{constant})\phi(1-\phi)^4/\{(1+2\phi)^2 - \phi^3(4-\phi)\} \qquad (4.3.1e)$$

where ϕ is assumed to be made up of the oil, the surfactant and an estimated number of bound water molecules per surfactant. For the purposes of the calculations presented here, it was assumed that there was one water molecule per E group, for all surfactants. Leaver *et al* [6] estimated there to be 3 water molecules per E group for the $C_{12}E_5$ with decane system. However, it was found that in these calculations changing the number of bound water molecules to 5 per E group did not significantly affect the results. The term (constant)ϕ is given by the right hand side of equation 4.3.1*b*, with NV_p being equivalent to ϕ.

Equation 4.3.1*b* predicts that turbidity is proportional to λ^{-4}. This was checked for a sample containing 0.09 M $C_{12}E_6$ with decane at R = 1.38, measured at 42.8°C. As shown in Figure 4.3.1*b*. the wavelength dependence is correctly predicted within the experimental uncertainty.

4.3.2 The temperature dependence of turbidity

The turbidity of a microemulsion at constant composition was found to increase with increasing temperature. Figure 4.3.2 illustrates the typical behaviour with data from a sample containing 0.09 M $C_{12}E_5$ with decane at R=4.14. The temperature dependence and its relation to droplet clustering or growth is the subject of chapter 5. This section is concerned only with the turbidity, τ_o, at the solubilisation phase boundary (SPB) where the microemulsion droplets are known to behave as hard spheres.

---

[11] P. D. I. Fletcher, J. F. Holzwarth, J. Phys Chem., 1991, 96, 2550.
[12] A.M.Cazabat, D. Langevin and A. Pouchelon, J. Coll. Int. Sci., 1980, 73, 1.

Figure 4.3.1*b*

Confirmation of λ^{-4} dependence of turbidity measured at 42.8°C, for a sample containing 0.09 M $C_{12}E_6$ with decane at R = 1.38.

The open circles are the experimental points with error bars reflecting the increasing effect of the experimental error in turbidity readings at the lower turbidities. The solid line shows the "best fit" slope of -4.

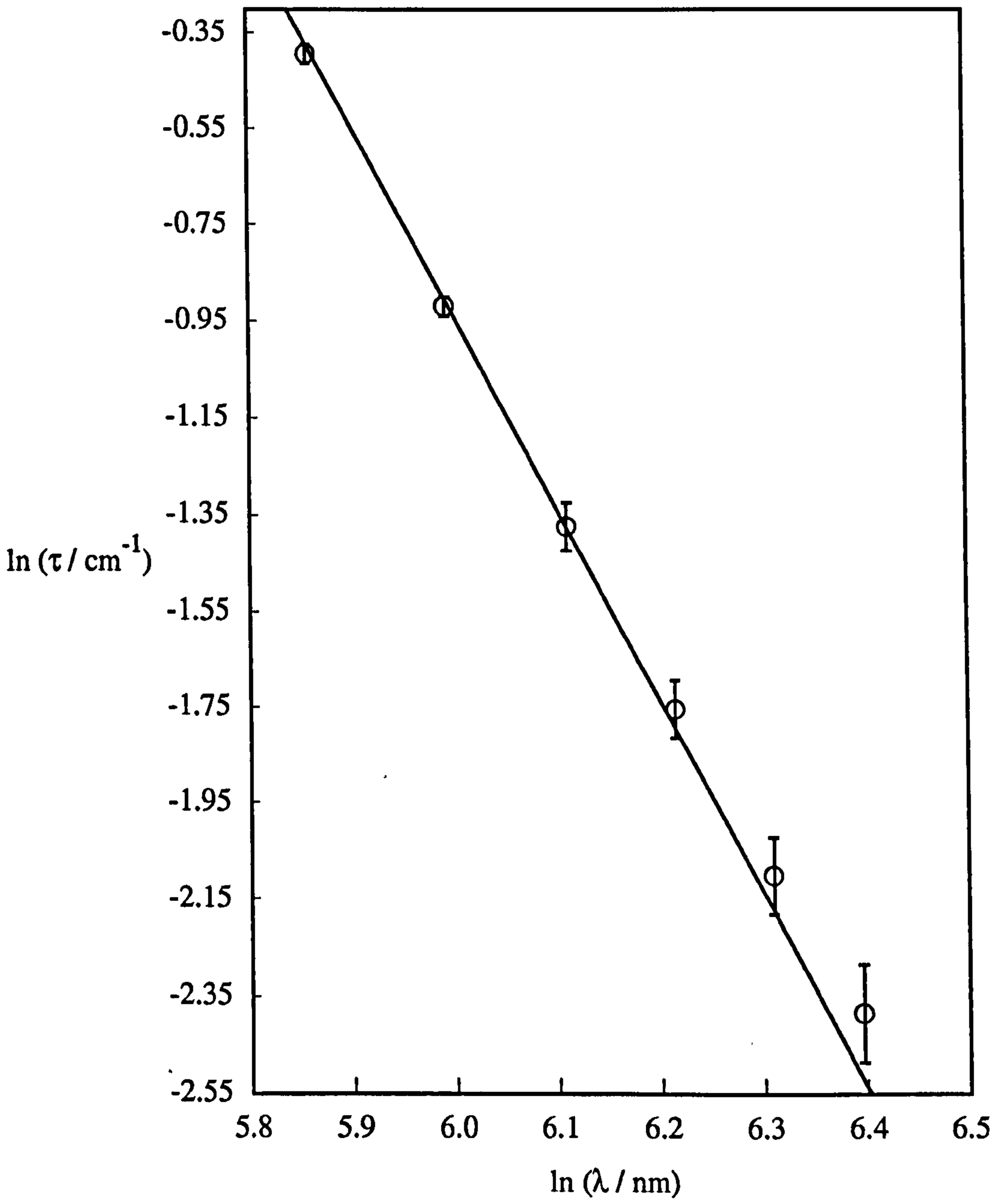

Figure 4.3.2

The temperature dependence of the turbidity for a microemulsion of 0.09 M $C_{12}E_5$ with decane at R = 4.14.

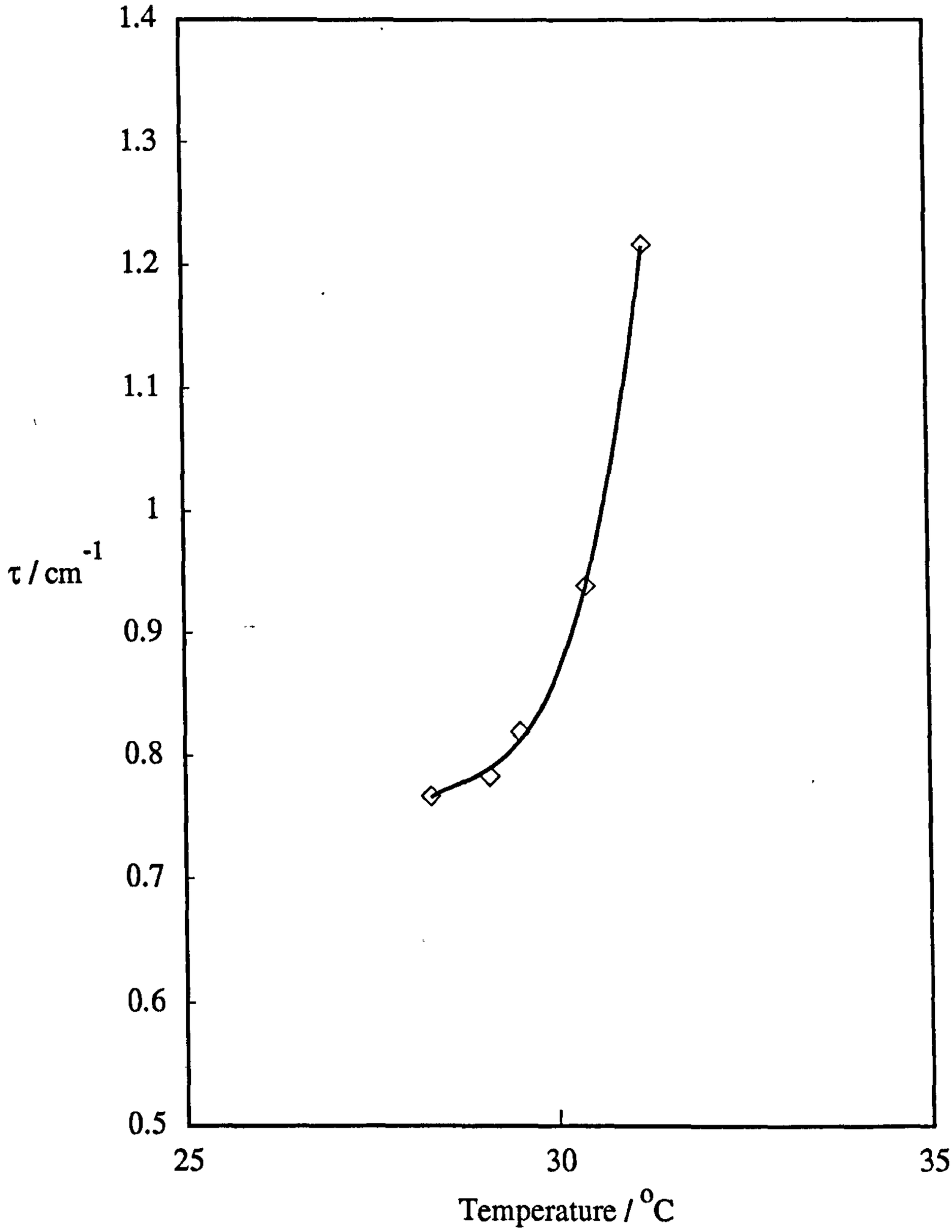

4.3.3 *The dependence of τ on R at the solubilisation phase boundary.*

Turbidity is predicted to be proportional to NV_p^2 (equation 4.3.1*b*). Calculation then shows that τ is expected to increase with increasing R (i.e. τ is proportional to R^4). Typical plots for different R values are shown in Figure 4.3.3*a* for 0.09 M $C_{12}E_5$ with decane, from which the turbidity values at the SPB are used to estimate the size of the individual microemulsion droplets.

The variation of τ_o with R was modelled using a computer program which used an algorithm based on a combination of equations 4.1*a* and 4.3.1*e*, using 4.3.1*c* or *d* as appropriate for the two different microemulsion droplet refractive index models. The program iteratively obtains the values of A_s and δ which produce the best fit to the experimental data of τ_o versus R. Copies of the computer programs for the two models are given in Appendix I. Refractive index data were obtained from Van Os *et al*[13], and also, for the surfactants, from the Nikkol catalogue. Since only very limited refractive index data for the surfactants was available, some interpolation of the available data was necessary to estimate the values at the temperature and wavelength required.

The best fit curves obtained for both models for the experimental data for $C_{12}E_5$ / decane are shown in Figure 4.3.3*b* for data obtained from Figure 4.3.3*a*. Both models gave equally good fits to the experimental data and yielded similar values of A_s. Values of A_s are valid for the high R values, as described in section 4.2.3. All the estimates of A_s and δ are collected together in table 4.4. where it can be seen that models 1 and 2 generally give the same value of A_s within 10% or so.

The best fit values of δ were slightly different for the two models. This is expected since (as described in section 4.3.1) the quantity δ has a different significance in the two models. The δ values from model 1 are expected to correspond approximately to the thickness of the surfactant tail region whereas those from the model 2 fits should correspond to the overall surfactant shell thickness. However, the values in table 1 show that the model 1 δ values are generally slightly *larger* than those from model 2. The model 1 values are generally larger than the all-trans length of the surfactant tail and are probably a consequence of the fact that the surfactant headgroup region is unlikely to have a refractive index equal to that of water. Faced with the high uncertainty in assigning refractive index values to the different regions of the

---

[13]N. M. Van Os, J. R. Haak, L. A. M. Rupert. "Physico-chemical properties of selected anionic, cationic and nonionic surfactants", 1993, Elsevier Science Publishers B. V. Sara Burgerhartstraat 25, P. O. Box 211, 1000 AE Amsterdam, The Netherlands.

microemulsion droplets, the paramter δ is probably best regarded as an adjustable fitting constant.

Figure 4.3.3*a*
The variation of turbidity with temperature for a series of R values of 0.09 M $C_{12}E_5$ with decane.

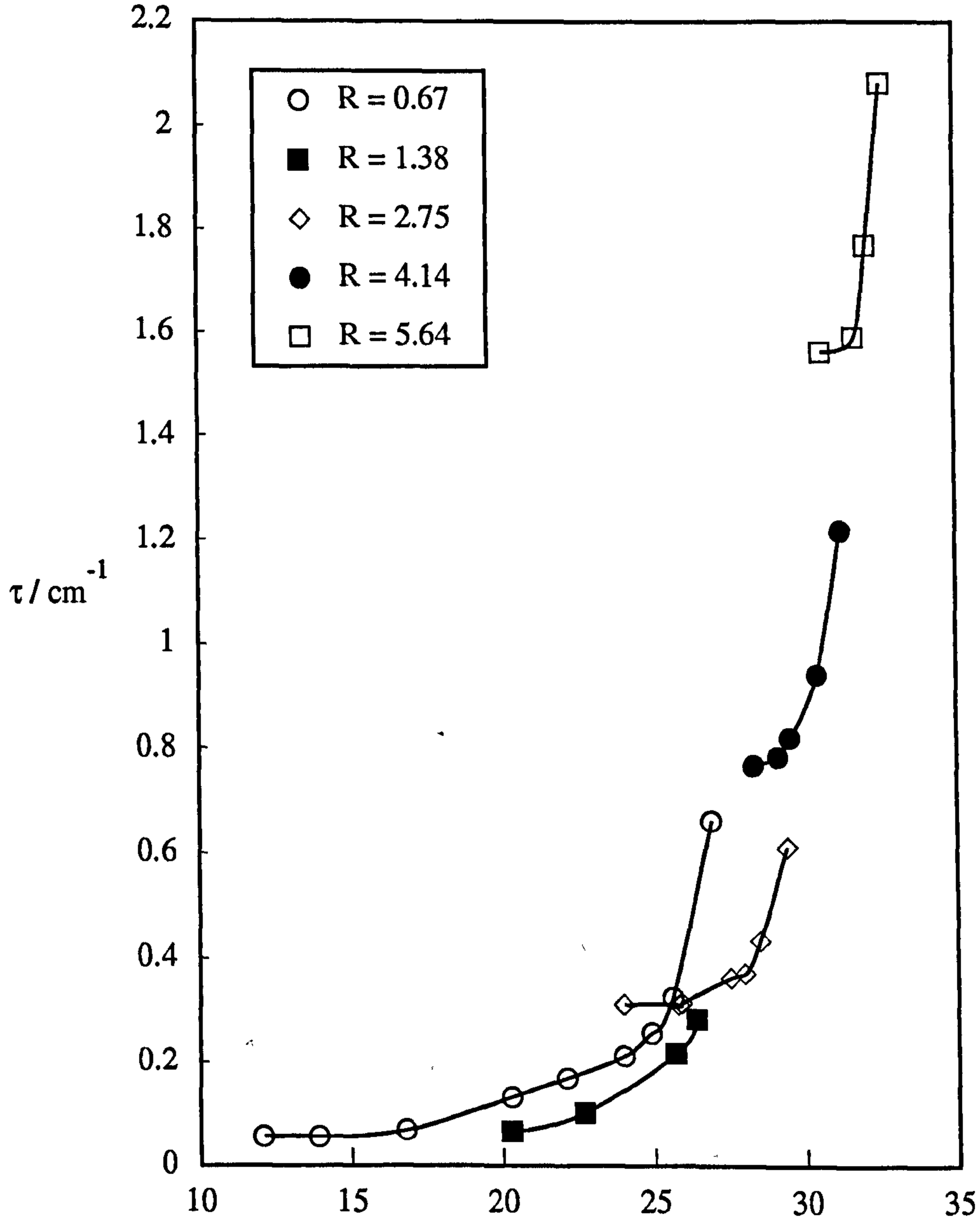

Figure 4.3.3*b*

The variation of the turbidity at the SPB, τ_o, with R for 0.09 M $C_{12}E_5$ with decane. The best fits to the two refractive index models are shown. The open circles are the experimental data points.

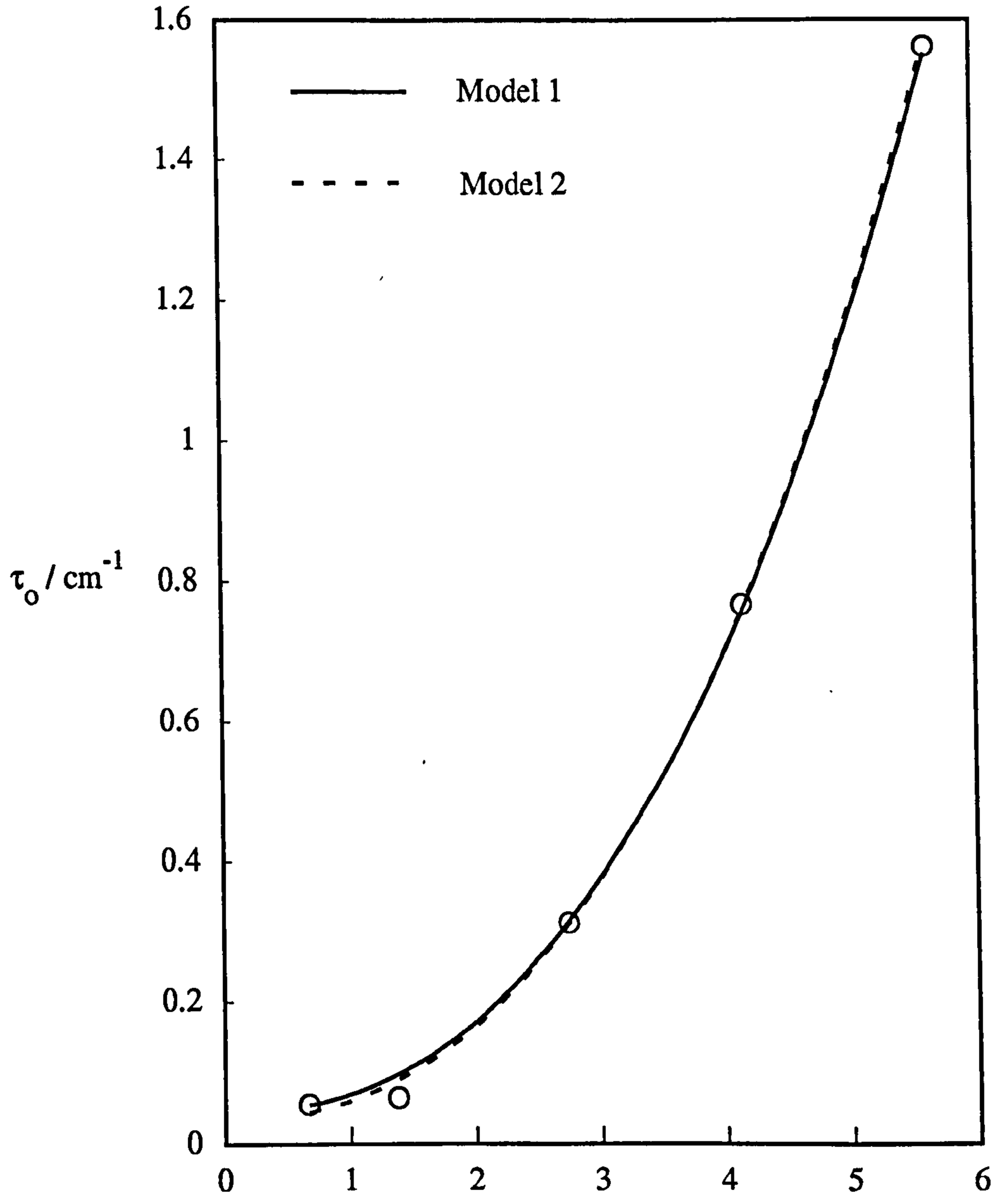

4.3.4 Effect of surfactant concentration.

The turbidities at the SPB of microemulsions of $C_{12}E_6$ with decane at three different surfactant concentrations were measured. As shown in table 4.4, the values of A_s and δ were found to agree within experimental error for the different surfactant concentrations which correspond to different droplet volume fractions. This data set supports the view (postulated in equation 4.1 *a*), that the droplet size at constant R is independent of droplet concentration. This independence of droplet size with droplet volume fraction is also supported by data reported in previous work for $C_{12}E_5$ with decane[14]. Additionally, it appears that the variation of turbidity with droplet volume fraction is correctly described by the hard sphere potential used in equation 4.3.1 *e*.[15]

4.4 Comparison and discussion of A_s measured by both turbidity and PCS data.

We now consider the values of A_s (which refer to high R values) collected together in table 4.4. We first compare the estimates from PCS and from turbidity. With the exception of the $C_{14}E_7$/decane system, the values all agree within approximately 10% which is estimated to be the uncertainty of the values. One possible cause of the lack of agreement in this case may arise from possible non-sphericity of the $C_{14}E_7$ droplets. Previous studies[16] have shown that in the binary system of 1.5% (0.029 M) $C_{14}E_7$ with water, the relative viscosity of the $C_{14}E_7$ solution to pure water increases considerably on increasing the temperature of the solution indicating a possible change of shape of the droplets, whereas with shorter surfactants the viscosity changes very little with temperature until the cloud point is reached. These findings could indicate that the microemulsion droplets of $C_{14}E_7$ with decane might not be spherical even at the SPB. Non-sphericity is expected to affect measurements from PCS and turbidity differently. The apparent droplet radius obtained from turbidity is derived from the measured scattering volume. In PCS, the radius is estimated from the measured diffusion coefficient on the assumption of sphericity. There could be many particles of the same volume but having different shapes and therefore different diffusion coefficients, and hence this disparity could result in contrasting apparent radii found by the two methods. Comparison of the enthalpy of clustering to the aggregation number for these systems (chapter 5, Table 5.3) suggests

---

[14]M. S. Leaver, U. Olsson, H. Wennerstrom, R. Strey, J. Phys. II France 1994, 4 ,515-531
[15] P. D. I Fletcher, J. F. Holzwarth, J. Phys. Chem. 1991, 95, 2550-2555

Table 4.4

Values for A_s (nm^2) and δ (nm) obtained by turbidity and PCS, listed by system variation for easy comparison.

System		τ Model 1		τ Model 2		PCS	
		A_s	δ_1	A_s	δ_2	A_s	δh
n-variations							
$C_{10}E_5$	+	0.35	2.7	0.38	2.1	0.32	2.0
$C_{12}E_5$	decane	0.38	2.6	0.39	2.0	0.41	3.0
$C_{12}E_7$	+	0.41	2.9	0.45	2.2	0.43	3.1
$C_{14}E_7$	decane	0.42	2.9	0.47	2.3	0.55	4.0
m-variations							
$C_{12}E_4$		0.38	2.9	0.39	2.2	0.42	3.6
$C_{12}E_5$	+	0.38	2.6	0.39	2.0	0.41	3.0
$C_{12}E_6$	decane	0.42	3.0	0.46	2.3	0.41	3.2
$C_{12}E_7$		0.41	2.9	0.45	2.2	0.43	3.1
oil length variations							
Heptane		0.42	3.5	0.47	2.2	0.39 *	3.3 *
Decane	+ $C_{12}E_5$	0.38	2.6	0.39	2.0	0.41	3.0
Tetradecane		0.29†	1.5	0.29	1.1	0.29*	3.0 *
n/m = 2							
$C_{10}E_5$		0.35	2.7	0.38	2.1	0.32	2.0
$C_{12}E_6$	+ decane	0.42	3.0	0.46	2.3	0.41	3.2
$C_{14}E_7$		0.42	2.9	0.47	2.3	0.55	4.0
[surf] variations							
0.016 M	$C_{12}E_6$	0.43	3.2	0.44	2.3	-	-
0.033 M	+	0.41	2.8	0.42	2.1	-	-
0.093 M	decane	0.42	3.0	0.46	2.3	-	-

† Calculation from data by Fletcher e*t al*[15] .

* PCS data for $C_{12}E_5$ with heptane and tetradecane from reference 2.

---

[16]M. Corti, C. Minero, V. Degiorgio, J. Phys. Chem. 1984, 88, 309.

that the turbidity data gave the more appropriate value for A_S of 0.42 nm^2, as other systems having the same A_S yielded similar enthalpies.

The effect on A_S by the variation of the structure of the surfactant and oil can be summarised as follows (and shown graphically in Figures 4.4 (i) - (iv)):

(i) Increasing the length of the surfactant tail group leads to an increase in A_S and therefore a decrease in the surfactant packing density of the monolayer (Figure 4.4 (i)).

(ii) Altering the size of the surfacant head group has no significant effect on A_S.(Figure 4.4 (ii))

(iii) Increasing the alkane oil chain length leads to a decrease in A_S, and hence the monolayer is more closely packed. An explanation of this could be that the longer chain alkanes penetrate the tail area of the surfactant monolayer less than the shorter chains[2], allowing closer packing of the surfactant monolayer (Figure 4.4 (iii))

(iv) Increasing the overall surfactant length (at n/m = 2) increases A_S and therefore the monolayer is less closely packed, the dominant factor being the increase in the surfactant tail length since, as established earlier, head group size has no effect (Figure 4.4 (iv)).

There has been little previous literature in which A_S values are quoted as defined here - as the area occupied by the surfactant tail at the curved interface between the droplet oil core and the surfactant monolayer at the preferred curvature. However it is interesting to compare these A_S values to other published values of area per surfactant molecule. In contrast to (ii) above, the area per surfactant molecule at the planar air/water interface has been found to increase with increasing head group size. $C_{12}E_4$, $C_{12}E_6$, $C_{12}E_7$, $C_{12}E_8$ measured at 25°C yield areas of 0.44, 0.45, 0.48, and 0.61nm^2 respectively [13,17]). At the planar air/water interface there is no limiting effect of the surfactant tails as at the curved interface of the microemulsion droplets. The head groups are therefore more free to interact with the surrounding water molecules reducing the packing density at the interface and thus resulting in a greater area per surfactant molecule for the larger head groups.

---

[17]M. J. Rosen, "Surfactants and interfacial phenomena", J. Wiley and Sons Inc. U.S.A.

Figure 4.4

The variation of A_s with n,m or x for C_nE_m/C_x systems.

Open squares = PCS data. Closed squares = turbidity data fitted to model 1.

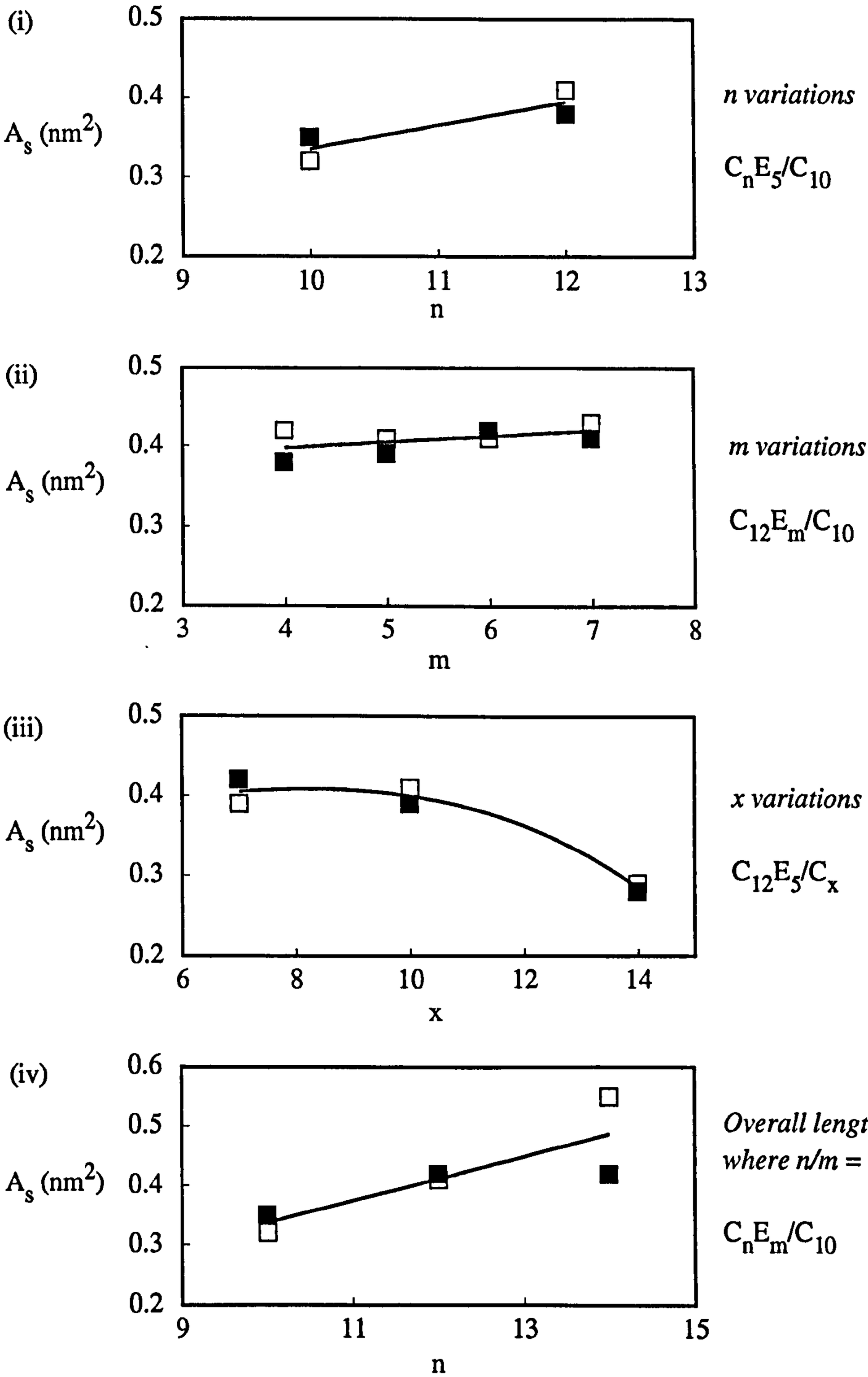

Calculation from data produced by Fukuda *et al*[18] in complementary work for the $C_{12}E_5$ with decane system at a surfactant to oil weight ratio of 52/48 (corresponding to R=2.65), yields a value of 0.44 nm^2 for the area per surfactant (A_i) at the polar/apolar interface separating the hydrocarbon tail group from the head group of the surfactant. Noting that also, as reported earlier in section 4.2.3, the hydrodynamic radius measured for this system by the same research group agrees with this work, this value is in accord with the A_s of 0.41nm^2 reported here, since for geometric reasons the area at the polar/apolar interface would be expected to be larger than that at the oil core/surfactant monolayer interface.

[18]K. Fukuda, U. Olsson, Langmuir, 1994, 10, 3222.

CHAPTER FIVE

5 Equilibrium behaviour of the clustering/growth process for oil-in-water microemulsion droplets.

5.1 Introduction

Turbidity and PCS measurements are consistent with the theory that microemulsion droplets at the SPB behave as weakly interacting spheres (with the possible exception of the system $C_{14}E_7$ with decane), and that measurements at the SPB therefore correspond to individual droplets. The size of the scattering particle increases with increasing temperature, either by clustering of the droplets, while retaining the original size of the individual droplets, or by growth forming larger droplets, or a combination of the two (as discussed in chapter 4). Calculation of the increased size of the scattering particle is possible from turbidity measurements. The turbidity of a sample of fixed composition is proportional to the average volume of the scattering particle (V_p in equation 4.3.1*a*) for increasing temperature. If the turbidity τ_o at the SPB (at temperature T_o), relates to the individual non-interacting droplets, then the ratio of the turbidity (τ) at a temperature (T) *above* the SPB with τ_o, gives the average number (n) of original droplets in each scattering particle as a function of temperature. See figure 5.1.a.

$$n = \tau/\tau_o \qquad (5.1a)$$

Assuming that only clustering occurs and no droplet growth, n corresponds to the number of droplets per cluster. If droplet growth occurs n is a measure of the extent of the growth.

The mechanism for the droplet clustering or droplet growth process assumed in the ensuing calculations can be represented as a series of equilibria.

$$\begin{aligned} &(1) && D + D <=> D_2 \\ &(2) && D + D_2 <=> D_3 \\ &(3) && D + D_3 <=> D_4 \\ &(i) && D + D_i <=> D_{(i+1)} \end{aligned} \qquad (5.1b)$$

Figure 5.1a

The variation of turbidity with temperature for 0.093 M $C_{12}E_6$ with decane at R = 1.0. n, the number of original sized droplets in a particle at temperature T is given by τ/τ_o as described in the text (section 5.1).

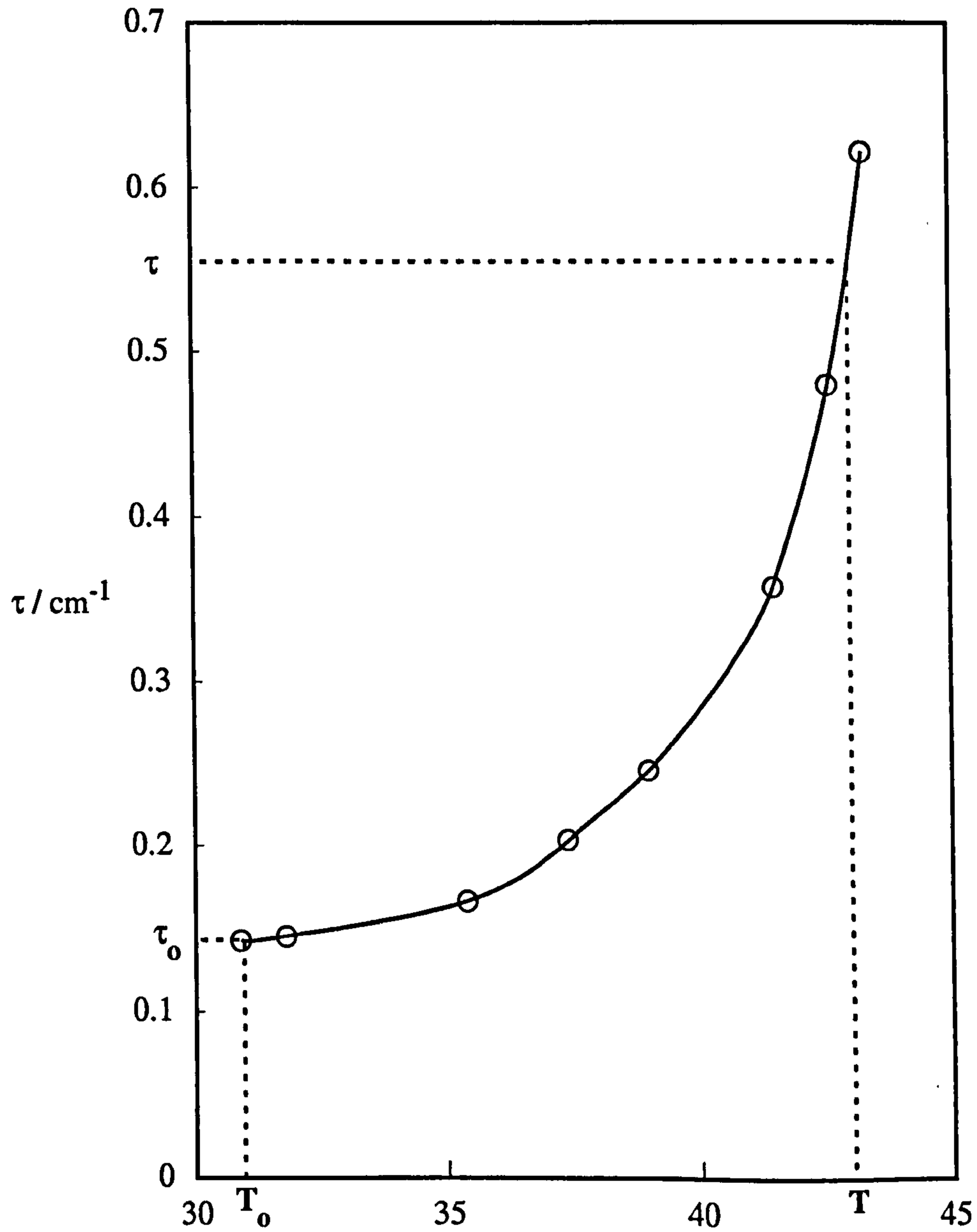

D represents a droplet of the size found at the SPB, i.e. of the original size, and D_i a cluster containing i original droplets. The following work assumes that the equilibrium constant for each addition of one drop are equal i.e:

$$K_1 = K_2 = K_3 \cdots\cdots K_i = K.$$

Note that implicit within this model is that the equilibrium constant for the formation of one particular cluster size is the same for any combination i.e the equilibrium constant for the formation of D_7 is the same for combinations of $(D_1 + D_6)$ or $(D_3 + D_4)$ etc.
The total concentration of original droplets C_d, and of droplet clusters C_c are given by:

$$C_d = [D] + 2[D_2] + 3[D_3] + \cdots i[D_i] \qquad (5.1c)$$

$$C_c = [D] + [D_2] + [D_3] + \cdots + [D_i] \qquad (5.1d)$$

The average number of original sized droplets in the cluster/coalesced particle is thus related by:

$$n = C_d / C_c \qquad (5.1e)$$

And n is related to the equilibrium constant, K, for this linear aggregation model by the following derivation[1].

Clustering may proceed by any combination of droplets, and the clustering rate (forward rate R_f) is given by

$$R_f = k_f([D_1]+[D_2]+[D_3]+.....[D_i])^2 = k_f C_c^2 \qquad (5.1f)$$

where k_f = the forward rate constant.

The rate of *unclustering* depends on the equilibrium concentration (α) of droplet-droplet "bonds", i.e. for 4 clustered droplets the number of droplet-droplet bonds = 3, (Figure 5.1b)

[1]D. Pörschke, F. Eggers, Eur. J. Biochem, 1972, 26, 490.

Figure 5.1b

Schematic diagram of the number of droplet-droplet bonds between four clustered droplets.

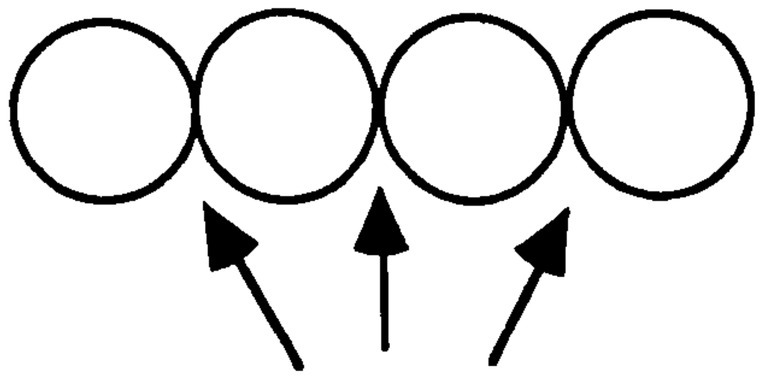

3 bonds between

4 droplets

The concentration of bonds between droplets is given by:

$$\alpha = [D_2]+2[D_3]+3[D_4]+4[D_5]+.....(i-1)[D_i] \qquad (5.1g)$$

the rate of unclustering (reverse rate R_r) is therefore given by:

$$R_r = k_r\alpha \qquad (5.1h)$$

where k_r = the reverse rate constant.

The rate of change of droplet bond formation is therefore:

$$d\alpha/dt = k_f C_c^{\,2} - k_r\alpha \qquad (5.1i)$$

at equilibrium $d\alpha/dt = 0$ therefore

$$k_f C_c^{\,2} = k_r\alpha \qquad (5.1j)$$

The equilibrium constant $K = k_f/k_r$

and therefore $$K = \alpha / C_c^{\,2} \qquad (5.1k)$$

note that $\alpha = C_d - C_c$ therefore:

$$K = (C_d - C_c)/C_c^2 \qquad (5.1l)$$

$$K = (C_d/C_c^2) - (C_c/C_c^2) \qquad (5.1m)$$

remembering that $n = C_d/C_c$, then:

$$K = (n/C_c) - (1/C_c) \qquad (5.1n)$$

and hence: $$KC_d = n^2 - n \qquad (5.1o)$$

The equilibrium constant K can therefore be simply calculated from turbidity measurements.

The validity of the equilibrium model can be tested for different droplet concentrations, varied by changing the surfactant concentration for a fixed R value, and checking the constancy of K.

The temperature dependence of K can be used to yield the enthalpy change of the clustering/growth process using van't Hoff plots from the equation:

$$d(\ln K)/d(1/T) = -\Delta H^o/ R' \qquad (5.1p)$$

where ΔH^o is the change in enthalpy of the clustering/growth process

R' is the gas constant.

T is the absolute temperature.

The standard entropy change (ΔS^o) can also be obtained using:

$$\Delta G^o = -R'T\ln K \qquad (5.1q)$$

and

$$\Delta G^o = \Delta H^o - T\Delta S^o \qquad (5.1r)$$

5.2. Testing the validity of the equilibrium model using van't Hoff plots for different droplet concentrations

Plots of ln K versus 1/T (equation 5.1p) are shown in Figures 5.2.1(a - j) for a series of C_nE_m/x alkane oil/water microemulsion systems, each varying in surfactant (droplet) concentration but at a fixed R value (fixed droplet size). The results show that, as predicted, K increases with increasing temperature i.e. that clustering/growth becomes more favourable. From the theory, K should be the same for all droplet concentrations at a particular temperature, therefore the plots for all concentrations should be represented by a single line. The results show that the model fits reasonably well for the middle surfactant concentration range of 0.04 - 0.10 M. At the lower droplet concentrations the calculated n values are more inaccurate, since at these concentrations the turbidities are less, hence the error in the absorbance readings becomes more significant (up to 30 %). The value of K is observed to decrease with increasing droplet concentration indicating that the model is then no longer applicable. The deviation from the model could be partly explained by shape changes affecting the clustering/growing behaviour. The higher surfactant (droplet) concentrations for the $C_{14}E_7$ with decane system produce curved van't Hoff plots as seen clearly in Figure 5.2.1j. As discussed in section 4.4 $C_{14}E_7$ may form non-spherical droplets even at the SPB which may be the cause of the different droplet behaviour. Previous studies[2,3,4] have also shown that microemulsion systems containing C_nE_m surfactants and alkane oils are likely to undergo changes from spherical droplets/globular clusters into rods or cylindrical shapes with increasing temperature. Previous work by Garland and Christian[5] suggested a statistical argument for an equilibrium scheme of multiple aggregation of nucleoside bases, in which the equilibrium constant decreases for an *increasing* number of bases in the aggregate (equivalent to n in this work). However, a calculation of n (as described in section 5.1) near the UTPB shows that n tends to be smaller for increased surfactant (droplet) concentration (Table 5.2(a)). In this work therefore K decreases with a *decreasing* n and thus such a model would not describe the behaviour observed in this work. A model which would incorporate the change in K with higher droplet concentrations would be highly complex, and involve the use of further estimated parameters. At this stage therefore it was deemed appropriate to employ the simple model for comparisons at the relevant droplet concentrations.

---

[2]M. Leaver, I. Furo, U. Olsson, Langmuir, 1995, 11, 5, 1524.
[3]P.-G. Nilsson, B. Lindman, J. Phys. Chem. 1984, 88, 4764.
[4]R. Aveyard, B. P. Binks, P. D. I. Fletcher, Langmuir, 1989, 5, 5, 1210.
[5]F. Garland, S. D. Christian, J. Phys. Chem. 1975, 79, 1247.

Figure 5.2.1
Van't Hoff plots obtained for C_nE_m surfactants with alkane oils at varying surfactant concentration.

(a) $C_{10}E_5$ with decane at R = 1.5.

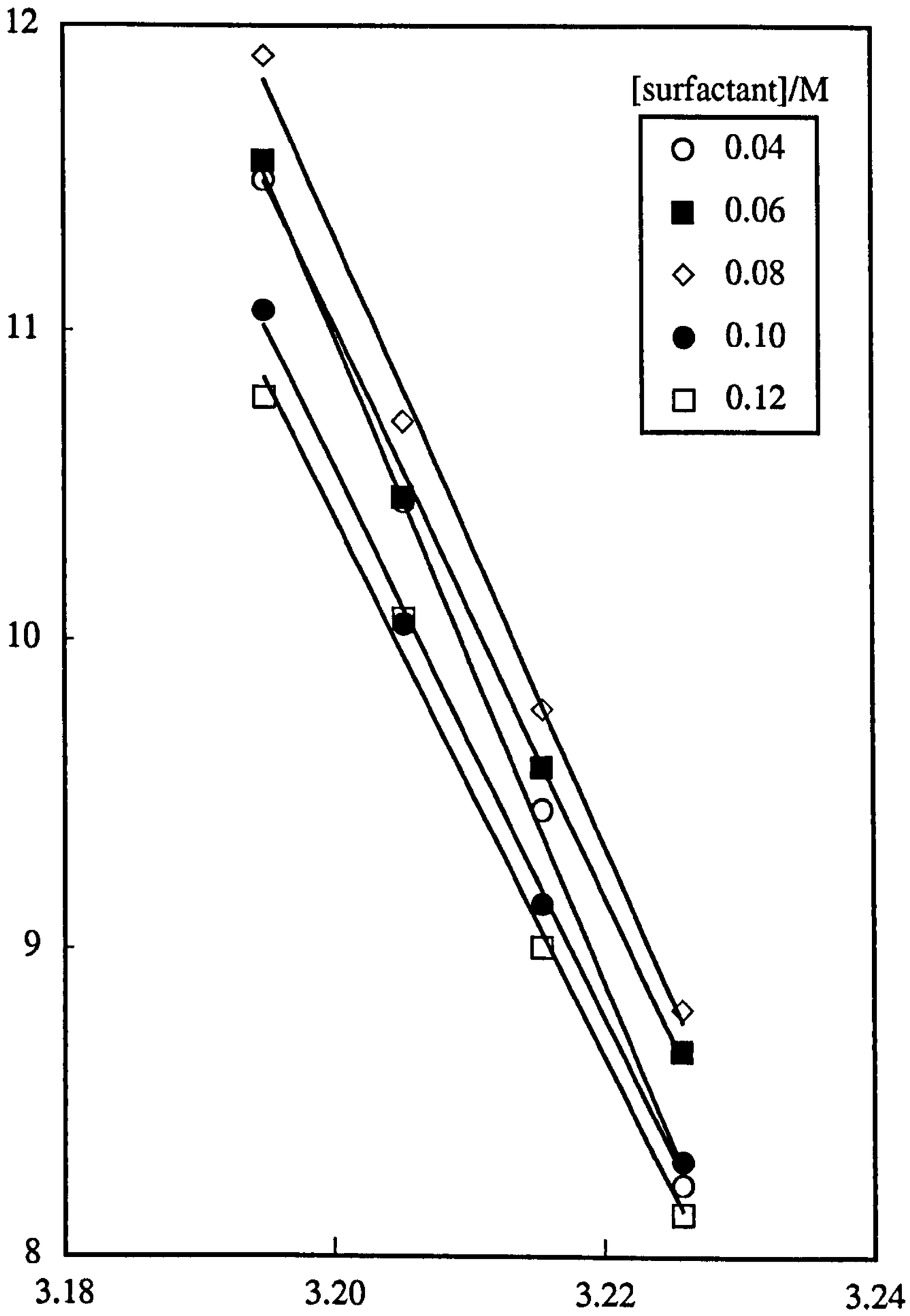

Figure 5.2.1
Van't Hoff plots obtained for C_nE_m surfactants with alkane oils at varying surfactant concentration.

(b) $C_{10}E_5$ with decane at R = 2.5.

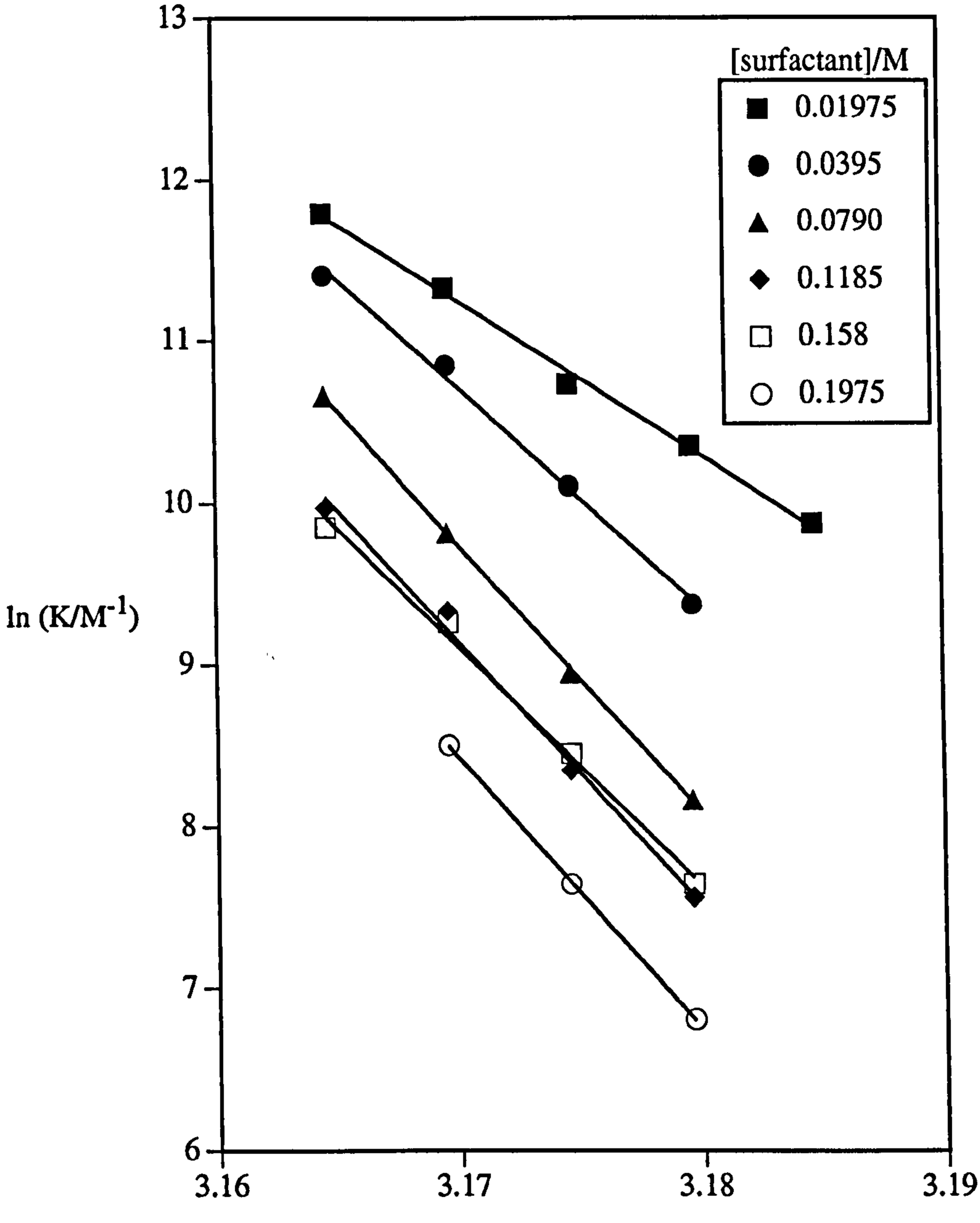

From unpublished experimental results by P. D. I. Fletcher, University of Hull.

Figure 5.2.1
Van't Hoff plots obtained for C_nE_m surfactants with alkane oils at varying surfactant concentration.

(c) $C_{12}E_5$ with heptane at R = 2.5.

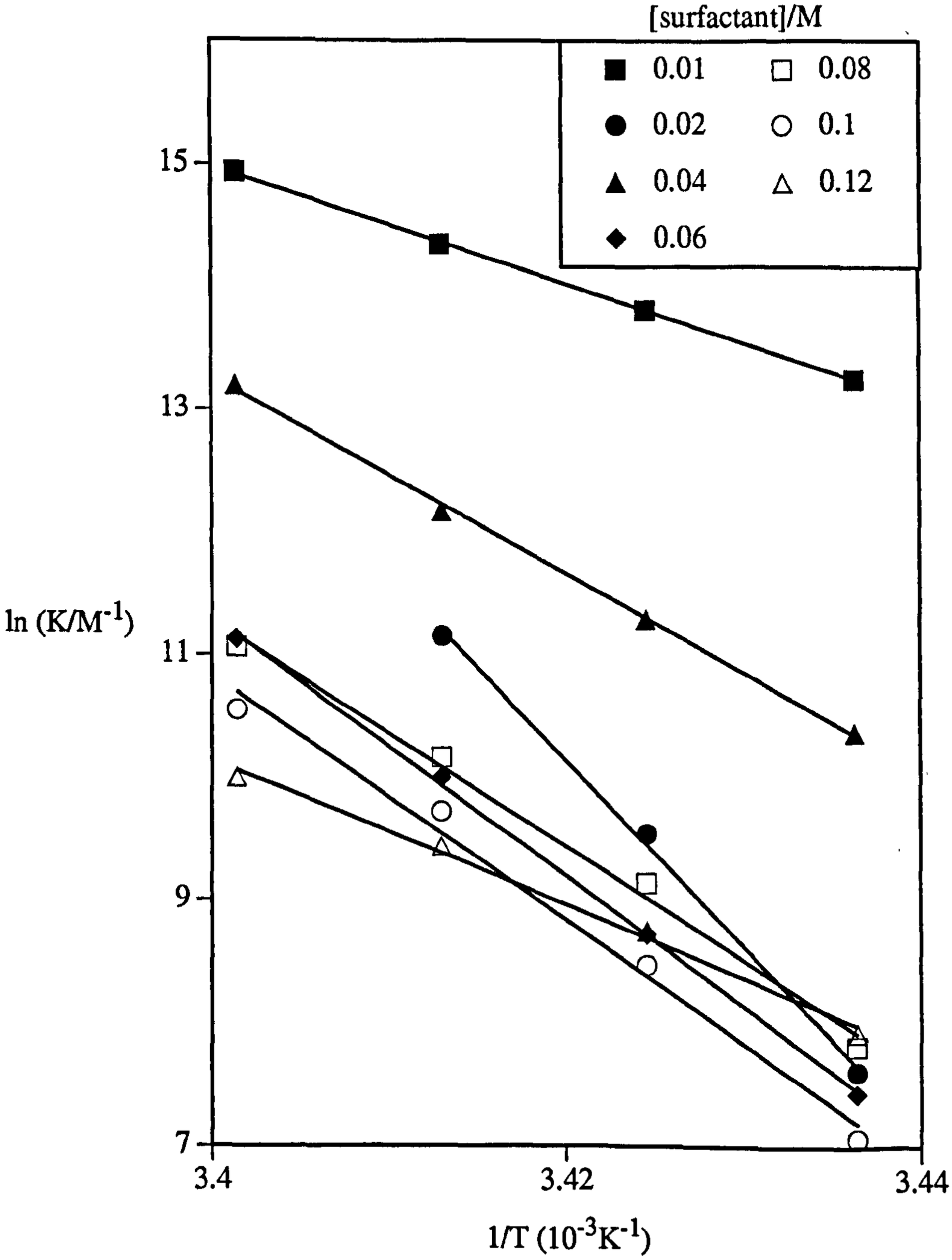

Figure 5.2.1
Van't Hoff plots obtained for C_nE_m surfactants with alkane oils at varying surfactant concentration.

(d) $C_{12}E_5$ with decane at R = 1.5.

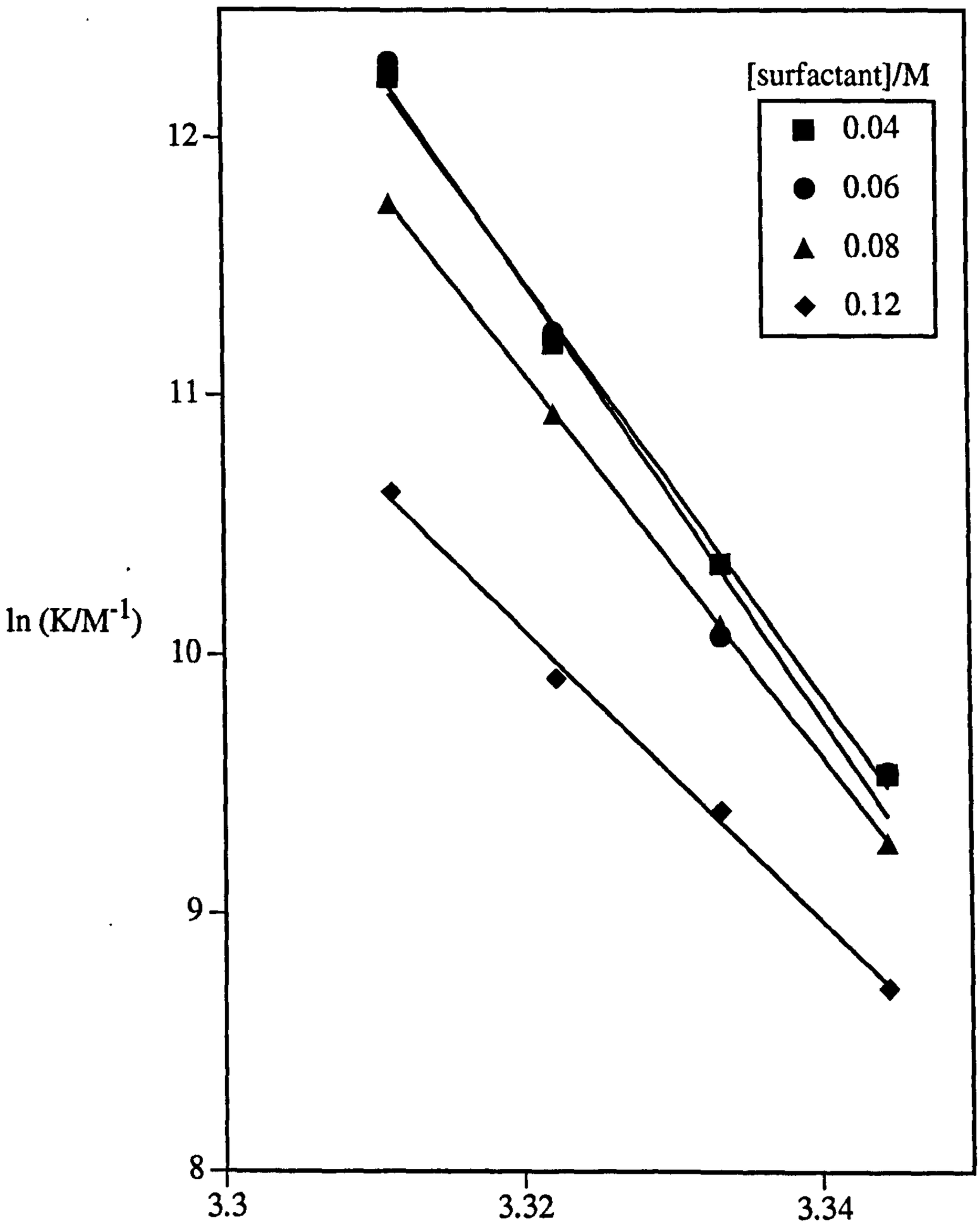

Figure 5.2.1
Van't Hoff plots obtained for C_nE_m surfactants with alkane oils at varying surfactant concentration.

(e) $C_{12}E_5$ with decane at R = 2.5.

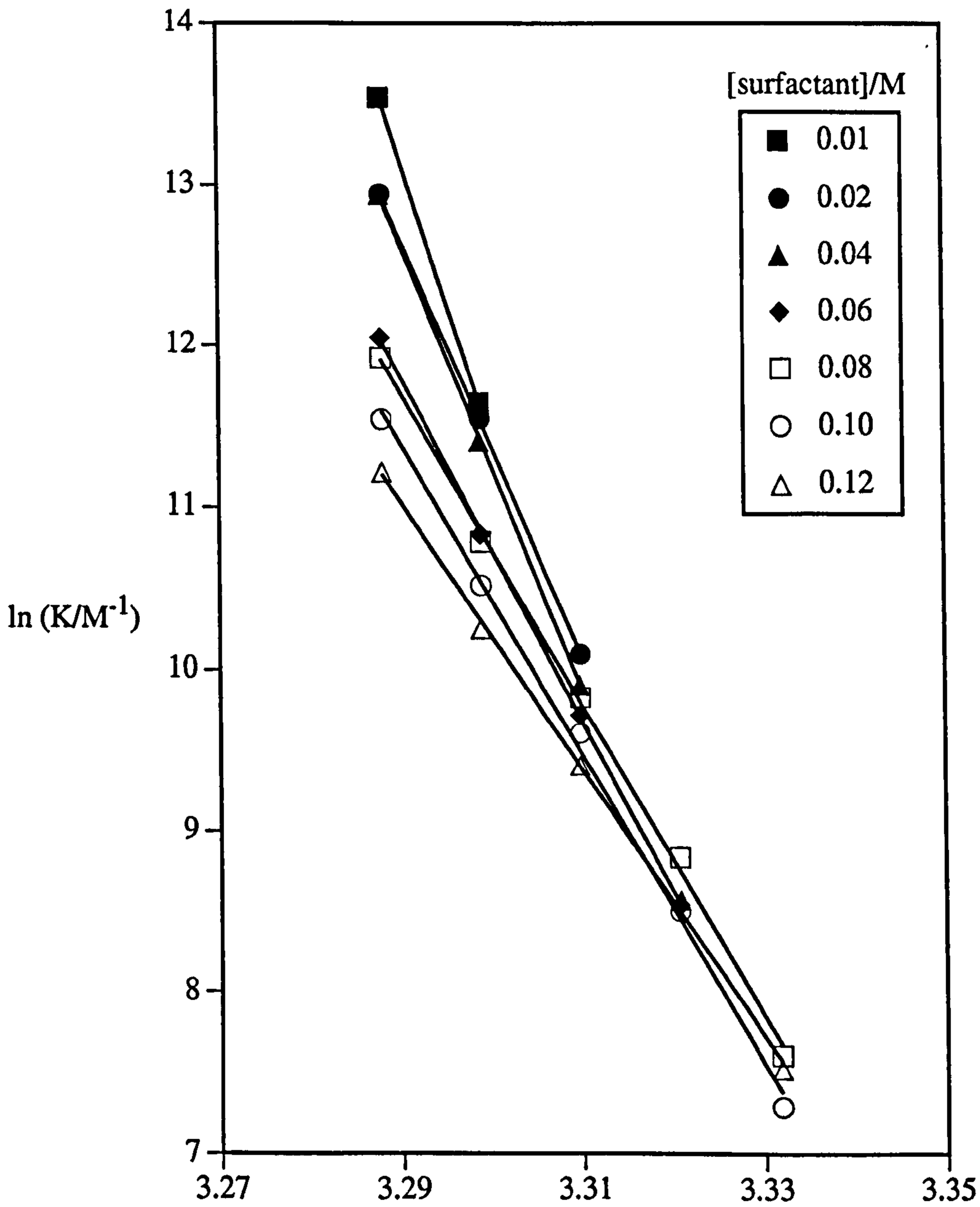

Figure 5.2.1
Van't Hoff plots obtained for C_nE_m surfactants with alkane oils at varying surfactant concentration.

(f) $C_{12}E_5$ with tetradecane at R = 1.26.

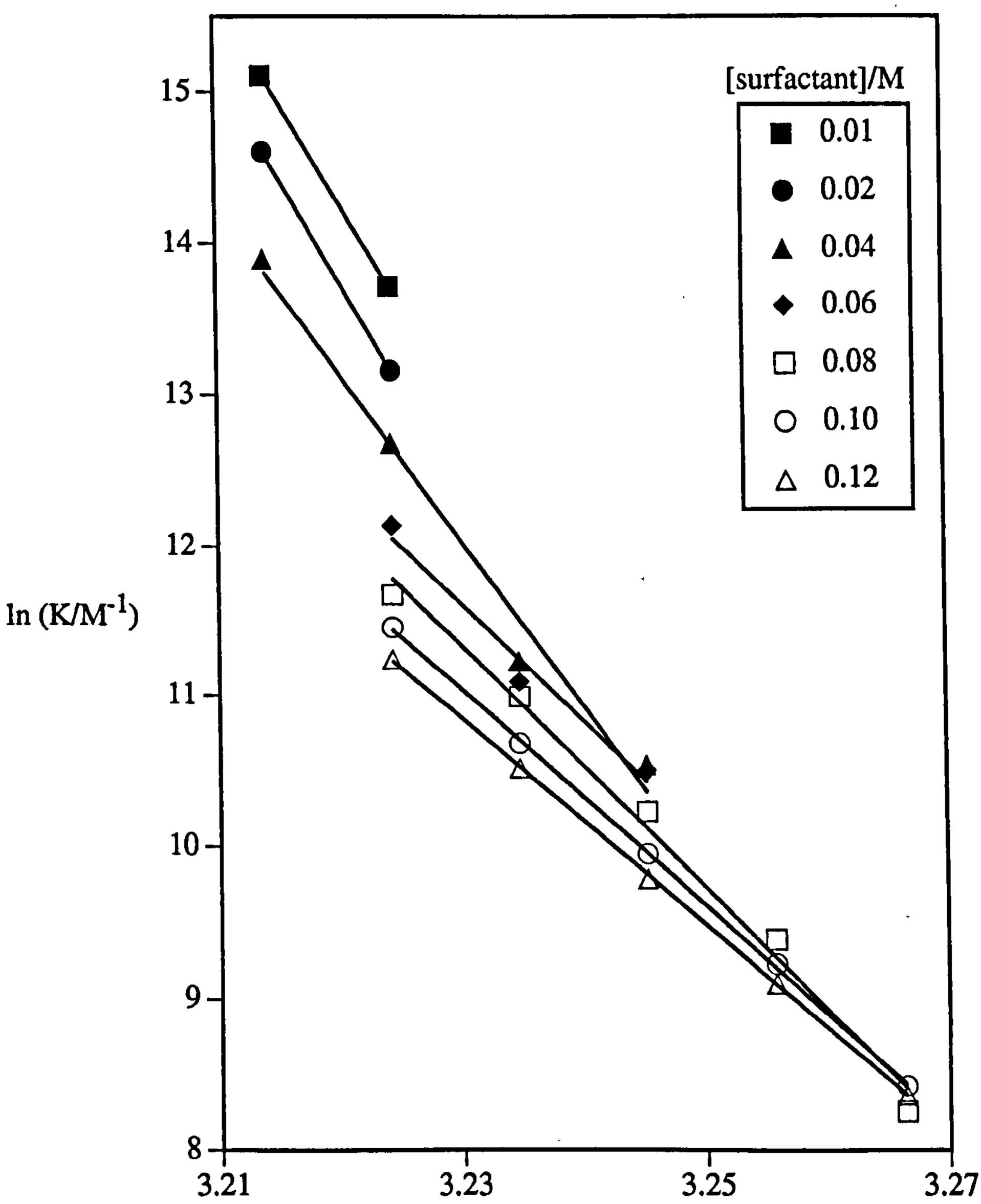

Figure 5.2.1
Van't Hoff plots obtained for C_nE_m surfactants with alkane oils at varying surfactant concentration.

(g) $C_{12}E_6$ with decane at R = 1.5.

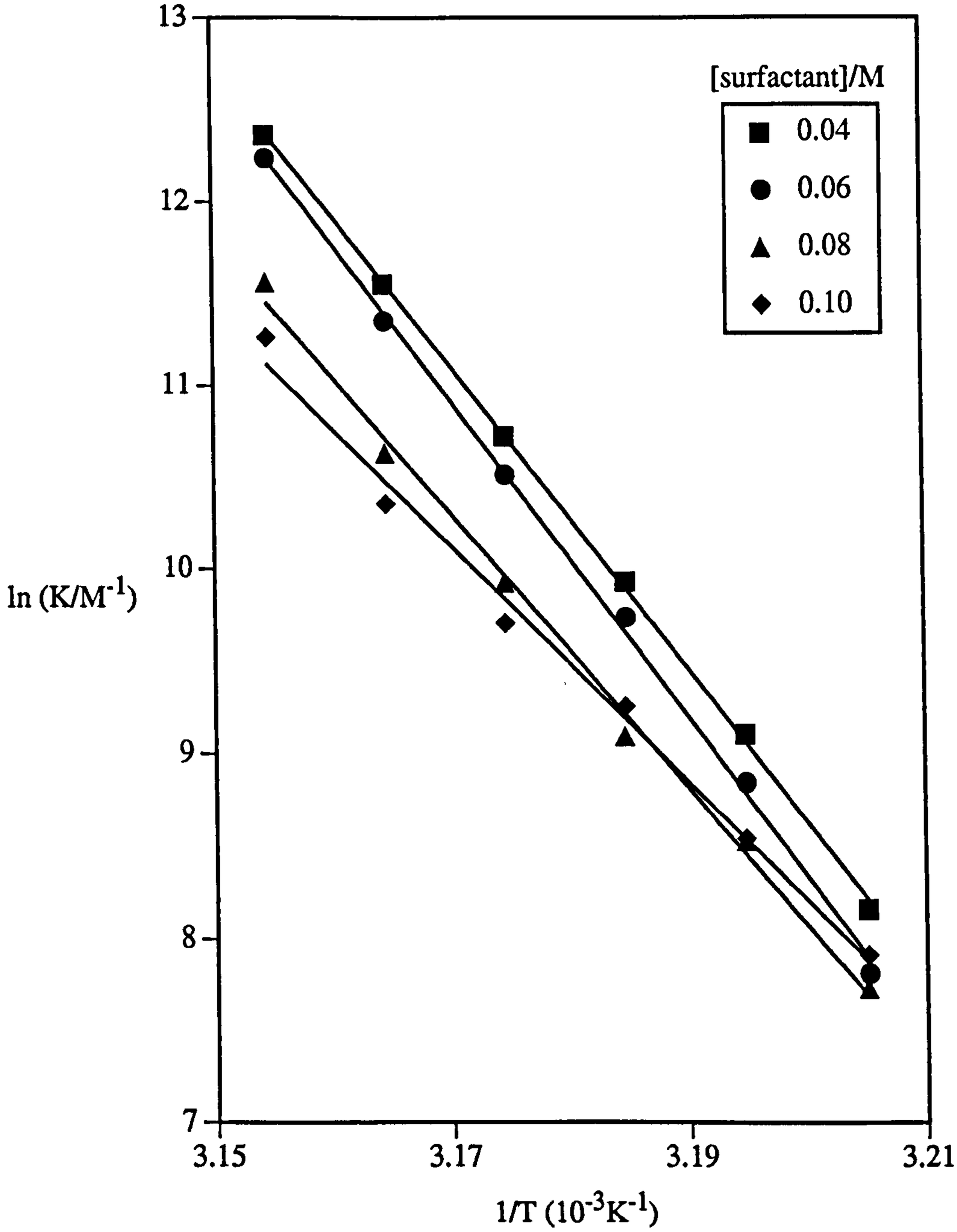

Figure 5.2.1
Van't Hoff plots obtained for C_nE_m surfactants with alkane oils at varying surfactant concentration.

(h) $C_{12}E_6$ with decane at R = 2.5.

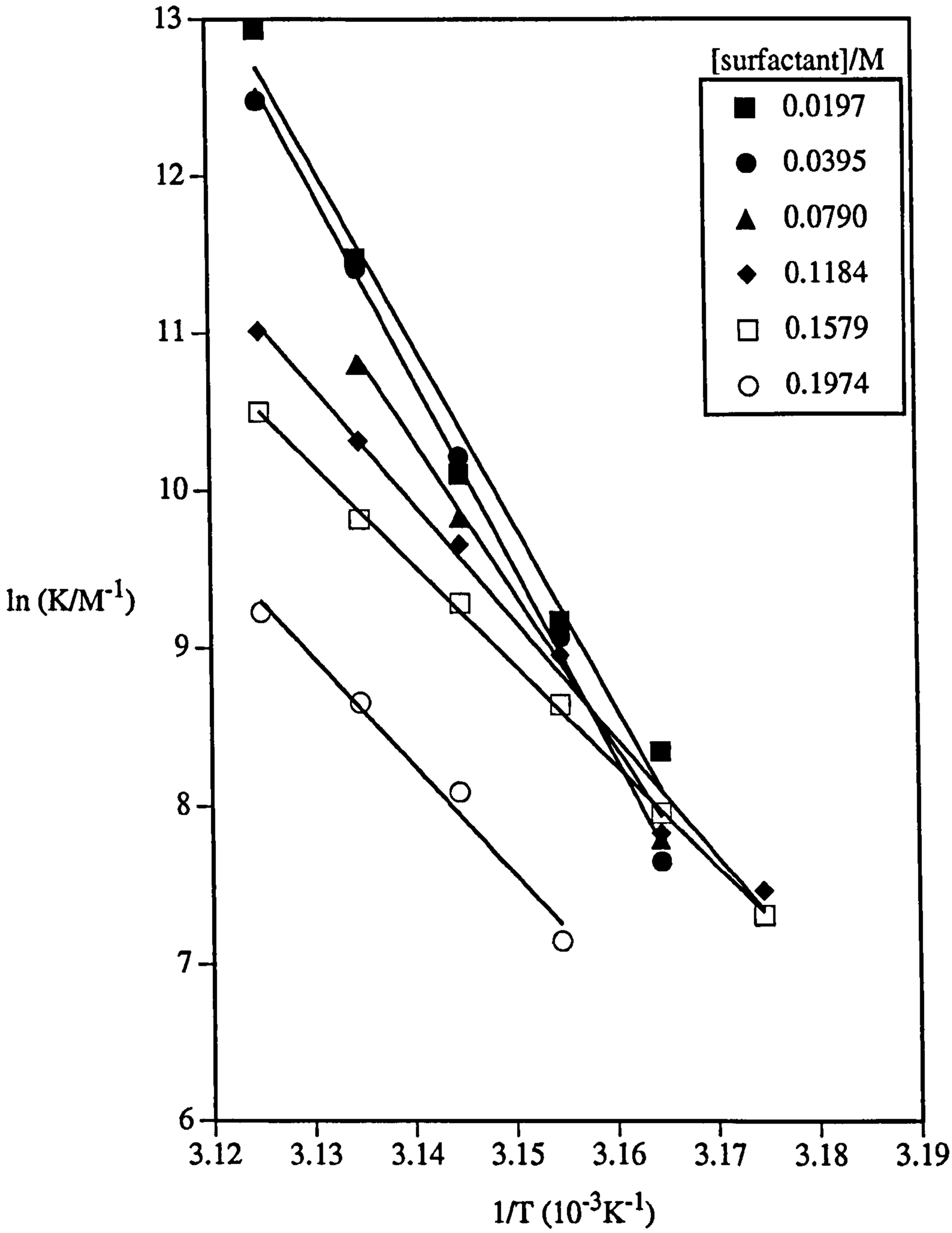

From unpublished experimental results by P. D. I. Fletcher, University of Hull.

Figure 5.2.1
Van't Hoff plots obtained for C_nE_m surfactants with alkane oils at varying surfactant concentration.

(i) $C_{12}E_7$ with decane at R = 2.5.

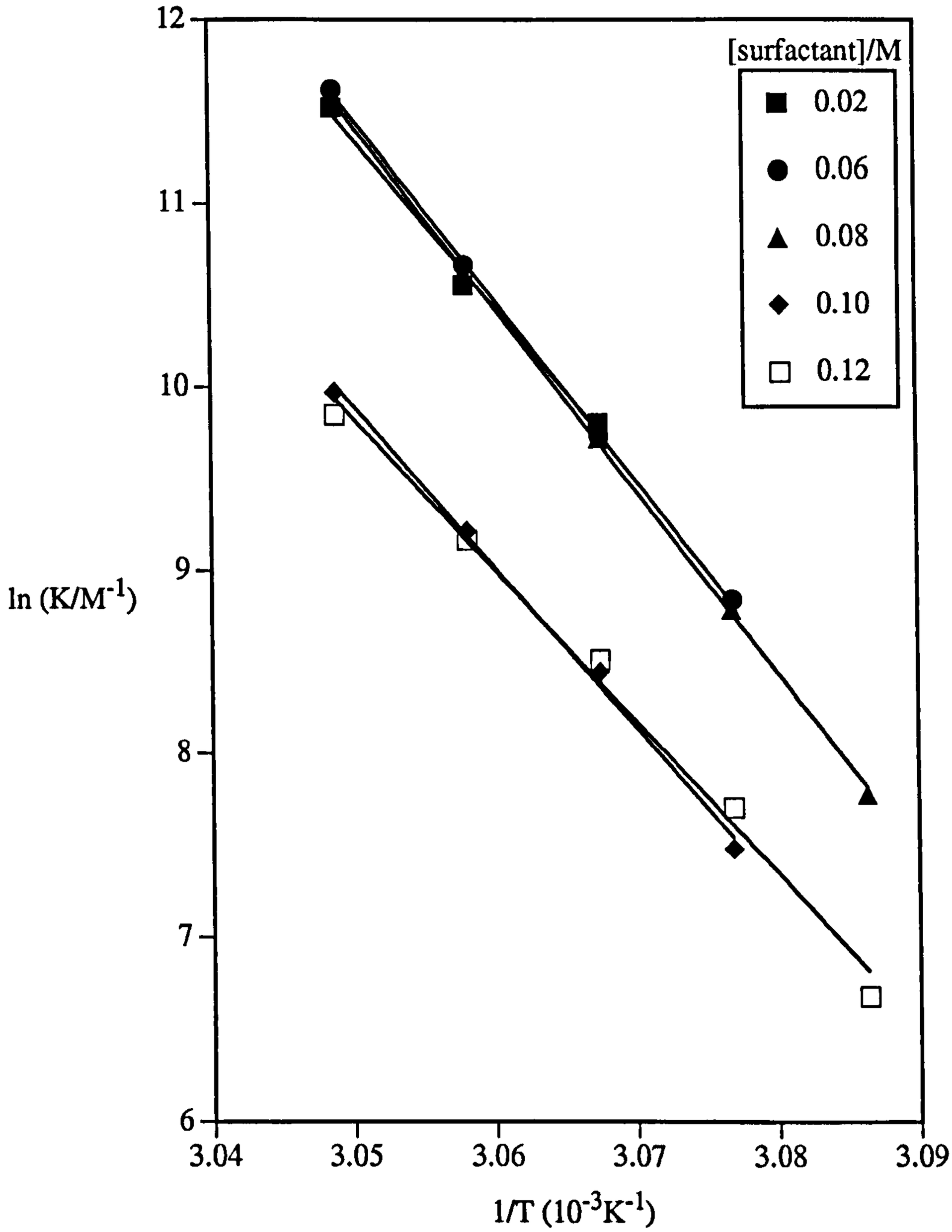

Figure 5.2.1
Van't Hoff plots obtained for C_nE_m surfactants with alkane oils at varying surfactant concentration.

(j) $C_{14}E_7$ with decane at R = 2.5.

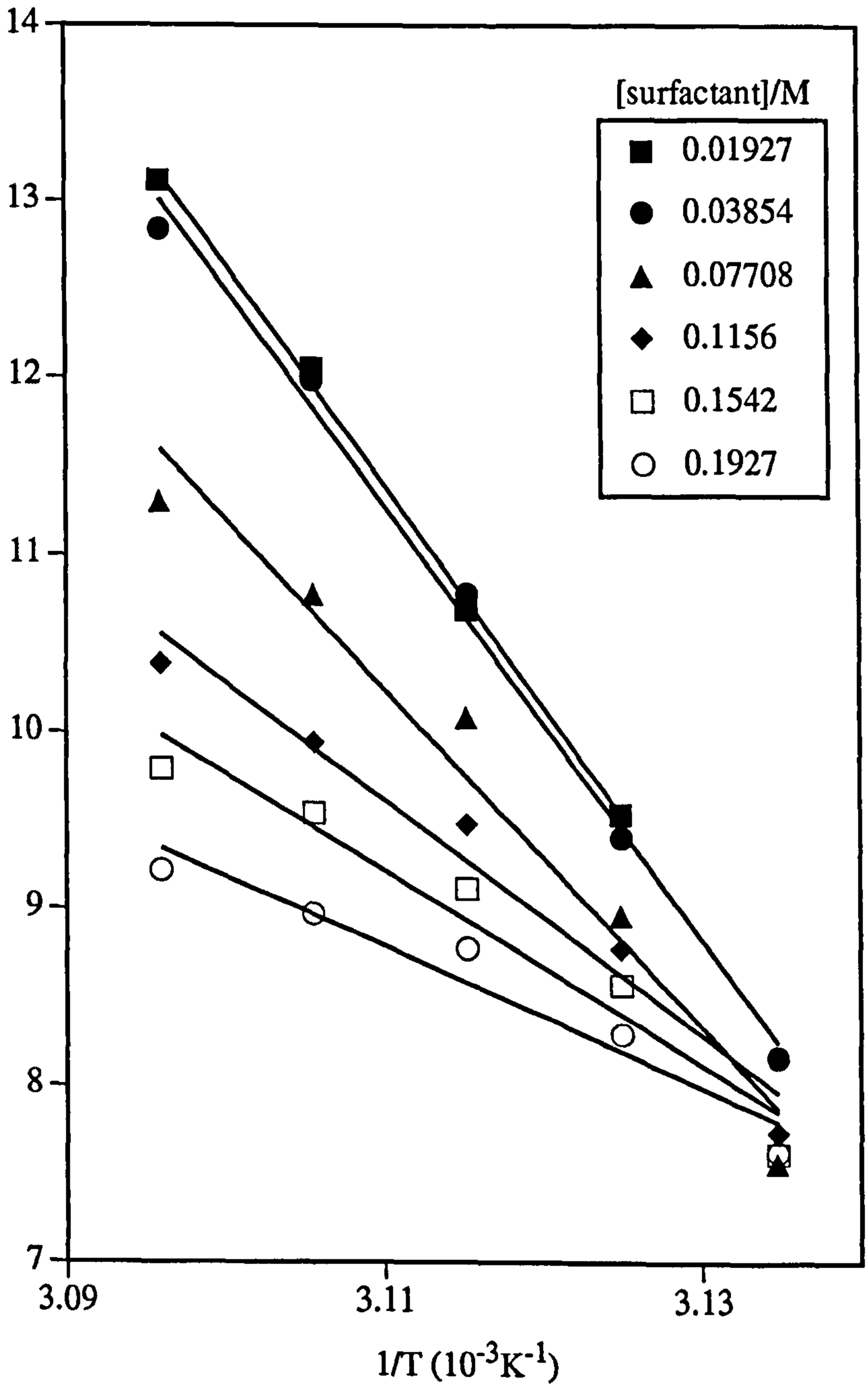

From unpublished experimental results by P. D. I. Fletcher, University of Hull.

Table 5.2 Calculation of n from turbidity data at temperatures approximately 0.1°C below the UTPB.

(a) For varying surfactant concentration.

$C_{12}E_7$ with decane at R = 2.5

[Surfactant] / M	T / °C	n
0.04	55.4	8.7
0.06	56.4	6.4
0.08	55.6	4.6
0.10	56.5	3.6
0.12	56.5	3.2

$C_{12}E_6$ with decane at R = 1.5.

[Surfactant] / M	T / °C	n
0.04	44.7	10.0
0.06	44.7	11.2
0.08	44.7	8.2
0.10	44.7	7.7

(b) For varying R value.

0.093 M $C_{12}E_6$ with decane

R	T (°C)	n
0.5	42.8	9.5
1.0	43.5	5.3
2.0	45.0	3.0
3.0	45.8	2.5
4.0	47.2	1.4

The van't Hoff plots for systems having varying R values at fixed surfactant concentration are shown in Figures 5.2.2(a - g). A comparison of K *at a particular temperature* shows that K decreases with increasing R value, i.e. for increasing drop size and decreasing droplet concentration. This is as expected since for these systems the temperature boundaries of the single phase microemulsion region increases for increasing R value. A particular temperature will therefore represent a different stage in the clustering behaviour for different R values, i.e. it could represent a point approaching the upper temperature phase boundary for a lower R value (almost maximum clustering hence a high K) compared to a point just above the solubilisation phase boundary for a high R value (little clustering, low K). Highly curved plots are again found for $C_{14}E_7$ systems at high droplet concentration (lower R values) (Figure 5.2.2g). A calculation of the number of droplets in a cluster near the UTPB for the different R values shows that n decreases for increasing R (Table 5.2(b)), indicating that a critical size or curvature is reached before phase separation occurs.

Figure 5.2.2
Van't Hoff plots obtained for C_nE_m surfactants with alkane oils at varying R values.

(a) 0.08 M $C_{10}E_5$ with decane.

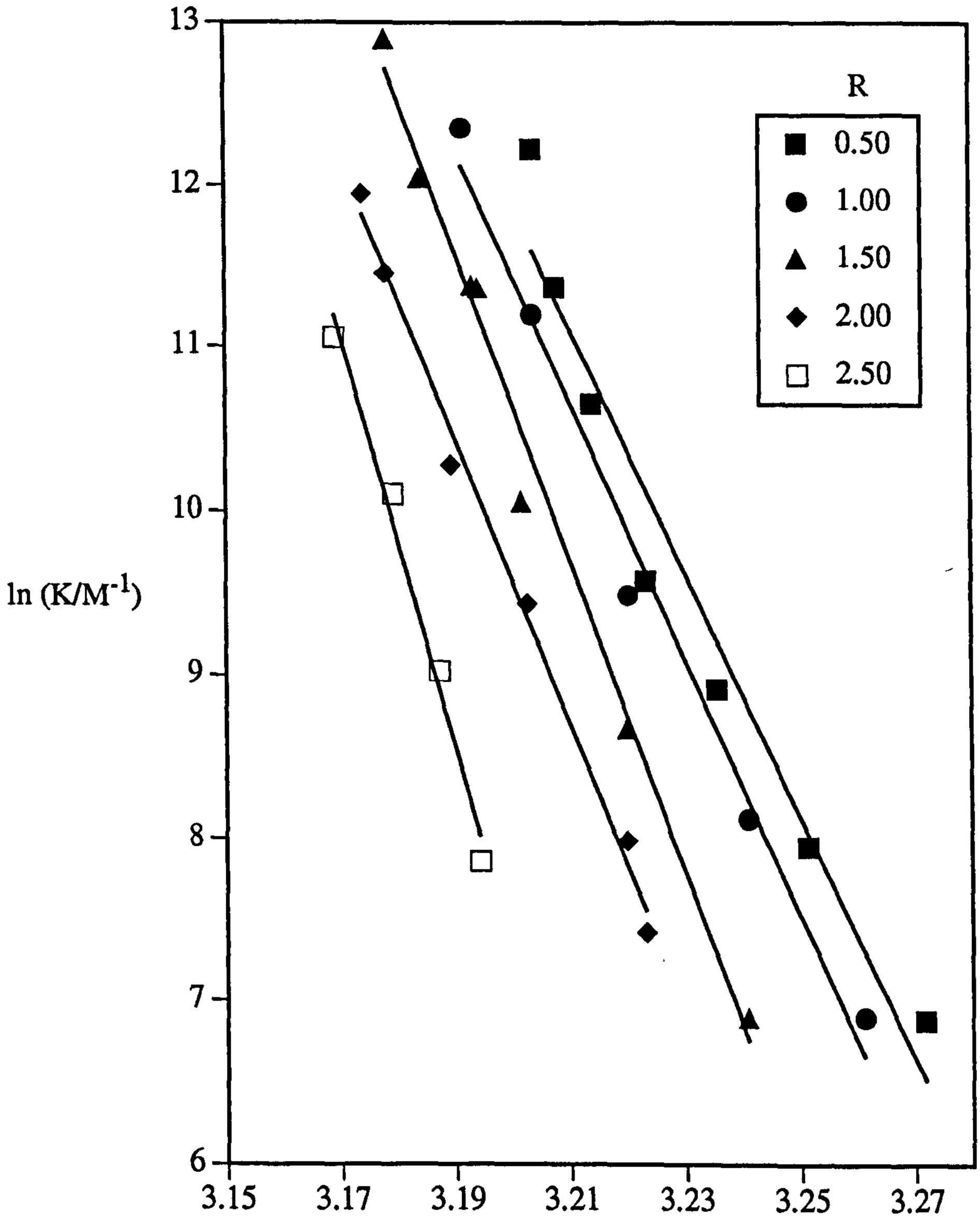

Figure 5.2.2
Van't Hoff plots obtained for C_nE_m surfactants with alkane oils at varying R values.

(b) 0.09 M $C_{12}E_5$ with heptane.

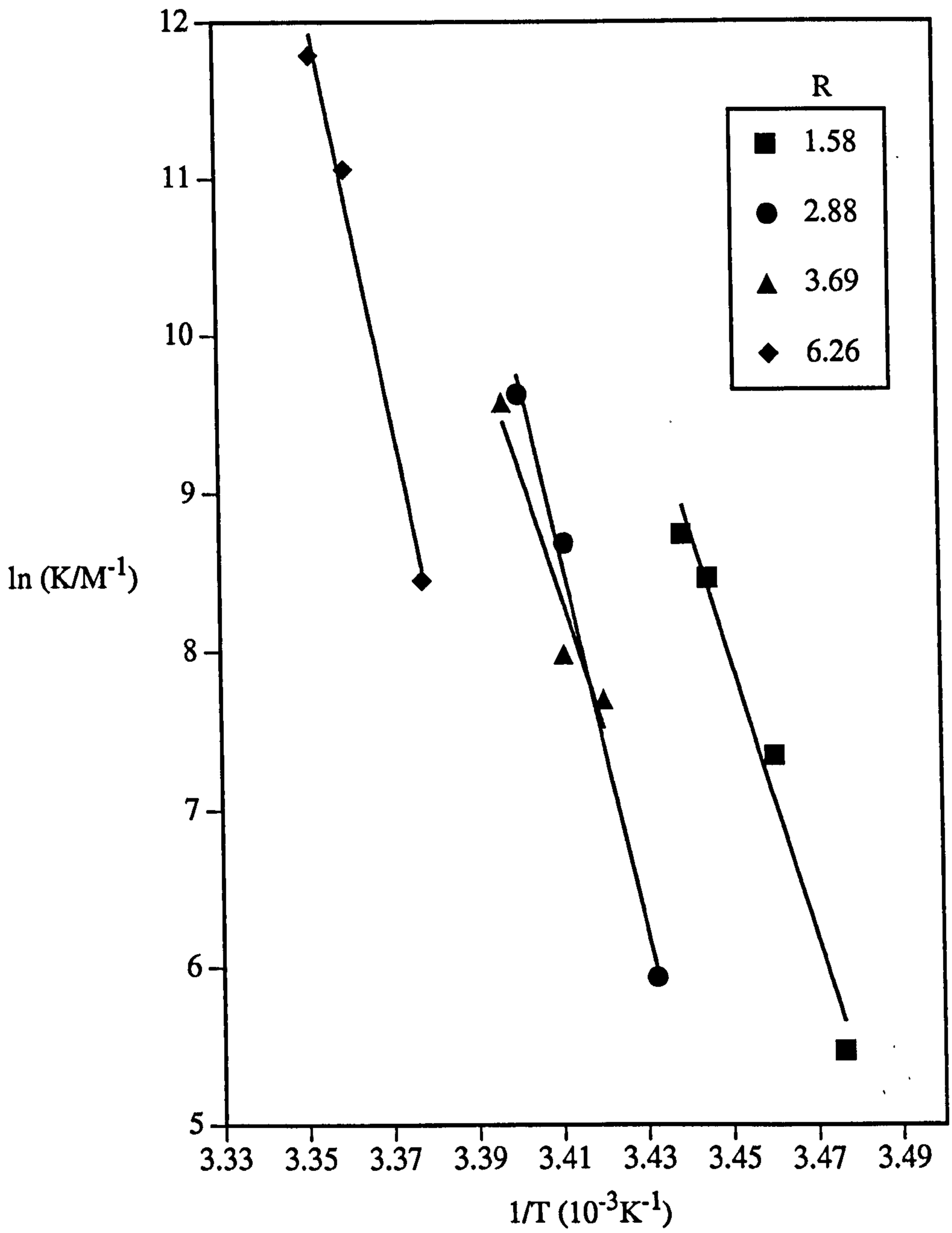

Figure 5.2.2
Van't Hoff plots obtained for C_nE_m surfactants with alkane oils at varying R values.

(c) 0.09 M $C_{12}E_5$ with decane.

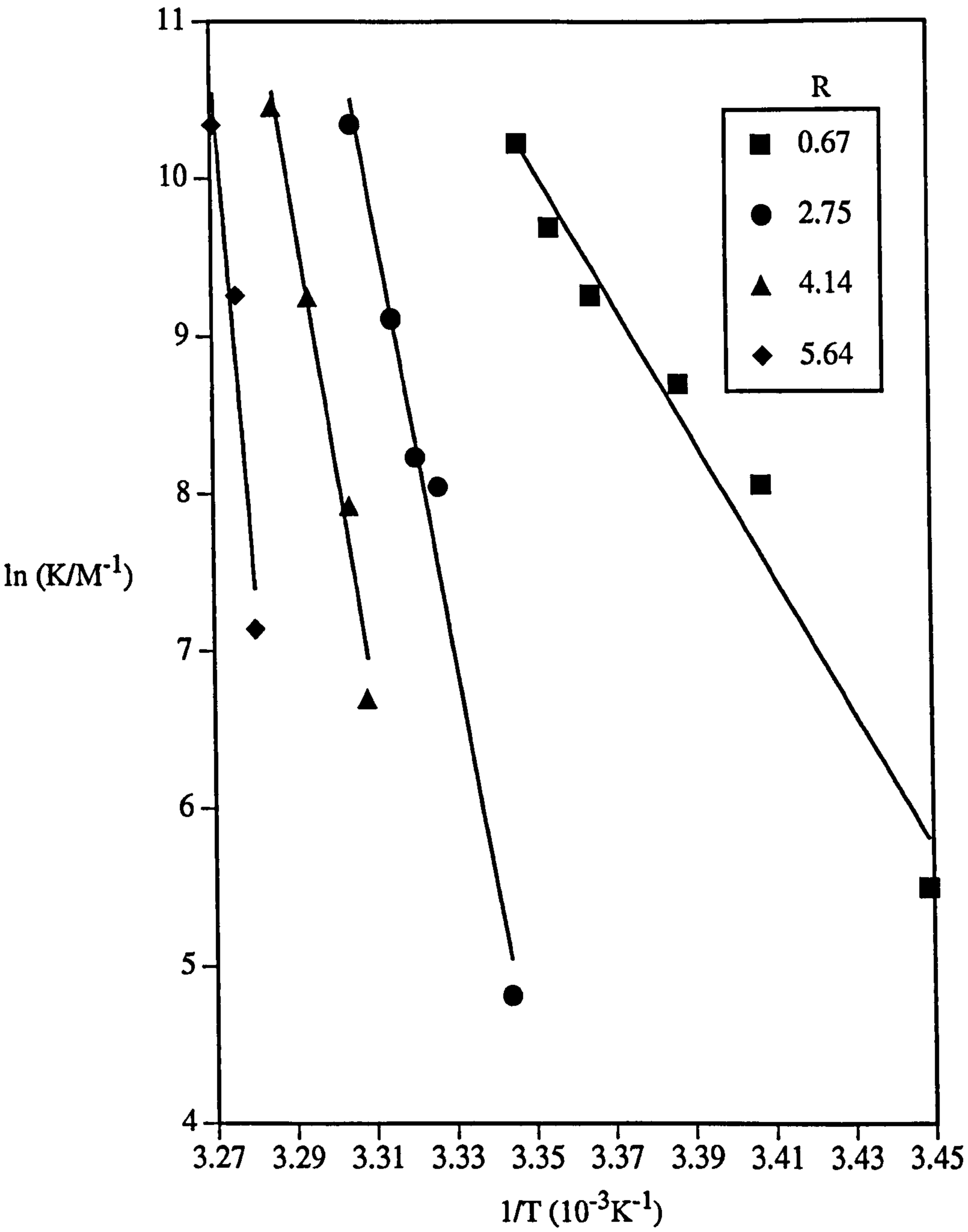

Figure 5.2.2
Van't Hoff plots obtained for C_nE_m surfactants with alkane oils at varying R values.

(d) 0.014 M $C_{12}E_5$ with tetradecane.

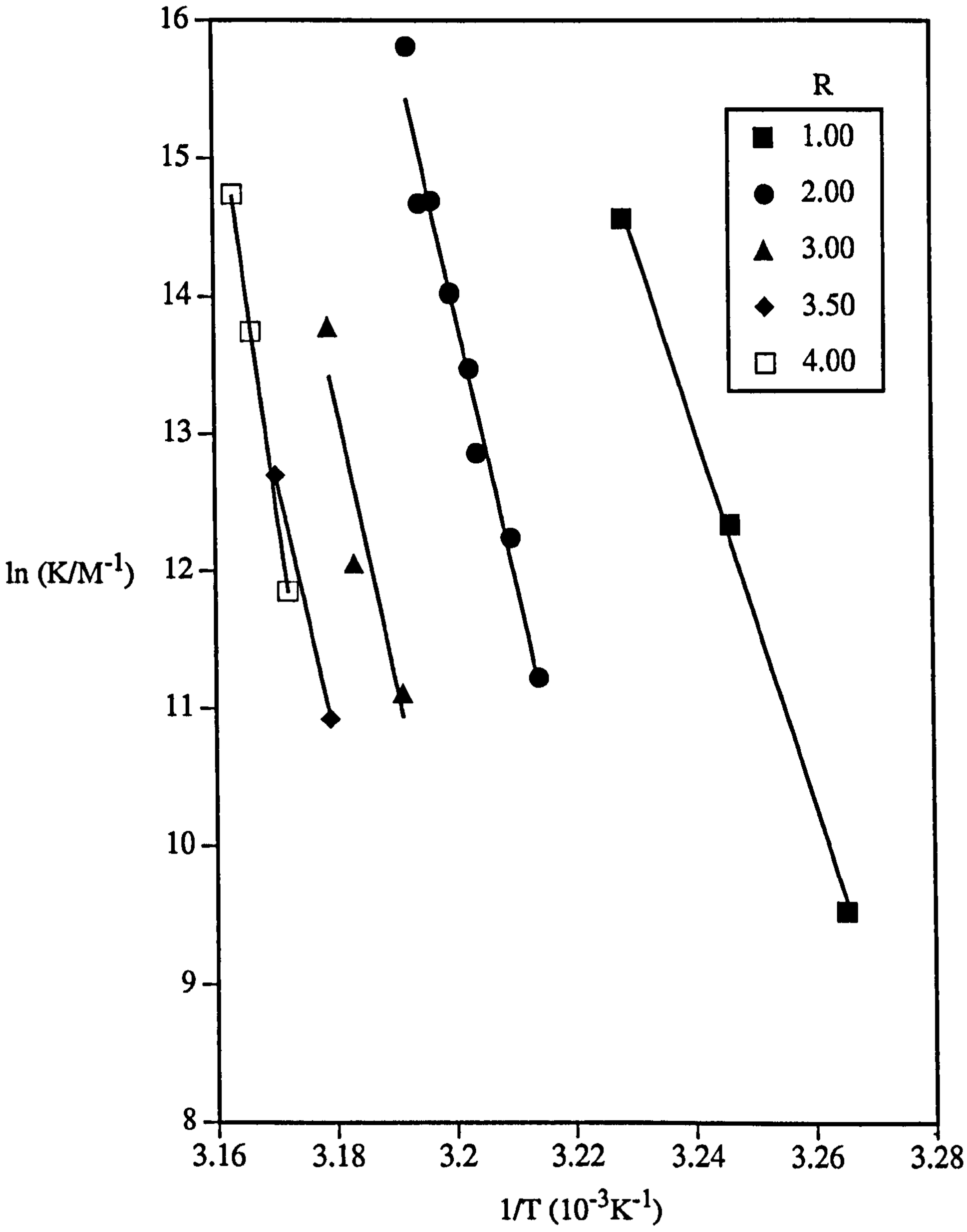

Figure 5.2.2
Van't Hoff plots obtained for C_nE_m surfactants with alkane oils at varying R values.

(e) 0.09 M $C_{12}E_6$ with decane.

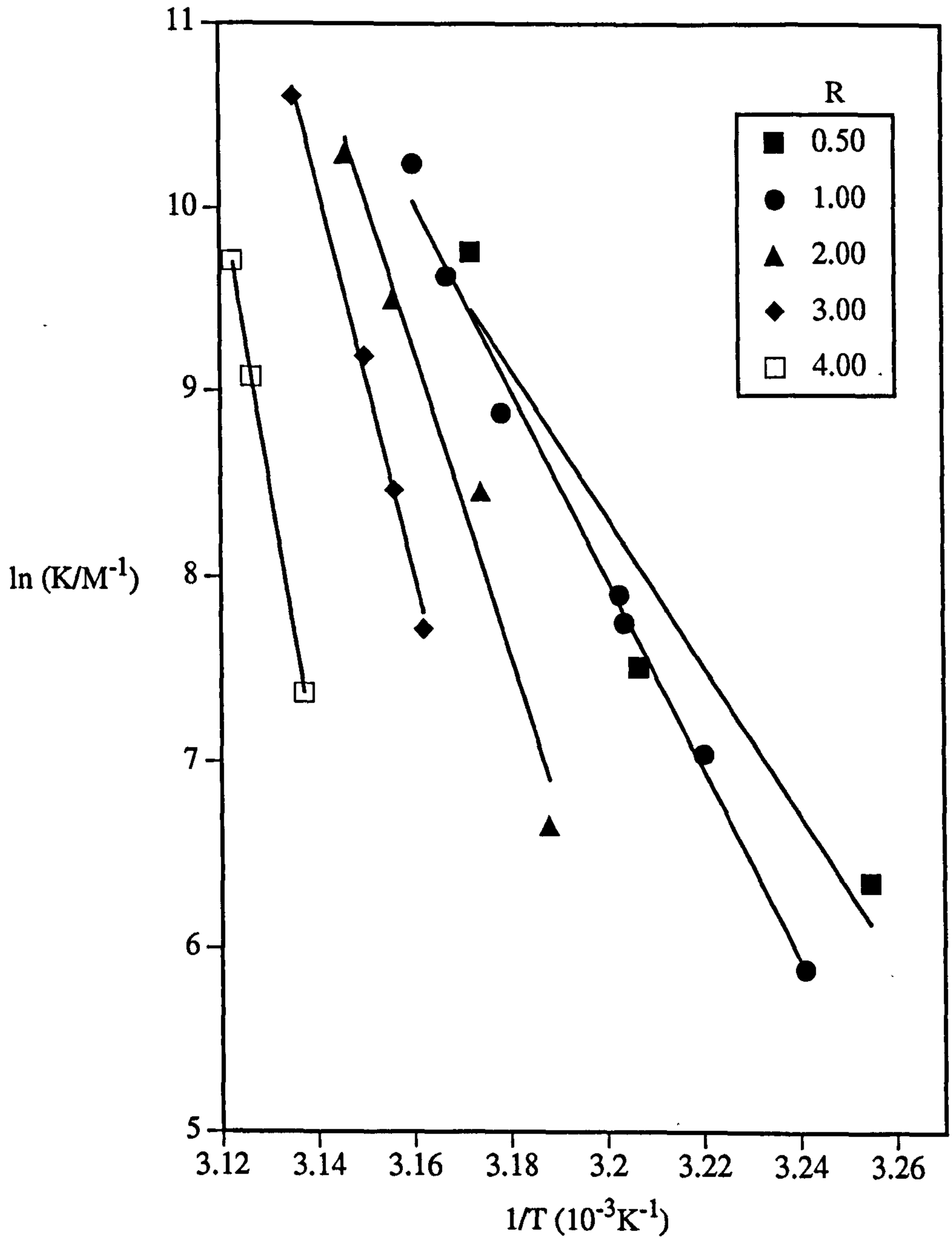

Figure 5.2.2
Van't Hoff plots obtained for C_nE_m surfactants with alkane oils at varying R values.

(f) 0.09 M $C_{12}E_7$ with decane.

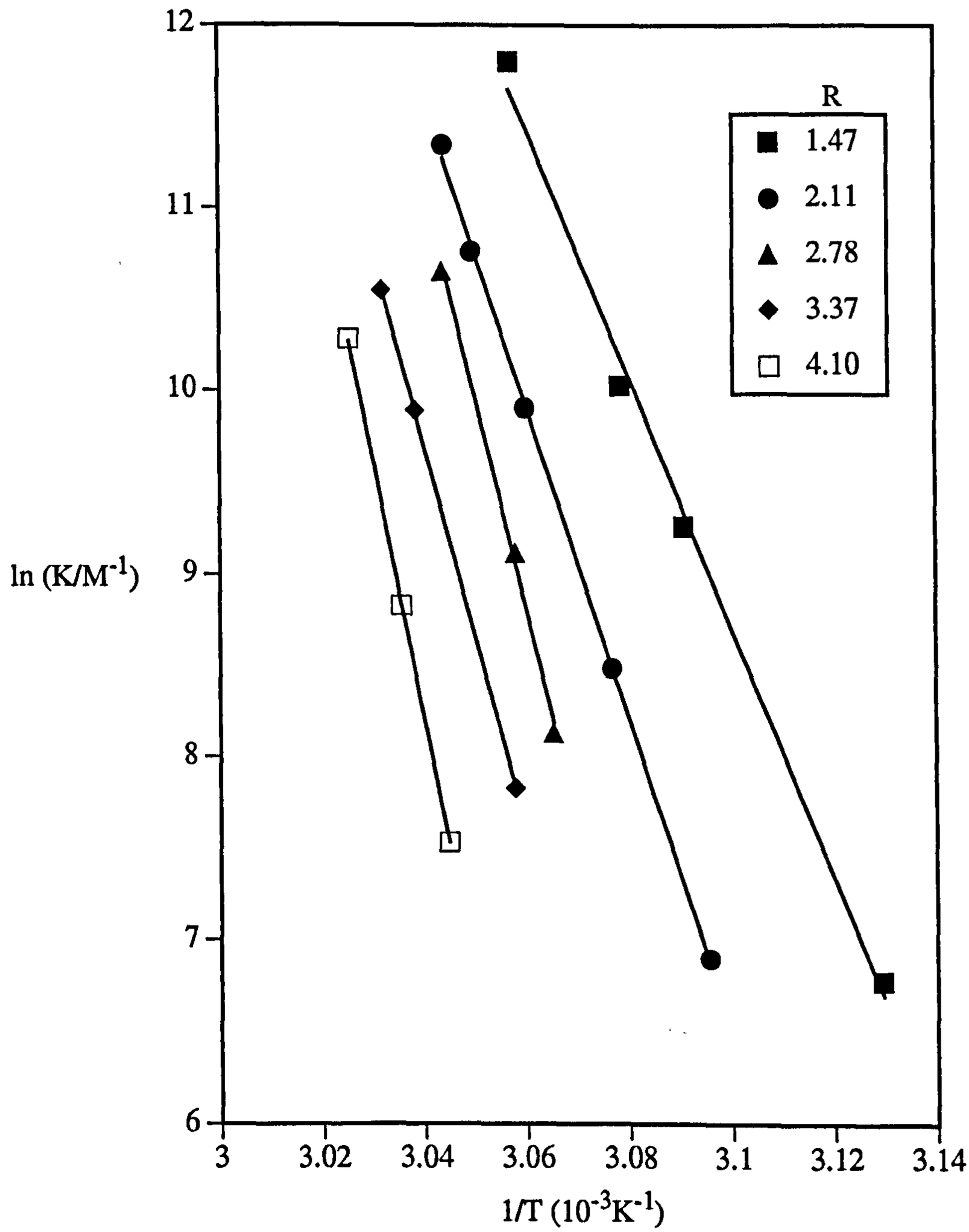

Figure 5.2.2
Van't Hoff plots obtained for C_nE_m surfactants with alkane oils at varying R values.

(g) 0.04 M $C_{14}E_7$ with decane.

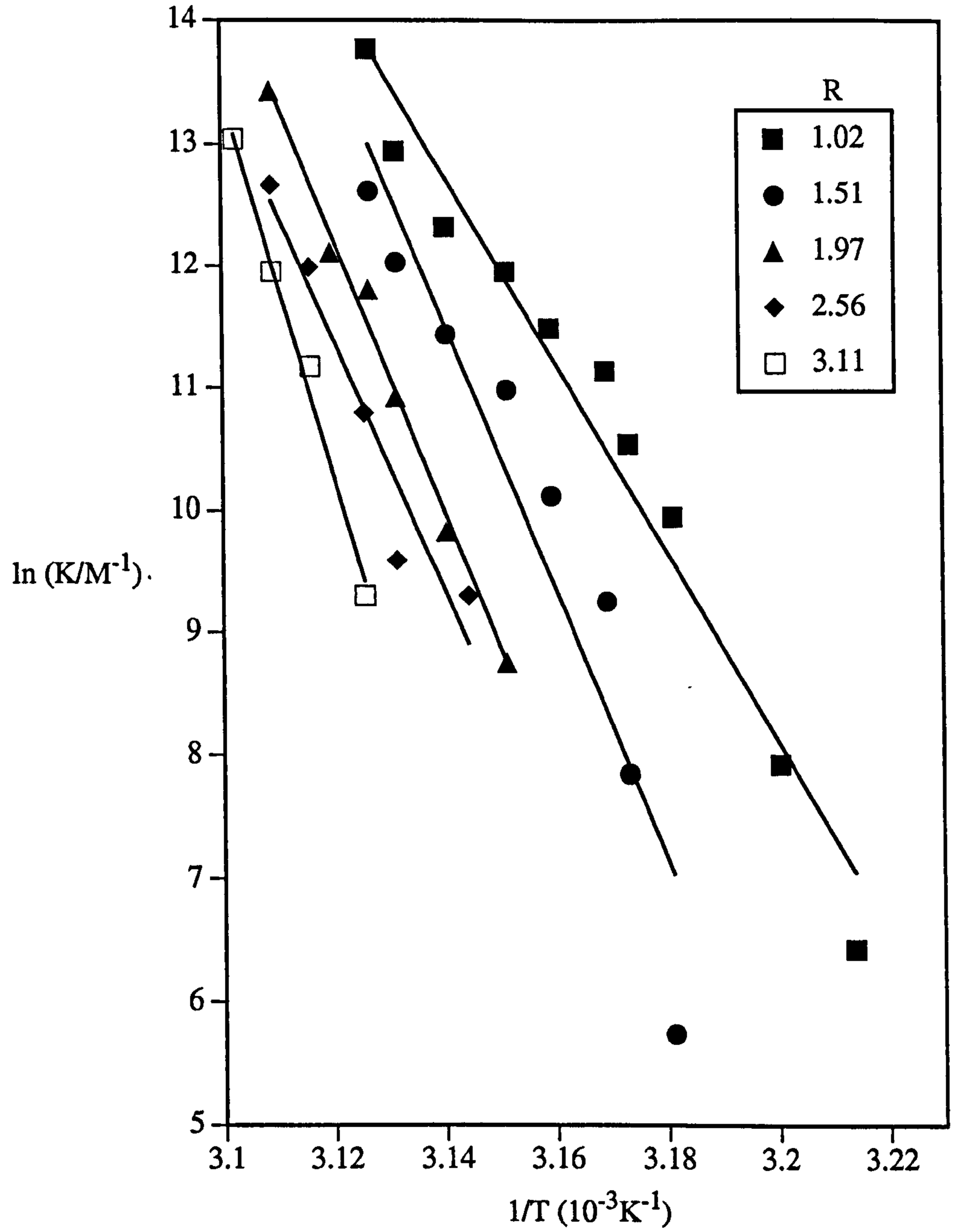

5.3 Relating the equilibrium constant and the thermodynamic changes of the clustering/growth process with the packing density of the surfactant monolayer.

5.3.1 Describing the calculation of thermodynamic data from the van't Hoff plots.

The slope of the van't Hoff plots yields the standard enthalpy change per mole of droplets (ΔH^o_d) resulting from the clustering/growth process. The Gibbs free energy (ΔG^o_d) and the entropy (ΔS^o_d) involved in the process have also been calculated, as described in section 5.1. Due to the variation in the plots with surfactant concentration the thermodynamic values for each system at a fixed concentration of 0.08 M is compared in Table 5.3. All parameters have been calculated at a temperature approximately 0.1°C above the SPB, where it is assumed that the behaviour associated with the temperature change is likely to be that of two droplets clustering (and no growth). A value of energy per mole of droplets however does not yield information about what is happening at the molecular level, since the aggregation numbers are different for the different systems. Assuming the clustering process is involved, only a fraction of the surface of a droplet is involved in the contact zone between the two droplets, and therefore the changes in energies are envisaged to be attributable only to that small section of the droplet surface. Calculations have therefore been made of the energies per mole of surfactant molecules involved in the contact zone of clustering, as described in detail in Appendix II. The average aggregation number of surfactant molecules in the droplets obtained from the average value of A_s calculated from both PCS and turbidity data is also shown, calculated using equation 5.3a.

$$N_{agg} = (36\pi V_m^2 R^2)/A_s^3 \qquad (5.3a)$$

Table 5.3

The variation of thermodynamic parameters with system variation, calculated at approximately 0.1 ^{o}C above the SPB.

$\grave{A}_s$, $\grave{r}_h$ denote the average values calculated from turbidity and PCS data. † calculated from turbidity data ‡ calculated from PCS data. A_h is calculated from $4\pi r_h^2/N_{agg}$. ΔH_d^o, ΔG_d^o, ΔS_d^o, denote parameters per mole of droplets. ΔH_m^o, ΔG_m^o, ΔS_m^o, denote parameters per mole of surfactant molecules involved in the contact area of clustering, K_m is the associated equilibrium constant, calculated as described in Appendix II.

Surfactant	$\grave{A}_s$ (nm^2)	A_h (nm^2)	$\grave{r}_h$ (nm)	T (K)	N_{agg}	ln K	ΔH_d^o $kJmol^{-1}$	ΔG_d^o $kJmol^{-1}$	ΔS_d^o $kJK^{-1}mol^{-1}$	ln K_m	ΔH_m^o $kJmol^{-1}$	ΔG_m^o $Jmol^{-1}$	ΔS_m^o $JK^{-1}mol^{-1}$
i *x variation* at ≈ drop size													
$C_{12}E_5$/C7	0.39	1.2	7.90	289.0	630	5.71	770	-14	2.7	0.08	10.3	-184	36
$C_{12}E_5$/C14	0.29	0.6	8.00	303.3	1400	5.95	667	-15	2.2	0.04	4.1	-91	14
ii At R = 1.5 (≈ drop size) *n variations*													
$C_{10}E_5$	0.34	0.8	7.00	307.2	735	5.85	825	-15	2.7	0.06	8.5	-153	28
$C_{12}E_5$	0.40	1.2	6.50	294.1	438	5.13	618	-13	2.1	0.08	9.9	-202	34
m variations													
$C_{12}E_5$	0.40	1.2	6.50	294.1	438	5.13	618	-13	2.1	0.08	9.9	-202	34
$C_{12}E_6$	0.42	1.5	6.70	309.3	388	5.60	619	-14	2.0	0.11	11.6	-269	38
n/m =2													
$C_{10}E_5$	0.34	0.8	7.00	307.2	735	5.85	825	-15	2.7	0.06	8.5	-153	28
$C_{12}E_6$	0.42	1.5	6.70	309.3	388	5.60	619	-14	2.0	0.11	11.6	-269	38

Table 5.3 *continued*

Surfactant	`A_s (nm^2)	A_h (nm^2)	`r_h (nm)	T (K)	N_{agg}	ln K	ΔH_d^o/ $kJmol^{-1}$	ΔG_d^o/ $kJmol^{-1}$	ΔS_d^o kJK^{-1} mol^{-1}	ln K_m	ΔH_m^o $kJmol^{-1}$	ΔG_m^o $Jmol^{-1}$	ΔS_m^o JK^{-1} mol^{-1}
iii At R=2.5 (≈ drop size) *n variations*													
$C_{10}E_5$	0.34	0.6	9.70	313.6	2050	6.63	1380	-17	4.4	0.03	6.9	-86	22
$C_{12}E_5$	0.40	0.8	9.00	298.8	1200	6.23	802	-15	2.7	0.05	6.4	-123	22
$C_{12}E_7$	0.42	0.9	9.00	322.0	1100	5.89	829	-16	2.6	0.05	7.2	-137	23
$C_{14}E_7$	†0.42 ‡0.55	0.8	8.60	317.6	1100 468	6.54	798	-17	2.5	0.05	6.6	-143	21
m variations													
$C_{12}E_5$	0.40	0.8	9.00	298.8	1200	6.23	802	-15	2.7	0.05	6.4	-123	22
$C_{12}E_6$	0.42	0.9	9.00	315.3	1100	7.24	816	-19	2.6	0.06	7.1	-164	23
$C_{12}E_7$	0.42	0.9	9.00	322.0	1100	5.89	829	-16	2.6	0.05	7.2	-137	23
n/m = 2													
$C_{10}E_5$	0.34	0.6	9.70	313.6	2050	6.63	1380	-17	4.4	0.03	6.9	-86	22
$C_{12}E_6$	0.42	0.9	9.00	315.3	1100	7.24	816	-19	2.6	0.06	7.1	-164	23
$C_{14}E_7$	†0.42 ‡0.55	0.8	8.60	317.6	1100 468	6.54	798	-17	2.5	0.05	6.6	-143	21
iv *R(drop size) variations* 0.093 M $C_{12}E_6$/C10													
R = 0.5	0.42	5.5	4.30	297.8	42	1.98	334	-5	1.1	0.23	38.7	-568	132
R = 1.0	0.42	2.2	5.50	304.1	172	3.46	426	-9	1.4	0.12	15.0	-308	50
R = 2.0	0.42	1.1	7.80	310.8	693	4.49	687	-12	2.2	0.05	8.3	-140	27
R = 3.0	0.42	0.8	10.20	314.9	1566	6.36	888	-17	2.8	0.04	6.1	-114	20
R = 4.0	0.42	0.7	12.60	318.6	2801	7.17	1319	-19	4.1	0.03	6.2	-89	20

5.3.2 General discussion of thermodynamic data.

The large positive value of the enthalpy change noted for all systems accounts for the strong temperature dependence observed for the turbidity of the single phase O/W microemulsion region. The favourable positive entropy change represents an increase in disorder with increasing temperature. This can be postulated to be attributable to the dehydration of the surfactant head groups thus allowing clustering or growth to take place with possible penetration of the surfactant monolayers from the clustered droplets (Figure 5.3.2). If dehydration occurs the water molecules are released from the ordered constraint of bonding either to the surfactant head groups or to each other in the inter head group area, resulting in an increase in entropy. The favourable negative value of the Gibbs free energy indicates that clustering/growth is spontaneous for increasing temperature of these systems, and that the process is entropically driven.

5.3.3 The effect of the surfactant monolayer packing density on the equilibrium constant and the associated energy changes.

First we compare systems at constant drop size for $C_{12}E_5$ with a variation in alkane oil chain length (Table 5.3.(i)) and for varying systems at R = 1.5 (Table 5.3.(ii)). It can be seen that per mole of surfactant molecules involved in the contact area of clustering, the value of the equilibrium constant (K_m) and associated energy changes (ΔH_m^o, ΔG_m^o, and ΔS_m^o) are generally greater for systems having the less closely packed monolayers (larger A_h). The same trend with A_h is observed for systems at different drop sizes (Table 5.3. (iv), and comparing 5.3.(ii) with 5.3.(iii)). This could be attributed to the hydration of the head groups. If the head groups are more widely spaced they are more accessible for bonding by water molecules (Figure 5.3.3). The head groups will therefore be more hydrated and thus the temperature would need to be increased further for dehydration and therefore clustering to take place, resulting in correspondingly larger enthalpy, entropy, and Gibbs free energy changes. This is consistent with the observed variation in the temperature range of the single phase O/W microemulsion region for varying alkane oil chain length (Chapter 3, Figure 3.3 (d)). Although the actual temperatures are lower, the temperature *range* is longer for the shorter alkane. The phase diagrams for the systems where n/m = 2 (Figure 3.3(c)) show an increasing temperature range for the longer surfactants

Figure 5.3.2
Schematic representation of clustering of microemulsion droplets.
"Enmeshed" monolayers from two clustered droplets A and B.

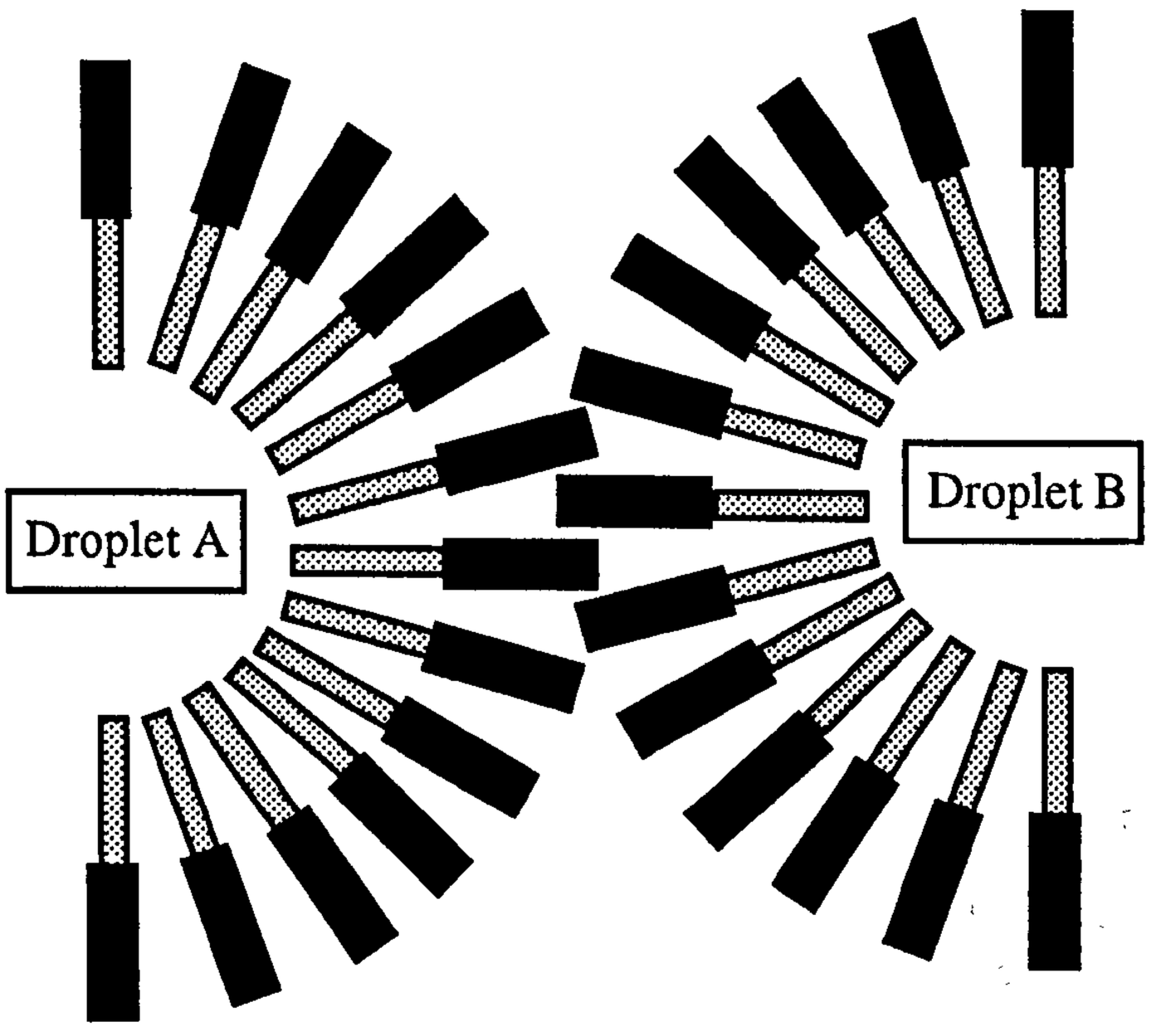

Figure 5.3.3
Schematic representation of the clustering of microemulsion droplets, showing approaching monolayers from two equally sized droplets.

(i) Clustering of droplets (W and X) having sparsley packed monolayers.

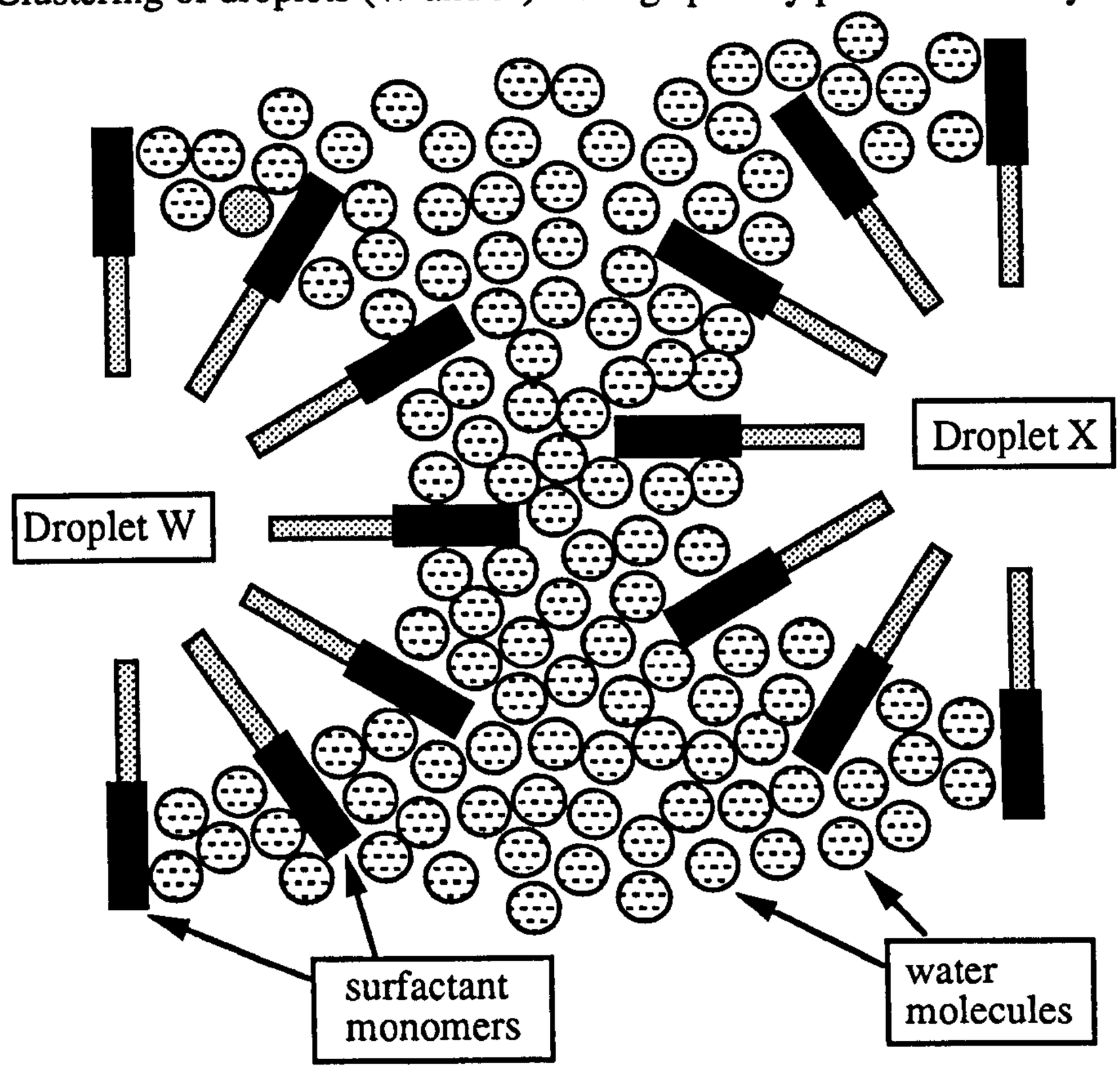

(ii) Clustering of droplets (Y and Z) having closeley packed monolayers.

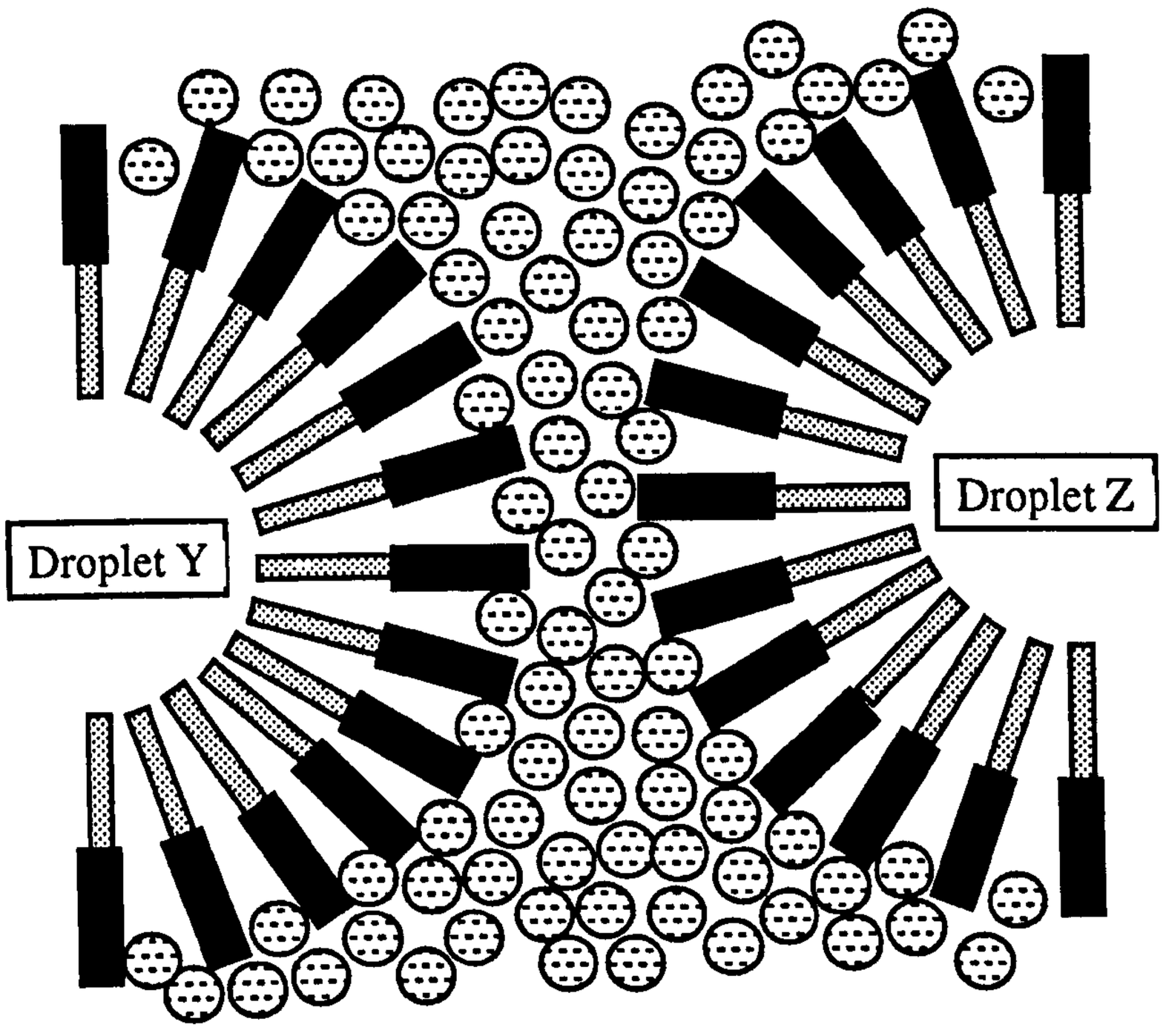

(having a larger A_h). The phase diagrams for all systems show an increase in the temperature range of the single phase microemulsion region with decreasing R value (and therefore increasing A_h) (Figures 3.3(a) - (d)).

For reasons which are as yet unclear the systems at constant drop size at an R value of 2.5 do not show these trends in energy changes with A_h.

The parameters per mole of surfactant molecules involved in the contact zone have been compared for an arbitrary 1 nm penetration depth of the two droplet monolayers on clustering (see Appendix II for a full explanation of this parameter). However, calculations involving penetrations of 0.5 nm and 0.1 nm make no difference to the *trends* observed (as shown for example in Table 5.3.2 for ΔS_m^o calculated for the systems with varying alkane chain length).

Table 5.3.2

The variation in the change in entropy per mole of molecules involved in the contact zone of clustering (ΔS_m^o) for varying penetration distance (z nm) of clustering droplet surfaces, calculated for $C_{12}E_5$ systems with a variation in alkane oil chain length.

	ΔS_m^o ($JK^{-1}mol^{-1}$)		
System	z = 0.1	z = 0.5	z = 1.0
$C_{12}E_5$/C7	342	70	36
$C_{12}E_5$/C14	129	27	14

The greater numbers of molecules involved for systems having the more closely packed monolayers outweighs the effects on the energy changes at the molecular level and thus *per mole of droplets* the reverses trends are observed for K, ΔH_d^o, ΔG_d^o, ΔS_d^o, with A_h.

5.4 Conclusions

- The particle size increases with increasing temperature due to either clustering or growth of droplets.

- Turbidity measurements are a simple method of measuring the extent of this clustering or growth.

- The aggregation model postulated in section 5.1 is found to fit well to the middle droplet concentration range 0.04 - 0.10 $moll^{-1}$. As expected the equilibrium constant (K) for the clustering/growth process is found to increase with increasing temperature.

- The large positive value observed for the enthalpy change accounts for the strong temperature dependence observed for the single phase O/W microemulsion region. The associated positive entropy is attributed to the dehydration of water molecules from the surfactant head groups, resulting in loss of the ordering caused by the restraints of bonding The negative Gibbs free energy indicates that clustering/growth is spontaneous and is entropically driven.

- The energy changes *per mole of molecules* involved in the contact area of clustering, and the associated equilibrium constant are found to be greater for the systems having the more widely spaced head groups (larger A_h, less closely packed monolayers.). This is consistent with the theory of the temperature dependence on the dehydration of the head groups. Monolayers which have more widely spaced head groups will be more hydrated and require a greater input of heat to dehydrate, with a corresponding greater change in entropy, and Gibbs free energy.

- Due to the greater numbers of molecules involved the energy changes *per mole of droplets* , and the associated equilibrium constant, are greater for systems having the more closely packed monolayers (smaller A_h).

CHAPTER SIX

6. The kinetics of the clustering/growth process for alkane-in-water microemulsions stabilised by C_nE_m surfactants.

6.1 Introduction

The rates of the clustering/growth process for the alkane-in-water microemulsion systems stabilised by C_nE_m surfactants were obtained using the iodine laser temperature jump technique (section 2.2.4) in which the time taken for the microemulsion to relax to a new greater turbidity following the temperature jump was recorded. The reciprocal of this relaxation time is the observed first order rate constant (k_{obs}) for the clustering/growth process, from which the forward (clustering/growth) and reverse (unclustering/shrinking) rate constants can be derived (k_f and k_r respectively). The turbidity, measured as absorbance, of the same stock microemulsion sample used for the T-jump experiments is measured as described in section 2.2.3, from which the change in absorbance following the temperature jump is calculated as described later in this section.

The mechanism assumed for the process is as described in chapter 5, where the rate of change of droplet bond formation (in terms of clustering) is given by equation 5.1i repeated below:

$$d\alpha/dt = k_f C_c^2 - k_r \alpha$$

Defining the deviation of α from equilibrium as $-\Delta\alpha$, the rate expression becomes:

$$d\alpha_t/dt = k_f(C_c+\Delta\alpha)^2 - k_r(\alpha-\Delta\alpha) \qquad (6.1a)$$

and

$$d\alpha_t/dt = k_f(C_c^2+2C_c\Delta\alpha+\Delta\alpha^2) - k_r(\alpha-\Delta\alpha) \qquad (6.1b)$$

where α_t is the concentration of bonds at time t, and α is the value at equilibrium. At equilibrium $d\alpha/dt = 0$, therefore $k_f C_c^2$ cancels with the negative term $-k_r\alpha$. Also for a small deviation from equilibrium $\Delta\alpha$ is small compared to α therefore $\Delta\alpha^2$ can be ignored. The expression then becomes:

$$d\alpha_t/dt = (k_f 2C_c+k_r)\Delta\alpha \qquad (6.1c)$$

Since $d\alpha_t = d\alpha - d\Delta\alpha$, and at equilibrium $d\alpha = 0$, therefore $d\alpha_t = - d\Delta\alpha$, hence:

$$- d\Delta\alpha/dt = (k_f 2C_c + k_r)\Delta\alpha \qquad (6.1d)$$

so $$- d\Delta\alpha/\Delta\alpha = (k_f 2C_c + k_r)dt \qquad (6.1e)$$

rewritten: $$d\Delta\alpha/\Delta\alpha = -(k_f 2C_c + k_r)dt \qquad (6.1f)$$

This is now a simple first order rate law, and integration yields a simple exponential decay for $\Delta\alpha$ by:

$$\ln \Delta\alpha = -(k_f 2C_c + k_r)t + \text{constant} \qquad (6.1g)$$

At time t=0, $\Delta\alpha$ has the value $\Delta\alpha_0$ therefore integrating equation 6.1f between the limits t=0 to t eliminates the constant of integration and yields:

$$\ln \Delta\alpha - \ln \Delta\alpha_0 = -(k_f 2C_c + k_r)t \qquad (6.1h)$$

hence $$\Delta\alpha = \Delta\alpha_0 \exp(-(k_f 2C_c + k_r)t) \qquad (6.1i)$$

The rate constant term is equivalent to the observed first order rate constant, k_{obs} :

$$k_{obs} = k_f 2C_c + k_r = (2k_f C_d/n) + k_r \qquad (6.1k)$$

a plot of k_{obs} versus C_d/n for a fixed temperature therefore yields a slope of $2k_f$ and an intercept of k_r .

The value of n, the average number of original droplets in the scattering particle is obtained from the absorbance versus temperature plot measured for the same sample (as described in chapter 4). The temperature at which n should be calculated is not obvious. The derivation of equation 6.1k assumes that the change in temperature, and therefore n, is negligible, thus calculation of n at either the initial or the final temperature of the T-jump is equally appropriate, and that strictly the median temperature is probably the most suitable. The final temperature following the T-jump is obtained from a calculation of the change in absorption as follows. The amplitude of the T-jump is given by the change in intensity of light detected by the CW laser caused by the increase in turbidity (measured as absorbance) of the microemulsion sample.

Noting that the amplitude is negative (the intensity of light decreases following the T-jump due to the increase in turbidity)

$$\text{amplitude} = (I_f - I_i) / I_i = (I_f / I_i) - 1 \qquad (6.1l)$$

where I_f = the final intensity following the T-jump

and I_i = the initial intensity prior to the T-jump

The change in absorbance of the sample is given by:

$$\Delta Abs = A_f - A_i \qquad (6.1m)$$

where A_f is the final absorbance following the T-jump,

$$A_f = \log_{10} (I_o / I_f) \qquad (6.1n)$$

and A_i is the initial absorbance prior to the T-jump

$$A_i = \log_{10} (I_o / I_i) \qquad (6.1o)$$

and I_o is the incident intensity of the CW laser.

hence $A_f - A_i = \log_{10} (I_o / I_f) - \log_{10} (I_o / I_i)$

$$= \log_{10} \{(I_o / I_f) / (I_o / I_i)\}$$

since I_o cancels $A_f - A_i = \log_{10} (I_i / I_f)$ (6.1p)

from equation 6.11 $I_i/I_f = 1/ (1+ \text{amplitude})$

hence $\Delta Abs = -\log_{10} (1+ \text{amplitude})$ (6.1q)

Note that ΔAbs will be positive since the amplitude is negative. In this work the amplitude is calculated as the (negative) change in the voltage recorded. The value of n at the final temperature following the T-jump is then found from this change in absorbance by calculation (explained in Figure 6.1.1) from the plot of absorbance versus temperature.

Figure 6.1.1

The calculation of n obtained following a T-jump, shown for 0.08 M $C_{12}E_7$ with decane at R=2.5 as an example. The value of n is found by:

(i) Finding the absorbance (A_i) which corresponds to the initial temperature (T_i) of the sample before the T-jump.

(ii) Adding the change in absorbance resulting from the T-jump experiment (see section 6.1) to find the final absorbance (A_f) [which then yields the final temperature (T_f)].

Note that this also allows calculation of the size of the temperature jump, i.e. $\Delta T = T_f - T$

(iii) The ratio of the final absorbance to that at the solubilisation phase boundary yields n. i.e. $A_f/A_o = n$.

(cf. chapter 4, remembering that turbidity, $\tau = 2.303$ x Absorbance (equation 2.2.3) therefore the absorbance ratio = the turbidity ratio).

(iv) In this example $\Delta Abs = 0.0265$, $n = 2.11$, and $\Delta T = 0.8\ ^oC$.

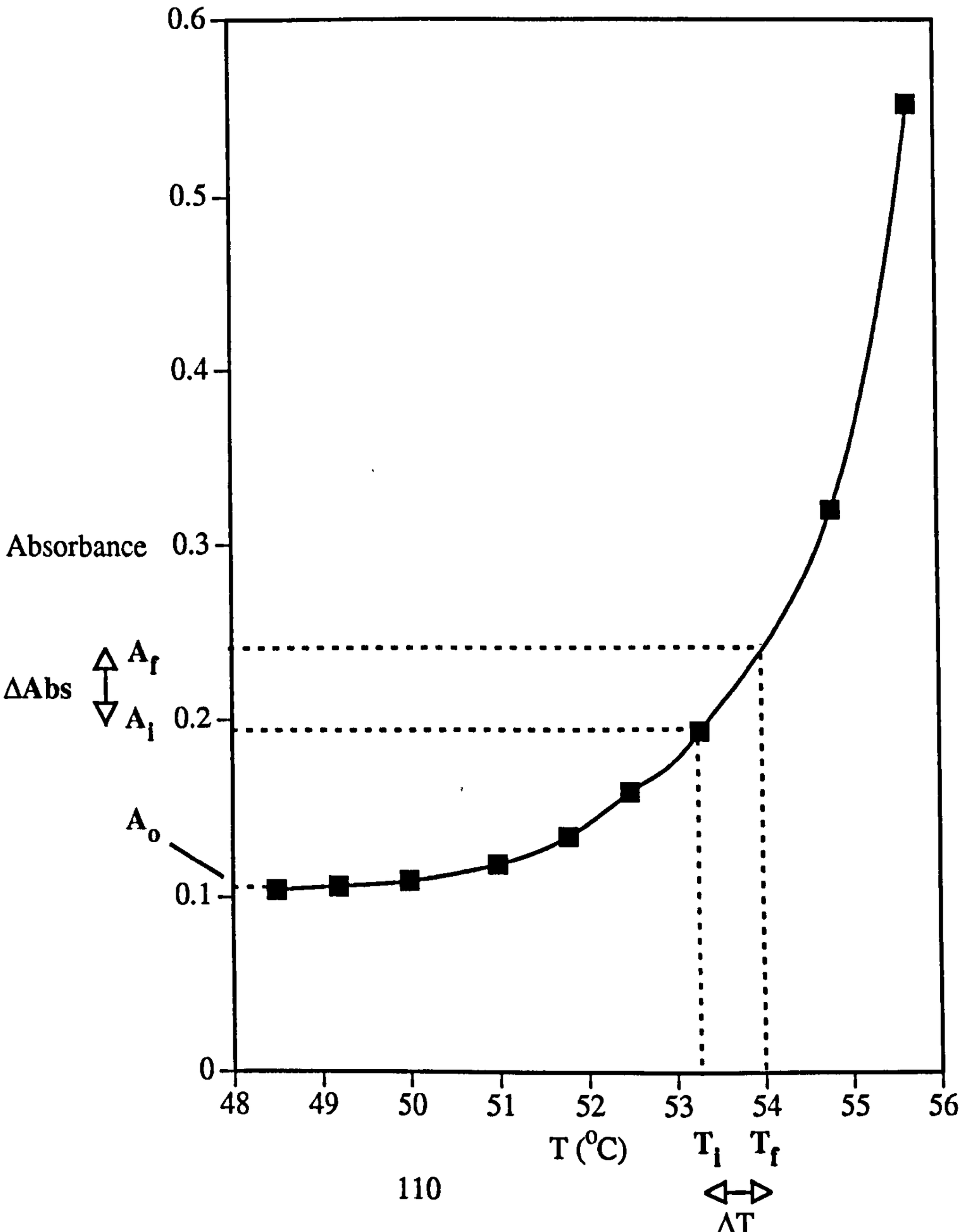

Figure 6.1.2 shows a comparison of k_{obs} versus C_d/n plots for one system calculated from both the initial and final temperatures which yields a 20% greater slope for the final temperature, with a corresponding 80% increase in the intercept (the greatest uncertainty is in the intercept, so a large error is to be expected here). A median temperature would therefore give an error of ±10% in k_f, and ±40% in k_r. As this work is concerned mainly with the qualitative comparison between systems rather than strictly quantitative factors, the more complex calculation of median temperatures is not necessary for the minimal difference found, and therefore initial temperatures were used.

6.2 The variation in observed rate constant with temperature and system variation.

The range of observed rate constants (k_{obs}) obtained for the different systems are given in Table 6.2. The values for k_{obs} varies considerably between systems, and although there are temperature differences between the systems for the one phase microemulsion region, this does not explain the variation in k_{obs}, shown clearly in the $C_{10}E_5/C_{12}E_6/C_{14}E_7$ series, where in fact the rate has an inverse relation to the temperature. Varying a factor in the system leads to trends in the rate behaviour, k_{obs} is shown to *decrease* with (i)*increasing* surfactant carbon chain length (n) to a point where the rate is too slow to be detectable (for $C_{14}E_5$), (ii)*increasing* oil chain length (x), and (iii) *decreases* with *decreasing* surfactant head group (m), again to a point where the rate is no longer dectectable (for $C_{12}E_4$).

The values for k_{obs} near the SPB have been plotted versus the cluster concentration ($C_c = C_d/n$) (Figures 6.2 (a-k)). In agreement with the kinetic scheme described in section 6.1, k_{obs} increases linearly with cluster concentration. There is a pattern of behaviour with changing temperature, an increase in temperature increases the slope, and therefore k_f (the rate of clustering/growth), while decreasing the intercept and therefore k_r (the rate of unclustering/shrinking). This consolidates the observation that clustering/growth becomes more favourable with increasing temperature.

Figure 6.1.2

Comparison of the k_{obs} versus C_d/n plot for n calculated at the initial and final temperature of the T-jump. Data for $C_{12}E_5$ with decane at R=2.5 for the initial temperature of 30 °C. The temperature jump was found to be on average 0.55 °C, making the final temperature 30.55 °C.

See text section 6.1 for further discussion.

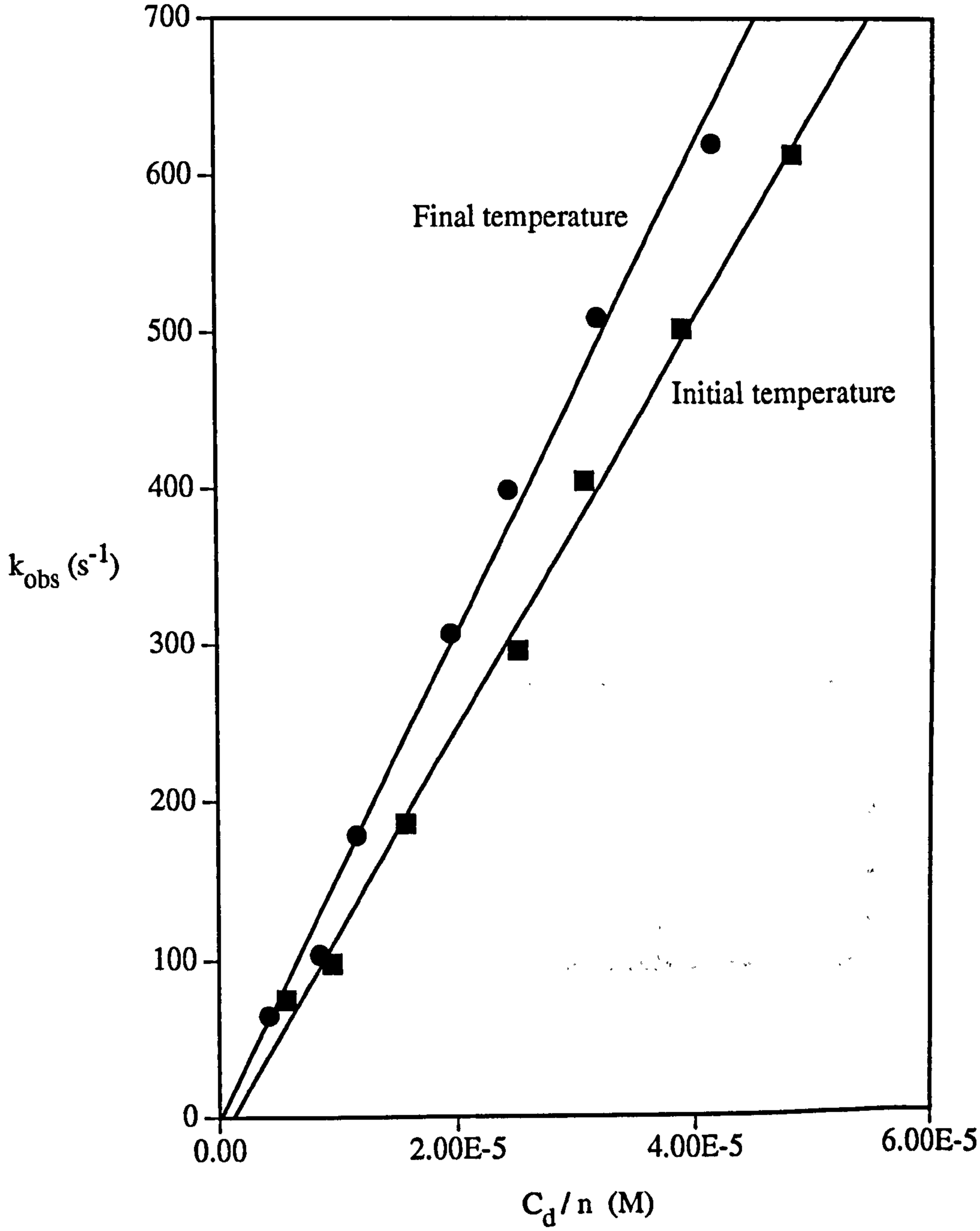

Table 6.2

Comparison of the observed rate constant (k_{obs}) with system variation

System	Temperature Range (^oC)	k_{obs} Range (s^{-1})
n-variations		
$C_{10}E_5$	37 - 43	4000 - 16000
$C_{12}E_5$ with decane	26 - 31	50 - 700
$C_{14}E_5$	14 - 17	not detectable
$C_{12}E_7$ with	51 - 54	1000 - 5000
$C_{14}E_7$ decane	44 - 49	0 - 600
m-variations		
$C_{12}E_4$	4 - 10	not detectable
$C_{12}E_5$ with	26 - 31	50 - 700
$C_{12}E_6$ decane	41 - 46	800 - 4000
$C_{12}E_7$	51 - 54	1000 - 5000
n/m = 2		
$C_{10}E_5$	37 - 43	4000 - 16000
$C_{12}E_6$ with decane	41 - 46	800 - 4000
$C_{14}E_7$	44 - 49	0 - 600
oil length variations		
with $C_{12}E_5$ at equivalent drop size		
C7	18 - 21	0 - 160
C14	35 - 38	1000 - 3000

Figure 6.2
Observed rate constant (k_{obs}) versus cluster concentration ($C_c = C_d/n$)

(a) $C_{10}E_5$with decane at R = 1.51.

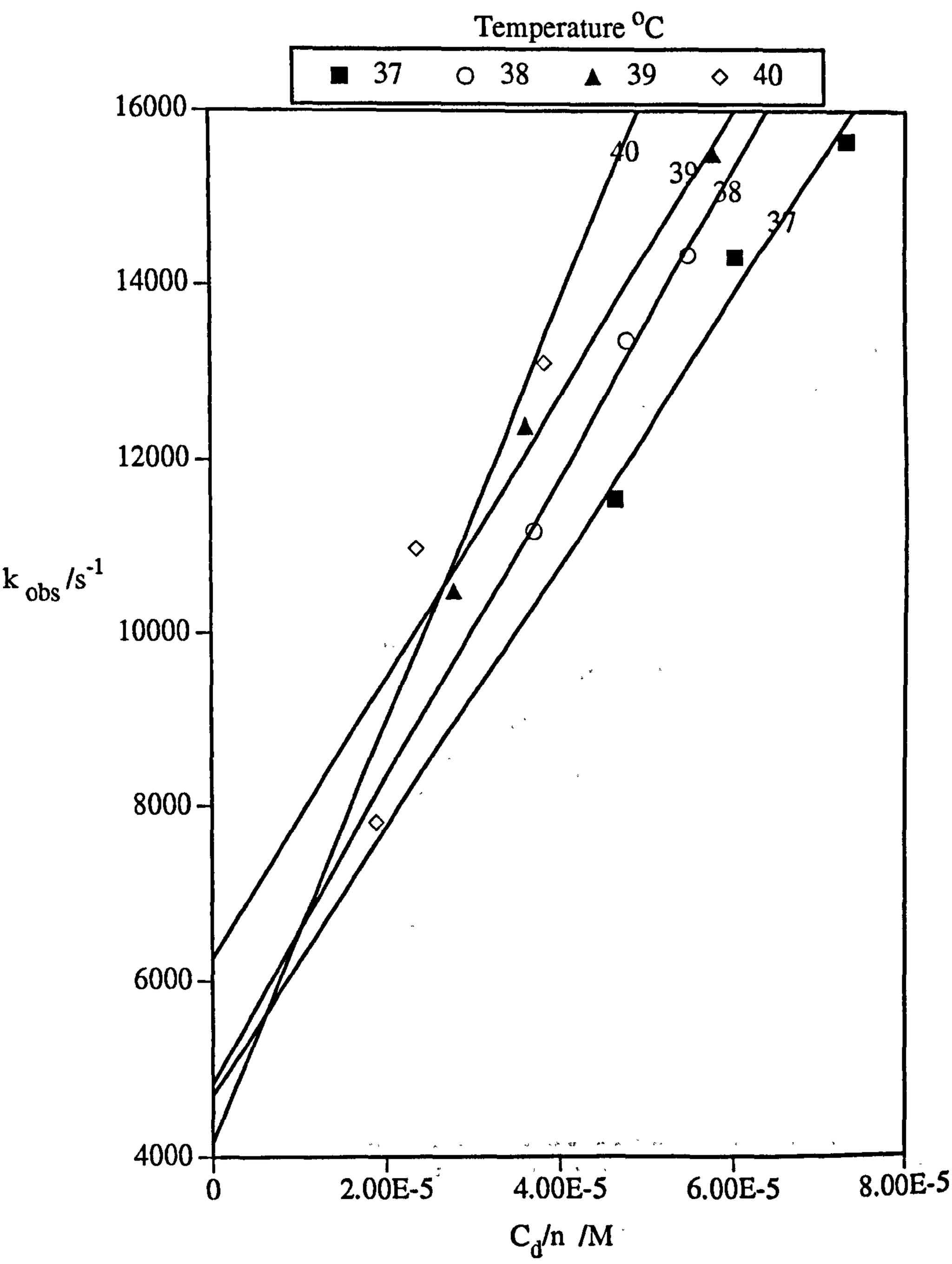

Figure 6.2
Observed rate constant (k_{obs}) versus cluster concentration ($C_c = C_d/n$).

(b) $C_{10}E_5$ with decane at R = 2.5

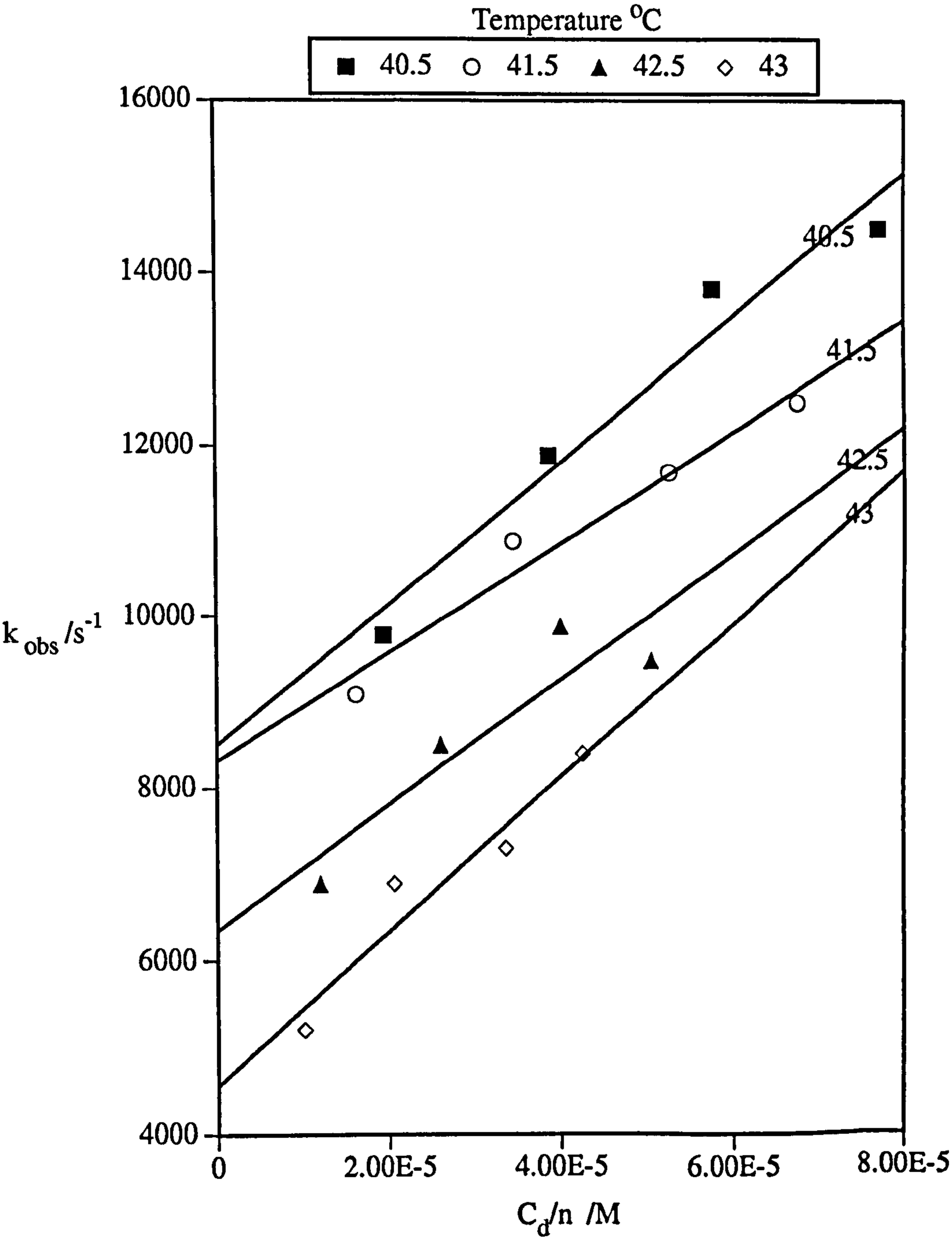

Figure 6.2
Observed rate constant (k_{obs}) versus cluster concentration ($C_c=C_d/n$).

(c) $C_{12}E_5$ with heptane at R = 2.5

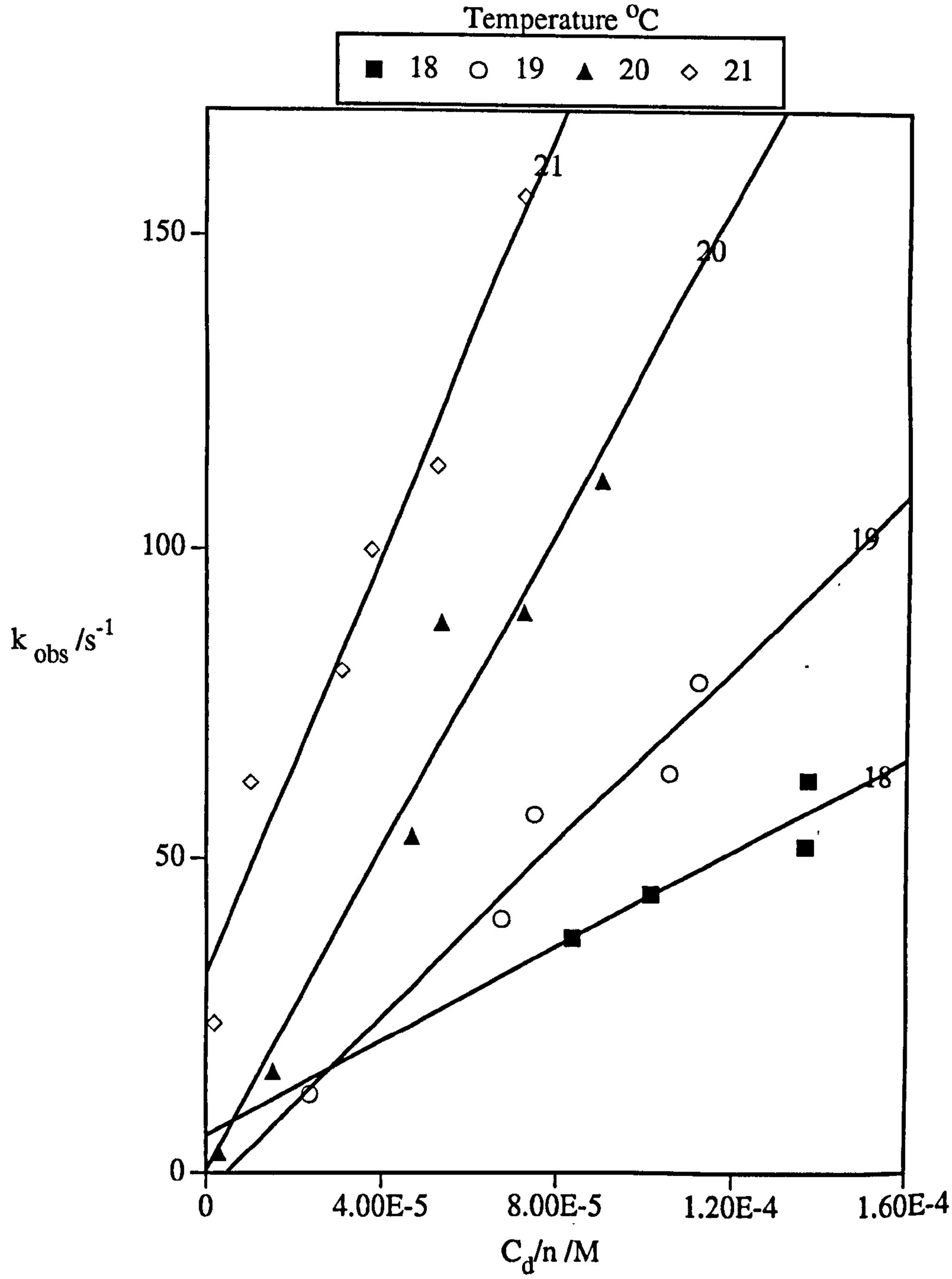

Figure 6.2
Observed rate constant (k_{obs}) versus cluster concentration ($C_c=C_d/n$).

(d) $C_{12}E_5$ with decane at R = 1.5

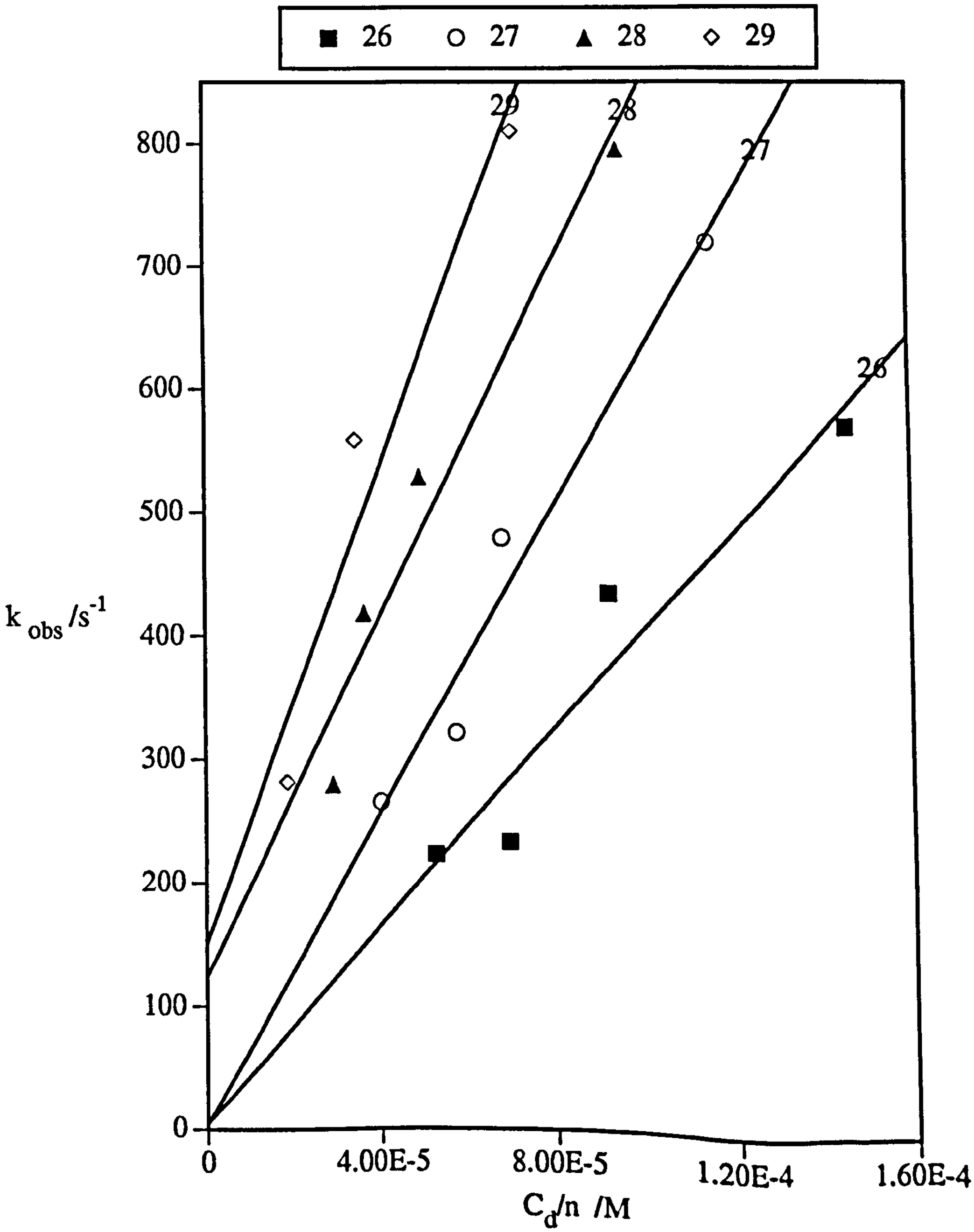

Figure 6.2
Observed rate constant (k_{obs}) versus cluster concentration ($C_c=C_d/n$).

(e) $C_{12}E_5$ with decane at R = 2.5

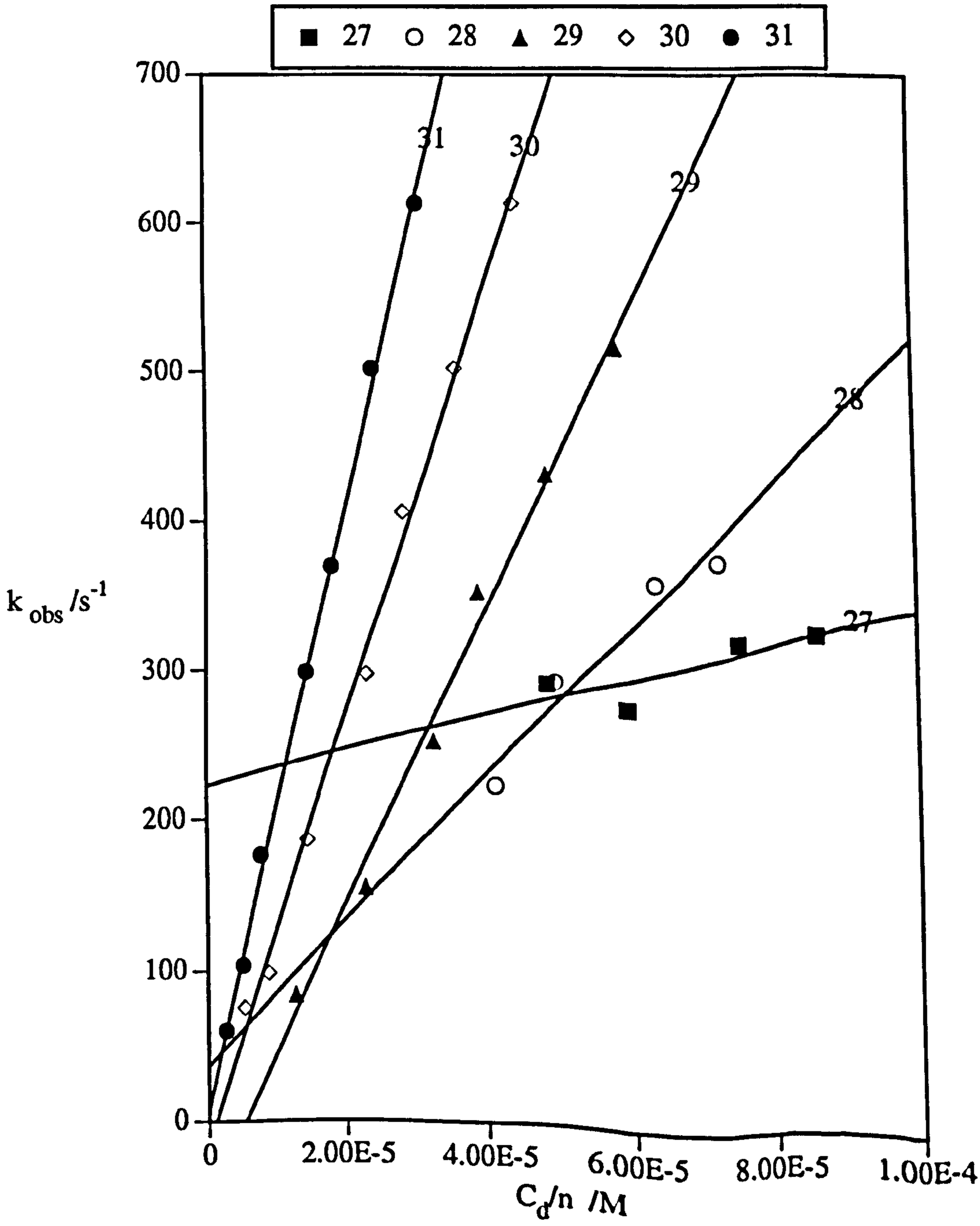

Figure 6.2
Observed rate constant (k_{obs}) versus cluster concentration ($C_c=C_d/n$).

(f) $C_{12}E_5$ with tetradecane at R = 1.26

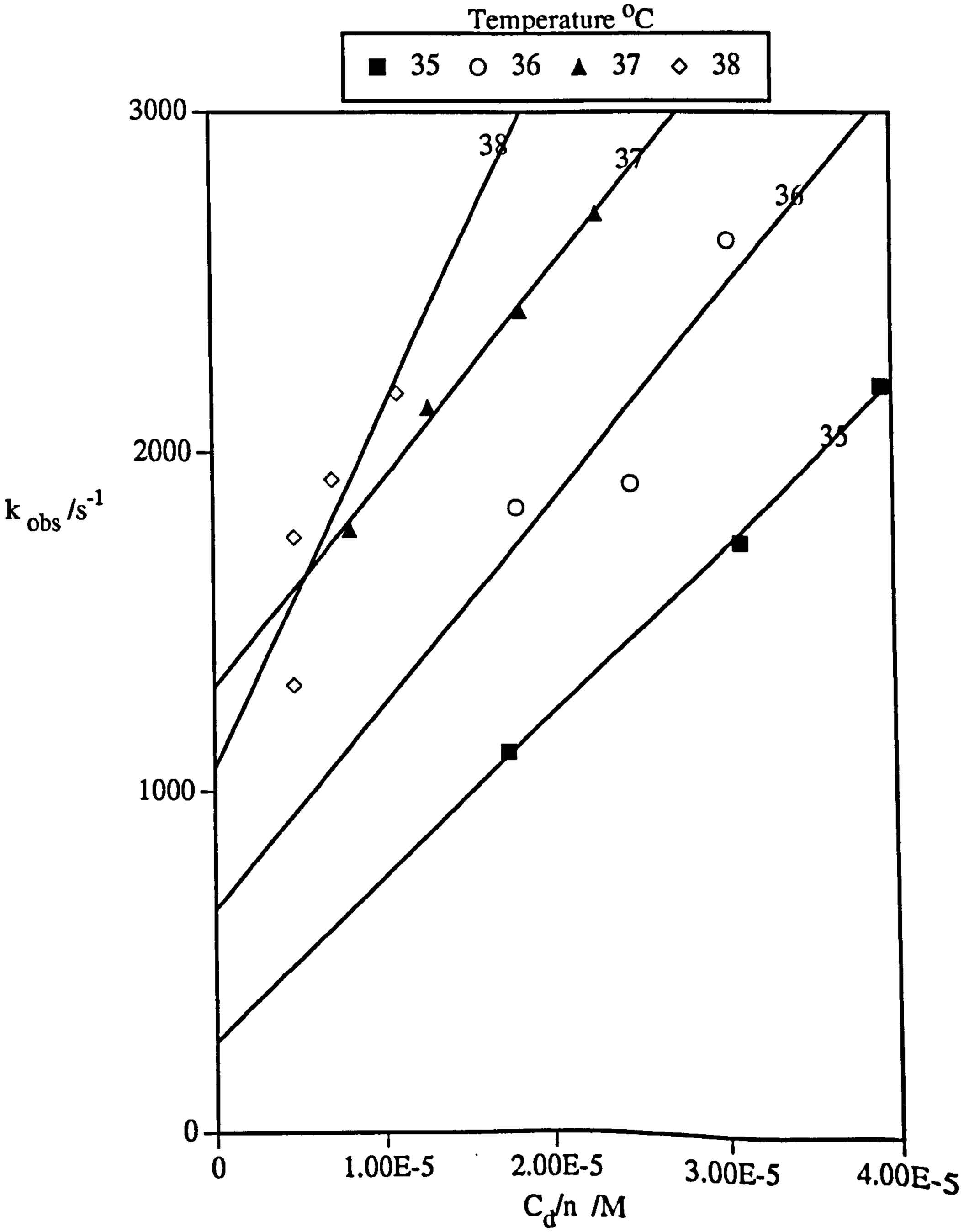

Figure 6.2

Observed rate constant (k_{obs}) versus cluster concentration ($C_c=C_d/n$).

(g) $C_{12}E_5$ with tetradecane at R = 2.5

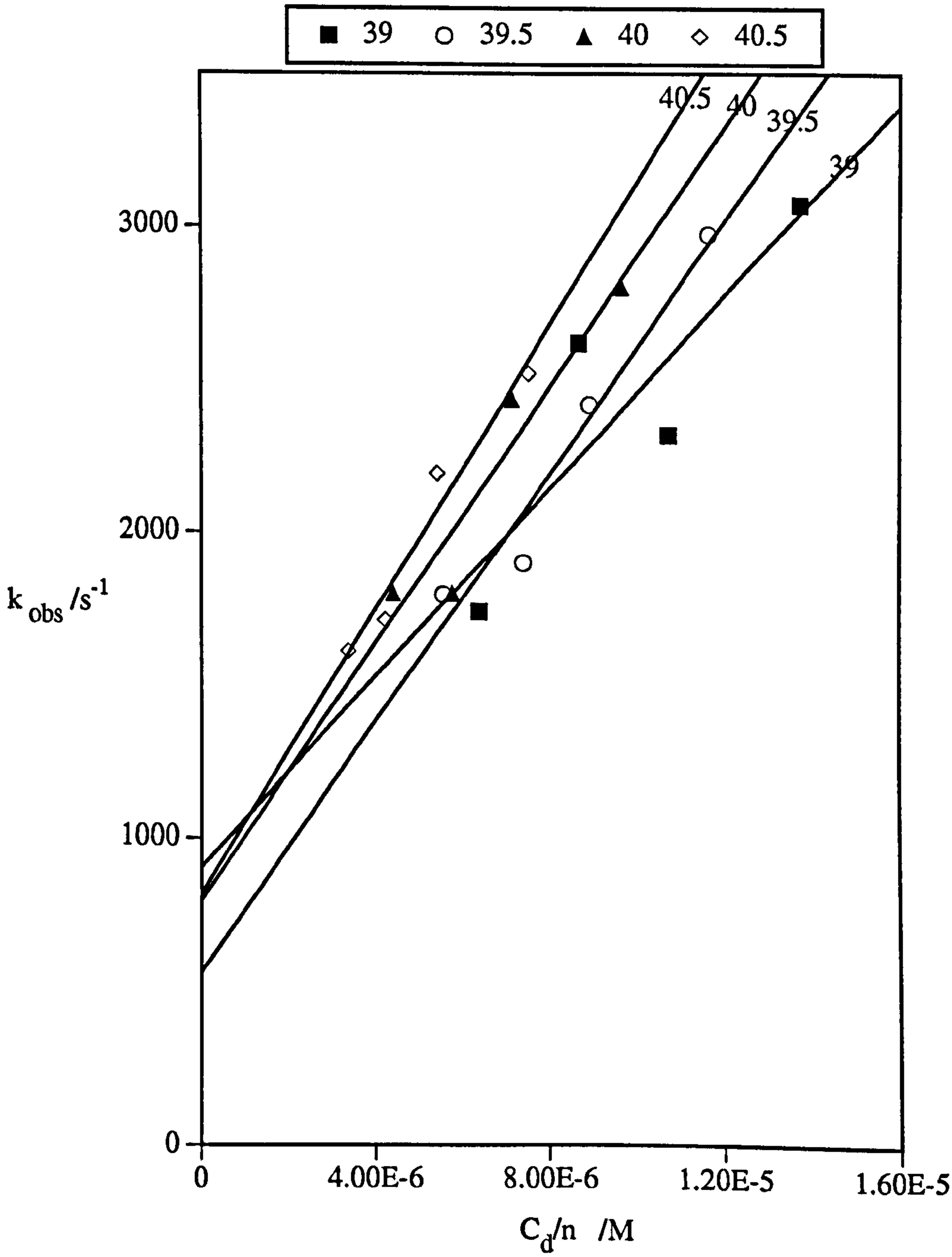

Figure 6.2
Observed rate constant (k_{obs}) versus cluster concentration ($C_c=C_d/n$).

(h) $C_{12}E_6$ with decane at R = 1.5

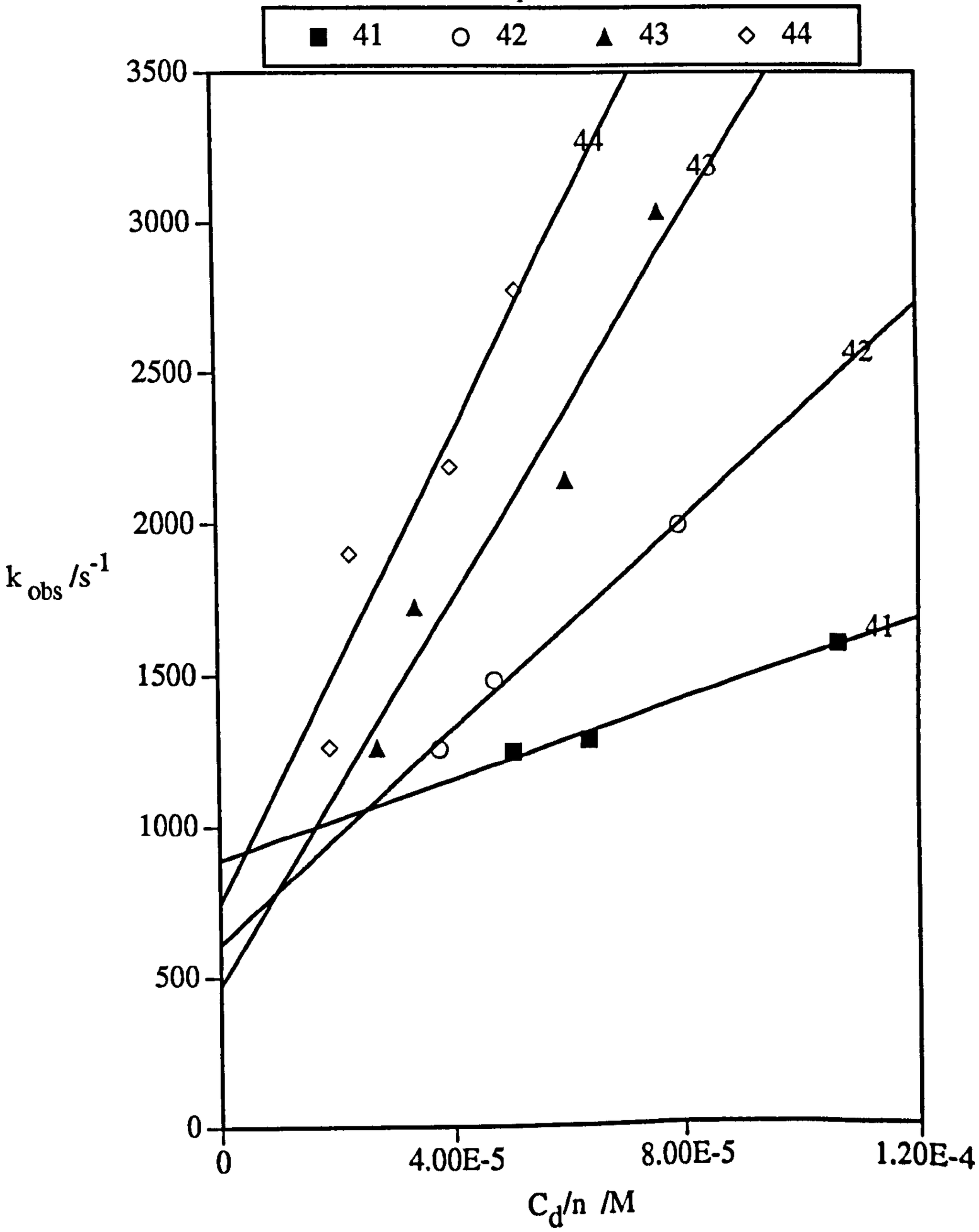

Figure 6.2
Observed rate constant (k_{obs}) versus cluster concentration ($C_c=C_d/n$).

(i) $C_{12}E_6$ with decane at R = 2.5

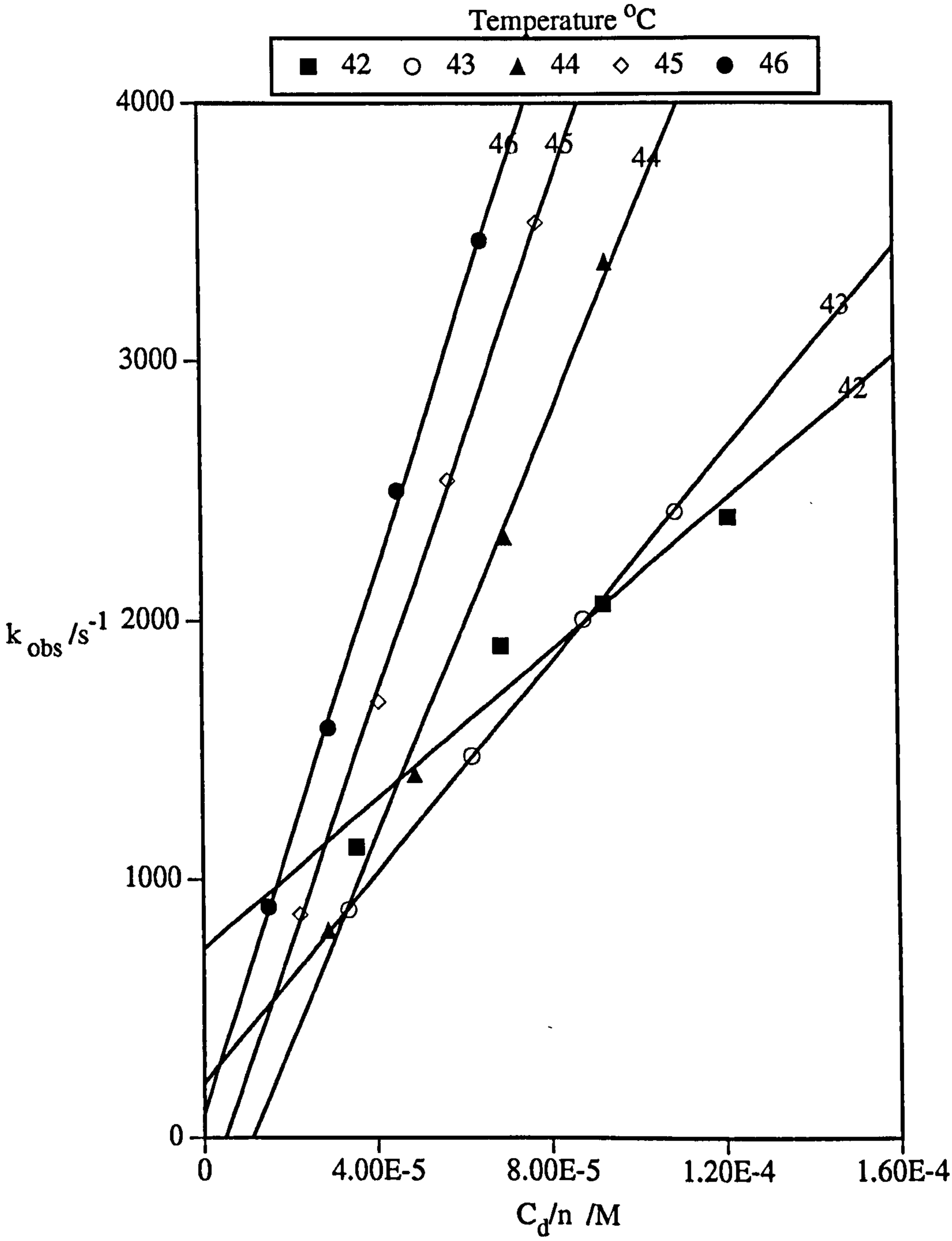

Figure 6.2
Observed rate constant (k_{obs}) versus cluster concentration ($C_c=C_d/n$).

(j) $C_{12}E_7$ with decane at R = 2.5

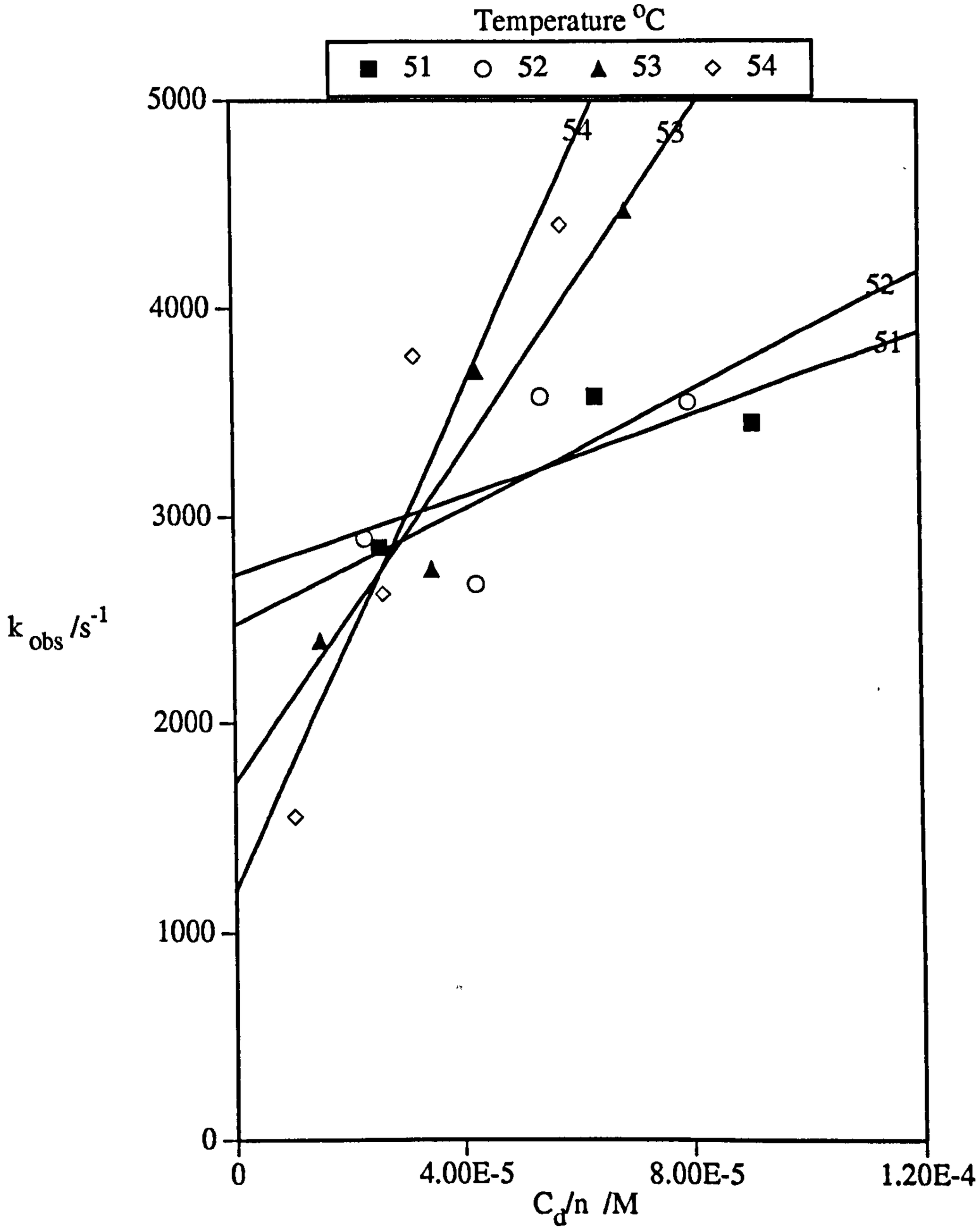

Figure 6.2
Observed rate constant (k_{obs}) versus cluster concentration ($C_c=C_d/n$).

(k) $C_{14}E_7$ with decane at R = 2.5

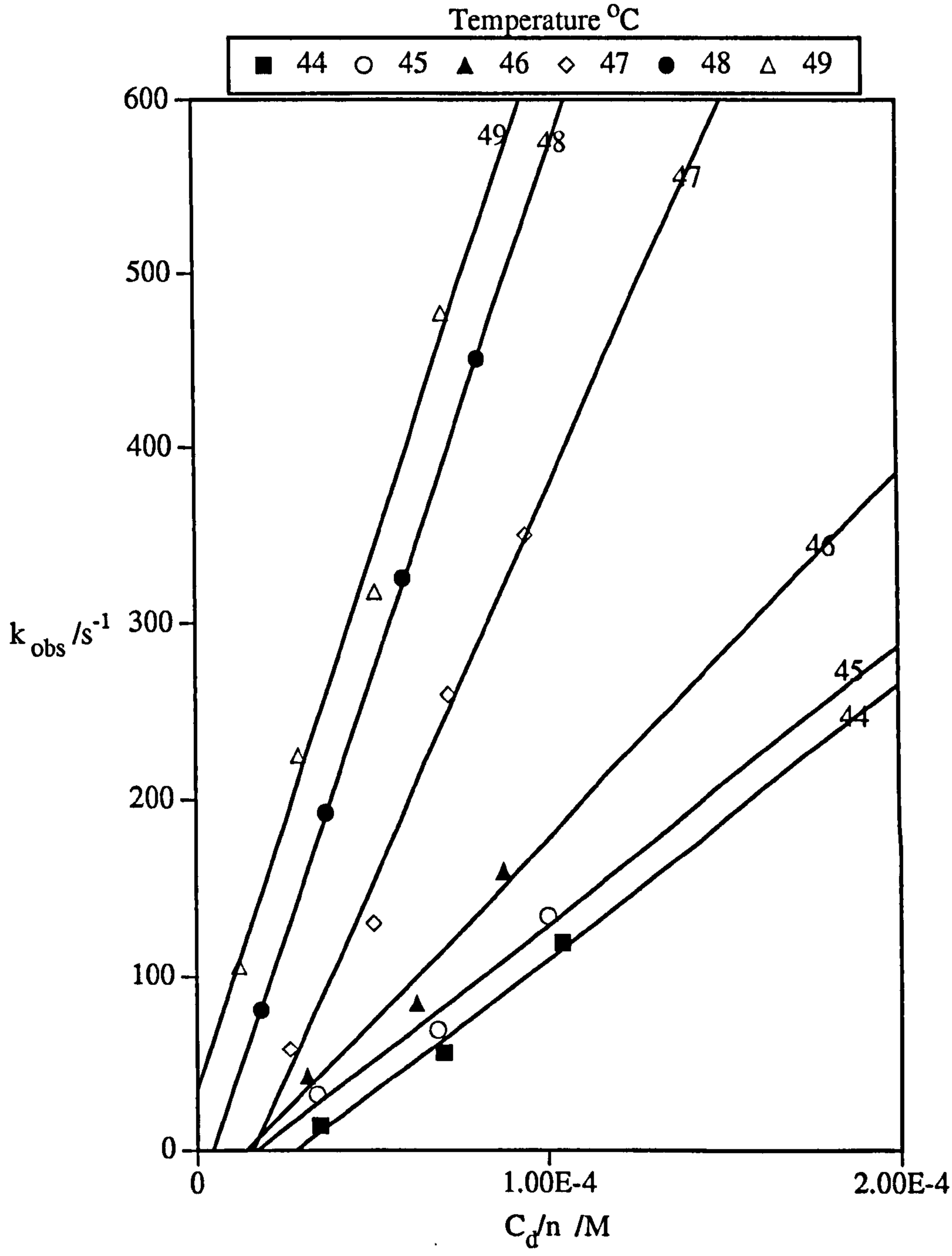

6.3 The variation in the foward and reverse rate constants due to varying n, m, or x, for C_nE_m/C_x microemulsions

The forward (k_f) and reverse (k_r) rate constants calculated as described in section 6.1 are given in Table 6.3.1 for temperatures just above the SPB. The values for k_r are generally uncertain as they are obtained from the intercept of the k_{obs} v C_d/n plots. The variation between the systems is more clearly observed from the plots of k_f and k_r versus system variation at constant drop size in Figures 6.3.1(a) and (b). The trends for the different series are the same for both k_f and k_r with the exception of k_r for the series of increasing head group size (Figure 6.3.1b (ii) - see later discussion). It could be thought that the rates could be merely related to the temperature since the single phase O/W microemulsion region for the different systems exists over different temperature ranges. However, these figures also include the temperatures at which the measurements were made for the different systems, and show that the temperature is not a controlling factor. The results for the series of systems varying in overall surfactant length (Figure 6.3.1a (iv)) shows that whereas the temperature slightly increases from 40°C to 44 °C for $C_{10}E_5$ to $C_{14}E_7$, the rate *decreases* by two orders of magnitude. For the series of systems having an increasing surfactant head group size, (Figure 6.3.1b (ii)), although the temperature increases from 27°C to 51°C a minimal change in the rate of clustering is observed. The reverse rate for this series however is observed to increase with increasing head group size, indicating that although the rate of clustering/growth remains the same for the different head groups, clusters of droplets having the longer head groups uncluster more quickly. It could be postulated that assuming clustering to take place, monolayers having surfactants with shorter head groups are more able to interpenetrate (*cf.* the greater ability of shorter alkane oils to penetrate the surfactant tail group area as discussed in chapter 4, section 4.4) creating a more stable clustered species.

As discussed by Fletcher *et al* [1], the forward rate constant for the clustering/growth process is much slower than the diffusion controlled limiting rate constant k_{dc} defined by the Smoluchowski equation 6.3a[2].

$$k_{dc} = 8RT/3\eta \qquad 6.3(a)$$

---

[1]P. D. I. Fletcher, J. F. Holzwarth, J. Phys. Chem. 1991, 95, 2550-2555.
[2]M. Z. Smoluchowski, Phys. Chem. Stoechiom. Verwandtschaftsl, 1917, 92, 129.

Table 6.3.1

Comparison of forward (k_f - clustering/growth) and the reverse (k_r) rate constants between system variations, measured at temperatures just above the SPB.

R = 2.5 data from unpublished experimental results by P. D. I. Fletcher, Hull University. * The intercept was indeterminate (apparently negative) but assumed to be 0 within the error.

		R = 1.5		R = 2.5	
System		k_f ($M^{-1}s^{-1}$)	k_r (s^{-1})	k_f ($M^{-1}s^{-1}$)	k_r (s^{-1})
n-variations					
$C_{10}E_5$ #	with	7.6×10^7	4.7×10^3	4.2×10^7	8.5×10^3
$C_{12}E_5$	decane	2.0×10^6	4.6×10^0	2.4×10^6	3.7×10^1
$C_{12}E_7$	with	-	-	4.8×10^6	2.7×10^3
$C_{14}E_7$ #	decane	-	-	7.7×10^5	0^*
m-variations					
$C_{12}E_5$		2.0×10^6	4.6×10^0	2.4×10^6	3.7×10^1
$C_{12}E_6$ #	with decane	3.2×10^6	8.9×10^2	7.2×10^6	7.3×10^2
$C_{12}E_7$		-	-	4.8×10^6	2.7×10^3
n/m = 2					
$C_{10}E_5$ #		7.6×10^7	4.7×10^3	4.2×10^7	8.5×10^3
$C_{12}E_6$ #	with decane	3.2×10^6	8.9×10^2	7.2×10^6	7.3×10^2
$C_{14}E_7$ #		-	-	7.7×10^5	0^*
oil length variations with $C_{12}E_5$ at equivalent drop size					
C7	R = 2.5	1.9×10^5	6.0×10^0		
C14	R = 1.26	2.4×10^7	2.7×10^2		
C14	R = 2.5			6.0×10^7	1.6×10^3

Figure 6.3.1a

k_f variation (just above the SPB) with n,m or x at constant drop size (9 nm). The temperatures refer to those at which the measurements were taken.

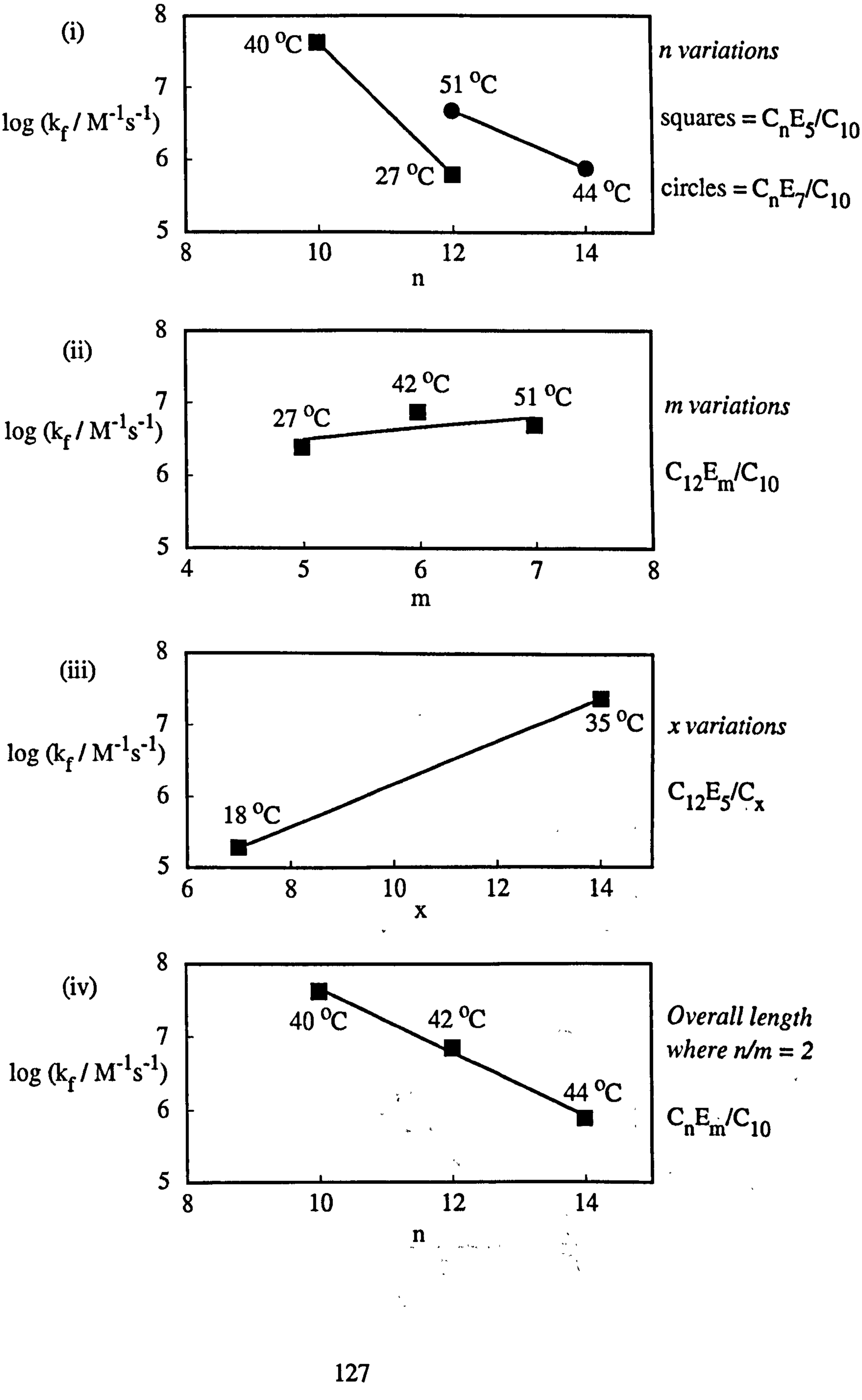

Figure 6.3.1b

k_r variation with n,m or x at constant drop size (9nm). (Note k_r for the $C_{14}E_7$ system is uncertain, see text.) The temperatures refer to those at which the measurments were taken.

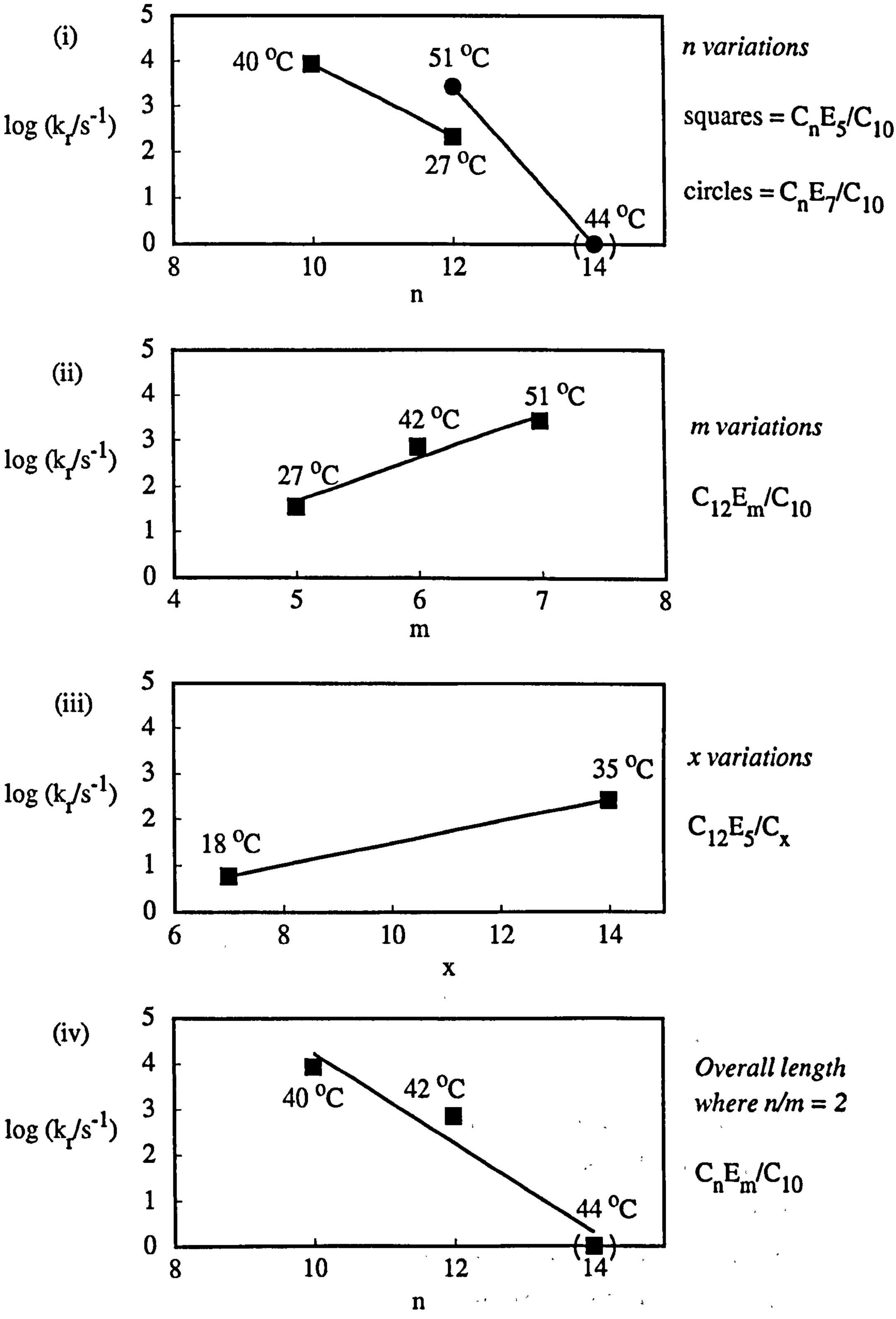

where η is the viscosity of the continuous solvent. There must therefore be an energy barrier which must be overcome before clustering/growth can take place. In chapter 5 (section 5.3.3) it was observed that the enthalpy change per surfactant molecule involved in the clustering/growth process was dependent on the packing density of the surfactant head groups in the monolayer - a lower packing density yielded a greater enthalpy change, relating to the dehydration of the head groups. A comparison of the plots of the *rate constants* versus system variation in Figures 6.3.1(a) and (b) with the corresponding plots of the variation of A_s with system variation (chapter 4, Figure 4.4) shows that there is an inverse relationship between the rates and A_s. A larger A_s (and therefore a lower packing density of the surfactant head groups) yields a slower rate. The effects of systems variation are summarised in Table 6.3.2.

Table 6.3.2

Correlation between the rate constants of the clustering/growth of microemulsion droplets at constant drop size and the packing density of the surfactant monolayer.

Increase in variable	Effect on A_s	Effect on packing density	Effect on k_f	Effect on k_r
n	increase	decrease	decrease	decrease
m	none	none	none	increase
x	decrease	increase	increase	increase
Total length of surfactant (n/m = 2)	increase	decrease	decrease	decrease

A comparison of the rates at varying R values (drop sizes) (Figure 6.3.2) shows that minimal differences in the rates are observed between varying R's up to R = 2.5. This would appear to be contrary to the expected behaviour, since in section 5.3.3 it was shown that assuming a constant A_s the area per head group (A_h) decreases with increasing R, thus increasing the packing density of the monolayer at the droplet surface, hence a faster rate would be expected for the larger R's. Indeed, Fletcher *et al*[1] observed an increased rate for R = 1 - R = 4 for the $C_{12}E_5$ with tetradecane system. It has been previously postulated[3] that A_s increases with R to a maximum value at perhaps R = 1 or 2. If this is the case then it is possible that the variation in A_s between

[3]P. D. I. Fletcher, R. Johannsson, J. Chem. Soc. Faraday Trans., 1994, 90, 23, 3567.

Figure 6.3.2
The variation in the rate constants with varying R value (drop size).

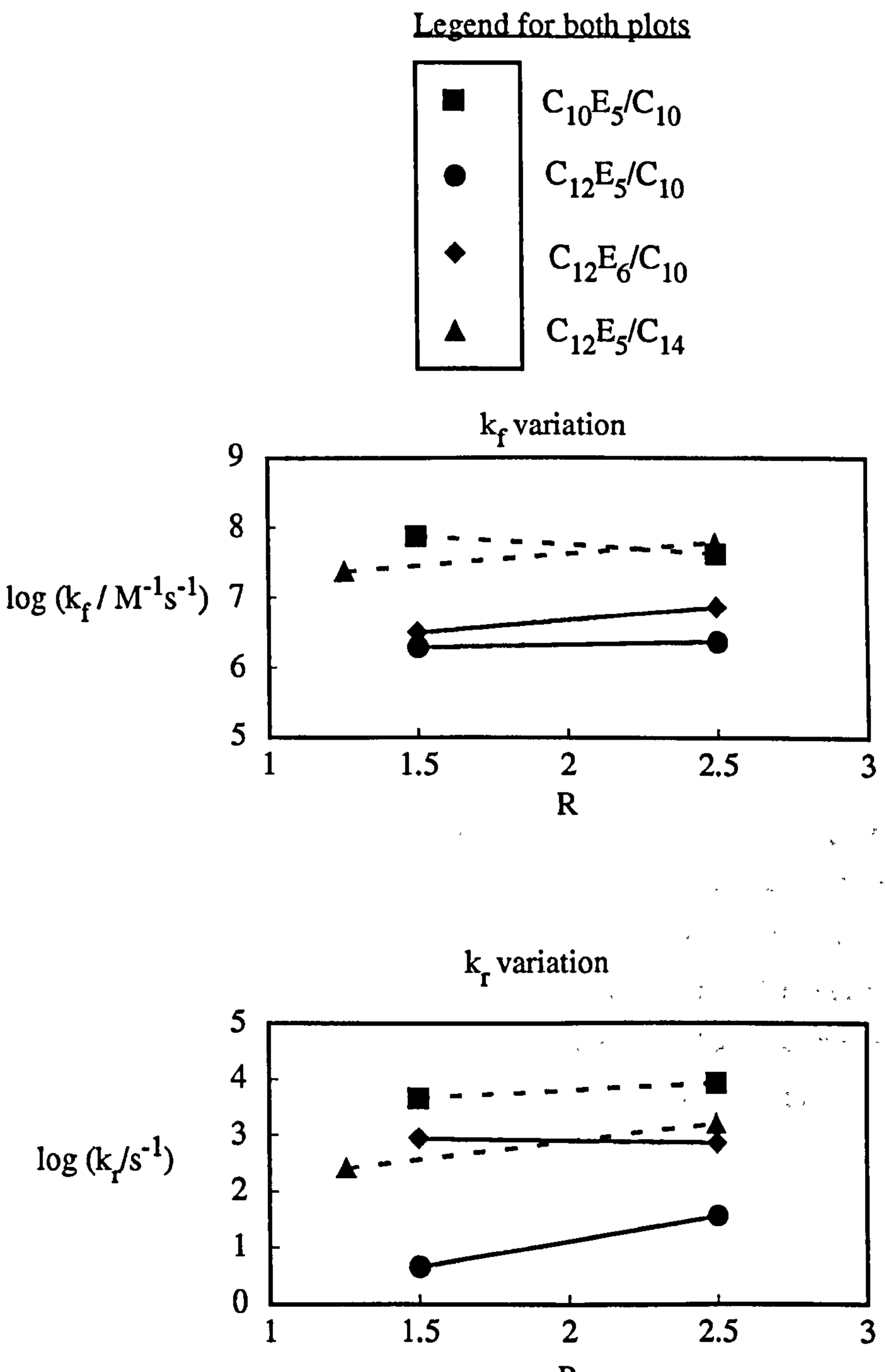

those R values studied results in the packing density of the head groups remaining the same and thus no effect on the rates is observed.

6.4 The activation energy for the clustering/growth process.

The activation energy associated with the clustering/growth proces can be obtained from the slope of the plot of ln k_x versus 1/T, from equation 6.4a:

$$d(\ln k_x)/d(1/T) = -\Delta E_{act}/R \qquad (6.4a)$$

where k_x refers to k_f or k_r as appropriate.

The results are given in Table 6.4, where it can be seen that the activation energy for the clustering/growth process is of the order of a few hundred $kJmol^{-1}$. There seems to be no obvious trends between the systems. An example of the plots obtained is given in Figure 6.4a for the $C_{12}E_m/C_{10}$ series. As discussed earlier the reverse rate constants are uncertain since they are obtained from the intercept of the k_{obs} versus C_d/n plots, however, where good data has been obtained, the ln k_r versus 1/T plot yields a positive slope, indicating apparently negative activation energies as shown in Figure 6.4b(ii) for the $C_{12}E_5/C_{14}$ system at different R values. Figure 6.4b(i) shows the plot obtained for the forward rate constant for these systems. Clark *et al* [4]observed similar negative activation energies for coalescence of water-in-heptane microemulsion droplets stabilised by $C_{12}E_5$. They also observed a slower rate of exchange of probe molecules between droplets near the SPB, consistent with the slower clustering/growth rates observed in this work at these temperatures.

---

[4]S. Clark, P. D. I. Fletcher, and X. Ye, Langmuir, 1990, 6, 1301.

Table 6.4

Comparison between the system variaton of the activation energies of the forward clustering/growth process (E_{act-f}).

R = 2.5 data from unpublished experimental results by P. D. I. Fletcher, Hull University.

System		R = 1.5 E_{act-f} ($kJmol^{-1}$)	R = 2.5 E_{act-f} ($kJmol^{-1}$)
n-variations			
$C_{10}E_5$ #	with	105	23
$C_{12}E_5$	decane	210	507
$C_{12}E_7$	with	-	574
$C_{14}E_7$ #	decane	-	283
m-variations			
$C_{12}E_5$		210	507
$C_{12}E_6$ #	with decane	490	512
$C_{12}E_7$		-	574
n/m = 2			
$C_{10}E_5$ #		105	23
$C_{12}E_6$ #	with decane	490	512
$C_{14}E_7$ #		-	283
oil length variations with $C_{12}E_5$ at equivalent drop size			
C7	R = 2.5	528	-
C14	R = 1.26	186	-
$C_{12}E_5$/C14 @ R = 2.5		-	249

Figure 6.4 a

ln k_f versus 1/T plots obtained for $C_{12}E_m$ surfactants with decane at R = 2.5.

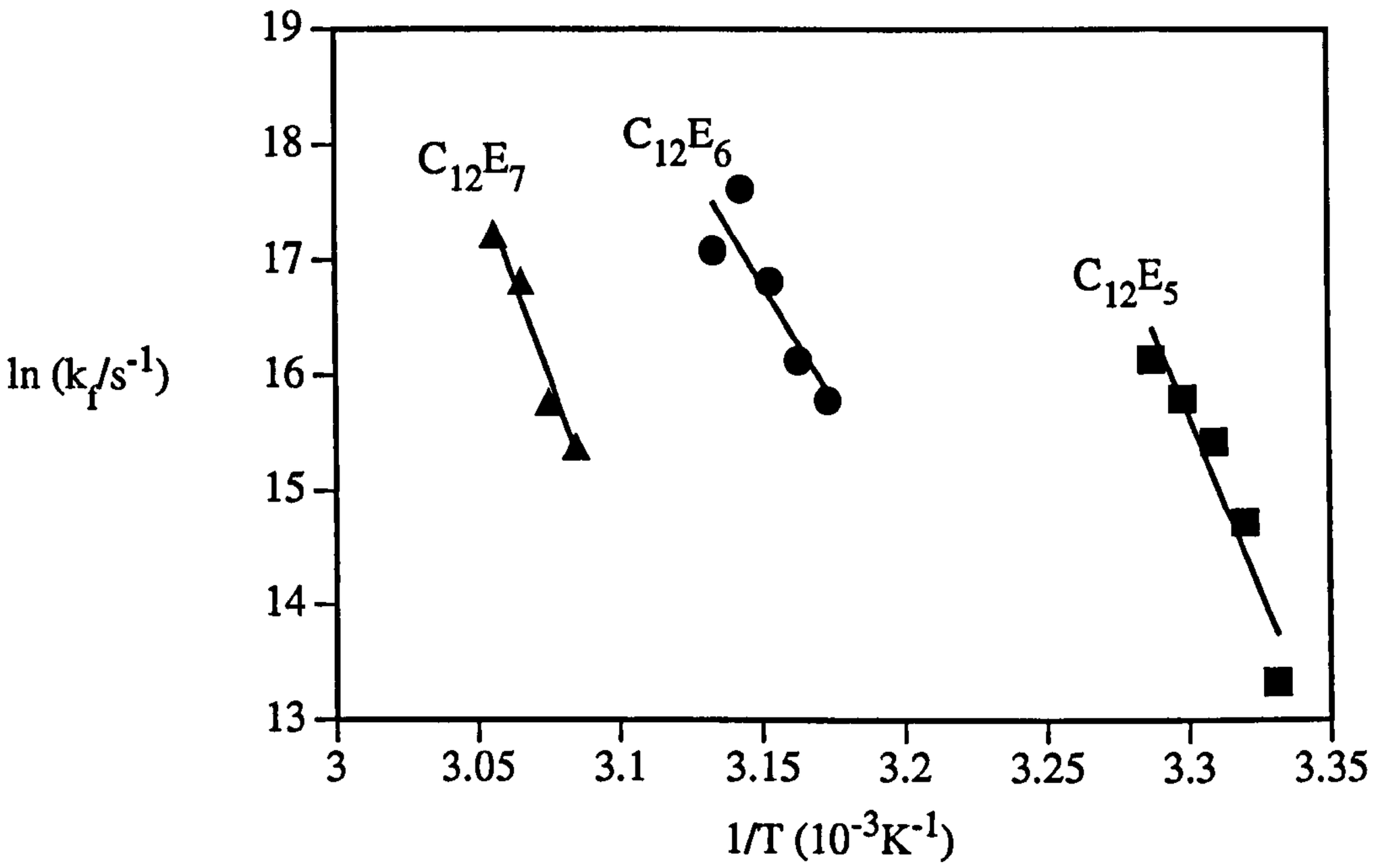

Figure 6.4 b

ln k_f and ln k_r versus 1/T plots obtained for different drop sizes of $C_{12}E_5$ with tetradecane. Circles denote R = 1.5, squares denote R = 2.5.

(i) Forward rate constants.

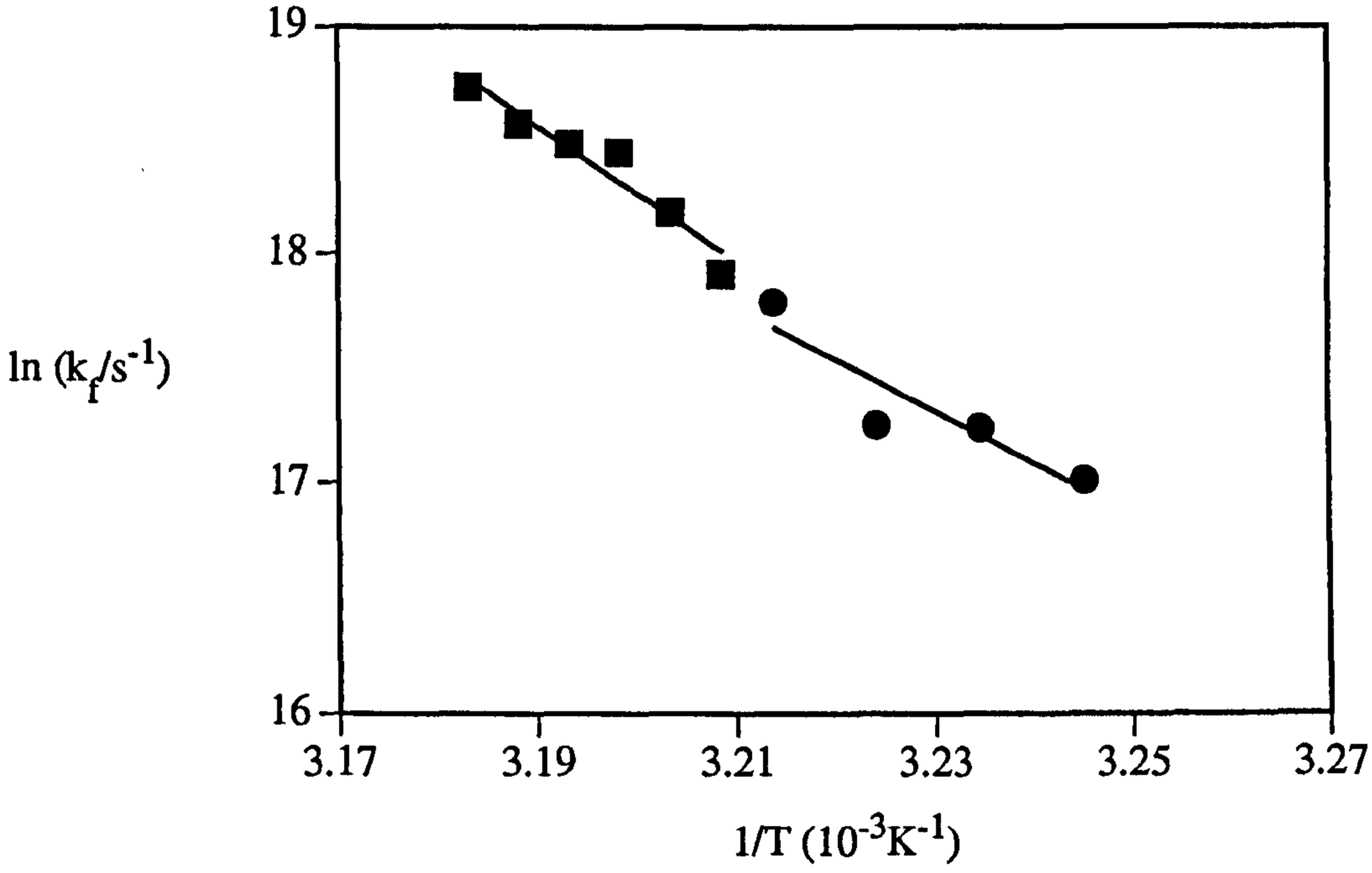

(ii) Reverse rate constants

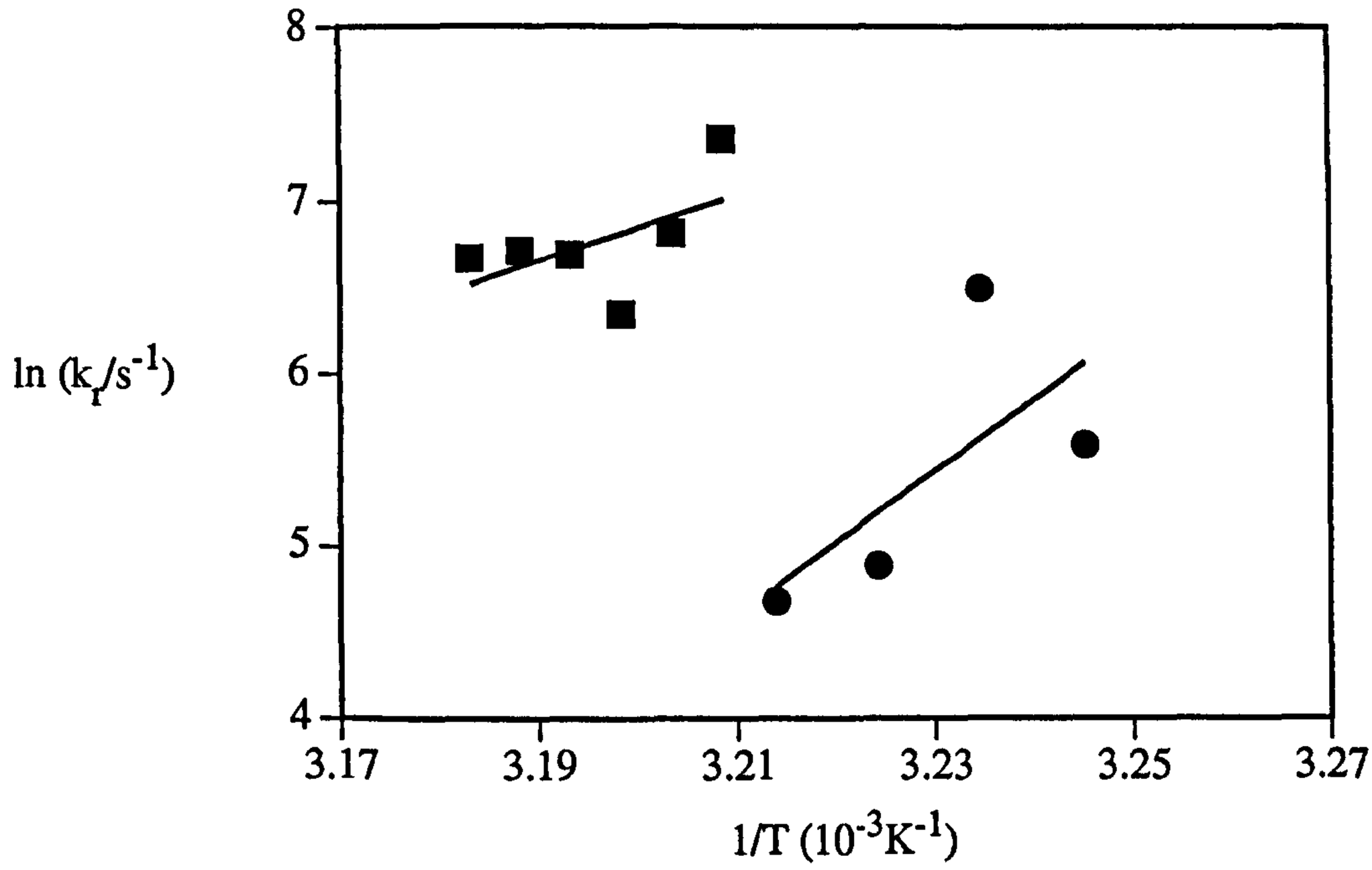

6.5 Summary

- The results from the kinetic study are consistent with the study of the equilibrium behaviour in that the clustering/growth process appears to be dependent on the packing density of the head groups in the surfactant monolayer. A higher packing density promotes a greater rate of clustering/growth, the rates are of the order of $10^6\ M^{-1}s^{-1}$.

- The reverse process is of the order of $10^3\ s^{-1}$, and shows a similar dependency on the packing density. Where the packing density is constant, assuming clustering occurs, it is postulated that the ability of the monolayers from the two clustering drops to interpenetrate determines the stability of the clustered species. Shorter head groups are more able to interpenetrate and hence the rate of unclustering is slower.

- The activation energy is found to be of the order of a few hundred $kJmol^{-1}$ but no obvious trends between systems emerge from the data.

CHAPTER SEVEN

7 Summary

The concern of this thesis was to study the single phase alkane oil-in-water microemulsions stabilised by the non-ionic C_nE_m surfactants, and to characterise their behaviour in terms of the effect of the different constituents n, m, and x-alkane oil. The main conclusions from this work are summarised below.

1) Initially the limiting temperature boundaries of the single phase microemulsion regions were determined to enable further detailed work to be carried out. The boundaries were determined by measurements of the turbidity of the system. The turbidity was observed to be at a minimum at the lower temperature phase boundary corresponding to the solubilisation phase boundary, and a maximum at the upper temperature limit. The temperature range over which the 1ϕ region exists was found to be dependent on the structure of the surfactant and the alkane oils and the amount of oil. The concentration of surfactant has little effect on its position.

For these C_nE_m/alkane oil/water systems the temperature of this region is:

(a) *increased* by increasing the head group size of the surfactant (m) or the alkane oil chain length (x);

(b) *decreased* by increasing the length of the surfactant hydrocarbon chain (n);

(c) For surfactant systems where n/m = 2, the SPB temperature was found to be constant due to the opposing effects of the tail and head group, whereas the UTPB is increased i.e. the 1ϕ region is stable over a wider temperature range.

2) Microemulsion droplet sizes were determined by both static and dynamic light scattering methods - turbidity and PCS respectively. The particle size was observed to be at a minimum at the SPB and to increase with temperature corresponding to clustering or growth of the droplets. The size of the particle at the SPB was assumed to correspond to the individual microemulsion droplets at their preferred size, and this value (the hydrodynamic radius) was used to calculate the area (A_s) occupied per surfactant molecule at the interface between the droplet oil core and the surfactant monolayer. A_s was found to depend on n and x as described below, whereas m was found to have no significant effect.

A_S, and therefore the packing density, of the surfactant monolayer was found to be:

(a) *increased* by:

- Increasing the length of the surfactant tail group (n)
- Increasing the overall surfactant length (at n/m = 2), the dominant factor being the increase in the surfactant tail length since, as established earlier, head group size has no effect.

(b) *decreased* by:

- Increasing the alkane oil chain length (x). An explanation of this could be that the longer chain alkanes penetrate the tail area of the surfactant monolayer less than the shorter chains allowing closer packing of the surfactant monolayer.

3) Turbidity measurements were found to be a simple method of measuring the extent of the increase in size of the particle with temperature. This information was then used to determine the equilibrium constant for the clustering/growth process, from which the associated enthalpy (ΔH^o), Gibbs free energy (ΔG^o) and the entropy (ΔS^o) could then be calculated both per mole of droplets, and, assuming clustering occurs, per mole of surfactant molecules involved in the clustering region. The main conclusions are summarized below:

- The simple aggregation scheme described in section 5.1 was found to fit well to the middle droplet concentration range of 0.04 - 0.10 $moll^{-1}$. As expected the equilibrium constant was found to increase with increasing temperature.

- The large positive value of the enthalpy change (of the order of 1000 kJ mol^{-1}) noted for all systems accounts for the strong temperature dependence observed for the turbidity of the single phase O/W microemulsion region. The favourable positive entropy change (of the order of 3 $kJK^{-1}mol^{-1}$) can be attributed to the dehydration of the surfactant head groups. If dehydration occurs the water molecules are released from

the ordered constraint of bonding either to the surfactant head groups or to each other in the inter head group area. The favourable negative value of the Gibbs free energy (of the order of -14 kJ mol^{-1}) indicates that clustering/growth is spontaneous and driven mainly by entropy.

- The clustering/growth process appears to be dependent on the packing density of the surfactant head groups in the monolayer at the droplet surface. The energy changes per mole of surfactant molecules involved in the clustering region, and the associated equilibrium constant, are found to be greater for systems having the more widely spaced head groups. This is consistent with the theory of the dependence of clustering/growth on the dehydration of the head groups. The more widely spaced head groups are likely to be more hydrated and require more heat to dehydrate, with the corresponding increase in entropy, Gibbs free energy and equilibrium constant.

- Due to the larger numbers of molecules involved between droplets having a greater packing density, the total energy change per mole of droplets, and the equilibrium constant is greater for these systems.

4) The results from the kinetic study are consistent with those of the equilibrium behaviour in that the clustering/growth process appears to be dependent on the packing density of the head groups in the surfactant monolayer. The main conclusions are summarised below:

- A higher packing density promotes a greater rate of clustering/growth. The rates were found to be of the order of 10^6 $M^{-1}s^{-1}$. Again this is an indication of the ease with which the head groups can be dehydrated. A higher packing density of head groups suggests that they would require less dehydration, and would therefore be able to cluster/grow more quickly.

- The reverse process was found to be of the order of 10^3 s^{-1}, and showed a similar dependency on the packing density.

- Where the packing density is constant, assuming clustering occurs, it was postulated that the ability of the monolayers of the two clustering drops to interpenetrate determines the stability of the clustered species. Shorter head groups are more able to interpenetrate and hence the rate of unclustering is slower.

- The activation energy for the clustering/growth process was found to be of the order of a few hundred $kJmol^{-1}$ but no obvious trends between systems were observed. Apparently negative activation energies were observed for the reverse process.

5) In final summary, the behaviour of these oil-in-water microemulsion systems is affected by the packing density of the surfactant monolayer, which in turn is altered by changing one or more of the constituents of the system - the surfactant tail group length (n), the surfactant head group size (m), or the length of the alkane oil (x). The effects of these constituents are summarised below:

Increase in variable	Effect on:				
	Temperature of 1ϕ region	A_s, A_h	Packing density	K	Rate of clustering/growth
n	decreased	increased	decreased	decreased	decreased
m	increased	none	none	none	none
x	increased	decreased	increased	increased	increased

and can be rationalised as follows:

- Increasing **n** promotes micellisation, and hence the 1ϕ region occurs at a lower temperature. A larger tail group occupies more space within the surfactant monolayer and thus the packing density of the surfactants is decreased requiring greater heat to dehydrate the head groups, thus reducing the rate of clustering/growth.

- Increasing **m** opposes micellisation and therefore the temperature of the 1ϕ region is increased. The packing density is not significantly affected, and therefore no effect on the rate of clustering is observed. However the rate of unclustering is increased for the longer head groups, indicating that such droplets are less stable in the clustered state. The monolayers having a shorter head groups are possibly more able to interpenetrate, thus making the clustered species more stable and slower to uncluster.

- Increasing **x** reduces the ability of the alkane oil to penetrate the surfactant tail group which has the same effect as decreasing the tail group length. Micellisation is therefore less favourable and hence the temperature of the one phase region is increased. The surfactant molecules are able to pack together more closely thus less heat is required to dehydrate the head groups and the rate of clustering/growth is increased.

APPENDICES

APPENDIX I

Computer programs for turbidity models 1 and 2 used in chapter 4 to calculate A_S.

Computer program used in chapter 4 to calculate A_S from turbidity data for model 1. Shown with parameters from $C_{12}E_5$ with decane.

```
>LIST

   10 REM PROGRAM TURBHE POIF/JM 4/3/92

   20 REM INPUT FIXED PARAMETERS

   30 REM NP IS THE REFRACTIVE INDEX OF THE  PARTICLE (PURE OIL)

   40 NP = 1.4218

   50 REM NS IS THE REFRACTIVE INDEX OF THE  SOLVENT (PURE WATER)

   60 NS = 1.3416

   70 REM DELTAT IS THE LENGTH OF THE SURFACTANT TAIL

   80 DELTAT = 2.6

   90 REM LAMBDA IS THE WAVELENGTH OF LIGHT IN VACUUM (I.E. LAMBDA 0)AT WHICH T
E TURBIDITY MEASUREMENTS WERE MADE(NM).

  100 LAMBDA = 407

  105 LAMBDA = LAMBDA/NE

  110 REM MV IS THE MOLAR VOLUME OF THE OIL (MWT/DENSITY)

  120 MV = 196.21

  130 REM MVS IS THE MOLAR VOLUME OF THE SURFACTANT

  140 MVS = 406.58

  150 REM NBW IS THE NUMBER OF BOUND WATER MOLECULES

  160 NBW = 5

  170 REM SURFC IS THE SURFACTANT CONCENTRATION

  180 SURFC = 0.09

  190 REM NE IS THE NUMBER OF EXPERIMENTAL POINTS

  200 NE = 5

  210 DIM RE(NE):DIM TE(NE)

  220 REM CALCULATE CONSTANT TERMS IN THE RAYLEIGH EQUATION

  230 C1 = (24*PI*PI*PI/(LAMBDA*1E-7)^4)

  240 C2 =(((NP*NP-NS*NS)/(NP*NP+2*NS*NS))^2)

  250 C3 = C1*C2

  260 REM C3 IS IN CM-4

  270 REM INPUT EXPERIMENTAL VALUES OF R(RE) AND ABSORBANCE (TE)
```

```
280 RE(1) = 0.67:TE(1) = .024
290 RE(2) = 1.38: TE(2) = 0.028
300 RE(3) = 2.75: TE(3) = 0.135
310 RE(4) = 4.14: TE(4) = 0.333
320 RE(5) = 5.64: TE(5) = 0.678
330 REM AS IS THE AREA OCCUPIED PER SURFACTANT MOLECULE
340 REM INPUT THE ESTIMATED RANGE FOR  AS - START OF RANGE = ASINIT
    END OF RANGE IN LINE 340                SIZE OF INCREMENT = ASSTEP
RUN PROGRAM FOR DIFFERENT VALUES OF DELTAT TO FIND BEST FIT (GGF)
350 ASSTEP = .005
360 ASINIT = 0.1
370 FLAG = 0
380 FOR AS = ASINIT TO 1.7 STEP ASSTEP
390 REM CALCULATE TURBIDITY FOR DIFFERENT R VALUES
400 IF AS = ASINIT THEN GOTO 420
410 GGFO = GGFN:GGFN = 0
420 FOR DP = 1 TO NE
430 R = RE(DP):TAUE = TE(DP)
440 RC = 3*MV*R/(AS*1E-14)/6.023E23
450 REM RC IS THE RADIUS OF THE OILY   CORE (CM)
460 VPC = (4*PI*RC^3)/3
470 REM VPC IS THE VOLUME OF OIL IN THE PARTICLE (CM3)
480  N = SURFC*R*MV*1E-3/VPC
490 REM N IS THE NUMBER OF PARTICLES PER UNIT VOLUME (CM-3)
500 VP = 4*PI*((RC+DELTAT*1E-7)^3)/3
510 REM VP IS THE VOLUME OF THE PARTICLE (CM3)
520 REM PHI- IS THE VOLUME FRACTION OF O = OIL, S = SURFACTANT, W = WATER.
530 PHIO = SURFC*R*MV/1000
540 PHIS = SURFC*MVS/1000
550 PHIW = SURFC*NBW*0.018
560 PHI = PHIO + PHIW + PHIS
570 HSF =((1-PHI)^4)/((1+2*PHI)^2-(PHI^3)*(4-PHI))
580 TAU = C3*N*VP*VP*HSF/2.303
585 REM THE FACTOR 2.303 CONVERTS CALCULATED TURBIDITY TO ABSORBANCE (I.E TAU
MEASURED ABS * 2.303)
```

```
590 GF = (SQR((TAU-TAUE)^2))
600 GGFN = GGFN + GF
610 IF FLAG < 1 THEN GOTO 640
620 PRINT "R = "R
630 PRINT "TAU = "TAU
 640 NEXT DP
 650 IF FLAG > 0 THEN STOP
 660 IF AS = ASINIT THEN GOTO 680
 670 IF GGFN > GGFO THEN GOTO 690
 680 NEXT AS
 690 AS = AS - ASSTEP:FLAG = 1:PRINT "BEST AS ="AS:PRINT"GGF = "GGFO:PRINT "DE
TAT ="DELTAT
 700 GOTO 390
 710 END
```

Result

```
>RUN
BEST AS =      0.375
GGF = 1.87444237E-2
DELTAT =        2.6
R =         0.67
TAU = 2.3807125E-2
R =         1.38
TAU = 4.27516902E-2
R =         2.75
TAU = 0.13688464
R =         4.14
TAU =  0.3318913
R =         5.64
TAU = 0.678806518

 STOP at line 650
```

Computer program used in chapter 4 to calculate A_s from turbidity data for model 2. Shown with parameters from $C_{12}E_5$ with decane.

```
10 REM PROGRAM TURBHS PDIF/JM 4/3/92
20 REM INPUT FIXED PARAMETERS
30 REM N1 IS THE REFRACTIVE INDEX OF THE  CORE (PURE OIL)
35 N1 = 1.4222
40 REM N2 IS THE REFRACTIVE INDEX OF THE SHELL (SURFACTANT)
45 N2 = 1.4621
50 REM N3 IS THE REFRACTIVE INDEX OF THE  SOLVENT (PURE WATER)
55 N3 = 1.3417
70 REM DELTAT IS THE LENGTH OF THE SURFACTANT TAIL
80 DELTAT = 1.95
90 REM LAMBDA IS THE WAVELENGTH OF LIGHT IN VACUUM (I.E. LAMBDA 0)AT WHICH T
E TURBIDITY MEASUREMENTS WERE MADE(NM).
100 LAMBDA = 407
105 LAMBDA = LAMBDA/N3
110 REM MV IS THE MOLAR VOLUME OF THE OIL (MWT/DENSITY)
120 MV = 195.95
130 REM MVS IS THE MOLAR VOLUME OF THE SURFACTANT
140 MVS = 405.55
150 REM NBW IS THE NUMBER OF BOUND WATER MOLECULES
160 NBW = 5
170 REM SURFC IS THE SURFACTANT CONCENTRATION
180 SURFC = 0.09
190 REM NE IS THE NUMBER OF EXPERIMENTAL POINTS
200 NE = 5
210 DIM RE(NE):DIM TE(NE)
220 REM CALCULATE CONSTANT TERMS IN THE RAYLEIGH EQUATION
260 REM C3 IS IN CM-4
270 REM INPUT EXPERIMENTAL VALUES OF R(RE) AND ABSORBANCE (TE)
280 RE(1) = 0.67:TE(1) = .024
290 RE(2) = 1.38: TE(2) = 0.028
300 RE(3) = 2.75: TE(3) = 0.135
310 RE(4) = 4.14: TE(4) = 0.333
320 RE(5) = 5.64: TE(5) = 0.678
```

```
330 REM AS IS THE AREA OCCUPIED PER SURFACTANT MOLECULE

340 REM INPUT THE ESTIMATED RANGE FOR  AS - START OF RANGE = ASINIT
    END OF RANGE IN LINE 340                    SIZE OF INCREMENT = ASSTEP
RUN PROGRAM FOR DIFFERENT VALUES OF DELTAT TO FIND BEST FIT (GGF)

350 ASSTEP = .005

360 ASINIT = 0.1

370 FLAG = 0

380 FOR AS = ASINIT TO 1.7 STEP ASSTEP

390 REM CALCULATE TURBIDITY FOR DIFFERENT R VALUES

400 IF AS = ASINIT THEN GOTO 420

410 GGFO = GGFN:GGFN = 0

420 FOR DP = 1 TO NE

430 R = RE(DP):TAUE = TE(DP)

440 RC = 3*MV*R/(AS*1E-14)/6.023E23

450 REM RC IS THE RADIUS OF THE OILY   CORE (CM)

460 VPC = (4*PI*RC^3)/3

470 REM VPC IS THE VOLUME OF OIL IN THE PARTICLE (CM3)

480  N = SURFC*R*MV*1E-3/VPC

490 REM N IS THE NUMBER OF PARTICLES PER UNIT VOLUME (CM-3)

500 VP = 4*PI*((RC+DELTAT*1E-7)^3)/3

510 REM VP IS THE VOLUME OF THE PARTICLE (CM3)

520 REM PHI- IS THE VOLUME FRACTION OF O = OIL, S = SURFACTANT, W = WATER.

530 PHIO = SURFC*R*MV/1000

540 PHIS = SURFC*MVS/1000

550 PHIW = SURFC*NBW*0.018

560 PHI = PHIO + PHIW + PHIS

  570 HSF =((1-PHI)^4)/((1+2*PHI)^2-(PHI^3)*(4-PHI))

  571 C1 = (24*PI*PI*PI/(LAMBDA*1E-7)^4)

  572 Q = RC/(RC+DELTAT*1E-7)

  573 M1 = N1/N3

  574 M2 = N2/N3

  575 C2 = (((M2*M2-1)*(M1*M1+2*M2*M2)+Q*Q*Q*(2*M2*M2+1)*(M1*M1-M2*M2))/((M2*M
2)*(M1*M1+2*M2*M2)+Q*Q*Q*(2*M2*M2-2)*(M1*M1-M2*M2)))^2

  576 C3 = C1*C2
```

```
 580 TAU = C3*N*VP*VP*HSF/2.303

 585 REM THE FACTOR 2.303 CONVERTS CALCULATED TURBIDITY TO ABSORBANCE (I.E TAU
MEASURED ABS * 2.303)

 590 GF = (SQR((TAU-TAUE)^2))

 600 GGFN = GGFN + GF

 610 IF FLAG < 1 THEN GOTO 640

 620 PRINT "R = "R

 630 PRINT "TAU = "TAU

 640 NEXT DP

 650 IF FLAG > 0 THEN STOP

 660 IF AS = ASINIT THEN GOTO 650

 670 IF GGFN > GGFO THEN GOTO 690

 680 NEXT AS

 690 AS = AS - ASSTEP:FLAG = 1:PRINT "BEST AS ="AS:PRINT"GGF = "GGFO:PRINT "DE
TAT ="DELTAT

 700 GOTO 390

 710 END
```

Result

```
>RUN
BEST AS =      0.385
GGF = 2.31376008E-2
DELTAT =       1.95
R =         0.67
TAU = 1.88342438E-2
R =         1.38
TAU = 3.98491238E-2
R =         2.75
TAU = 0.136932635
R =         4.14
TAU = 0.334418285
R =         5.64
TAU = 0.680771801

STOP at line 650
```

APPENDIX II

Calculation of the contact area for the clustering of two spherical microemulsion droplets. Used in chapter 5.

Calculation of the contact area for the clustering of two spherical microemulsion droplets .

(i)

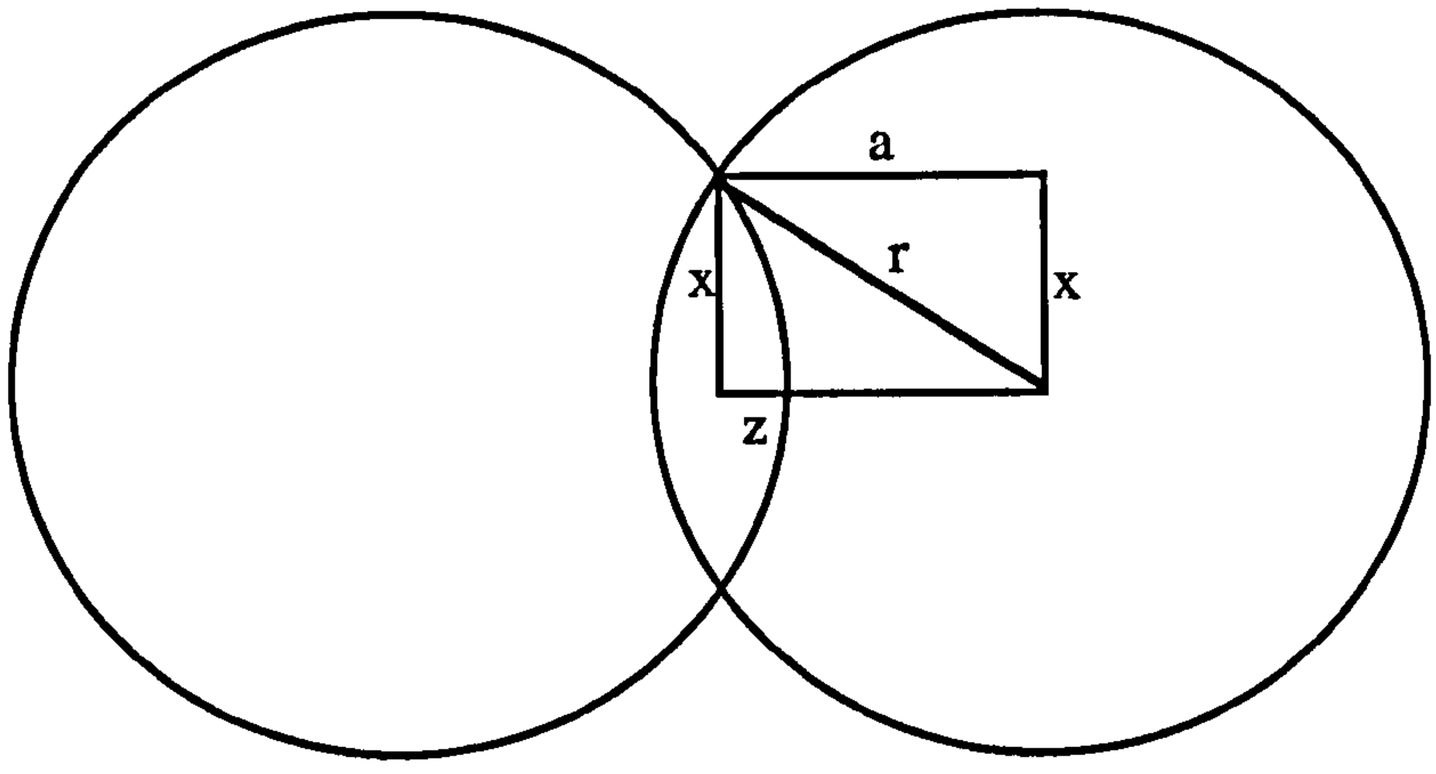

The radius, x, of the contact area between two clustered droplets can be calculated by simple geometric considerations.

From Pythagoras' Theorem

$$x^2 = r^2 - a^2$$

noting that

$$a = r - z$$

then

$$x^2 = r^2 - (r - z)^2$$

so

$$x = \{r^2 - (r - z)^2\}^{1/2}$$

where r is the radius of the droplet, and z can be regarded as a measure of the depth of penetration of the two monolayers.

(ii) A plot of the variation of x with z for droplets of different radius.

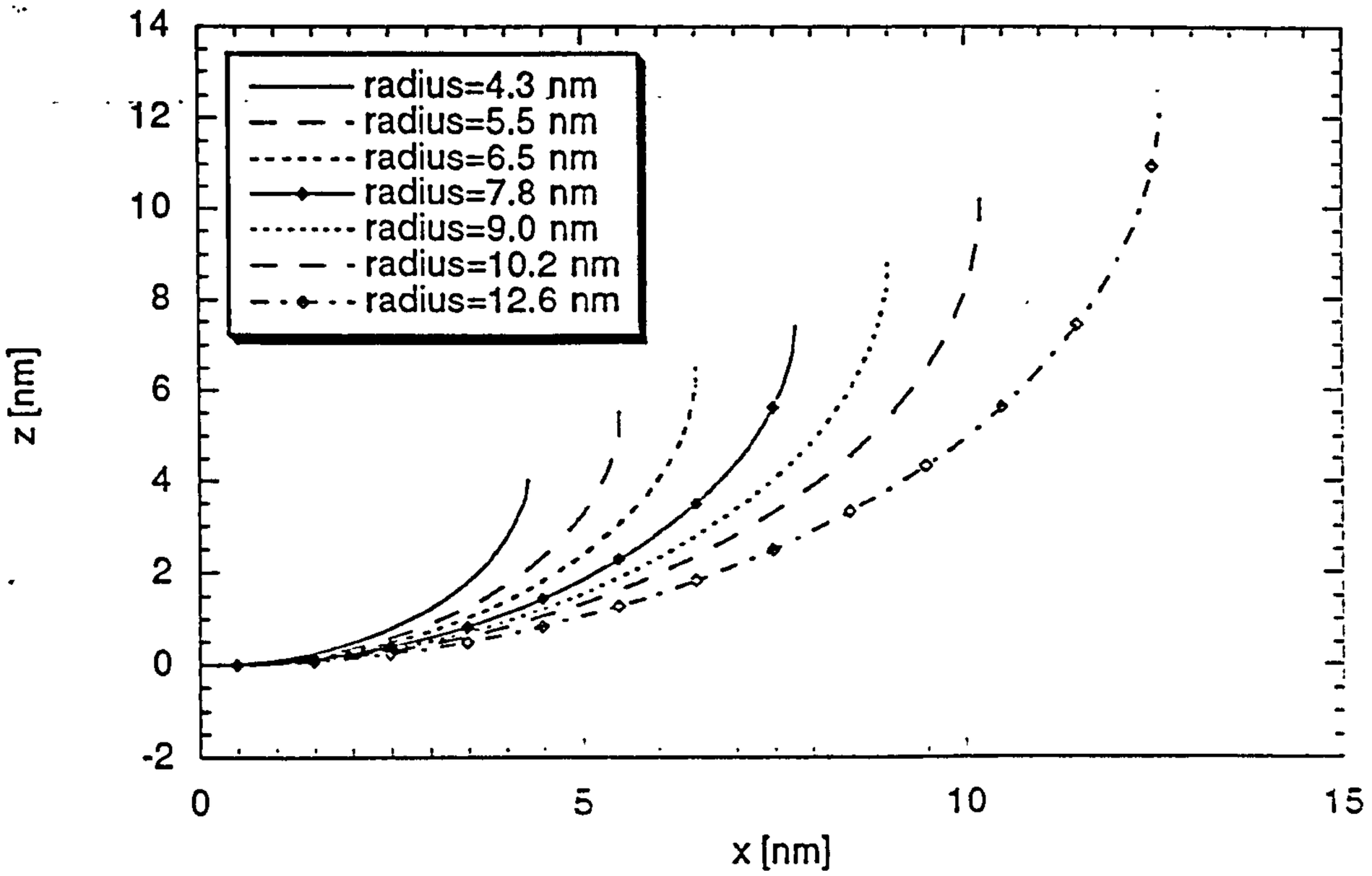

(iii) The variation in the contact radius x (nm) with hydrodynamic radius r_h (nm) for a constant (arbitrary) value of 1 nm for z. The equation of the line is given by:

$$x = 1.26\ r_h^{0.539}.$$

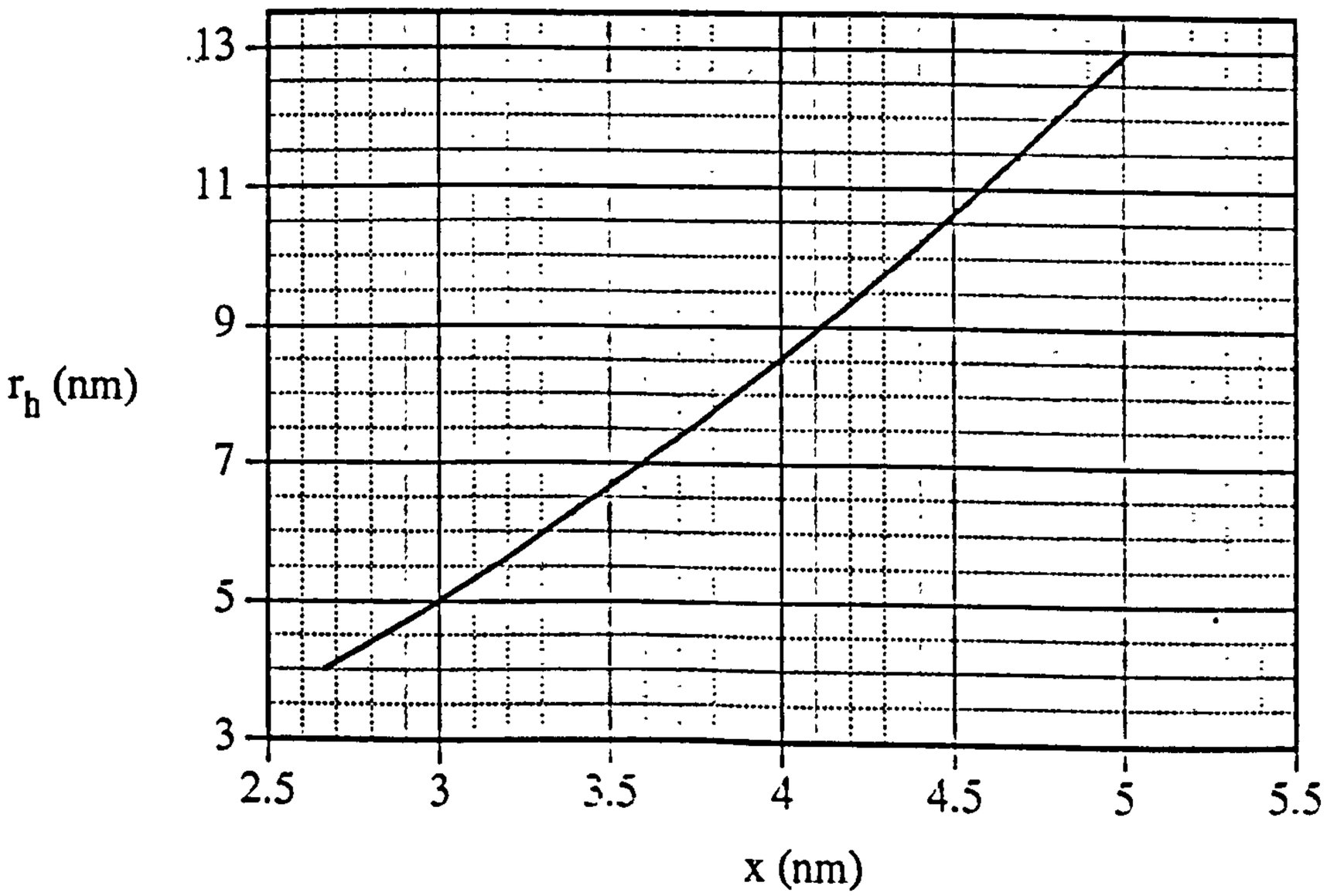

(iv) The fraction, F, of the surface of a droplet involved in the contact area can be calculated as follows:

$$\text{Area of contact} = \pi x^2$$

$$\text{Surface area of the droplet} = 4\pi r_h^2$$

$$\text{Fraction of the droplet involved in the contact area, } F = \pi x^2 / 4\pi r_h^2$$

The thermodynamic parameters can therefore be calculated per mole of surfactant molecules involved in the contact area by:

$$\text{Energy per mole of surfactant molecules} = \text{Energy per mole of droplets} / 2FN_{agg}$$

Noting that F should be doubled since the surfaces of two droplets are involved in the contact area.

APPENDIX III

The absorbance values, measured at 406 nm, for varying temperatures (^{o}C) of the O/W microemulsion single phase domains of C_nE_m/x-alkane oil/water systems.at varying R value. Data used in chapters 4 and 5.

The minimum absorbance values measured for each C_nE_m/C_x alkane oil/water system with varying R value, at X M surfactant concentration.

System	R	Minimum Absorbance
$C_{10}E_5/C_{10}$ *0.08 M*	0.50	0.022
	1.00	0.030
	1.50	0.041
	2.00	0.066
	2.50	0.121
$C_{12}E_4/C_{10}$ *0.09 M*	2.88	0.180
	3.48	0.293
	4.38	0.477
	4.82	0.619
	5.47	0.780
$C_{12}E_5/C_7$ *0.09 M*	1.58	0.038
	2.88	0.077
	3.69	0.110
	4.42	0.142
	6.26	0.271
	7.46	0.371
$C_{12}E_5/C_{10}$ *0.09 M*	0.67	0.024
	1.38	0.028
	2.75	0.135
	4.14	0.333
	5.64	0.678
$C_{12}E_5/C_{14}$ *0.014 M* [1]	1.00	0.011
	2.00	0.034
	3.00	0.154
	3.50	0.261
	4.00	0.407

System	R	Minimum Absorbance
$C_{12}E_6/C_{10}$ *0.016 M*	2.00	0.024
	2.50	0.044
	3.00	0.058
	4.00	0.102
	5.00	0.189
0.033M	0.50	0.009
	1.00	0.021
	2.00	0.039
	3.00	0.088
	4.00	0.171
0.093 M	0.50	0.035
	1.00	0.062
	2.00	0.098
	3.00	0.130
	4.00	0.267
$C_{12}E_7/C_{10}$ *0.09 M*	1.36	0.012
	2.11	0.076
	2.78	0.124
	3.37	0.180
	4.10	0.256
$C_{14}E_7/C_{10}$ *0.09 M*	0.50	0.033
	1.00	0.032
	2.00	0.096
	3.00	0.127
	3.50	0.188

[1] P. D. I. Fletcher, J. F. Holzwarth, J. Phys. Chem. 1991, 95, 1210.

The absorbance values measured at 406 nm for varying temperature (^{o}C) at different R values of **0.093 M $C_{12}E_6$ with decane** . Data used in chapters 4 and 5.

R	Temperature	Absorbance
0.5	24.6	0.035
	27.1	0.036
	34.1	0.060
	38.7	0.089
	42.1	0.231
1.0	30.9	0.062
	31.8	0.063
	35.4	0.072
	37.4	0.088
	39.0	0.106
	39.1	0.111
	41.5	0.155
	42.6	0.208
	43.3	0.270
2.0	37.6	0.098
	38.6	0.099
	40.5	0.107
	41.9	0.140
	43.7	0.187
	44.7	0.247
3.0	41.7	0.130
	43.1	0.145
	43.7	0.159
	44.3	0.182
	45.8	0.273
4.0	45.2	0.267
	45.6	0.280
	46.7	0.328
	47.1	0.369
	46.7	0.328
	47.1	0.369

APPENDIX IV

The absorbance values, measured at 406 nm, for varying temperatures (^{o}C) of the O/W microemulsion single phase domains of C_nE_m/x-alkane oil/water systems at varying surfactant concentrations. Data used in chapters 5 and 6.

$C_{10}E_5$ with decane at R = 1.5

The absorbance values measured at 406 nm for varying temperature (^{o}C) at different surfactant concentrations. Data used in chapters 5 and 6.

[Surfactant]	Temperature	Absorbance
0.04 M	33.8	0.023
	35.3	0.023
	37.1	0.027
	37.5	0.030
	38.7	0.040
	39.1	0.048
	40.2	0.074
	40.9	0.122
	41.6	0.199
0.06 M	33.8	0.030
	35.3	0.032
	37.1	0.041
	37.5	0.046
	38.7	0.061
	39.1	0.079
	40.2	0.128
	40.9	0.217
0.08 M	33.8	0.037
	35.3	0.041
	37.1	0.055
	37.5	0.064
	38.7	0.089
	39.1	0.114
	40.2	0.188
	40.9	0.406
0.10 M	34.0	0.043
	35.7	0.050
	36.4	0.054
	37.5	0.065
	38.1	0.076
	39.1	0.103
	39.7	0.137
	40.5	0.241
	41.0	0.278
	41.5	0.426
0.12 M	32.4	0.049
	34.0	0.049
	35.7	0.057
	36.4	0.062
	37.5	0.075
	38.1	0.087
	39.1	0.116
	39.7	0.154
	40.5	0.202
	41.0	0.320
	41.5	0.502

$C_{10}E_5$ with decane at R = 2.5

The absorbance values measured at 406 nm for varying temperature (^{o}C) at different surfactant concentrations. Data used in chapters 5 and 6.

[Surfactant]	Temperature	Absorbance
0.01975 M	40.1	0.033
	40.9	0.039
	41.8	0.044
	42.7	0.055
	43.5	0.070
	44.1	0.096
	44.6	0.120
0.0395 M	40.9	0.082
	41.8	0.101
	42.7	0.135
	43.5	0.186
	44.1	0.334
	44.6	0.525
0.079 M	40.9	0.145
	41.8	0.165
	42.7	0.223
	43.5	0.304
	44.1	0.508
	44.6	0.961
0.1185 M	41.2	0.166
	42.0	0.199
	42.9	0.267
	43.4	0.327
	43.8	0.404
	44.3	0.579
0.158 M	41.2	0.168
	42.0	0.204
	42.9	0.275
	43.4	0.347
	43.8	0.429
	44.3	0.614
0.1975 M	41.2	0.149
	42.0	0.175
	42.9	0.221
	43.4	0.260
	43.8	0.311
	44.3	0.402

$C_{12}E_5$ with heptane at R = 2.5.

The absorbance values measured at 406 nm for varying temperature (^{o}C) at different surfactant concentrations. Data used in chapters 5 and 6.

[Surfactant]	Temperature	Absorbance
0.01 M	12.2	0.005
	13.2	0.006
	14.2	0.008
	16.1	0.012
	17.6	0.016
	18.9	0.022
	19.7	0.025
	20.7	0.029
	21.0	0.035
	21.3	0.041
	21.7	0.054
	21.8	0.050
	21.9	0.138
0.02 M	15.8	0.015
	16.7	0.016
	18.1	0.017
	18.6	0.018
	19.8	0.026
	20.3	0.035
	21.1	0.368
0.04 M	15.8	0.018
	16.7	0.028
	18.1	0.031
	18.6	0.037
	19.8	0.051
	20.3	0.073
	20.9	0.090
	21.1	0.095
0.06 M	13.9	0.039
	14.6	0.039
	15.8	0.039
	16.7	0.040
	18.1	0.045
	18.6	0.054
	19.8	0.073
	20.3	0.099
	20.9	0.115
	21.1	0.121
0.08 M	15.2	0.040
	15.2	0.040
	16.3	0.041
	16.8	0.043
	17.9	0.049
	18.5	0.062
	19.6	0.083
	20.1	0.106
	20.9	0.131
	21.3	0.143
0.10 M	16.3	0.049
	16.8	0.062
	17.9	0.056
	18.5	0.082
	19.6	0.092
	20.1	0.114
	20.9	0.137
	21.3	0.160
0.12 M	15.2	0.053
	15.2	0.054
	16.3	0.055
	16.8	0.058
	17.9	0.066
	18.5	0.081
	19.6	0.101
	20.1	0.118
	20.9	0.139
	21.3	0.146

$C_{12}E_5$ with decane at R=1.5

The absorbance values measured at 406 nm for varying temperature (^{o}C) at different surfactant concentrations. Data used in chapters 5 and 6.

[Surfatant]	Temperature	Absorbance
0.04 M	20.3	0.031
	21.1	0.032
	23.0	0.033
	25.4	0.043
	25.9	0.053
	27.2	0.072
	27.8	0.099
	28.7	0.139
	29.5	0.214
	29.8	0.270
0.06 M	20.3	0.035
	21.1	0.035
	23.0	0.037
	25.4	0.056
	25.9	0.072
	27.2	0.100
	27.8	0.131
	28.7	0.181
	29.5	0.282
	29.8	0.360
0.08 M	20.3	0.044
	21.1	0.045
	23.0	0.047
	25.4	0.075
	25.9	0.093
	27.2	0.123
	27.8	0.153
	28.7	0.204
	29.5	0.307
	29.8	0.383
0.12 M	20.7	0.043
	22.2	0.045
	23.9	0.053
	25.5	0.078
	27.1	0.111
	28.8	0.165
	29.7	0.229

$C_{12}E_5$ with decane at R = 2.5

The absorbance values measured at 406 nm for varying temperature (^{o}C) at different surfactant concentrations. Data used in chapters 5 and 6.

[Surfactant]	Temperature	Absorbance
0.01 M	24.4	0.017
	25.9	0.018
	27.6	0.018
	29.0	0.021
	30.1	0.030
	30.7	0.038
	31.7	0.071
	32.1	0.184
	32.5	0.829
0.02 M	24.4	0.039
	25.9	0.039
	27.6	0.041
	29.0	0.051
	30.1	0.077
	30.7	0.103
	31.7	0.196
	32.1	0.330
0.04 M	24.4	0.056
	25.9	0.057
	27.6	0.061
	29.0	0.082
	30.1	0.165
	30.7	0.174
	31.7	0.413
0.06 M	26.8	0.094
	27.1	0.099
	28.2	0.114
	28.4	0.125
	29.6	0.180
	30.0	0.211
	31.0	0.311
	31.6	0.439
0.08 M	24.6	0.099
	25.4	0.100
	26.1	0.102
	27.7	0.117
	29.1	0.174
	29.6	0.213
	30.6	0.294
	31.9	0.644
0.10 M	24.6	0.109
	25.4	0.110
	26.1	0.112
	27.7	0.131
	29.1	0.192
	29.6	0.228
	30.6	0.297
	31.9	0.623
0.12 M	24.6	0.104
	25.4	0.106
	26.1	0.108
	27.7	0.128
	29.1	0.184
	29.6	0.217
	30.6	0.270
	31.9	0.508

$C_{12}E_5$ with tetradecane at R = 1.26

The absorbance values measured at 406 nm for varying temperature (^{o}C) at different surfactant concentrations. Data used in chapters 5 and 6.

[Surfactant]	Temperature	Absorbance
0.01 M	32.3	0.008
	33.8	0.009
	35.4	0.011
	35.8	0.014
	36.9	0.021
	37.5	0.032
	37.9	0.042
	38.2	0.055
	38.5	0.062
0.02 M	32.3	0.021
	33.8	0.023
	35.4	0.032
	35.8	0.041
	36.9	0.062
	37.5	0.094
	37.9	0.122
	38.2	0.179
	38.5	0.225
0.04 M	28.4	0.037
	30.4	0.037
	31.4	0.038
	33.1	0.041
	34.7	0.052
	35.2	0.066
	36.3	0.094
	37.0	0.136
	37.8	0.209
	38.4	0.315
0.06 M	28.4	0.050
	30.4	0.051
	31.4	0.052
	33.1	0.058
	34.7	0.080
	35.2	0.102
	36.3	0.144
	37.0	0.206
	37.8	0.315
	38.4	0.483
0.08 M	28.4	0.065
	30.4	0.065
	31.4	0.067
	33.1	0.076
	34.7	0.107
	35.2	0.135
	36.3	0.181
	37.0	0.250
	37.8	0.379
	38.4	0.574
0.10 M	28.6	0.070
	30.1	0.071
	31.9	0.074
	33.2	0.086
	34.6	0.126
	35.6	0.158
	37.0	0.277
	37.2	0.241
	37.6	0.337
	38.0	0.450
0.12 M	28.6	0.070
	30.1	0.070
	31.9	0.074
	33.2	0.087
	34.6	0.125
	35.6	0.155
	37.0	0.254
	37.2	0.228
	37.6	0.302
	38.0	0.385

$C_{12}E_6$ with decane at R = 1.5

The absorbance values measured at 406 nm for varying temperature (^{o}C) at different surfactant concentrations. Data used in chapters 5 and 6.

[Surfactant]	Temperature	Absorbance
0.04 M	35.8	0.025
	37.5	0.026
	39.0	0.030
	40.6	0.045
	42.3	0.079
	43.1	0.105
	44.0	0.153
	44.7	0.251
0.06 M	35.8	0.034
	37.5	0.036
	39.0	0.044
	40.6	0.067
	42.3	0.109
	43.1	0.144
	44.0	0.217
	44.7	0.379
0.08 M	35.8	0.049
	37.5	0.053
	39.0	0.065
	40.6	0.092
	42.3	0.140
	43.1	0.171
	44.0	0.250
	44.7	0.403
0.10 M	34.2	0.040
	36.0	0.043
	37.6	0.048
	39.3	0.062
	40.9	0.089
	42.6	0.127
	42.8	0.145
	44.1	0.212
	44.7	0.308

$C_{12}E_6$ with decane at R = 2.5

The absorbance values measured at 406 nm for varying temperature (^{o}C) at different surfactant concentrations. Data used in chapters 5 and 6.

[Surfactant]	Temperature	Absorbance
0.0197 M	42.3	0.031
	42.8	0.033
	43.5	0.032
	44.6	0.036
	45.1	0.043
	45.6	0.045
	46.4	0.068
	47.5	0.110
0.0395 M	41.2	0.068
	42.3	0.070
	42.8	0.072
	43.4	0.076
	44.6	0.095
	45.1	0.115
	45.5	0.126
	46.4	0.186
	47.4	0.297
0.0790 M	42.8	0.120
	43.3	0.130
	44.4	0.162
	45.0	0.187
	45.3	0.201
	46.1	0.273
	47.2	0.312
0.1184 M	39.1	0.092
	40.6	0.101
	42.4	0.105
	44.4	0.148
	45.4	0.185
	46.3	0.227
	47.2	0.307
0.1579 M	39.1	0.092
	40.6	0.098
	42.4	0.109
	44.4	0.147
	45.4	0.178
	46.3	0.208
	47.2	0.266
0.1974 M	39.1	0.084
	40.6	0.107
	42.4	0.099
	44.4	0.122
	45.4	0.146
	46.3	0.162
	47.2	0.191

$C_{12}E_7$ with decane at R = 2.5

The absorbance values measured at 406 nm for varying temperature (^{o}C) at different *surfactant concentrations. Data used in* chapters 5 and 6.

[Surfactant]	Temperature	Absorbance
0.01 M	49.8	0.019
	50.8	0.029
	51.4	0.021
	53.6	0.022
	55.4	0.037
	55.7	0.043
	56.4	0.054
0.02 M	48.1	0.036
	49.8	0.036
	50.8	0.039
	51.4	0.038
	53.6	0.047
	55.4	0.084
	55.7	0.099
	56.4	0.138
0.04 M	46.5	0.049
	48.1	0.049
	49.8	0.058
	50.8	0.067
	51.4	0.077
	53.6	0.148
	55.4	0.426
0.06 M	46.6	0.071
	48.3	0.069
	50.1	0.074
	51.0	0.077
	51.8	0.087
	53.6	0.129
	54.6	0.179
	55.3	0.239
	56.4	0.443
0.08 M	48.5	0.104
	49.2	0.106
	50.0	0.109
	51.0	0.118
	51.8	0.134
	52.5	0.159
	53.3	0.193
	54.8	0.320
	55.7	0.552

[Surfactant]	Temperature	Absorbance
0.10 M	51.0	0.114
	51.8	0.127
	53.6	0.168
	54.6	0.206
	55.3	0.253
	56.4	0.371
0.12 M	48.3	0.127
	50.1	0.132
	51.0	0.132
	51.8	0.148
	53.6	0.195
	54.6	0.233
	55.3	0.276
	56.4	0.401

$C_{14}E_7$ with decane at R = 2.5

The absorbance values measured at 406 nm for varying temperature (^{o}C) at different surfactant concentrations. Data used in chapters 5 and 6.

[Surfactant]	Temperature	Absorbance
0.01927 M	44.4	0.042
	45.3	0.043
	46.1	0.052
	47.1	0.050
	48.0	0.063
	48.8	0.086
	49.7	0.125
	50.3	0.161
	50.7	0.186
0.03854 M	44.4	0.056
	45.3	0.057
	46.1	0.062
	47.1	0.074
	48.0	0.104
	48.8	0.148
	49.7	0.204
	50.3	0.251
	50.7	0.292
0.07708 M	44.4	0.085
	45.3	0.088
	46.1	0.095
	47.1	0.119
	48.0	0.159
	48.8	0.200
	49.7	0.230
	50.3	0.264
	50.7	0.293
0.1156 M	42.8	0.097
	43.7	0.097
	44.6	0.100
	45.4	0.106
	46.3	0.121
	47.1	0.147
	47.7	0.164
	48.8	0.194
	49.6	0.218
	50.5	0.253
0.01542 M	42.8	0.080
	43.7	0.082
	44.6	0.083
	45.4	0.088
	46.3	0.101
	47.1	0.121
	47.7	0.146
	48.8	0.154
	49.6	0.165
	50.5	0.184
0.1927 M	43.7	0.076
	44.6	0.079
	45.4	0.087
	46.3	0.100
	47.1	0.112
	47.7	0.123
	48.8	0.131
	49.6	0.140
	50.5	0.150

APPENDIX V

The hydrodynamic radii measured by PCS at the SPB for each C_nE_m/x-alkane oil/water system. Data used in chapter 4.

The hydrodynamic radii (r_h) measured by PCS at the SPB for each C_nE_m/x-alkane oil/water system. Data used in chapter 4.

System	R	r_h (nm)
$C_{10}E_5/C_{10}$	0.93	4.49
	1.05	6.20
	1.17	5.95
	1.31	6.63
	1.50	7.02
	1.90	7.24
	1.90	8.80
	2.26	7.06
	2.26	10.5
	2.31	5.49
	2.50	11.4
	3.07	10.1
	3.10	10.6
	3.12	11.1
	3.16	10.9
	3.41	14.3
	3.50	9.65
	3.53	16.3
	3.60	15.9
	3.99	13.4
$C_{12}E_4/C_{10}$	2.83	10.5
	2.89	10.7
	3.48	11.0
	4.28	12.7
	4.63	14.0
	5.62	17.0
$C_{12}E_5/C_{10}$	0.81	5.53
	1.59	6.48
	2.75	8.92
	3.73	12.5
	5.36	16.0
	5.41	14.4
	7.23	21.0
$C_{12}E_5/C_7$	2.0	6.40
	5.0	11.9
	10.0	21.6
$C_{12}E_6/C_{10}$	1.11	5.55
	1.97	8.18
	3.27	11.43
	4.33	13.5
	5.10	15.3
	6.09	17.8
$C_{12}E_7/C_{10}$	0.85	5.25
	2.16	8.20
	3.19	10.1
	3.70	10.8
	4.40	13.5
	4.68	14.5
	5.18	15.1
$C_{14}E_7/C_{10}$	0.96	6.30
	1.88	7.15
	1.97	7.82
	3.13	7.79
	3.36	10.6
	4.15	11.7
	4.89	13.2
	5.17	14.1
	5.22	11.7
	5.79	15.0
	7.09	16.8

APPENDIX VI

The observed rate constants measured for each C_nE_m/x-alkane oil/water system.
Data used in chapter 6.

The observed rate constants (k obs/s^{-1}) for varying temperatures (^{o}C) measured for different concentrations of **$C_{10}E_5$ with decane at R = 1.51**

[Surfactant]	Temperature	K_{obs}
0.04 M	37.1	11500
	38.9	10700
	39.9	8660
	40.8	8410
	41.8	5020
0.06 M	36.4	14850
	38.9	12500
	39.9	11300
	40.8	9190
	41.8	5600
0.08 M	36.4	20600
	37.1	14700
	39.9	13500
	40.8	9745
	41.3	8140
	41.8	6260
0.10 M	35.7	21750
	36.4	16450
	37.1	14850
	38.9	15850
	39.9	13750
	40.8	10670
	40.8	8050
	41.3	8405
0.12 M	36.4	18700
	37.1	18200
	38.9	16200
	40.8	8980
	40.8	9010
	41.3	9575

The observed rate constants (k obs/s^{-1}) for varying temperatures (^{o}C) measured for different concentrations of **$C_{10}E_5$ with decane at R = 2.5**

(Data from unpublished experimental results by P. D. I. Fletcher, Hull University)

[Surfactant]	Temperature	k_{obs}
0.01975 M	40.6	7400
	41.6	7390
	42.0	5640
	42.5	5220
	43.0	4610
	43.5	3240
	43.9	1460
0.0395 M	40.1	11300
	40.6	98800
	41.4	9880
	41.6	8740
	42.0	8490
	42.5	7150
	43.0	5540
0.079 M	40.1	14700
	40.6	12600
	41.1	12000
	41.6	11600
	42.0	10100
	42.5	85600
0.1185 M	40.1	13200
	40.6	14300
	41.1	14000
	41.6	11800
	42.0	11200
	42.5	9580
	43.0	7880
0.158 M	40.1	14400
	40.6	13000
	41.4	13500
	41.6	11100
	42.0	9200
	42.5	8650
	43.0	9180
	43.0	7530
0.1975 M	39.7	19800
	40.1	18100
	40.6	15600
	41.1	13700
	41.6	12300
	42.0	11600
	42.5	8970

The observed rate constants (k_{obs}/s^{-1}) for varying temperatures (^oC) measured for different concentrations of **$C_{12}E_5$ with decane at R = 1.5**

[Surfatant]	Temperature	k_{obs}
0.04 M	25.3	184
	27.2	269
	28.2	280
	29.2	280
0.06 M	24.3	215
	25.3	182
	26.3	249
	28.2	439
	29.2	566
0.08 M	25.3	329
	26.3	474
	27.2	627
	28.2	542
	29.2	562
	29.7	484
0.12 M	24.3	391
	25.3	597
	26.3	558
	27.2	784
	29.2	819

The observed rate constants (k_{obs}/s^{-1}) for varying temperatures (^oC) measured for different concentrations of **$C_{12}E_5$ with decane at R = 2.5**

[Surfactant]	Temperature	k_{obs}
0.01 M	29.4	51.0
	29.9	76.8
	30.4	67.0
	31.3	56.5
	31.8	30.3
0.02 M	29.0	82.6
	29.4	95.9
	29.9	97.6
	30.9	104
	31.3	101
	31.8	56.1
0.04 M	27.6	657
	28.5	227
	29.0	157
	29.4	179
	29.9	186
	30.9	178
	31.8	189
0.06 M	27.1	277
	27.6	227
	28.0	223
	28.4	243
	28.7	225
	29.6	279
	30.9	301
0.08 M	27.1	278
	28.0	294
	29.0	351
	29.9	404
	30.4	413
	31.3	350
0.10 M	27.1	324
	28.0	361
	28.5	388
	29.0	431
	29.4	491
	29.9	495
	30.4	508
	30.9	511
	31.3	463
0.12 M	27.1	329
	27.6	339
	28.0	455
	29.0	510
	29.4	589
	29.9	612
	30.9	620
	31.3	583
	31.8	419

The observed rate constants (k_{obs}/s^{-1}) for varying temperatures (^oC) measured for different concentrations of **$C_{12}E_6$ with decane at R = 1.5**

[Surfactant]	Temperature	k_{obs}
0.04 M	38.9	1250
	39.9	1230
	41.8	1250
	43.8	1265
	44.7	1250
0.06 M	38.9	523
	40.8	1250
	42.8	1640
	43.8	2040
	44.7	1470
0.08 M	37.5	1390
	39.9	1090
	41.8	1960
	43.8	2260
	44.7	1955
0.10 M	37.5	2340
	38.9	1820
	39.9	2320
	41.8	3405
	43.8	2795
	44.7	2710

The observed rate constants (k obs/s^{-1}) for varying temperatures (^{o}C) measured for different concentrations of **$C_{12}E_6$ with decane at R = 2.5**

(Data from unpublished experimental results by P. D. I. Fletcher, Hull University)

[Surfactant]	Temperature	k_{obs}
0.0197 M	43.0	730
	43.9	546
	44.9	505
	45.9	495
	46.8	472
0.0395 M	42.5	1000
	43.5	775
	44.4	821
	45.4	883
	46.3	888
0.0790 M	42.5	14600
	43.0	13500
	44.0	16000
	45.4	17100
	46.3	15700
0.1184 M	40.6	3420
	42.5	2050
	44.4	2430
	45.4	2580
	46.3	2450
0.1579 M	39.9	4900
	40.9	2460
	41.8	2410
	42.8	2350
	43.8	3300
	44.7	3500
	45.7	3600
	46.6	3220
	47.6	2270
0.1974 M	42.5	4230
	43.5	4880
	44.5	5250
	45.4	4980
	46.4	4230
	47.3	3670
	47.8	3650

The observed rate constants (k_{obs}/s^{-1}) for varying temperatures (^oC) measured for different concentrations of **$C_{12}E_7$ with decane at R = 2.5**

[Surfactant]	Temperature	k_{obs}	[Surfactant]	Temperature	k_{obs}
0.01 M	53.2	232	0.10 M	50.4	4570
	53.6	727		51.3	2930
	54.1	951		52.2	3860
	54.6	658		53.2	4650
	55.0	740		54.1	4400
				54.6	4260
0.02 M	53.2	1360		55.0	3810
	53.6	1520			
	54.1	1200	0.12 M	49.4	4260
	54.6	1220		50.3	4210
	55.0	1090		50.4	3010
	55.5	868		51.3	4230
				52.2	4010
0.04 M	51.3	2750		52.8	4090
	52.2	3010		53.2	4700
	52.7	2050		53.6	5250
	53.2	2320		53.9	4990
	53.6	1970		54.6	4930
	54.1	1440		55.0	4290
0.06 M	51.3	2390			
	51.7	2100			
	52.2	3190			
	52.7	2850			
	53.2	2760			
	53.6	2910			
	54.1	2700			
	54.6	2300			
	55.0	2200			
0.08 M	49.4	4680			
	50.4	3580			
	51.3	3480			
	52.2	3580			
	52.7	3730			
	53.2	3660			
	54.1	3780			
	54.6	3010			
	55.0	2670			

The observed rate constants (k obs/s^{-1}) for varying temperatures (^{o}C) measured for different concentrations of **$C_{14}E_7$ with decane at R = 2.5**

(Data from unpublished experimental results by P. D. I. Fletcher, Hull University)

[Surfactant]	Temperature	k_{obs}
0.01927 M	44.9	8.5
	45.9	23.1
	46.8	26.5
	47.8	38.1
	48.7	47.0
	49.7	56.9
0.03854 M	44.0	8.0
	44.9	34.2
	45.9	46.8
	46.8	54.8
	47.8	75.0
	48.7	98.8
	49.7	114
0.07708 M	44.0	83
	44.9	87.8
	45.9	84.5
	46.8	120
	47.8	136
	48.2	200
	48.7	222
	49.2	223
0.1156 M	44.9	129
	45.9	154
	46.8	232
	47.8	331
	48.7	322
	49.7	306
0.01542 M	43.5	45
	44.4	162
	45.4	221
	46.8	316
	47.8	456
	48.7	458
	49.2	527
0.1927 M	44.4	190
	46.3	492
	47.3	437
	48.2	581
	49.2	738